Recommended Resistance Factors for Load and Resistance Factor Design of Drilled Shafts in Iowa

Final Report
April 2019

BRIDGE ENGINEERING CENTER

IOWA STATE UNIVERSITY
Institute for Transportation

Sponsored by
Iowa Department of Transportation
(InTrans Project 14-512)

About the Bridge Engineering Center

The mission of the Bridge Engineering Center (BEC) is to conduct research on bridge technologies to help bridge designers/owners design, build, and maintain long-lasting bridges.

About the Institute for Transportation

The mission of the Institute for Transportation (InTrans) at Iowa State University is to develop and implement innovative methods, materials, and technologies for improving transportation efficiency, safety, reliability, and sustainability while improving the learning environment of students, faculty, and staff in transportation-related fields.

The preparation of this report was financed in part through funds provided by the Iowa Department of Transportation through its "Second Revised Agreement for the Management of Research Conducted by Iowa State University for the Iowa Department of Transportation" and its amendments.

Technical Report Documentation Page

1. Report No.	2. Government Accession No.	3. Recipient's Catalog No.
InTrans Project 14-512		

4. Title and Subtitle

Recommended Resistance Factors for Load and Resistance Factor Design of Drilled Shafts in Iowa

5. Report Date

April 2019

6. Performing Organization Code

7. Author(s)

Philippe Kalmogo (orcid.org/0000-0002-9727-5945), Sri Sritharan (orcid.org/0000-0001-9941-8156), and Jeramy C. Ashlock (orcid.org/0000-0003-0677-9900)

8. Performing Organization Report No.

InTrans Project 14-512

9. Performing Organization Name and Address

Bridge Engineering Center
Iowa State University
2711 South Loop Drive, Suite 4700
Ames, IA 50010-8664

10. Work Unit No. (TRAIS)

11. Contract or Grant No.

12. Sponsoring Organization Name and Address

Iowa Department of Transportation
800 Lincoln Way
Ames, IA 50010

Federal Highway Administration
U.S. Department of Transportation
1200 New Jersey Avenue SE
Washington, DC 20590

13. Type of Report and Period Covered

Final Report

14. Sponsoring Agency Code

SPR RB03-12

15. Supplementary Notes

Visit www.intrans.iastate.edu for color PDFs of this and other research reports.

16. Abstract

The Federal Highway Administration (FHWA) mandated utilization of the Load and Resistance Factor Design (LRFD) approach for all new bridges initiated in the US after October 1, 2007. To achieve part of this goal, a database for Drilled SHAft Foundation Testing (DSHAFT) was developed and reported on by the researchers in 2012. DSHAFT is aimed at assimilating high-quality drilled shaft test data from Iowa and the surrounding regions. Using the available data in DSHAFT, preliminary resistance factors were calibrated and proposed by the researchers in a previous project. Compared to the American Association of State Highway and Transportation Officials (AASHTO) LRFD specifications, the preliminary values showed increased efficiency in some cases. DSHAFT is currently housed on a project website (http://srg.cce.iastate.edu/dshaft) and has been expanded to include 51 drilled shaft tests from the previous number of 41.

As additional load test data became available, resistance factors were expected to be recalibrated; thus, the objective of this research was to utilize the expanded DSHAFT database to refine and recommend final resistance factor values for implementation. This was done by examining current design and construction practices used by the Iowa Department of Transportation (DOT) as well as recommendations given in the AASHTO LRFD Bridge Design Specifications and the FHWA drilled shaft design guidelines, and by reviewing calibration studies conducted by Iowa and other states.

Various static design methods were used to estimate side resistance and end bearing of drilled shafts in cohesive soil, cohesionless soil, intermediate geomaterial (IGM), and rock. The extrapolation procedures developed by the researchers and reported in 2014 were found to have significant limitations; therefore, a t-z analysis approach was adopted instead to obtain the measured resistances necessary for the calibration.

Using the estimated and measured resistances, regional resistance factors were calibrated at a target reliability of 3.0 following the AASHTO LRFD calibration framework and the modified first-order second-moment (FOSM) reliability method. Two different procedures (Approach I and Approach II) were used in the calibration of skin friction resistance factors. The calibration initially considered load tests performed in Iowa solely before including all usable load tests available in the database. Based on the calibration results, final resistance factors, which show improvement compared to preliminary values and AASHTO recommended values, are recommended for implementation.

17. Key Words

bridge design—drilled shafts—end bearing—load factors—resistance factors—side resistance

18. Distribution Statement

No restrictions.

19. Security Classification (of this report)	20. Security Classification (of this page)	21. No. of Pages	22. Price
Unclassified.	Unclassified.	196	NA

RECOMMENDED RESISTANCE FACTORS FOR LOAD AND RESISTANCE FACTOR DESIGN OF DRILLED SHAFTS IN IOWA

Final Report
April 2019

Principal Investigator
Sri Sritharan, Professor
Civil, Construction, and Environmental Engineering, Iowa State University

Co-Principal Investigator
Jeramy C. Ashlock, Assistant Professor
Civil, Construction, and Environmental Engineering, Iowa State University

Research Assistant
Philippe Kalmogo

Authors
Philippe Kalmogo, Sri Sritharan, and Jeramy C. Ashlock

Sponsored by
Iowa Department of Transportation
(InTrans Project 14-512)

Preparation of this report was financed in part
through funds provided by the Iowa Department of Transportation
through its Research Management Agreement with the
Institute for Transportation

A report from
Bridge Engineering Center
Iowa State University
2711 South Loop Drive, Suite 4700
Ames, IA 50010-8664
Phone: 515-294-8103 Fax: 515-294-0467
www.intrans.iastate.edu

TABLE OF CONTENTS

LIST OF FIGURES

LIST OF TABLES

ACKNOWLEDGMENTS

The authors would like to thank the Iowa Department of Transportation (DOT) for sponsoring this research, the Federal Highway Administration for state planning and research (SPR) funds used for this project, and the technical advisory committee (TAC) for their guidance.

The following individuals served on the TAC: Ahmad Abu-Hawash, Mark Dunn, Kyle Frame, Steve Megivern, Michael Nop, and Bob Stanley. The members of this committee represented Bridges and Structures, Soils Design, Construction, and Research and Analytics for the Iowa DOT.

EXECUTIVE SUMMARY

The Federal Highway Administration (FHWA) mandated utilization of the Load and Resistance Factor Design (LRFD) approach for all new bridges initiated in the US after October 1, 2007. To achieve part of this goal, a database for Drilled SHAft Foundation Testing (DSHAFT) was developed and reported on by the researchers in 2012. DSHAFT is aimed at assimilating high-quality drilled shaft test data from Iowa and the surrounding regions.

Using the available data in DSHAFT, the researchers subsequently calibrated and proposed preliminary resistance factors in 2014. Compared to the American Association of State Highway and Transportation Officials (AASHTO) LRFD specifications, the preliminary values showed increased efficiency in some cases.

DSHAFT is currently housed on a project website (http://srg.cce.iastate.edu/dshaft) and has been expanded to include 51 drilled shaft tests from the previous number of 41. As additional load test data became available, resistance factors were expected to be recalibrated; thus, the objective of this research was to utilize the expanded DSHAFT database to refine and recommend final resistance factor values for implementation. This was done by examining current design and construction practices used by the Iowa Department of Transportation (DOT) as well as recommendations given in the AASHTO LRFD Bridge Design Specifications and the FHWA drilled shaft design guidelines, and by reviewing calibration studies conducted by Iowa and other states.

Various static design methods recommended by others were used to estimate side resistance and end bearing of drilled shafts in cohesive soil, cohesionless soil, intermediate geomaterial (IGM), and rock. The extrapolation procedures developed by the researchers prior to this were found to have significant limitations; therefore, a t-z analysis approach was adopted instead to obtain the measured resistances necessary for the calibration.

Using the estimated and measured resistances, regional resistance factors were calibrated at a target reliability of 3.0 following the AASHTO LRFD calibration framework and the modified first-order second-moment (FOSM) reliability method. Two different procedures (Approach I and Approach II) were used in the calibration of skin friction resistance factors. The calibration initially considered load tests performed solely in Iowa before including all usable load tests available in the database. Based on the calibration results, final resistance factors, which show improvement compared to preliminary established values and AASHTO recommended values, are recommended for implementation.

CHAPTER 1. OVERVIEW

1.1. Background

Despite the advantages of drilled shafts over other foundations types, the state of Iowa has commonly used driven steel H-piles for bridge foundations. Although drilled shafts can be the most cost-effective foundation option for certain construction and soil conditions found in several regions of Iowa, they have been used infrequently due to three primary reasons including (1) the lack of a formal process for selection of appropriate foundation types, especially in evaluating the advantages of drilled shafts over driven piles; (2) limited design guidelines and details for drilled shafts in the Iowa Bridge Design Manual; and (3) the absence of standard construction inspection checklists for drilled shafts. The addition of the Federal Highway Administration's (FHWA's) drilled shaft construction procedures and Load and Resistance Factor Design (LRFD) methods by Brown et al. (2010) to the latest Iowa Department of Transportation (DOT) LRFD manual, however, overcame some of these shortcomings, resulting in an increase of drilled shaft use in recent years.

Conforming to the FHWA mandate, the Iowa DOT Office of Bridges and Structures has relied on the resistance factors recommended by the American Association of State Highway and Transportation Officials (AASHTO) LRFD Bridge Design Specifications for drilled shaft design. However, AASHTO recommended resistance factors were developed using various calibration methods, including both reliability theory with statistical analysis of drilled shaft load tests from a general national database and fitting to the allowable stress design (ASD) factor for safety, as well as a combination of the two. In some cases, engineering judgement was exercised to settle on the final resistance factor with due consideration of the quantity and quality of the load test data used in the calibration. Consequently, the set of resistance factors recommended by AASHTO does not fully embrace LRFD fundamental concepts. Neither are the resistance factors able to accurately reflect soil variability and construction practices that are specific to a given state or region.

Given the successful development and implementation of regional LRFD guidelines that improved the reliability of bridge foundations designed with driven piles and elevated the cost-competitiveness of driven pile foundations, a similar endeavor has been initiated for drilled shafts. In the initial phase of the research project sponsored by the Iowa DOT, Garder et al. (2012) collected, reviewed, and integrated available drilled shaft load test data into a Microsoft Access database for Drilled SHAft Foundation Testing (DSHAFT). An earlier version of DSHAFT included 31 load tests, which was later expanded to include 10 additional load tests for a preliminary calibration by Ng et al. (2014). The necessary load test data was retrieved from 11 states including Colorado, Iowa, Illinois, Kansas, Kentucky, Minnesota, Missouri, Nebraska, Nevada, South Dakota, and Tennessee. DSHAFT is housed on the project website: http://srg.cce.iastate.edu/dshaft/, and it has been updated with 10 additional load tests performed in Iowa.

1.2. Scope of Research Project

This research project had the overall objective to develop and recommend refined regionally calibrated resistance factors that increase drilled shaft design efficiency in Iowa. This overall objective was accomplished by the following:

- Conducting a literature review on regional LRFD calibration studies conducted by the Iowa DOT and various states as well as recommendations given in AASHTO LRFD Bridge Design Specifications (2017) and the FHWA drilled shaft guidelines reported by Brown et al. (2010)
- Reviewing the analysis procedures and outcomes of the preliminary calibration
- Examining and analyzing the expanded DSHAFT data sets
- Performing static analyses
- Quantifying the measured capacity of each test drilled shaft
- Determining regional LRFD resistance factors

1.3. Report Layout

The purpose of this report is to clearly illustrate the development of regional LRFD resistance factors for the design of drilled shafts under axial load in Iowa. This report consists of five chapters and four appendices. The content of each chapter is briefly described as follows:

Chapter 1: Overview – A brief description of the background of the deep foundations implemented in Iowa and the scope of the research project

Chapter 2: Literature Review – A summary of a literature review on of the LRFD calibration framework, drilled shaft design methods and construction procedures, AASHTO LRFD specifications, and state of regional LRFD studies in various states including preliminary calibration in Iowa

Chapter 3: Examination and Analysis of Expanded DSHAFT Data – A brief summary of the DSHAFT expanded database, and drilled shaft resistance estimations and measurements including extrapolation procedure of load test data

Chapter 4: Resistance Factor Calibration – A brief description of the statistical characterization of the resistance bias; resistance factor calculations for side resistance, end bearing, and total resistance; resistance factor calculations based on various failure defining criteria; and presents a summary of recommended resistance factors

Chapter 5: Summary and Future Research – A summary of the research outcomes for the development of regional LRFD procedures for drilled shafts in Iowa, and proposes several topics for future research

CHAPTER 2. LITERATURE REVIEW

2.1. ASD vs. LRFD Philosophy

Uncertainties are an inherent part of drilled shafts design. They stem from various sources and may lead to variability in the drilled shafts' anticipated loads and resistance. Consequently, engineers have, over the years, developed various strategies to account for the unknowns and provide a margin of safety against undesired performance defined whether in terms of excessive settlement or complete geotechnical failure. Historically, a factor of safety (FS) was used in the allowable stress design (ASD) framework to ensure that the drilled shafts' applied loads were always less than the available resistance regardless of any variation during the design life of the structure as shown in Figure 2.1.

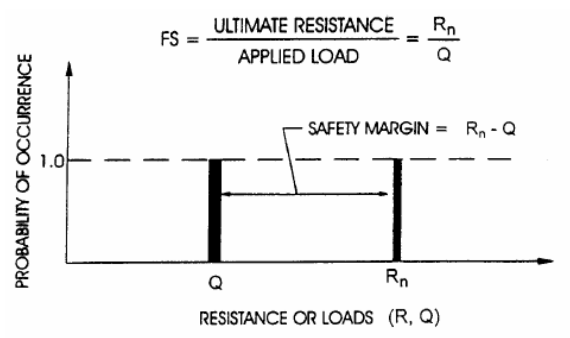

After Withiam et al. 1998

Figure 2.1. ASD principle

The factor of safety used in the ASD framework was selected based on the design method, successful past practices, and the designer's engineering judgment. Despite its simplicity, this approach could not guarantee a consistent level of reliability across designs due to its inability to accurately and quantitatively account for the different levels of uncertainty associated with load and resistance.

LRFD overcomes the deficiencies associated with ASD by providing a more rational approach to quantify and account for all sources of uncertainty involved in the design process. As illustrated by the basic LRFD equation (2.1), uncertainties associated with various types of load and resistance at a given limit state can be taken into account by load and resistance factors, respectively.

$$\sum \gamma_i Q_i \leq \varphi R_n \tag{2.1}$$

where,

Q_i = Load type i (e.g., dead load, live load, etc.)
γ_i = Factor for load type i
R_n = Nominal resistance
Φ = Resistance factor

In LRFD, the load and resistance are treated as independent random variables with some probability of occurrence (Figure 2.2).

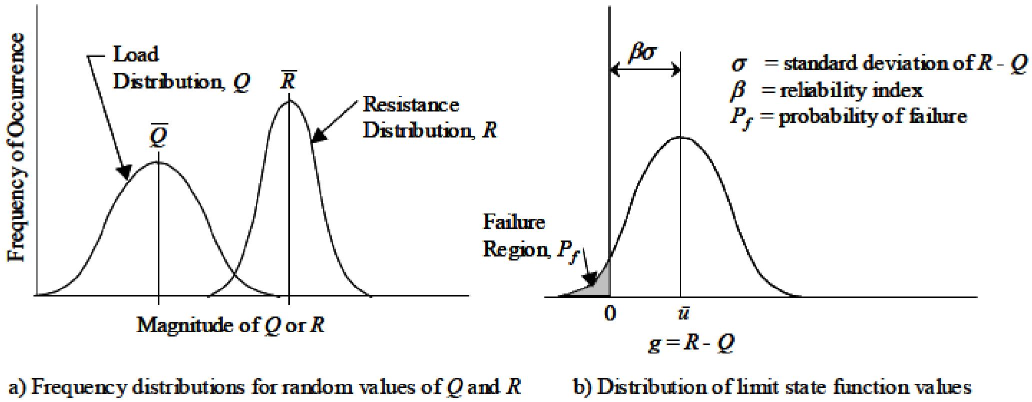

After Withiam et al. 1998

Figure 2.2. Load and resistance distribution and reliability index

Using their known variabilities, the load and resistance factors can be calibrated to ensure that the probability of the factored loads exceeding the available resistance is at an acceptable level. This failure region, represented by the shaded area in Figure 2.2b, is related to a reliability index, β, for which a value must be specified in the calibration process.

2.2. Calibration Approach

Resistance factor calibration can be accomplished by judgment, fitting to ASD, reliability theory, or a combination of them, but only calibration using reliability theory can fulfill the true goal of LRFD to ensure more uniform and consistent levels of safety across designs. In calibration by judgment, experience, which includes records of past satisfactory and poor performance, is relied upon to select appropriate values for the resistance factors. Calibration by fitting to ASD is simply a format change consisting in the selection of resistance factors that would result in the same designs as ASD factors of safety. This approach only eliminates the discrepancy between load values used for substructure and superstructure designs, thereby reducing possible miscommunications between structural and geotechnical engineers. Calibration by reliability theory involves the application of probabilistic methods of varying levels of complexity. The Level III method (fully probabilistic) is the most accurate, but it is rarely used in LRFD calibration because of the difficulty in obtaining the required load and resistance information. Level II includes approximate probabilistic methods such as the first-order second-moment (FOSM) method, and it only requires the first two moments (i.e., mean and standard deviation) of the load and resistance variables to define the probability distributions associated with each variable. This approach, through an iterative procedure, can determine the safety or reliability index associated with a combination of selected values of load and resistance factors. Level I probabilistic methods are the least accurate, and they also use a second moment reliability method. The difference between Level I and Level II methods, however, lies in the limit state function being linearized at the mean values of the load and resistance rather than at the design point on the nonlinear failure surface.

The use of any of these probabilistic methods requires the existence of an extensive record of test data to statistically characterize the different variables involved in the limit state function. A calibration using a combination of any of the approaches previously detailed is warranted when the data required for a proper reliability-based calibration is not available, or when the quality of the data at hand is questionable. As Allen (2005) stated, "if the adequacy of the input data is questionable, the final load and resistance factor combination selected should be more heavily weighted toward a level of safety that is consistent with past successful design practice, using the reliability theory results to gain insight as to whether or not past practice is conservative or non-conservative."

The first step in the calibration by reliability theory consists in developing the performance function that incorporates all random variables describing the failure mechanism of a drilled shaft. Rearranging LRFD limit state in equation (2.1) and considering only dead load (Q_D) and live load (Q_L) consistent with Strength I limit state leads to:

$$\varphi R_n - \left(\gamma_{Q_D} Q_D + \gamma_{Q_L} Q_L\right) \geq 0 \tag{2.2}$$

where,
Q_D = Dead load
Q_L = Live load
γ_{Q_D} = Dead load factor
γ_{Q_L} = Live load factor

If the load and resistance are assumed to be random variables, then the performance limit function corresponding to equation (2.2) can be written as:

$$g(R, Q) = R_m - Q_m \tag{2.3}$$

where, g is a random variable representing the margin of safety, and Q_m and R_m are random variables representing the actual loads and resistance. The parameters necessary to statistically characterize these random variables include the mean (μ), standard deviation (σ), and coefficient of variation (COV).

$$\mu = \frac{1}{N} \sum x_i \tag{2.4}$$

$$\sigma = \sqrt{\frac{\sum (x_i - \mu)^2}{N-1}} \tag{2.5}$$

$$COV = \frac{\sigma}{\mu} \tag{2.6}$$

where, N is the total number of data values and x_i the individual value of the random variable being considered.

The variation of actual load and resistance values from predicted values can be expressed in terms of the bias λ, defined as the ratio of the measured to predicted values.

Using this relationship between measured and predicted values, equation 2.3 can be rewritten as:

$$g(R, Q) = \lambda_R R_n - \left(\lambda_{Q_D} Q_D + \lambda_{Q_L} Q_L\right) \tag{2.7}$$

The minimum R_n required to satisfy the limit state design equation is obtained when equation (2.2) is equated to zero, which represents the boundary line between satisfactory structure performance and adverse performance.

$$R_n = \frac{\gamma_{Q_D} Q_D + \gamma_{Q_L} Q_L}{\varphi} \tag{2.8}$$

Substituting equation (2.8) into equation (2.7) yields:

$$g(R, Q) = \lambda_R \frac{\gamma_{Q_D} Q_D + \gamma_{Q_L} Q_L}{\varphi} - \left(\lambda_{Q_D} Q_D + \lambda_{Q_L} Q_L\right) \tag{2.9}$$

Factoring out Q_L from each term in equation (2.9) gives:

$$\frac{g(R,Q)}{Q_L} = \lambda_R \frac{\gamma_{Q_D} \frac{Q_D}{Q_L} + \gamma_{Q_L}}{\varphi} - \left(\lambda_{Q_D} \frac{Q_D}{Q_L} + \lambda_{Q_L}\right) \tag{2.10}$$

Redefining g(R, Q)/Q_L as g(R, Q), the performance function can be written as:

$$g(R, Q) = \lambda_R \frac{\gamma_{Q_D} \frac{Q_D}{Q_L} + \gamma_{Q_L}}{\varphi} - \left(\lambda_{Q_D} \frac{Q_D}{Q_L} + \lambda_{Q_L}\right) \tag{2.11}$$

Equation (2.11) can be solved using the various reliability methods described previously. If both the load and resistance random variables are assumed to follow a perfect lognormal distribution as consistent with the basis of current AASHTO specifications, then a closed-form solution relating the resistance factor, φ, to the reliability index, β, developed by Withiam et al. (1998) using the FOSM reliability method can be expressed as:

$$\varphi = \frac{\lambda_R\left(\frac{\gamma_D Q_D}{Q_L} + \gamma_L\right)\sqrt{\left[\frac{\left(1+COV_D^2+COV_L^2\right)}{1+COV_R^2}\right]}}{\left(\frac{\lambda_D Q_D}{Q_L} + \lambda_L\right)\exp\left\{\beta_T\sqrt{\ln\left[\left(1+COV_R^2\right)\left(1+COV_D^2+COV_L^2\right)\right]}\right\}} \tag{2.12}$$

where,
COV_R = Coefficient of variation of resistance

COV_D = Coefficient of variation of dead load
COV_L = Coefficient of variation of live load
β_T = Target reliability index
λ_R = Resistance bias factor
λ_D = Dead load bias factor
λ_L = Live load bias factor
γ_D = Dead load factor
γ_L = Live load factor
Q_D = Dead load
Q_L = Live load

A modified version of equation (2.12) was developed by Bloomquist et al. (2007) to minimize the difference between the results obtained from all three reliability methods. The proposed equation is presented below and subsequently used in the resistance factor calculation. As the actual distribution of the load and resistance bias factors deviate from the lognormal, equations (2.12) and (2.13) become approximations, and the Monte Carlo simulation should be used to provide more accurate results.

$$\varphi = \frac{\lambda_R\left(\frac{\gamma_D Q_D}{Q_L}+\gamma_L\right)\sqrt{\frac{\left(1+\frac{\frac{Q_D^2}{Q_L^2}\lambda_D^2 COV_D^2+\lambda_L^2 COV_L^2}{\frac{Q_D^2}{Q_L^2}\lambda_D^2+2\frac{Q_D}{Q_L}\lambda_D\lambda_L+\lambda_D^2}\right)}{\left(1+COV_R^2\right)}}}{\left(\frac{\lambda_D Q_D}{Q_L}+\lambda_L\right)\exp\left\{\beta_T\sqrt{\ln\left[\left(1+COV_R^2\right)\left(1+\frac{\frac{Q_D^2}{Q_L^2}\lambda_D^2 COV_D^2+\lambda_L^2 COV_L^2}{\frac{Q_D^2}{Q_L^2}\lambda_D^2+2\frac{Q_D}{Q_L}\lambda_D\lambda_L+\lambda_D^2}\right)\right]}\right\}} \tag{2.13}$$

The Monte Carlo simulation is a numerical technique that utilizes a given variable mean value, standard deviation, COV, and distribution type to randomly generate a chosen number of virtual observations of the variable allowing extrapolation of the cumulative density function values. It is able to deal with a variety of functions and can be easily implemented on a computer using Microsoft Excel or MATLAB. The steps necessary to implement a Monte Carlo simulation can be described as follows:

- Use the statistical parameters of each random variable to generate N random numbers for each variable. The value of N is a function of the desired accuracy, the target probability of failure, and the coefficient of variation.
- Assume a trial resistance factor, φ, and evaluate the performance function for each set of randomly generated load and resistance values.
- Calculate the probability of failure, pf, as the ratio of the number of failures ($g \leq 0$) to the total number of simulations, N, and determine the corresponding reliability index.
- Iterate until the calculated reliability index converges to the desired target value.

As reported by Paikowsky et al (2004) and Allen (2005), the difference between the resistance factors calculated from these methods is within 10% with first-order reliability method (FORM) and Monte Carlo simulation providing the highest values.

Upon developing the required performance function, the statistical characteristics of the load and resistance bias factors must be established in the next step of the calibration. Additionally, an appropriate distribution type must be assigned to the load and resistance data upon comparing the shape of their respective histograms generated from observed values with existing theoretical frequency distribution types including but not limited to the normal and lognormal distributions. The assumed distribution type must then be verified using probability plots as well as statistical tests such as the Anderson-Darling (AD) (1952) normality method or the Pearson's chi-squared (χ^2) test. Because of the lack of research on superstructure load transfer to the foundation and the difficulty of obtaining such information, the characteristics of the load uncertainties used in superstructure analysis are also used for substructures. Consequently, load factors associated with the Strength I limit state condition recommended by AASHTO are used in this study. The dead and live load random variables are assumed to follow a lognormal distribution with probabilistic characteristics presented in Table 2.1 (Nowak 1999).

Table 2.1. Statistical parameters of dead load and live load

Load (Q)	Load factor (γ)	Load bias (λ)	Coefficient of variation (COV_Q)
Dead (D)	1.25	1.05	0.1
Live (L)	1.75	1.15	0.2

Once the necessary statistical parameters are established and the assumed distribution type verified, the calibration can proceed with the selection of a desired target reliability and the calculation of the resistance factors.

The selection of a target reliability is a function of several factors including but not limited to the desired failure probability, the amount of redundancy present in the foundation system, the level of reliability inherent in past ASD practices, the extent of damage and potential human loss in the event of undesired structure performance, and the design life of the structure. Maintaining a uniform level of reliability across all limit states is also an important aspect to be considered. While resistance factors for bridge structural components have been calibrated to achieve a reliability index of 3.5, reliability analyses by Barker et al. (1991) have shown that the previously used factors of safety for foundation design in the ASD framework resulted in reliabilities less than 3.5. Based on their findings, target reliabilities of 3.5, 2.5 to 3.0, and 2.0 to 2.5 were recommended for single shaft supported foundations, non-redundant systems, and highly redundant systems, respectively. Based on Paikowsky et al. (2004), a foundation system with five or more shafts in a group can be considered redundant. Otherwise, it is classified as non-redundant. The higher reliability associated with highly redundant systems such as driven pile groups stem from the fact that the failure of a single component in a group may not automatically result in the collapse of the entire foundation. In contrast, a foundation composed of fewer components has a higher probability of failure in the event that a single element fails or is overloaded. AASHTO resistance factors were developed based on these recommendations.

Another parameter required in the resistance factor calibration is the dead to live load ratio. This parameter is a function of the bridge span, and it could vary between 1.0 and 4.0. Though a range of 2 to 2.5 and a value of 3.0 were recommended by Paikowsky et al. (2004) and Barker et al. (1991), respectively, this parameter has been found to have a negligible influence in the calibration.

2.3. Drilled Shaft Capacity Prediction Methods

2.3.1. Introduction

In drilled shaft design, static design methods of an empirical or semi-empirical nature are generally used to determine the shaft size, embedment length, and tip elevation required to transfer the superstructure loads to the ground. Depending on the soil conditions and construction quality, the required resistance can be derived from skin friction, end bearing, or a combination of both. While some states have developed their own in-house design methods based on regression analyses of local load test results, most design agencies routinely use the AASHTO LRFD Bridge Design Specifications recommended methods, which are based on the work of O'Neill and Reese (1999) and its subsequent update by Brown et al. (2010). Several design methods are available depending on the geomaterial type, and they require properties that can be determined from laboratory tests on field-collected soil/rock samples, or correlations to in situ measurements such as the Standard Penetration Test (SPT) blow count number. In a typical design process, the subsurface at the planned location of the drilled shaft is divided into several idealized geomaterial layers using boring logs and other relevant information. Depending on the geomaterial properties, the different layers are classified as cohesive soil, cohesionless soil, intermediate geomaterial (IGM), or rock. For drilled shaft design, cohesive soils can be defined as geomaterials with undrained shear strength less than 5 ksf (Brown et al. 2010), and they include clayey sands and gravels, lean and fat clay soils, and silts with a liquid limit over 50 (GC, SC, CL, CH, and MH from the Unified Soil Classification System and ASTM D2487). Cohesionless soils include gravels and sands with less than 5% fines, gravels and sands with silty fines, and non-plastic silts. Rock is defined as a high strength cohesive cemented geomaterial with unconfined compressive strength greater than 100 ksf. IGMs are geomaterials with strength characteristics transitional between soil and rock. They can be categorized as either cohesive or cohesionless. Cohesive IGMs have unconfined compressive strength ranging between 10 and 100 ksf whereas cohesionless IGMs are considered to be very dense granular geomaterials with SPT blow counts between 50 and 100. After the subsurface profile has been delineated and strength properties assigned to each zone, appropriate design methods are selected based on the site geology, extent of available soil parameters, and local practice, and they are used to estimate the nominal side and base resistance of a drilled shaft for each geomaterial layer. The ultimate axial capacity of a drilled shaft is given by:

$$Q_u = Q_b + Q_s = q_b A_b + \sum_{i=1}^{n} q_{si} A_{si} \tag{2.14}$$

where,
q_b = Unit end bearing resistance
A_b = Base cross sectional area
q_{si} = Unit side resistance of soil layer i
A_{si} = Shear area of soil layer i
n = Number of soil layers along shaft length

2.3.2. Side Resistance Prediction Methods

2.3.2.1. Cohesive Soils

Side resistance of drilled shafts in cohesive soil is commonly evaluated in terms of undrained shear strength consistent with short-term loading conditions using the α-method. The α-method, developed by Tomlinson (1971) and based on back-analysis of load test results on timber, pipe, and precast concrete piles in cohesive soils, suggests that the unit skin friction is related to the undrained shear strength by an empirical factor, α, which varies with depth and the strength of the cohesive soil. This relationship is expressed as:

$$q_s = \alpha S_u \tag{2.15}$$

where,
S_u = Undrained shear strength (ksf)
α = 0 from the ground surface to a depth of 5 ft or to the depth of seasonal moisture change whichever is greater
α = 0.55 for $\frac{S_u}{P_a} \leq 1.5$
α = $0.55 - 0.1\left(\frac{S_u}{P_a} - 1.5\right)$ for $1.5 \leq \frac{S_u}{P_a} \leq 2.5$
P_a = Atmospheric pressure (2.12 ksf)

In previous practice, the side resistance was neglected over a distance of one diameter above the base of the shaft based on numerical modeling that predicted the development of a zone of tension near the base. However, this recommendation has been discarded from current practice because of the lack of evidence from field load test data. The undrained shear strength parameter should ideally be determined in the laboratory from triaxial tests (consolidated undrained, unconsolidated undrained) on undisturbed soil samples or in situ from tests including vane shear test (VST) and cone penetration test (CPT). The undrained shear strength can also be estimated using various correlations available in the literature. Examples of such correlations include but are not limited to those proposed by Bjerrum (1972) (equation 2.16) and Bowles (1982) (Table 2.2).

$$S_u = \frac{f_1 N_{60} P_a}{100} \tag{2.16}$$

where,

f_1 = Empirical factor (4.5 for PI = 50 and 5.5 for PI = 15),
PI = Plasticity index
N_{60} = SPT blow count corrected for hammer efficiency
P_a = Atmospheric pressure (2.12 ksf)

Table 2.2. Undrained shear strength correlation to SPT blow count number

S_u, ksf	0	0.25	0.5	1	2	4
N, standard penetration resistance	0	2	4	8	16	32

Source: Bowles 1982

2.3.2.2. Cohesionless Soils

The unit side resistance of a drilled shaft in cohesionless soils is a function of the normal stress acting on the shaft-soil interface, and it can be estimated by the β-method expressed as:

$$q_s = K \tan \delta \sigma'_V = \beta \sigma'_V \tag{2.17}$$

where,
K = Lateral earth pressure coefficient at shaft-soil interface
δ = Effective stress angle of friction at shaft-soil interface
σ'_v = Vertical effective stress at mid-depth of soil layer (ksf)
β = Side resistance coefficient

To calculate the vertical effective stress as a function of depth, the soil unit weight was estimated from Table 2.3 and Table 2.4 based on the uncorrected SPT blow count number.

Table 2.3. Unit weight correlation to SPT blow count for granular soils

SPT N-value (blows/foot)	γ (lb/ft^3)
0–4	70–100
4–10	90–115
10–30	110–130
30–50	110–140
> 50	130–150

Source: Bowles 1982

Table 2.4. Unit weight correlation to SPT blow count for cohesive soils

SPT N-value (blows/foot)	γ_{sat} (lb/ft^3)
0–4	100–120
4–8	110–130
8–32	120–140

Source: Bowles 1982

In previous AASHTO recommendations, the β coefficient was determined as a function of depth below the ground surface. Based on back-analysis of load test data, O'Neill and Hassan (1994) developed the following expressions:

$$\beta = 1.5 - 0.135\sqrt{z} \text{ for sandy soils and } N_{60} \geq 15 \tag{2.18}$$

$$\beta = \frac{N_{60}}{15}\left(1.5 - 0.135\sqrt{z}\right) \text{ for all cohesionless soils and } N_{60} < 15 \tag{2.19}$$

$$\beta = 2.0 - 0.06(z)^{0.75} \text{ for gravelly sands and gravels and } N_{60} \geq 15 \tag{2.20}$$

where,

z = Depth below ground at soil layer mid depth (ft)

N_{60} = Average SPT blow count in the design zone under consideration and corrected for hammer efficiency

β coefficients calculated from equation (2.18) and equation (2.19) are limited to a minimum of 0.25 and maximum value of 1.20. For equation (2.20), and β is limited to minimum and maximum values of 0.25 and 1.80, respectively. Moreover, a limit of 4 ksf is imposed by O'Neill and Hassan (1994) on the unit side resistance calculated using this approach based on the maximum value observed in the load test database that served as the basis for the development of the expressions. Rollins et al. (2005) developed and proposed an additional expression for β as follows:

$$\beta = 3.4 \times e^{(-0.085z)} \text{ for gravels with } N_{60} \geq 50 \tag{2.21}$$

where,

z = Depth below ground at soil layer mid depth (ft)

N_{60} = Average SPT blow count in the design zone under consideration and corrected for hammer efficiency

β calculated from equation (2.21) is limited to a minimum of 0.25 and maximum value of 3.0.

Although the depth-dependent approach to estimating the β coefficient has been found to be conservative in practice, it fails to account explicitly for the in situ state of stress and soil shear strength, which is necessary for proper modeling of the mechanisms of soil-structure interaction controlling side resistance. A more rational approach that overcomes this major limitation was developed by Chen and Kulhawy (2002). In this approach, the β coefficient is determined as a function of in situ lateral earth pressure and interface friction angle as:

$$\beta = K_0\left(\frac{K}{K_0}\right)\tan\varphi' = (1 - \sin\varphi')\left(\frac{\sigma'_p}{\sigma'_v}\right)^{\sin\varphi'}\tan\varphi' \leq K_p\tan\varphi' \tag{2.22}$$

where,

φ' = Soil effective stress friction angle
σ'_p = Effective vertical preconsolidation stress
σ'_v = Vertical effective stress at mid-depth of soil layer (ksf)
K_p = Passive earth pressure coefficient
K_0 = At rest earth pressure coefficient

Depending on the type of cohesionless soils, the effective vertical preconsolidation stress can be estimated as follows:

$$\frac{\sigma'_p}{P_a} \approx 0.47(N_{60})^m \text{ for sands, silty sands and silts} \quad (2.23)$$

$$\frac{\sigma'_p}{P_a} = 0.15N_{60} \text{ for gravelly soils} \quad (2.24)$$

where m is 0.6 for clean quarzitic sands and 0.8 for silty sands to sandy silts.

2.3.2.3. Intermediate Geomaterials

Cohesive Intermediate Geomaterials

The intermediate geomaterial category was introduced by O'Neill and Reese (1999) to describe materials that are transitional between soil and rock. The cohesive type include argillaceous geomaterials such as heavily overconsolidated clays, clay shales, saprolites, and mudstones that are prone to smearing during drilling and calcareous rocks such as limestone, limerock, and argillaceous geomaterials that are not prone to smearing during drilling. From an engineering perspective, IGM are classified as materials with unconfined compressive strength ranging between 10 and 100 ksf. Based on the design methodology developed by Hassan et al. (1997), the unit side resistance of drilled shafts in cohesive IGM is given by:

$$q_s = \alpha\, \phi\, q_u \quad (2.25)$$

where,

α = Empirical factor determined from Figure 2.3
q_u = Uniaxial compressive strength of intact rock (ksf)
ϕ = Correction factor to account for the degree of jointing (see Table 2.5)

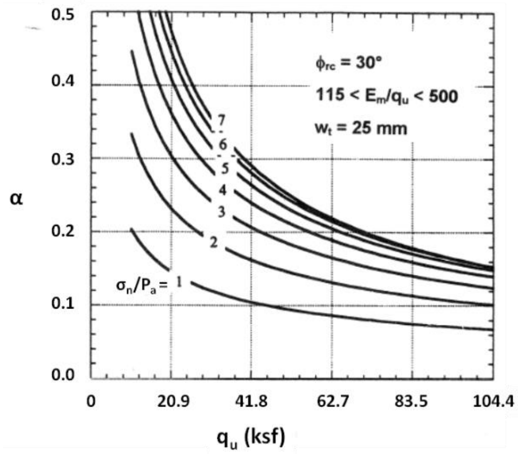

Adapted from O'Neill et al. 1996

Figure 2.3. Factor α for cohesive IGM

Table 2.5. Side resistance reduction factor for cohesive IGM

Rock Quality Designation, RQD (%)	Joint reduction factor, ϕ Closed joints	Joint reduction factor, ϕ Open or Gouge-filled joints
100	1.00	0.85
70	0.85	0.55
50	0.60	0.55
30	0.50	0.50
20	0.45	0.45

The method was developed assuming an interface friction angle (ϕ_{rc}) of 30°, a ratio of modulus of rock mass (E_m) to q_u between 115 and 500, and a total vertical displacement required to mobilize the full side resistance of 1 in. If the interface friction angle differs from the assumed value, then α can be adjusted using the following expression:

$$\alpha = \alpha_{\text{Figure 2.3}} \frac{\tan \phi_{rc}}{\tan 30^{\circ}} \tag{2.26}$$

The magnitude of α depends also on the pressure exerted by the freshly placed concrete. Assuming a minimum concrete slump of 7 in. and a placement rate of 40 ft per hour or greater, the concrete pressure, σ_n, at a given depth, z_i^*, below the cut-off elevation is given by:

$$\sigma_n = 0.65 \gamma_c z_i^* \tag{2.27}$$

where,

γ_c = Concrete unit weight (kcf)

z_i^* = Depth below the selected cutoff elevation to the middle of a material layer i, which is limited to 40 ft

The φ parameter accounts for the effect of joints on the unit skin resistance of cohesive IGMs. This effect can be estimated from Table 2.5 based on the Rock Quality Designation (RQD) and the joint characteristics (i.e., either closed joints or open/gouge-filled joints). No recommendations are made for RQD values less than 20%, and load tests are recommended to determine the side resistance in these circumstances.

Cohesionless Intermediate Geomaterials

O'Neill and Reese (1999) described cohesionless intermediate geomaterials as very dense granular tills or granular residual materials with SPT N_{60} value ranging between 50 and 100 blows per foot. As previously recommended by the 1999 FHWA drilled shaft manual, unit side resistance in cohesionless IGMs was estimated using the rational β method expressed by:

$$q_s = K_0 \tan(\phi') \ \sigma'_v \tag{2.28}$$

In current practice, this design method is recommended for both cohesionless soils and IGMs.

2.3.2.4. Rock

For drilled shaft design purposes, rock are geomaterials such as shales, sandstone, limestone, and mudstone with uniaxial compressive strength greater than 100 ksf or SPT blow count larger than 100. The unit side resistance of drilled shafts in rock can be evaluated based on the compressive strength of the rock as:

$$q_s = C \times p_a \sqrt{\frac{q_u}{p_a}} \tag{2.29}$$

where,
q_u = Mean uniaxial compressive strength for the rock layer in ksf
p_a = Atmospheric pressure (2.12 ksf)
C = Regression coefficient based on load test results

The value of q_u should be limited to the 28-day compressive strength of the drilled shaft concrete(f'_c). Different values of C have been proposed by various studies including but not limited to those of Horvath and Kenney (1979), Rowe and Armitage (1987), and Kulhawy and Phoon (1993). Based on their analyses, Horvath and Kenney (1979) recommended a value of 0.65, which was adopted by O'Neill and Reese (1999) and previous versions of AASHTO LRFD specifications. An empirical reduction factor, α_E, was added by O'Neill and Reese (1999) to account for the degree of jointing in the rock resulting in the following expression:

$$q_s = 0.65\alpha_E P_a \sqrt{\frac{q_u}{P_a}} \tag{2.30}$$

The reduction factor, α_E, is a function of the ratio of the rock mass modulus to intact rock modulus (E_m/E_i), which depends on the RQD, and it can be estimated from Table 2.6 and Table 2.7.

Table 2.6. Estimation of α_E

E_m/E_i	α_E
1.0	1.0
0.5	0.8
0.3	0.7
0.1	0.55
0.05	0.45

Source: Adapted from O'Neill and Reese 1999

Table 2.7. Estimation of E_m based on RQD

RQD (%)	E_m/E_i	
	Closed joints	Open joints
100	1.00	0.60
70	0.70	0.10
50	0.15	0.10
20	0.05	0.05

Source: Adapted from O'Neill and Reese 1999

$$q_s = 1.0\ P_a\sqrt{\frac{q_u}{P_a}} \tag{2.31}$$

Most recent studies by Kulhawy et al. (2005) suggest that, as shown in equation (2.31), a regression coefficient, C, of 1.0 is appropriate for the design of "normal" rock sockets that are not prone to smearing during drilling and that can be constructed without support, or special equipment or procedures. The reduction factor, αE, is only recommended where artificial support such as casing would be required during construction of the rock socket.

A significant increase of the drilled shaft side resistance can be achieved by artificial roughening of the rock socket using grooving tools. In this case, the unit side resistance can be estimated using the following expression proposed by Horvath et al. (1983):

$$q_s = 0.80\left[\frac{\Delta r}{r}\left(\frac{L'}{L}\right)\right]^{0.45} q_u \tag{2.32}$$

where,

q_u = Uniaxial compressive strength of rock (ksf)
Δr = Height of asperities or grooves in rock sidewall (ft)
r = Radius of drilled shaft (ft)
L' = Distance along surface of rock socket (ft)

L = Depth of rock socket (ft)

The geometric terms in equation (2.32) are illustrated in Figure 2.4. An accurate geometry of the socket must therefore be known for proper use of equation (2.32).

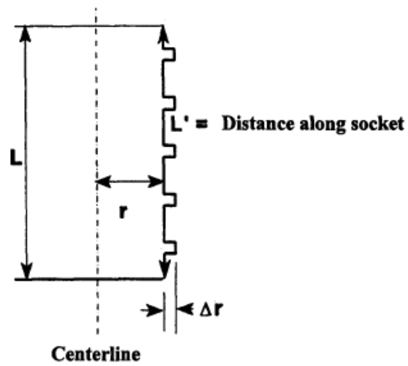

Adapted from O'Neill and Reese 1999

Figure 2.4. Definition of geometric terms in equation (2.32)

2.3.3. End Resistance Prediction Methods

2.3.3.1. Cohesive Soils

End bearing of drilled shafts in cohesive soils is determined from bearing capacity theory in terms of total stress analysis as:

$$q_p = N_c S_u \leq 80.0 \text{ ksf} \tag{2.33}$$

where,
N_c = Bearing capacity factor
S_u = Mean undrained shear strength of the cohesive soil over a depth of 2B below base

If the rigidity index of the soil is known, then N_c can be calculated as:

$$N_c = 1.33(\ln I_r + 1) \tag{2.34}$$

where,
I_r = Rigidity index = $\frac{E_s}{3S_u}$
E_s = Young's modulus
S_u = Undrained shear strength

If the rigidity index cannot be estimated, N_c can be determined as a function of the undrained shear strength as shown in Table 2.8.

Table 2.8. Bearing capacity factor

Undrained shear strength, S_u (ksf)	Rigidity index, $I_r = E_s/3S_u$	Bearing capacity factor, N_c
0.5	50	6.5
1	150	8.0
2	250–300	9.0

For cases where the shaft embedment length is at least three times the shaft diameter and the average shear strength is greater or equal to 2 ksf, N_c can be taken as 9.0. For embedment depth smaller than three times the shaft diameter, a reduction factor applies to the bearing capacity factor and the end bearing is calculated as:

$$q_p = \frac{2}{3}\left[1 + \frac{1}{6}\left(\frac{Z}{B}\right)\right] N_c S_u \qquad (2.35)$$

where,
Z = Embedded depth of shaft in cohesive soil (ft)
B = Diameter of drilled shaft (ft)

2.3.3.2. Cohesionless Soils

Due to soil disturbance resulting from the construction process, end resistance in cohesionless soils cannot be reliably determined from bearing capacity theory. Rather, direct empirical correlations developed from actual load tests data are relied upon to estimate drilled shaft base resistance. For routine design, the end resistance in cohesionless soils can be estimated using the following correlation proposed by Reese and O'Neill (1989):

$$q_p = 1.2\ N_{60} \leq 60 \text{ ksf} \qquad (2.36)$$

where N_{60} = Average SPT blow count between the base and two diameters below the base

The end resistance calculated using equation (2.36) is limited to a maximum value of 60 ksf based on the largest value observed in the load tests database used to develop the correlation. Equation (2.36) is not applicable to situations where the average SPT value exceeds 50. Load testing is recommended in this case. Otherwise, the upper bound value of 60 ksf can be used for design.

2.3.3.3. Cohesive Intermediate Geomaterials and Rock

End resistance in cohesive IGM and rock is affected by a variety of rock mass conditions such as rock mass strength, discontinuities, as well as the spacing, condition, and orientation of the discontinuities. Depending on these conditions, rock mass can be classified as intact or massive, jointed, layered, or fractured. Consequently, end bearing capacity may be controlled by various failure modes as illustrated in Table 2.9.

Table 2.9. Bearing capacity failure modes in rock

Rock mass condition			Failure	
Type	**Joint dip angle from horizontal**	**Joint spacing**	**Illustration**	**Mode**
INTACT/MASSIVE	N/A	S >> B	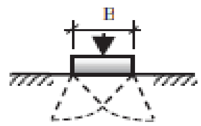	(a) Brittle rock: Local shear failure caused by localized brittle fracture
			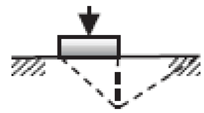	(b) Ductile rock: General shear failure along well-defined shear surface
STEEPLY DIPPING JOINTS	70° < α < 90°	S < B	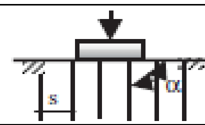	(c) Open joints: Compression failure of individual rock columns
			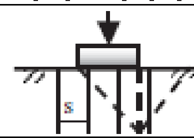	(d) Closed joints: General shear failure along well defined failure surfaces; near vertical joints
		S > B	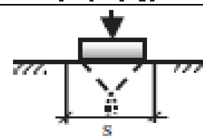	(e) Open or closed joints: Failure initiated by splitting leading to general shear failure; near vertical joints
JOINTED	20° < α < 70°	S < B or S > B if failure wedge can develop along joints	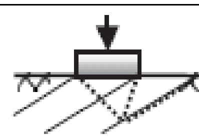	(f) General shear failure with potential for failure along joints; moderately dipping joint sets
LAYERED	0° < α < 20°	Limiting value of H with respect to B is dependent upon material properties	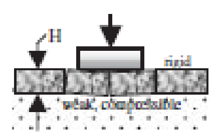	(g) Rigid layer over weak compressible layer: Failure is initiated by tensile failure caused by flexure of rigid upper layer
			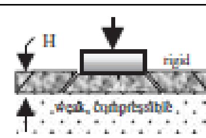	(h) Thin rigid layer over weak compressible layer: Failure is by punching shear through upper layer
FRACTURED	N/A	S << B	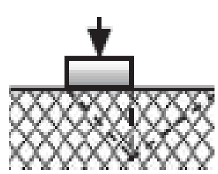	(i) General shear failure with irregular failure surface through fractured rock mass; two or more closely spaced joint sets

Source: U.S. Army Corps of Engineers 1994

Various expressions have been developed to predict end resistance for various rock mass conditions. However, some of these correlations require information related to rock conditions that is usually not available in routine drilled shaft design. When the available parameters are limited to the unconfined compressive strength (q_u) of the intact rock and the RQD, unit end resistance in rock or IGM can be expressed as:

$$q_p = N_{cr}^{*} q_u \tag{2.37}$$

where N_{cr}^{*} is an empirical bearing capacity factor.

The value of N_{cr}^{*} is a function of the rock mass condition below the shaft base. Based on the work of Rowe and Armitage (1987), a N_{cr}^{*} value of 2.5 can be used for intact rock when the following criteria are satisfied:

- The rock from the shaft base to a depth of two times the shaft diameter is either intact or tightly jointed with visible joint spacing much greater than the shaft diameter
- The depth of the rock socket is greater than one and one-half diameters
- Solution cavities or voids are not present below the shaft base
- The shaft base can be adequately cleaned using conventional clean-out equipment

For routine design, the rock can be considered to be intact when RQD is equal to 100%. When the RQD is between 70% and 100% and the joints are closed and approximately horizontal, O'Neill and Reese (1999) proposed the following expression for end resistance:

$$q_p(\mathrm{MPa}) = 4.83[q_u(\mathrm{MPa})]^{0.51} \tag{2.38}$$

When the joint spacing and condition below the shaft base can be characterized, the unit end resistance for rock mass with steeply dipping open joints and joint spacing smaller than the shaft diameter proposed by Sowers (1976) can be expressed as:

$$q_p = q_u \tag{2.39}$$

When the joint spacing is greater than 1 ft and the aperture of the discontinuity is as large as 0.25 in., the Canadian Geotechnical Society (1985) illustrated by equation (2.40) can be used.

$$q_p = 3 q_u K_{sp} d \tag{2.40}$$

where,

$$K_{sp} = \frac{3+\frac{s_v}{B}}{10\sqrt{1+300\frac{t_d}{s_v}}}$$

$$d = 1 + 0.4\frac{D_s}{B} \leq 3.4$$

s_v = Vertical spacing between discontinuities
t_d = Aperture (thickness) of discontinuities
B = Socket diameter
D_s = Socket embedment depth

For fractured rock mass where the joint spacing is significantly smaller than the shaft diameter, Carter and Kulhawy (1988), based on Hoek-Brown (1988) strength criterion, suggested that end resistance can be expressed as:

$$q_p = \left[\sqrt{s} + \sqrt{\left(m\sqrt{s} + s\right)}\right] q_u \tag{2.41}$$

where, s and m are the fractured rock mass parameters.

The s and m parameters are presented in Table 2.10, and they are function of the rock type as well as the rock mass rating (RMR).

Table 2.10. Approximate relationship between rock-mass quality and fractured rock-mass parameters used in defining nonlinear strength

		Rock type				
Rock quality	**Parameters**	**A**	**B**	**C**	**D**	**E**
Intact Rock Samples Laboratory size specimens free from discontinuities. RMR = 100	m s	7.00 1.00	10.00 1.00	15.00 1.00	17.00 1.00	25.00 1.00
Very Good Quality Rock Mass Tightly interlocking undisturbed rock with unweathered joint at 3 to 10 ft. RMR = 85	m s	2.40 0.082	3.43 0.082	5.14 0.082	5.82 0.082	8.567 0.082
Good Quality Rock Mass Fresh to slightly weathered rock, slightly disturbed with joints at 3 to 10 ft. RMR = 65	m s	0.575 0.00293	0.821 0.00293	1.231 0.00293	1.395 0.00293	2.052 0.00293
Fair Quality Rock Mass Several sets of moderately weathered joints spaced at 1 to 3 ft. RMR = 44	m s	0.128 0.00009	0.183 0.00009	0.275 0.00009	0.311 0.00009	0.458 0.00009
Poor Quality Rock Mass Numerous weathered joints at 2 to 12 in.; some gouge. Clean compacted waste rock. RMR = 23	m s	0.029 3×10^{-6}	0.041 3×10^{-6}	0.061 3×10^{-6}	0.069 3×10^{-6}	0.102 3×10^{-6}
Very Poor Quality Rock Mass Numerous heavily weathered joints spaced < 2 in. with gouge. Waste rock with fines. RMR = 3	m s	0.007 1×10^{-7}	0.010 1×10^{-7}	0.015 1×10^{-7}	0.017 1×10^{-7}	0.025 1×10^{-7}

RMR = rock mass rating; m and s = constants dependent on rock mass characteristics
A = Carbonate rocks with well-developed crystal cleavage: dolomite, limestone, and marble
B = Lithified argrillaceous rocks: mudstone, siltstone, shale, and slate (normal to cleavage)
C = Arenaceous rocks with strong crystals and poorly developed crystal cleavage: sandstone and quartzite
D = Fine grained polyminerallic igneous crystalline rocks: andesite, dolerite, diabase, and rhyolite
E = Coarse grained polyminerallic igneous and metamorphic crystalline rocks: amphibolite, gabbro gneiss, granite, norite, and quartz-diorite

Source: Hoek and Brown 1988

Although several methods are available in the literature to estimate end bearing in cohesive IGM and rock, their application in practice is generally difficult due to the lack of adequate information on the rock mass characteristics. End bearing determined from any of the methods previously discussed shall be limited to the compressive strength of a short reinforced concrete drilled shaft given by:

$$R_p \leq R_{sp} = \beta\left[0.85 f'_c\left(A_g - A_s\right) + A_s f_y\right] \tag{2.42}$$

where,

β = Reduction factor, 0.85 for spiral reinforcement and 0.80 for tie reinforcement
f'_c = Specified minimum 28-day compressive strength of concrete
A_g = Gross area of drilled shaft section
A_s = Total area of longitudinal steel reinforcement
f_y = Specified yield strength of steel reinforcement

Additional details related to the structural design of drilled shafts can be found in Brown et al. (2010).

As illustrated in Table 2.11, the RMR is influenced by five parameters including the strength of intact rock, RQD, joint spacing, joint condition, and groundwater conditions. The RMR is determined as the sum of the relative rating associated with each parameter.

Table 2.11. Geomechanics classification of rock masses

<table>
<tr><th colspan="3">Parameter</th><th colspan="7">Ranges of values</th></tr>
<tr><td rowspan="3">1</td><td rowspan="2">Strength of intact rock material</td><td>Point load strength index</td><td>> 175 ksf</td><td>85–175 ksf</td><td>45–85 ksf</td><td>20–45 ksf</td><td colspan="3">For this low range, uniaxial compressive test is preferred</td></tr>
<tr><td>Uniaxial compressive strength, q_u</td><td>> 4,320 ksf</td><td>2,160–4,320 ksf</td><td>1,080–2,160 ksf</td><td>520–1,080 ksf</td><td>215–520 ksf</td><td>70–215 ksf</td><td>20–70 ksf</td></tr>
<tr><td colspan="2">Relative rating</td><td>15</td><td>12</td><td>7</td><td>4</td><td>2</td><td>1</td><td>0</td></tr>
<tr><td rowspan="2">2</td><td colspan="2">Drill core quality RQD</td><td>90% to 100%</td><td colspan="2">75% to 90%</td><td colspan="2">50% to 75%</td><td colspan="2">25% to 50%</td><td>< 25%</td></tr>
<tr><td colspan="2">Relative rating</td><td>20</td><td colspan="2">17</td><td colspan="2">13</td><td colspan="2">8</td><td>3</td></tr>
<tr><td rowspan="2">3</td><td colspan="2">Spacing of joints</td><td>> 10 ft</td><td colspan="2">3–10 ft</td><td colspan="2">1–3 ft</td><td colspan="2">2 in.–1 ft</td><td>< 2 in.</td></tr>
<tr><td colspan="2">Relative rating</td><td>30</td><td colspan="2">25</td><td colspan="2">20</td><td colspan="2">10</td><td>5</td></tr>
<tr><td rowspan="2">4</td><td colspan="2">Condition of joints</td><td>• Very rough surface
• Not continuous
• No separation
• Hard joint wall rock</td><td colspan="2">• Slightly rough surfaces
• Separation < 0.05 in.
• Hard joint wall rock</td><td colspan="2">• Slightly rough surface
• Separation < 0.05 in.
• Soft joint wall rock</td><td colspan="2">• Slicken-sided surface or
• Gouge < 0.2 in thick or
• Joints open 0.05–0.2 in.
• Continuous joints</td><td>• Soft gouge > 0.2 in. thick or
• Joints open > 0.2 in.
• Continuous joints</td></tr>
<tr><td colspan="2">Relative rating</td><td>25</td><td colspan="2">20</td><td colspan="2">12</td><td colspan="2">6</td><td>0</td></tr>
<tr><td rowspan="4">5</td><td rowspan="3">Ground water conditions (use one of the three) evaluation criteria as appropriate to the method of exploration</td><td>Inflow per 30 ft tunnel length</td><td>None</td><td colspan="2">< 400 gal./hr</td><td colspan="2">400–2,000 gal./hr</td><td colspan="3">> 2,000 gal./hr</td></tr>
<tr><td>Ratio = joint water pressure/ major principal stress</td><td>0</td><td colspan="2">0.0–0.2</td><td colspan="2">0.2–0.5</td><td colspan="3">> 0.5</td></tr>
<tr><td>General conditions</td><td>Completely dry</td><td colspan="2">Moist only (interstitial water)</td><td colspan="2">Water under moderate pressure</td><td colspan="3">Severe water problems</td></tr>
<tr><td colspan="2">Relative rating</td><td>10</td><td colspan="2">7</td><td colspan="2">4</td><td colspan="3">0</td></tr>
</table>

Source: Bieniawski 1984 from AASHTO 2012

2.4. Drilled Shaft Construction Methods

Drilled shafts can be constructed using one or a combination of three methods including the dry method, the casing method, and the wet method. The selection of the most suitable method for a given project is dictated by subsurface conditions, local construction practices, and experience. A summary of the construction methods is presented in Table 2.12.

Table 2.12. Drilled shafts construction methods

Construction method	Subsurface conditions	General remarks
Dry method	Strong cohesive soil with low permeability, IGM, or rock with no presence of groundwater or above water table; minimal water seepage	Least expensive and allow visual inspection
Casing method	Caving geomaterials; below or above water table	Three construction sequences; permanent or temporary casing; expensive
Wet method	Soil with high permeability and seepage; boreholes with water; high water table	Moderately expensive

The dry method is suitable for strong cohesive geomaterials that are not prone to caving during excavation. It is the least expensive of the three methods, and it allows visual inspection of the borehole to assure its quality. The wet method is moderately expensive, and it is ideal to subsurface conditions with highly permeable soils and significant seepage. Temporary or permanent casing is required for excavation in unstable geomaterials, below or above the water table. Brown et al. (2010) and Ng et al. (2014) provide additional details on these methods.

2.5. Field Loading Tests

Although numerous correlations of drilled shaft resistance to geomaterial properties have been developed from various research studies, field load tests are still relied upon to verify the estimated capacity and ensure satisfactory performance. This is due to the fact that these methods are often developed from a database of load tests from several regions with different soil conditions and construction practices. Consequently, accurate drilled shaft resistance prediction from these methods is a difficult task. Field load testing at the actual site provides a direct measure of drilled shaft performance; thus, it is more reliable. It not only assures that the drilled shaft meets the design requirements but also provides details, given adequate instrumentation, on the load transfer characteristics of the various soil layers around and beneath the shaft. The latter data is crucial for research purposes such as the development of local design methods or the calibration of regional resistance factors. The number and location of load tests depends on several factors including the variability of the subsurface geology, the objectives of test programs, the characteristics of the supporting structures, the spatial variability of the geomaterial properties, and the type of construction procedures. Drilled shaft field load testing can be accomplished using either top-down static load test, Osterberg cell (O-cell) load test, statnamic load test, or high-strain dynamic load test. The advantages and limitations associated with each method are shown in Table 2.13.

Table 2.13. Advantages and limitations of drilled shaft field load test methods

Testing method	Advantages	Limitations
Top down static load test	• Apply testing load on top of drilled shafts	• Time consuming • Increasing cost as the drilled shaft capacity gets larger
O-cell load test	• Ability to test high capacity production or test drilled shafts • Ability to test at select segments of a drilled shaft • Allows investigation of creep effects	• Pre-arrangement of test setup is required • Does not allow testing on existing drilled shafts • The accuracy of the equivalent top load-displacement response may depend on the data interpretation • Discrepancy in skin resistance associated with upward loading vs. downward loading is not completely known, but treated with adjustment factors • High cost
Statnamic load test	• Ability to test both production and test shafts with relatively high capacity • Apply testing load on top of drilled shafts • Economies of scale for multiple tests • Does not require reaction system	• Duration and cost of mobilization • Test load limit 5,000 tons • The rate of loading must be considered in the resistance estimation
High strain dynamic load test	• Ability to apply relatively large load on production or test drilled shafts • Relatively cheap • Test can be performed with minimal setup • Does not require reaction system	• Limited testing capacity • Control and Provisioning of Wireless Access Points (CAPWAP) protocol analysis produces non-unique resistances • Damage of shaft top • Estimation is highly dependent on soil damping and elastic characteristics • Requires shaft structural properties and surrounding soil parameters in the analysis

Additional details regarding the principles and application of these methods can be found in Brown et al. (2010) and Ng et al. (2014).

2.6. AASHTO Drilled Shafts LRFD Specifications

Specifications for the design of drilled shafts at Strength I limit state in accordance with LRFD are recommended by AASHTO based on the work of Brown et al. (2010) as well as Allen (2005). Slight changes were made to these specifications to reflect a departure from O'Neill and Reese (1999) design methods, which served as the basis for previous editions of AASHTO. Current recommended design methods and their corresponding resistance factors are presented in Table 2.14.

Table 2.14. Latest AASHTO drilled shaft resistance factors for axial compression

	Method/Soil/Condition		Resistance factor
Nominal axial compressive resistance of single-drilled shafts, φ	Side resistance in clay	α-method Brown et al. 2010	0.45
	Tip resistance in clay	Total stress Brown et al. 2010	0.40
	Side resistance in sand	β-method Brown et al. 2010	0.55
	Tip resistance in sand	Brown et al. 2010	0.50
	Side resistance in cohesive IGM	Brown et al. 2010	0.60
	Tip resistance in cohesive IGM	Brown et al. 2010	0.55
	Side resistance in rock	Kulhawy et al. 2005, Brown et al. 2010	0.55
	Side resistance in rock	Carter and Kulhawy 1988	0.50
	Tip resistance in rock	Canadian Geotechnical Society 1985, pressuremeter method (Canadian Geotechnical Society 1985) Brown et al. 2010	0.50

With the exception of resistance factors for skin friction prediction in sand and rock, all other resistance factors remain unchanged from previous editions. Resistance factors for skin friction prediction in sand and rock were updated to reflect the transition of design methods from O'Neill and Reese (1999) to Brown et al. (2010). These resistance factors are recommended based on a calibration by fitting to current factors of safety until reliability analyses can be conducted for the new methods. A 20% reduction of the resistance factors is recommended when a single-drilled shaft is used to support a bridge pier. A resistance factor of 1.0 is recommended for serviceability limit state to ensure that the drilled shaft settlement does not exceed a tolerable value.

2.7. States' Regional LRFD Calibrations

Given the limitations associated with resistance factors recommended by AASHTO for drilled shaft design, local jurisdictions have, in recent years, dedicated significant efforts to research studies designed to develop and implement resistance factors that better (1) reflect local soil conditions and construction practices; (2) cover design methods other than those recommended by AASHTO; and (3) improve drilled shaft design efficiency, thereby reducing foundation cost.

2.7.1. Louisiana DOT

Citing the fact that AASHTO LRFD specifications were not specifically developed for any particular region and that their implementation in Louisiana or Mississippi could lead to a reduction in design efficiency and larger foundation sizes, a series of several calibration studies has been conducted in order to develop resistance factors consistent with the region's soil conditions and construction practices. The first calibration was conducted by Abu-Farsakh et al. (2010) considering a collection of 66 top down and O-cell load tests from Louisiana and Mississippi. Only 26 load tests were used in the actual calibration to maintain consistency in the soil conditions and to minimize excessive extrapolation of load test data when necessary. The majority of the load tests were conducted using the O-cell load testing method. The second calibration study, conducted by Abu-Farsakh et al. (2013), used an expanded database that included eight additional tests obtained from Louisiana DOT. All shafts were constructed and tested in soil types that included silty clay, clay, sand, clayey sand, and gravel. The shaft lengths range from 35.1 to 138.1 ft with diameters ranging from to 2 to 6 ft. The Monte Carlo simulation technique was implemented to evaluate skin friction and end bearing resistance factors associated with drilled shaft design methods recommended by O'Neill and Reese (1999) and Brown et al. (2010) for a settlement corresponding to 5% of the shaft diameter (AASHTO criterion) or the plunging load whichever occurred first. The exponential curve fitting method was selected to extrapolate a small number of drilled shafts that did not meet the 5% of the shaft diameter settlement criterion that was used in this study. Presented in Table 2.15 are the results from that calibration.

Table 2.15. Calibrated resistance factors

Design method	φ, side resistance	φ, tip resistance	φ, total resistance
O'Neill and Reese 1999	0.39	0.52	0.60
Brown et al. 2010	0.26	0.53	0.48

Source: Abu-Farsakh et al. 2013

On one hand, the regionally calibrated factors of 0.39 and 0.26 were far less than AASHTO recommended values of 0.45 for clay and 0.55 for sand or any average that would result from these two values. The calibrated values of 0.52 and 0.53 for tip resistance, on the other hand, showed some improvement compared to AASHTO values of 0.40 for clay and 0.50 for sand. If resistance factors for the combination of side and tip resistance are considered, the calibrated values either show some improvement or close agreement with AASHTO recommended values.

Following similar analysis procedures and using an updated database of 69 O-cell load tests, the latest calibration study was conducted by Fortier et al. (2016). In addition, to the Monte Carlo simulation technique, the FOSM reliability method was used to calibrate the resistance factors for comparison purposes. An additional strength criterion, i.e., 1 in. top displacement, was also considered. Table 2.16 illustrates the calibrated resistance factors obtained from the Monte Carlo simulation.

Table 2.16. Side and end bearing resistance factors

	1 in. criterion			AASHTO criterion		
Design method	**φ, side resistance**	**φ, tip resistance**	**φ, total resistance**	**φ, side resistance**	**φ, tip resistance**	**φ, total resistance**
O'Neill and Reese 1999	0.30	0.19	0.34	0.35	0.16	0.38
Brown et al. 2010	0.15	0.15	0.31	0.29	0.11	0.27

Source: Fortier et al. 2016

A direct comparison between the values shown in Table 2.15 and Table 2.16 shows that all resistance factors at the AASHTO criterion decreased significantly between the two calibration studies and compared to AASHTO. Another important observation in the two studies relates to the difference in the uncertainty involved with predicting the total resistance and the uncertainty associated with separate side and tip resistance prediction. From the higher resistance factors obtained for total resistance prediction compared to side and tip resistance in both studies, it is safe to conclude that the uncertainty in predicting the total resistance is less than that associated with predicting either side or tip.

Although these resistance factors might illustrate the true reliability associated with the design methods considered, their implementation would result in even larger foundations compared to AASHTO specifications, which are believed to be overly conservative in the first place. No discussion regarding this issue is offered in the study.

2.7.2. Kansas DOT

Calibration of resistance factors for drilled shafts in weak rocks in the state of Kansas was conducted by Yang et al. (2010). According to the study, the use of AASHTO LRFD specifications by Kansas DOT engineers led to designs that were often inconsistent with their past ASD practice. Thus, the calibration was justified by the need to develop regional factors that would resolve this issue and be reflective of the state's experience. To evaluate the uncertainty associated with the O'Neill and Reese (1999) design method for intermediate geomaterials (IGM), a database including 25 O-cell load tests collected from Kansas, Colorado, Missouri, Ohio, and Illinois was developed. Using the Monte Carlo simulation technique, resistance factors for skin friction and end bearing were calibrated at the AASHTO strength criterion and at a serviceability criterion corresponding to 0.25 in. Resistance factors associated with skin friction were calibrated following a total side resistance and layered unit side resistance approach. In addition to the target reliability of 3.0 commonly recommended for drilled shafts, the study also considered a target reliability of 2.3. Table 2.17 presents the resistance factors obtained from the calibration.

Table 2.17. Calibrated resistance factors modified

Situation			φ (β_t=3.0)	AASHTO φ (β_t=3.0)
Side resistance	Strength limit state	Total	0.50	0.60
		Layered	0.70	
	Service limit state	Total	0.35	1.00
		Layered	0.40	
Base resistance	Strength limit state		0.25	0.55
	Service limit state		0.15	1.00

Source: Yang et al. 2010

Considering the total side resistance approach, the calibrated factor of 0.50 represents a decrease from the AASHTO recommended value of 0.60. Following the layered side resistance approach, the regional resistance factor of 0.70 shows some improvement compared to AASHTO. This difference highlights the effect of the resistance bias calculation method on the calibrated resistance factor (uncertainty in total resistance prediction versus uncertainty in one or multiple layers of resistance prediction), which is not covered in the AASHTO LRFD calibration framework. For end bearing, the calibration did not result in any improvement.

2.7.3. Nevada DOT

In Nevada, Motamed et al. (2016) used a database of 41 load tests to calibrate resistance factors for axially loaded drilled shafts constructed in interbedded layers of silty clay and sand with seams of caliche. With the exception of one case, all load tests used in the calibration were O-cell load tests. The shafts' diameter ranged from 2 to 8 ft with lengths between 31.6 and 128 ft. Following the scoring system specifically developed for the study and illustrated in Table 2.18, the load tests were classified in three groups including (1) all data, (2) load tests with a mean score > 2, and (3) load tests with a mean score > 3.

Table 2.18. Load test quality scoring system

Score	Scoring criteria: Load test data	Scoring criteria: Geotechnical investigation data
1 (worst)	Extrapolation > 2% of the shaft diameter is required for both components of bi-directional movement or > 3% is required for a top-down test.	Incomplete boring logs with little to no SPT data or proper visual-manual classifications. No lab data.
2	Extrapolation > 2% of the shaft diameter is required for one component of bi-directional movement (second component may require < 2%) or > 2.5% but ≤ 3% is required for a top-down test.	Boring logs with minimal SPT data (i.e., missing for some geologic units) and useful visual-manual classifications. No lab data.
3	Extrapolation < 2% of the shaft diameter is required for both components of bi-directional movement or > 2% but ≤ 2.5% is required for a top-down test.	Boring logs are complete with SPT data, visual-manual classification and possibly torvane or pocket pen data. Limited lab data and/or additional in situ data is available.
4 (best)	Either no extrapolation is needed or extrapolation ≤ 2% of the shaft diameter is required for only one component of load-cell movement or in total for a top-down test.	Complete boring logs with detailed material classifications, SPT data, and possibly other data such as CPT or shear wave velocity measurements. Thorough lab data covering soil strengths is available.

Source: Motamed et al. 2016

As can be seen from the scoring system, load test quality ranges from 1 to 4 and is a function of the extent of available details on the site subsurface exploration as well as the amount of extrapolation of load test data necessary. Four design methods including M1, M2, M3, and M4 were investigated in the calibration. M1 treats caliche as very dense sand with unit weight of 140 pcf, effective friction angle of 40°, and SPT blow count of 50. M2 treats caliche as cohesive IGM with unconfined compressive strength of 100 ksf unless lower values are suggested from site-specific data. M3 treats caliche as rock with unconfined compressive strength of 729 ksf and RQD of 70% unless other values are suggested by site-specific data. M4 represents an approach proposed by the author based on the following assumptions:

- The skin friction is estimated using the following: $\frac{f_{SN}}{p_a} = 0.85\sqrt{\frac{q_u}{p_a}} \leq 15.8$
- Caliche layers with lack of information on their compressive strength are assigned a value of 729 ksf
- End bearing corresponds to the rock model or 100 ksf whichever is lower
- Strongly cemented materials with SPT blow count > 50 are assigned a skin friction of 6 ksf
- Treat moderately cemented materials with SPT blow count < 50 the same as the parent material.

Due to the inability to separate end bearing from skin friction based on the available data, the resistance factors were calibrated for total resistance only. The Monte Carlo simulation was implemented in two approaches, i.e., L1 and L2, to calibrate the resistance factors in this study. The resistance factors calibrated using L1 relate to the uncertainty of the overall resistance predicted using the best estimate of the geomaterial properties based on available data, while those calibrated from L2 approach capture the uncertainty associated directly with the testing method and interpretation used to determine the geomaterial properties. Following the general calibration procedure, resistance factors were calibrated at a target reliability of 3.0 for a strength criterion corresponding to shafts' settlement equal to 5% of the shaft diameter or plunging failure whichever occurred first. As illustrated in Table 2.19, the calibrated resistance factors ranged from 0.66 to 1.09 depending on the calibration level and the design method.

Table 2.19. Total resistance factors

Calibration level	Caliche model	ϕ at $\beta = 3$		
		All data	Mean score >2	Mean score > 3
L1	M1	1.05	0.78	0.79
	M2	0.81	0.85	0.85
	M3	0.90	0.91	0.91
	M4	0.73	0.77	0.72
L2	M1	1.09	0.86	1.02
	M2	0.84	0.87	0.76
	M3	0.90	0.91	0.77
	M4	0.71	0.74	0.66

Source: Motamed et al. 2016

The results also show that the influence of the data quality on the calibrated resistance factors was a function of the design method considered. For a given calibration level and design method, the lowest resistance factor was selected as the governing value.

2.7.4. New Mexico DOT

A database of 95 drilled shaft O-cell and top-down load tests collected from New Mexico and other states was developed by Ng and Fazia (2012) to assist in the calibration of resistance factor for skin friction in cohesionless soils. Among the available data, only 24 tests were selected for the calibration. It is important to also note that only five of the load tests considered were performed in New Mexico. The shafts' diameter ranged from 1.5 ft to 7 ft with lengths ranging from 24.3 ft to 134.5 ft. The study investigated the reliability of three methods for predicting skin friction in cohesionless soils: the O'Neill and Reese (1999) β-method, Brown et al. (2010) β-method, and Chua et al. (2000) unified design equation. The resistance bias corresponding to each method was calculated and statistically characterized. Assuming a lognormal or polynomial distribution for the resistance bias, the Monte Carlo simulation technique was used to calibrate the resistance factor associated with each design method for a reliability of 3.0. As seen from the results presented in Table 2.20, the use of a fitted polynomial regression model to characterize the resistance bias results in higher resistance factors compared to those obtained based on the assumption of a lognormal distribution. Nonetheless, all calibrated factors were lower than AASHTO recommended value of 0.55.

Table 2.20. Calibrated resistance factors

Design method	Lognormal	Polynomial
O'Neill and Reese 1999	0.32	0.45
Chua et al. 2000	0.26	0.49
Brown et al. 2010	0.37	0.47

Source: Ng and Fazia 2012

2.7.5. Iowa DOT

To overcome the deficiencies associated with code recommendations for LRFD of drilled shafts, a research plan composed of three phases was devised by researchers at Iowa State University. In Phase I of the project, an electronic database of load tests collected from Iowa and several neighboring states was developed by Garder et al. (2012). Available information on 32 drilled shaft load tests was collected, reviewed, and integrated into this Microsoft Access-based database for Drilled SHAft Foundation Testing (DHSAFT). The resulting database contained 29 O-cell load tests and 3 statnamic load tests. Preliminary reliability analyses were then performed on the 13 load tests from Iowa by Ng et al. (2012), and the calibrated resistance factor is presented in Table 2.21 along with those recommended by AASHTO.

Table 2.21. Summary of AASHTO and regionally calibrated resistance factors

<table>
<tr><th rowspan="2">Soil type</th><th rowspan="2">Shaft/Toe resistance</th><th colspan="2">Resistance factor (φ) for $\beta_T = 3.00$</th></tr>
<tr><th>AASHTO</th><th>DSHAFT</th></tr>
<tr><td rowspan="2">Clay</td><td>Shaft</td><td>0.45</td><td rowspan="8">0.66 (based on total resistance)</td></tr>
<tr><td>Toe</td><td>0.40</td></tr>
<tr><td rowspan="2">Sand</td><td>Shaft</td><td>0.55</td></tr>
<tr><td>Toe</td><td>0.50</td></tr>
<tr><td rowspan="2">Rock</td><td>Shaft</td><td>0.50–0.55</td></tr>
<tr><td>Toe</td><td>0.50</td></tr>
<tr><td rowspan="2">IGM</td><td>Shaft</td><td>0.60</td></tr>
<tr><td>Toe</td><td>0.55</td></tr>
</table>

Source: Ng et al. 2012

The calibrated resistance factor of 0.66 was higher than all values recommended by AASHTO. However, it should be noted that the resistance factor was calibrated based on a total resistance (skin friction + end bearing) scheme. Additionally, no distinction was made between geomaterial types; thus, the individual reliability associated with each design method is not reflected in the calibrated resistance factor. Even though the study focused on total resistance factor, results have shown that a calibration at the regional level can potentially improve resistance factors for the design of drilled shafts in axial compression, thus resulting in safer, more reliable, and cost-effective designs. To further investigate this potential during Phase II of the project, the database was expanded with nine additional O-cell load tests for another calibration. Because of missing key information such as boring logs and soil/rock strength parameters, 13 load tests could not be used in the statistical analyses. Additionally, the majority of the load tests in DSHAFT are terminated at relatively small shaft displacements or before full mobilization of the shaft resistance. Therefore, the ultimate resistance or the shaft resistance at the chosen failure criteria could not be determined from the LOADTEST, Inc. (2010) procedure for constructing the equivalent top load-displacement curve. To overcome this challenge, three different procedures for extrapolating the shaft top load-displacement curve were established by Ng. et al. (2014). These procedures were used to generate complete load-displacement curves that allowed resistance factors to be calibrated at specific shaft top displacements including 1 in. and 5% of the shaft diameter. Following the FOSM reliability method, resistance factors were determined for each geomaterial type and for individual resistance component, i.e., skin friction and end bearing.

Calibrated resistance factors for side resistance are presented in Table 2.22 along with those recommended by AASHTO, National Cooperative Highway Research Program (NCHRP), and National Highway Institute (NHI) reports. Resistance factors were calibrated at three strength criteria including load test criterion, Iowa DOT 1 in. top displacement, and AASHTO criterion corresponding to 5% of the shaft diameter.

Table 2.22. Comparison of resistance factors for skin friction

		Resistance factors for β_T = 3.00, φ						φ/λ
Geo material	**Failure criteria**	**NCHRP 343[e]**	**NCHRP 507[b]**	**NHI 05-052[a]**	**NHI 05-052[c]**	**AASHTO 2017[d]**	**DSHAFT**	**DSHAFT**
Clay	LTR	n/a	n/a	n/a	n/a	n/a	0.31	0.15
	1-in Δ	n/a	n/a	n/a	n/a	n/a	0.20	0.11
	5% D for Δ	0.65	0.36 (φ/λ: 0.41)	0.55	0.60	0.45	0.22	0.12
Sand	LTR	n/a	n/a	n/a	n/a	n/a	0.47	0.34
	1-in Δ	n/a	n/a	n/a	n/a	n/a	0.48	0.54
	5% D for Δ	n/a	0.31 (φ/λ: 0.28)	0.55	n/a	0.55	0.47	0.53
IGM	LTR	n/a	n/a	n/a	n/a	n/a	0.66	0.26
	1-in Δ	n/a	n/a	n/a	n/a	n/a	0.63	0.30
	5% D for Δ	n/a	0.51 (φ/λ: 0.41)	0.55	n/a	0.60	0.69	0.32
Rock	LTR	n/a	n/a	n/a	n/a	n/a	0.57	0.39
	1-in Δ	n/a	n/a	n/a	n/a	n/a	0.55	0.49
	5% D for Δ	0.65	0.38[f] (φ/λ: 0.32)	0.55	0.55	0.55	0.62	0.53

[a] calibration by fitting to ASD; [b] calibration performed using reliability theory (FORM); [c] calibration performed using reliability theory (Monte Carlo method); [d] selected value among NCHRP 343 (Barker et al. 1991), NCHRP 507 (Paikowsky et al. 2004), and Allen (2005); [e] recommended value; [f] based on Carter and Kulhawy (1988); LTR = load test report criterion; n/a = not available; Δ = shaft top displacement; D = shaft diameter

Source: Ng et al. 2014

Since resistance factors were only calibrated at the AASHTO criterion of 5% of the shaft diameter in other studies, direct comparison could only be made for this particular case. The calibrated resistance factor for side resistance in clay using the α-method was much lower compared to other recommended values regardless of the failure criterion. At the AASHTO failure criterion, the calibration resulted in a 51% decrease compared to AASHTO value. Calibrated factors for side resistance in sand using the β-method were also lower. Compared to AASHTO, a 17% decrease resulted from the calibration. For side resistance in IGM using the modified α-method, the calibration resulted in higher resistance factors compared to other recommended values. The resistance factor was increased by 13% compared to AASHTO. Regional resistance factor for side resistance in rock was calibrated for the Horvath and Kenney (1979) method. The calibrated factor of 0.62 was higher than the AASHTO recommended value of 0.55, which is based on a calibration by fitting to ASD factor of safety. The efficiency value of 0.53 shows that the Horvath and Kenney (1979) method would result in a more economical design compared to the Carter and Kulhawy (1988) method used in NCHRP 507 (Paikowsky et al. 2004). Because of insufficient data, resistance factor could not be calibrated for end bearing in clay. For end bearing in sand, the calibration resulted in a resistance factor of 0.75, which shows an improvement to the value of 0.50 recommended by AASHTO. The efficiency of 0.44 was also higher than the maximum value of 0.32 achieved in NCHRP 507 (Paikowsky et al. 2004). The resistance factors for end bearing in IGM and rock are presented in Table 2.23 and Table 2.24, respectively.

Table 2.23. Comparison of resistance factors of end bearing in IGM

Failure criteria	Analytical method	Resistance factors for β_T = 3.00, φ				φ/λ
		NCHRP 507[(a)]	NHI 05-052[(b)]	AASHTO 2017[(c)]	DSHAFT	DSHAFT
LTR	Rowe and Armitage 1987	n/a	n/a	n/a	0.32	0.29
	Goodman 1980	n/a	n/a	n/a	1.27	0.28
	Terzaghi 1943	n/a	n/a	n/a	0.29	0.26
	Carter and Kulhawy 1988	n/a	n/a	n/a	1.46	0.17
	Sowers 1979	n/a	n/a	n/a	0.67	0.24
	O'Neill and Reese 1999	n/a	n/a	n/a	0.15	0.18
	Proposed method	n/a	n/a	n/a	0.59	0.47
1 in. Δ	Rowe and Armitage 1987	n/a	n/a	n/a	0.32	0.33
	Goodman 1980	n/a	n/a	n/a	1.41	0.35
	Terzaghi 1943	n/a	n/a	n/a	0.24	0.23
	Carter and Kulhawy 1988	n/a	n/a	n/a	1.71	0.22
	Sowers 1979	n/a	n/a	n/a	0.64	0.27
	O'Neill and Reese 1999	n/a	n/a	n/a	0.17	0.22
	Proposed method	n/a	n/a	n/a	0.64	0.58
5% D for Δ	Rowe and Armitage 1987	n/a	n/a	n/a	0.44	0.36
	Goodman 1980	n/a	n/a	n/a	1.86	0.36
	Terzaghi 1943	n/a	n/a	n/a	0.49	0.39
	Carter and Kulhawy 1988	n/a	n/a	n/a	3.04	0.30
	Sowers 1979	n/a	n/a	n/a	1.06	0.33
	O'Neill and Reese 1999	0.57 to 0.65 (φ/λ: 0.44 to 0.48)	0.55	0.55	0.20	0.21
	Proposed method	n/a	n/a	n/a	0.85	0.62

[(a)] calibration performed using reliability theory (FORM); [(b)] calibration by fitting to ASD; [(c)] selected value among NCHRP 343 (Barker et al. 1991), NCHRP 507 (Paikowsky et al. 2004), and Allen (2005); LTR = load test report criterion; n/a = not available; Δ = shaft top displacement; D = shaft diameter

Table 2.24. Comparison of resistance factors of end bearing in rock

Failure criteria	Analytical method	Resistance factors for $\beta_T = 3.00$, φ NCHRP 507[a]	NHI 05-052[b]	AASHTO 2017[c]	DSHAFT	φ/λ DSHAFT
LTR	Rowe and Armitage 1987	n/a	n/a	n/a	0.11	0.38
	Goodman 1980	n/a	n/a	n/a	0.28	0.24
	Terzaghi 1943	n/a	n/a	n/a	0.15	0.18
	Carter and Kulhawy 1988	n/a	n/a	n/a	0.19	0.04
	Sowers 1979	n/a	n/a	n/a	0.28	0.38
	O'Neill and Reese 1999	n/a	n/a	n/a	0.25	0.39
	Proposed method	n/a	n/a	n/a	0.11	0.18
1 in. Δ	Rowe and Armitage 1987	n/a	n/a	n/a	0.10	0.30
	Goodman 1980	n/a	n/a	n/a	0.30	0.22
	Terzaghi 1943	n/a	n/a	n/a	0.13	0.13
	Carter and Kulhawy 1988	n/a	n/a	n/a	0.22	0.04
	Sowers 1979	n/a	n/a	n/a	0.26	0.30
	O'Neill and Reese 1999	n/a	n/a	n/a	0.22	0.29
	Proposed method	n/a	n/a	n/a	0.36	0.41
5% D for Δ	Rowe and Armitage 1987	n/a			0.16	0.38
	Goodman 1980	n/a			0.42	0.25
	Terzaghi 1943	n/a			0.22	0.19
	Carter and Kulhawy 1988	0.45 to 0.49 (φ/λ: 0.37 to 0.38)	0.55[d]	0.50[d]	0.31	0.04
	Sowers 1979	n/a			0.40	0.38
	O'Neill and Reese 1999	n/a			0.35	0.40
	Proposed method	n/a			0.71	0.68

[a] calibration performed using reliability theory (FORM); [b] calibration by fitting to ASD; [c] selected value among NCHRP 343 (Barker et al. 1991), NCHRP 507 (Paikowsky et al. 2004), and Allen (2005); [d] based on Canadian Geotechnical Society (1985); LTR = load test report criterion; n/a = not available; Δ = shaft top displacement; D = shaft diameter

Resistance factors were calibrated for various design methods. In the case of IGM, the calibration resulted in unrealistic resistance factors for the Goodman (1980), Carter and Kulhawy (1988), and Sowers (1976) design methods. Because these methods consistently underestimated the actual measured resistance, their corresponding resistance factors were greater than unity. For the O'Neill and Reese (1999) method, the calibrated resistance factor of 0.20 and corresponding efficiency of 0.21 were much lower than the values recommended by NCHRP 507 (Paikowsky et al. 2004) and AASHTO. The proposed method developed by Ng et al. (2014), which is an average of Rowe and Armitage (1987) and Carter and Kulhawy (1988), was the most efficient design method with a calibrated resistance factor of 0.85 and efficiency of 0.62 at the AASHTO failure criterion.

For end bearing in rock, comparison could only be made for the Carter and Kulhawy (1988) design method. The calibrated resistance factor of 0.31 and corresponding efficiency of 0.31

were lower than other recommended values. Similar to end bearing in IGM, the proposed method (Ng et al. 2014) was the most efficient design method with a resistance factor of 0.71 and an efficiency of 0.68.

CHAPTER 3. EXAMINATION AND ANALYSIS OF DSHAFT DATA

3.1. DSHAFT Database

The initial version of the database was developed by Garder et al. (2012) using Microsoft Access to provide efficient and easy access to original field records in an electronic format. At the time of the preliminary regional calibration, the database included a total of 41 load tests from Iowa and 10 other states. Out of the available load tests in the database, only 28 were deemed to have the required structural, subsurface, testing, and construction details for the calibration study. Since the preliminary calibration, eight additional load tests were performed in Iowa and have been included in DSHAFT. The distribution of the of the load tests currently available in the database according to state distribution, construction methods, testing methods, geomaterial type at the shaft bases, and geomaterial along the shafts is presented in Figure 3.1, Figure 3.2, Figure 3.3, Figure 3.4, and Figure 3.5, respectively.

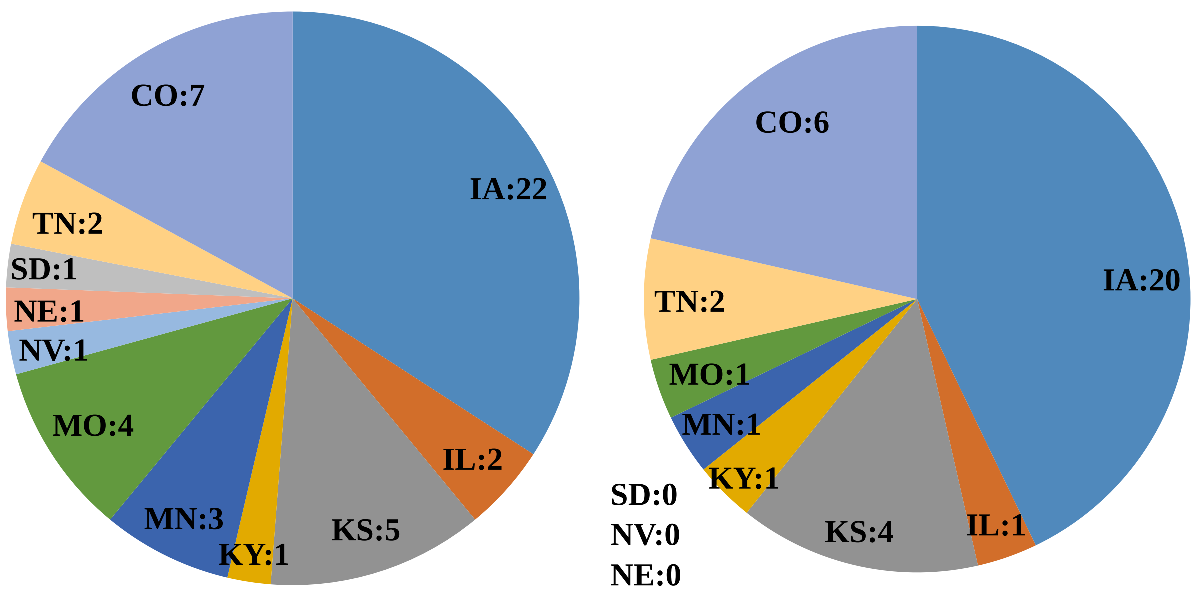

Figure 3.1. Distribution of drilled shaft load tests contained in DSHAFT by state: available data (left) and usable data (right)

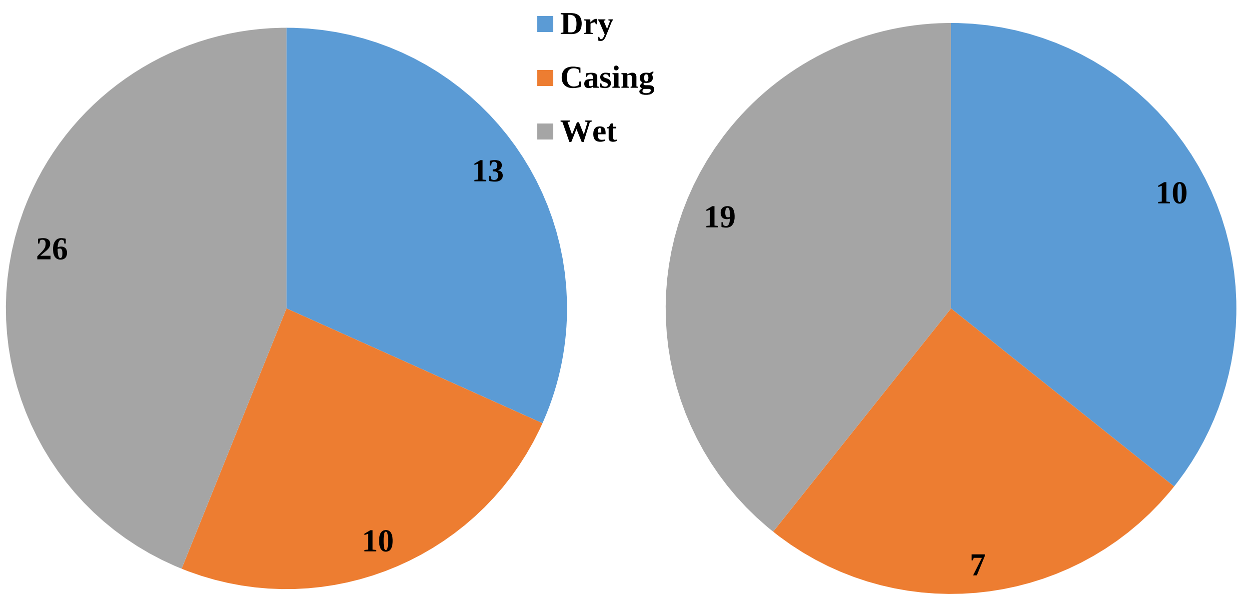

Figure 3.2. Distribution of drilled shaft load tests contained in DSHAFT by construction method: available data (left) and usable data (right)

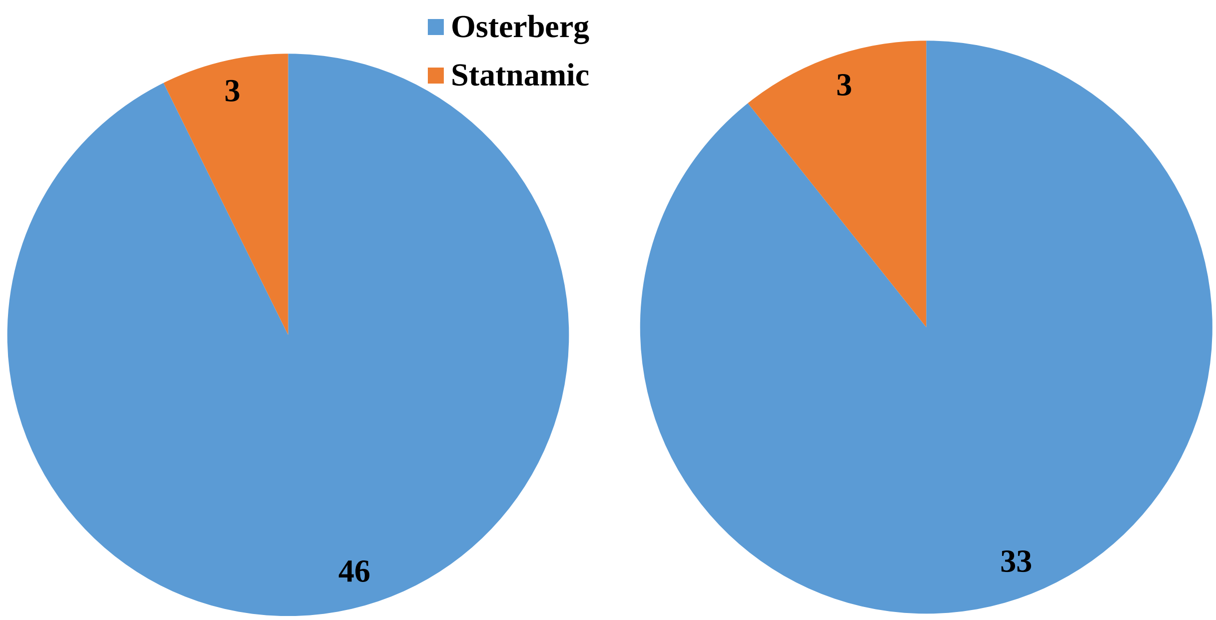

Figure 3.3. Distribution of drilled shaft load tests contained in DSHAFT by testing methods available data (left) and usable data (right)

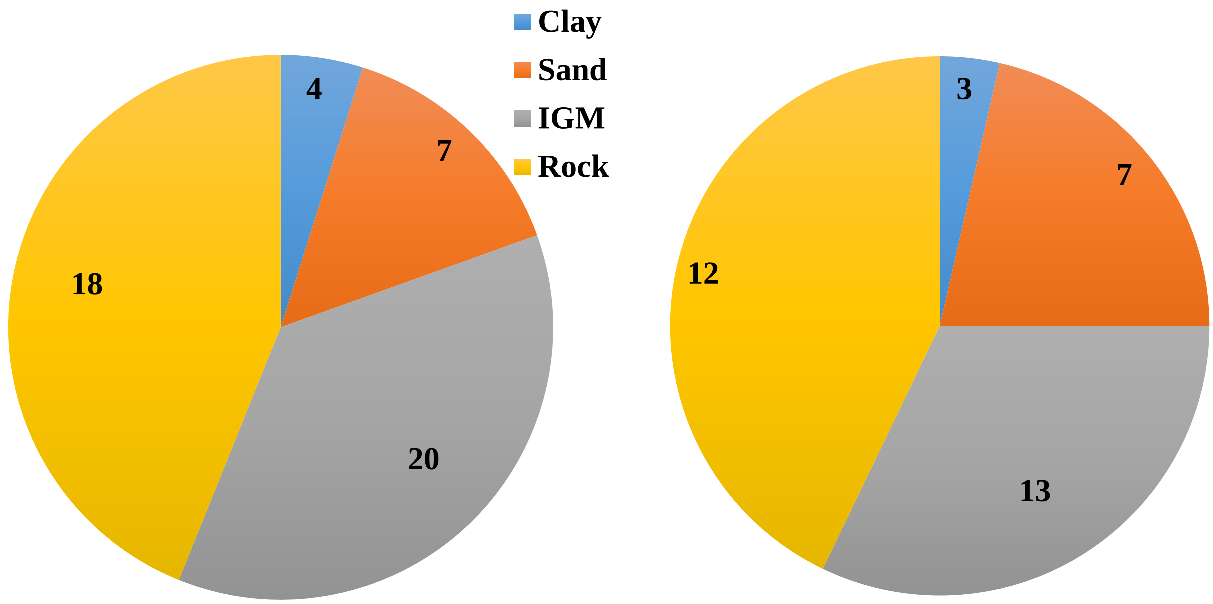

Figure 3.4. Distribution of drilled shaft load tests contained in DSHAFT by geomaterial along shaft length: available data (left) and usable data (right)

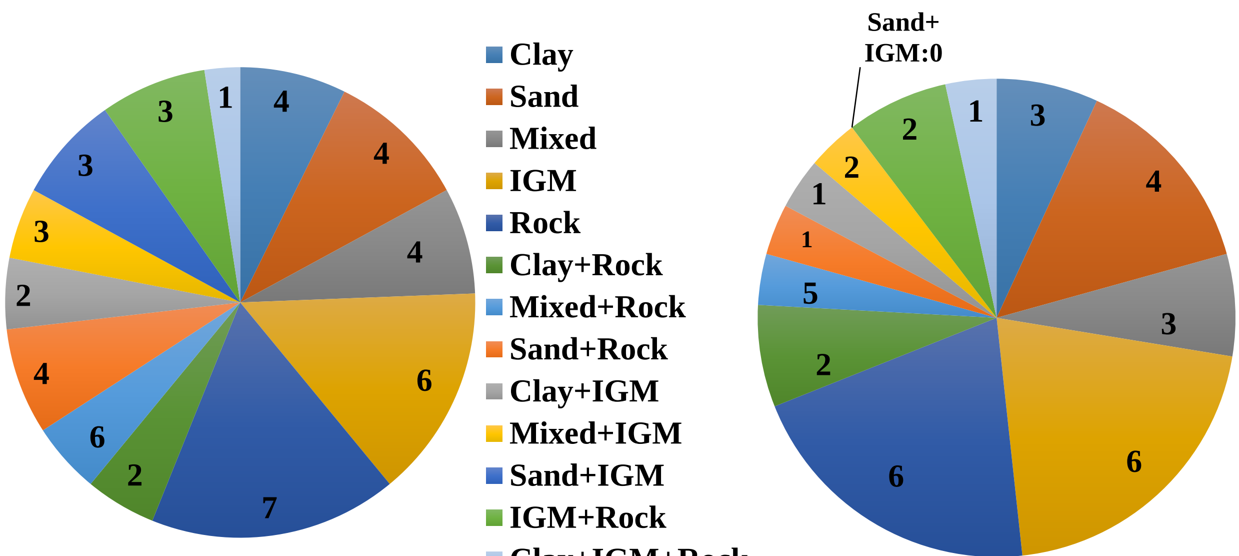

Figure 3.5. Distribution of drilled shaft load tests contained in DSHAFT by geomaterial along shaft length: available data (left) and usable data (right)

3.2. Data Categorization

It is common procedure in calibration studies to group load tests in databases based on the predominant soil type present along the shaft at each load test. This categorization allows the calibration of resistance factors for specific geomaterial type and corresponding design methods.

Load test sites are generally classified as clay, sand, mixed, IGM, or rock. Because of the lack of clear guidelines from AASHTO in this process of sorting load tests, a classification scheme termed the 70% rule was developed by Roling et al. (2010) in the regional calibration of resistance factors for driven piles in Iowa. Based on this criterion, a site is classified as sand or clay if 70% or more of the soil layers along the shaft length is composed of either geomaterial. Otherwise, the site is considered to be mixed. However, a classification based on an average soil profile or based on the most predominant type of soil ignores the true spatial variation of geomaterials, which can introduce some errors in the calibrated factors. Additionally, this classification scheme is only applicable to soils, and it does not offer any directions on how to approach test sites underlain by a mix of rock or IGM and soil. Others have sometimes neglected skin friction of soils overlying the bedrock in calibration studies. However, resistance from the overburden soils is not always negligible, and it cannot be neglected without introducing some errors in the calibrated resistance factors. To overcome these shortcomings, the analyses in this calibration focuses on a layered approach rather than classification based on an average soil profile. This approach, however, requires proper instrumentation along each test shaft and good quality strain gauge data in order to establish the load-deformation characteristic of individual soil layers. Using the strain gauge records, the soil profile at a given load test site can be divided into several shear zones. The database is then sorted based on the geomaterial type present in shear zones rather than along the entire shaft length. For instance the site shown in Figure 3.6 would be classified as mixed using an average soil profile classification scheme such as the 70% rule.

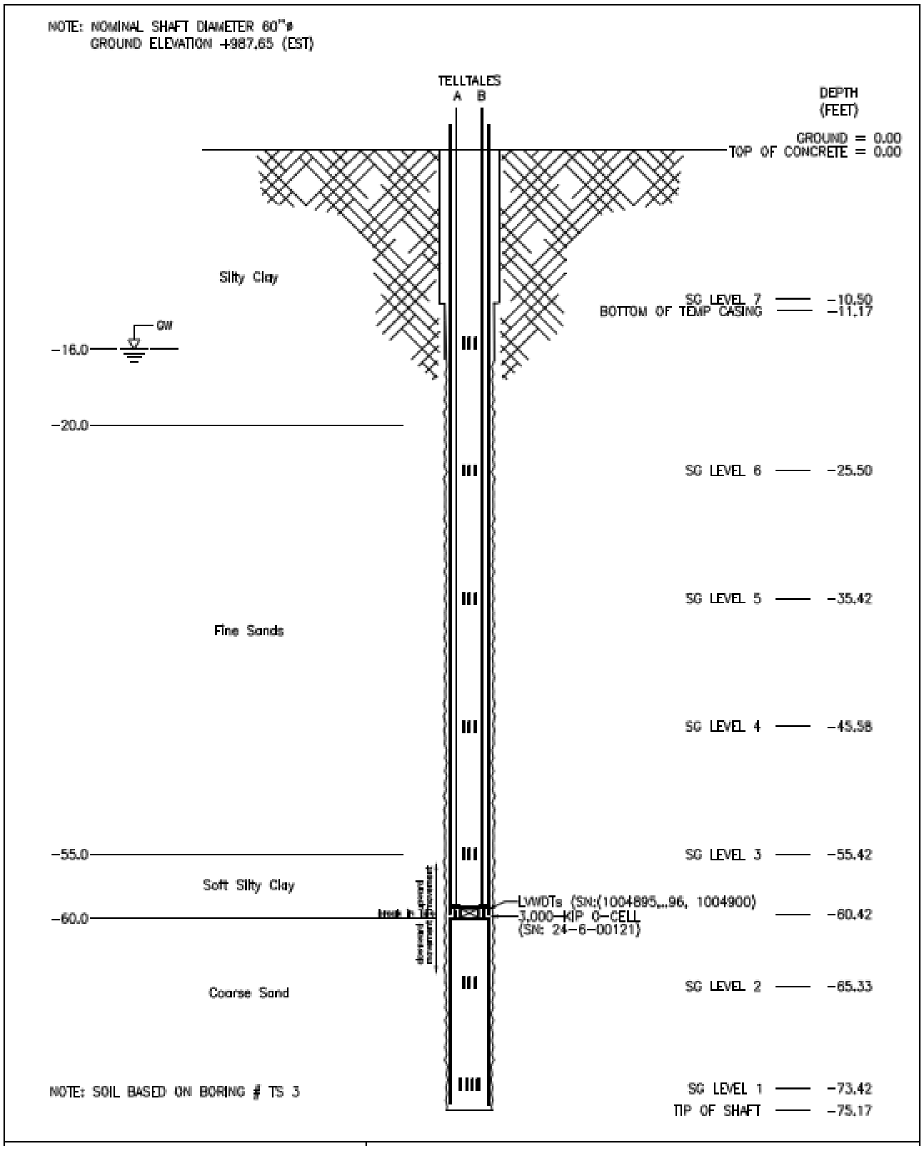

Figure 3.6. DST26 soil profile

Following a layered approach leads to two shear zones (top of concrete-SG7, SG3-O-cell) classified as clay, and five shear zones (SG6-SG5, SG5-SG4, SG4-SG3, O-cell-SG2, SG2-tip) classified as sand. Because of the presence of both sand and clay between SG7 and SG6, the shear zone between these strain gauges can be classified as mixed. Using this approach, the data in DHSAFT can be grouped in 35 clay shear zones, 53 sand, 27 cohesive IGM, and 22 rock, allowing proper evaluation of the uncertainty associated with each geomaterial type and resistance prediction method.

3.3. Shaft Measured Resistance and Extrapolation

The nominal resistance of the shafts' various shear zones and base from measured load-displacement curves are required for the calibration of resistance factors. Generally, the nominal resistance can be defined as the ultimate resistance established by one of the several methods available in literature, or as the resistance at a certain displacement of the shaft top. Available methods include but are not limited to Brinch-Hansen's, Butler and Hoy's, Chin's, Davisson's, De Beer's, and Hirany and Kulhawy's. Since the Iowa DOT defines drilled shafts' strength limit state in terms of shaft top displacement, the Iowa DOT 1 in. displacement criterion is used in this study. Resistance factors are also calibrated at the AASHTO criterion corresponding to 5% of the shaft diameter for top displacement so that a direct comparison can be made with code recommended resistance factors. Due to the fact that the majority of the load tests in DSHAFT are terminated before the target displacements are reached, extrapolation is necessary to quantify the required resistances. Three different extrapolation methods were developed by Ng et al. (2014) depending on whether ultimate resistance is achieved in side shear, end bearing, or neither. Case A represents a load test with side shear failure only, Case B a situation where only end bearing reaches ultimate, and Case C a load test in which failure is not achieved in either side shear or end bearing. Illustrations of these cases and respective extrapolation procedures are shown in Figure 3.7 through Figure 3.12.

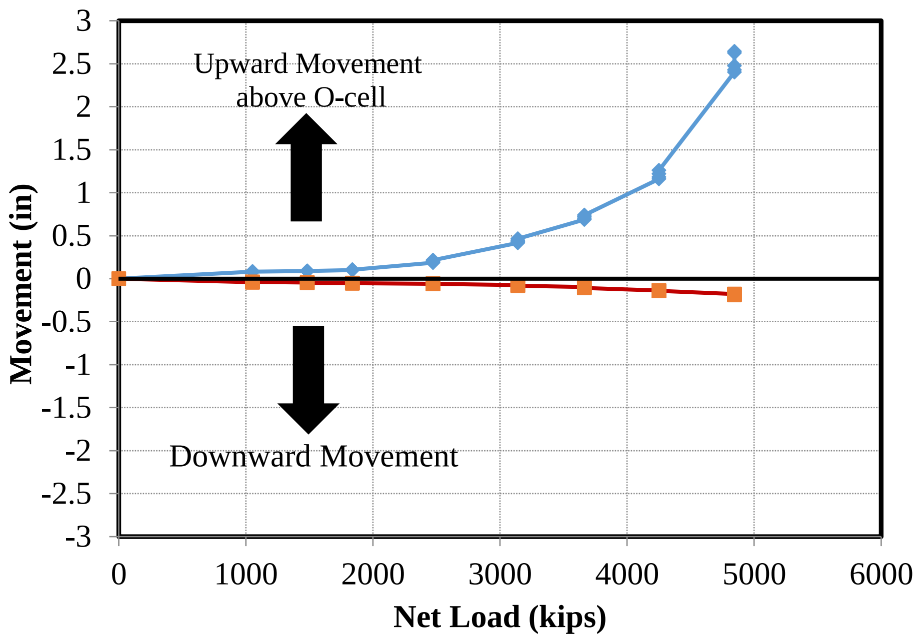

Figure 3.7. Case A: Fully mobilized side shear in DST2

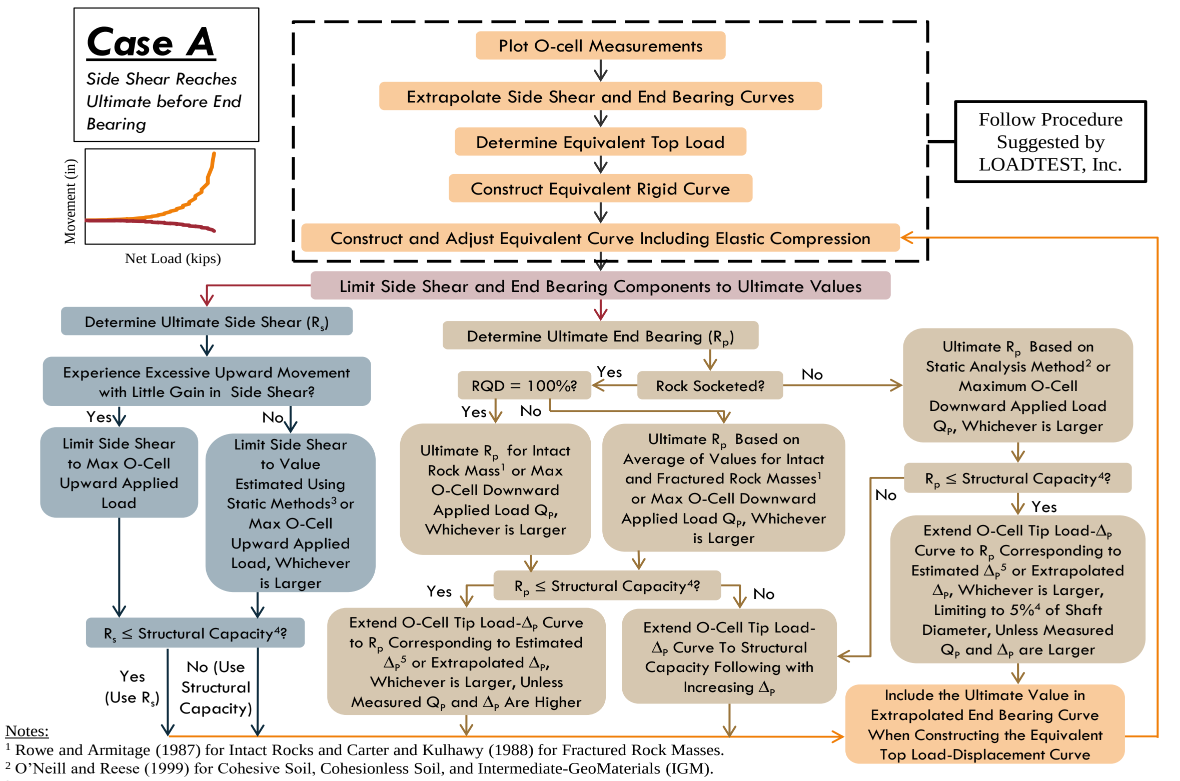

Notes:
[1] Rowe and Armitage (1987) for Intact Rocks and Carter and Kulhawy (1988) for Fractured Rock Masses.
[2] O'Neill and Reese (1999) for Cohesive Soil, Cohesionless Soil, and Intermediate-GeoMaterials (IGM).
[3] Alpha-method for Cohesive Soil, Beta-Method for Cohesionless Soil, O'Neill et al. (1996) for IGM, Horvath and Kenney (1979) for Rocks, or a Combination of All.
[4] AASHTO LRFD Bridge Design Specifications (2010).
[5] Estimated Tip Displacement: Vesic for Soils, O'Neill et al. (1996) for Cohesive IGM, Mayne and Harris (1993) for Granular IGM, and Kulhawy and Carter (1992) for Rock

Ng et al. 2014

Figure 3.8. Proposed procedure to generate an equivalent top load-displacement curve for Case A

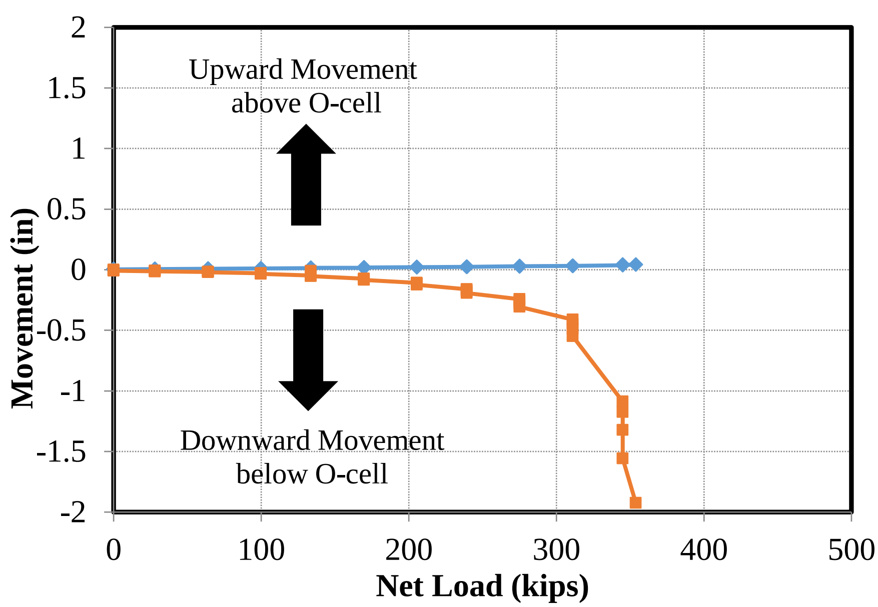

Figure 3.9. Case B: Fully mobilized end bearing in DST6

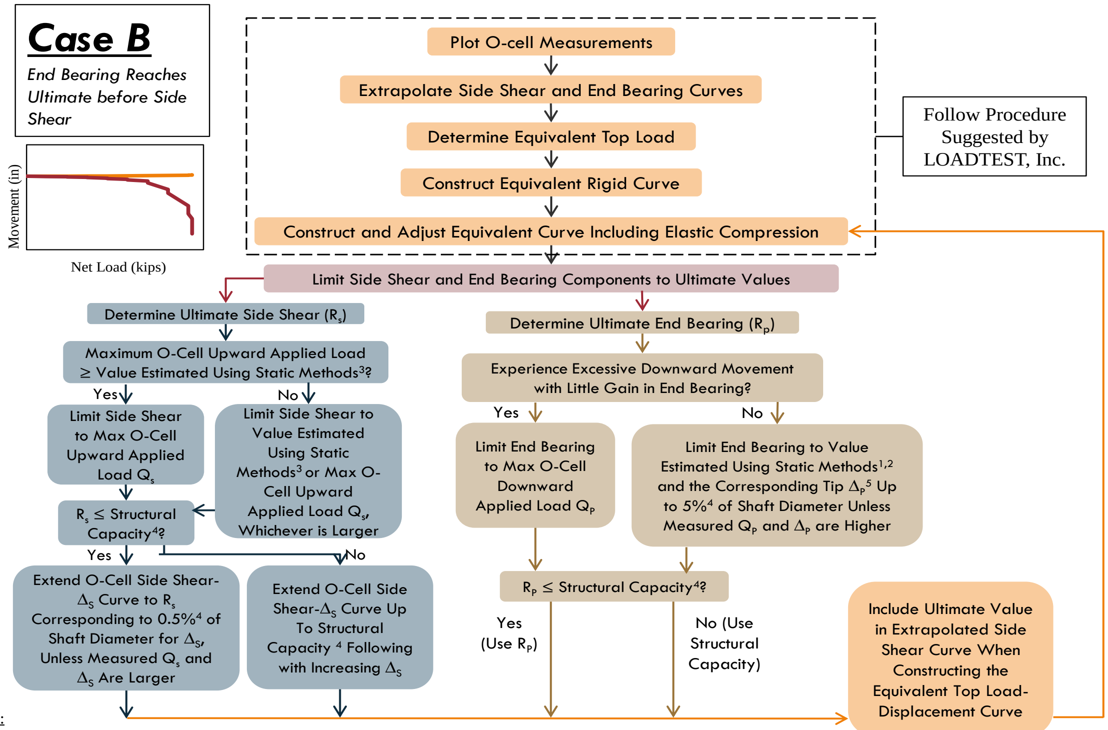

Notes:
[1] Rowe and Armitage (1987) for Intact Rocks and Carter and Kulhawy (1988) for Fractured Rock Masses.
[2] O'Neill and Reese (1999) for Cohesive Soil, Cohesionless Soil, and Intermediate-GeoMaterials (IGM).
[3] Alpha-method for Cohesive Soil, Beta-Method for Cohesionless Soil, O'Neill et al. (1996) for IGM, Horvath and Kenney (1979) for Rocks, or a Combination of All.
[4] AASHTO LRFD Bridge Design Specifications (2010).
[5] Estimated Tip Displacement: Vesic for Soils, O'Neill et al. (1996) for Cohesive IGM, Mayne and Harris (1993) for Granular IGM, and Kulhawy and Carter (1992) for Rock

Ng et al. 2014

Figure 3.10. Proposed procedure to generate an equivalent top load-displacement curve for Case B

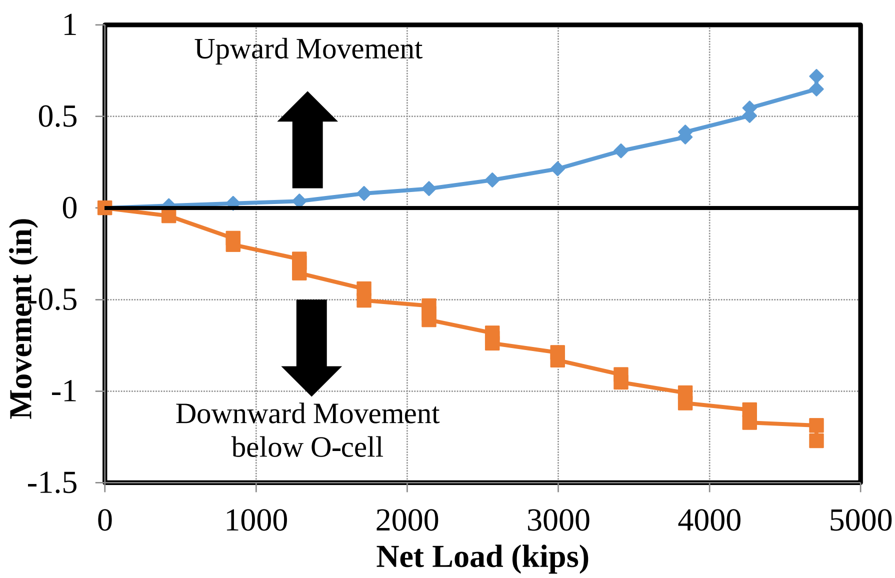

Figure 3.11. Case C: No failure achieved in either side shear or end bearing in DST39

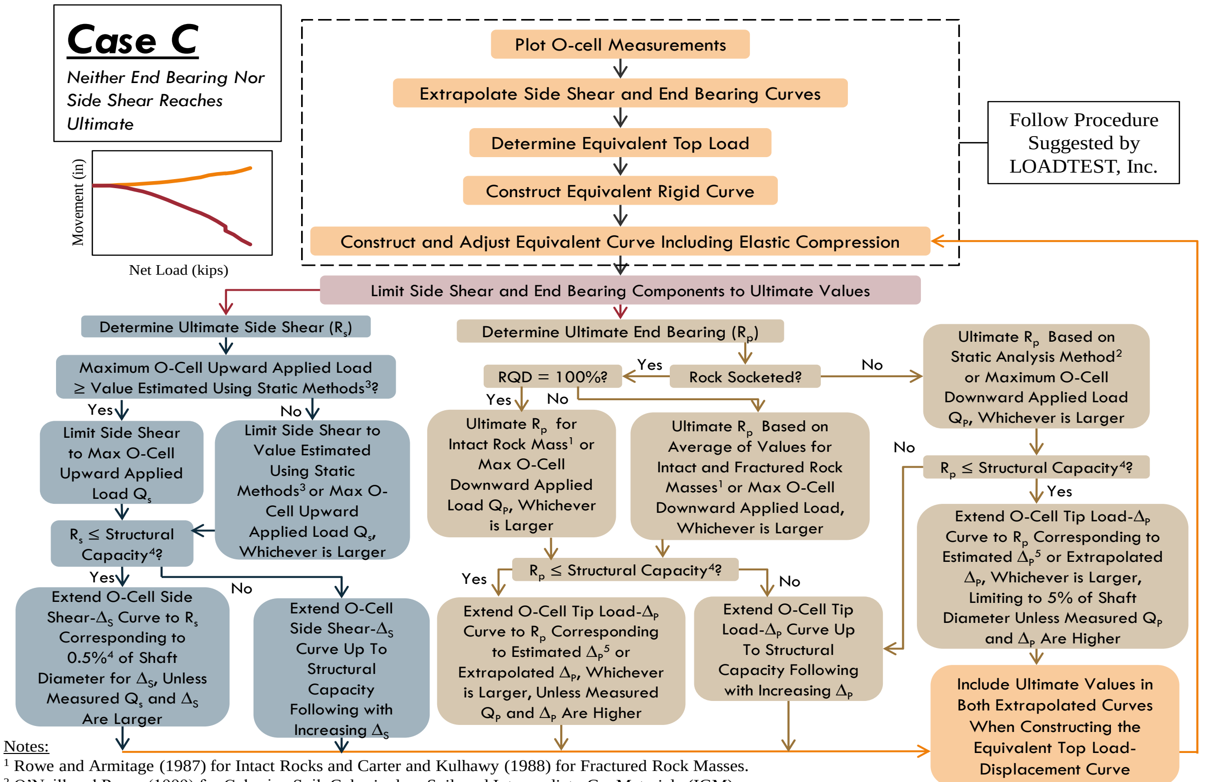

Notes:

[1] Rowe and Armitage (1987) for Intact Rocks and Carter and Kulhawy (1988) for Fractured Rock Masses.
[2] O'Neill and Reese (1999) for Cohesive Soil, Cohesionless Soil, and Intermediate-GeoMaterials (IGM).
[3] Alpha-method for Cohesive Soil, Beta-Method for Cohesionless Soil, O'Neill et al. (1996) for IGM, Horvath and Kenney (1979) for Rocks, or a Combination of All.
[4] AASHTO LRFD Bridge Design Specifications (2010).
[5] Estimated Tip Displacement: Vesic for Soils, O'Neill et al. (1996) for Cohesive IGM, Mayne and Harris (1993) for Granular IGM, and Kulhawy and Carter (1992) for Rock

Ng et al. 2014

Figure 3.12. Proposed procedure to generate an equivalent top load-displacement curve for Case C

Although the developed procedures can generate equivalent top load-displacement curves beyond the maximum displacement achieved during load testing, they have important limitations.

By relying on various drilled shaft static design methods, the proposed procedures introduce the uncertainty associated with these methods into the actual measured shaft capacities. The purpose of the calibration to evaluate the accuracy of the design methods at predicting the actual measured resistance is somewhat defeated when uncertainties from the design methods themselves are introduced into the measured resistance. Additionally, extrapolation of the equivalent top load-displacement curve in this fashion is not useful to the calibration of resistance factors using the layered approach adopted in this study.

The proposed procedures are not able to provide any information on the load-displacement characteristics of each shear zone. To overcome this issue, Ng et al. (2014) distributed the extrapolated total measured shaft resistance at a given top displacement among all layers based on their estimated contribution to the overall predicted shaft resistance. The uncertainties associated with the design methods are introduced once again into the measured capacities. Due to these limitations, a different approach to obtaining the required resistance values for the calibration was adopted in this study. This approach, which is based on the work of Lee and Park (2008) and Meyer et al. (1975), relies on t-z analyses using strain gauge data collected during load testing. Load-deformation behavior of all shear zones are established and used to quantify the mobilized resistance of each zone for a given top displacement with due consideration of the shaft elastic compression. For a given shaft segment, i, with an associated unit shear resistance, t_i, developed from strain gauge data as illustrated in Figure 3.13, three governing equations are solved iteratively until convergence of the output and input loads and displacements.

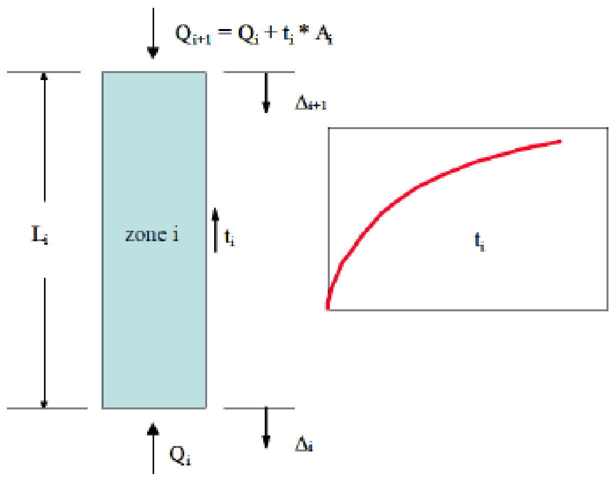

After LOADTEST, Inc. 2010

Figure 3.13. Sample shaft Section in t-z analyses

$$\delta_i = \frac{(Q_i + Q_{i+1})L_i}{2A_iE_i} \tag{3.1}$$

$$\Delta_{i+1} = \Delta_i + \delta_i \tag{3.2}$$

$$Q_{i+1} = Q_i + t\left(\frac{\Delta_i + \Delta_{i+1}}{2}\right)A_i \tag{3.3}$$

where,

δ_i	= Elastic compression of section i
Q_i and Q_{i+1}	= Load at bottom and top of section i, respectively
Δ_i and Δ_{i+1}	= Displacement at bottom and top of section i, respectively
A_i	= Cross-sectional area of section i
E_i	= Elastic modulus of section i

The same procedure is repeated for other segments until the complete shaft length is analyzed. A MATLAB code was written to facilitate the implementation of this approach.

The segment at the very bottom of the shaft has, in addition to skin resistance, an end bearing resistance component, which must be taken into account in the analysis. When necessary, extrapolation of the unit skin friction in each shear zone or end bearing can be performed using one of the functions recommended by Fellenius (2015) that best fit the measured data. Fitting functions include the ratio function, the Chin-Kondner hyperbolic function, the exponential function, the Hansen 80% function, and the Zhang function. The ratio function and the Chin-Kondner hyperbolic function are best suited for geomaterials that exhibit a strain-hardening behavior. The increase in resistance with larger displacement is more pronounced in the ratio function compared to the hyperbolic function. The Hansen 80% function and the Zhang function are strain-softening functions, and the exponential function is appropriate for geomaterials with an elasto-plastic trend. When extrapolation using any of these functions is doubtful, it can conservatively be assumed that the unit skin friction or end bearing remains constant beyond the maximum measured value. Because of the importance of the strain gauge data quality in this approach, some of the load tests that were deemed usable in the preliminary calibration could not be used in this study. The measured resistances corresponding to the two strength criteria considered are presented in Appendix A.

3.4. Side Resistance and End Bearing Estimations

The predicted resistance of the various shear zones and end bearings were estimated from the static design methods described in Section 2.3 using the necessary subsurface information available in DSHAFT. Additionally, the following assumptions were made:

- Closed joints were assumed in side resistance estimations in rock and IGM
- The reported SPT N-values were assumed based on a 60% hammer efficiency
- The undrained shear strength (S_u) of cohesive materials were approximated to (1) half of measured unconfined compressive strength, or (2) from Table 2.2 depending on the availability of material parameters
- The unit weight of geomaterials (γ) was estimated using N_{60} from Table 2.3 and Table 2.4
- The interface friction angle (ϕ_{rc}) in cohesive IGM required for unit side resistance estimation was assumed to be 30°
- The drilled shaft boreholes were not artificially roughened

A summary of these methods is presented in Table 3.1.

Table 3.1. Static design methods for skin friction and end bearing prediction

Geomaterial	Unit side resistance (q_s)	Unit end bearing (q_p)
Cohesive soil	α-method by O'Neill and Reese 1999: Section 2.3.2.1	Total Stress method by O'Neill and Reese 1999: Section 2.3.3.1
Cohesionless soils and Cohesionless IGM	β-method by and O'Neill and Reese 1999: Section 2.3.2.2 β-method by Brown et al. 2010: Section 2.3.2.3	Effective stress method by Reese and O'Neill 1989: Section 2.3.3.2
Cohesive IGM	Eq. (2.25) by O'Neill and Reese 1999: Section 2.3.2.3	Rowe and Armitage 1987, Carter and Kulhawy 1988, O'Neill and Reese 1999, Sowers 1976, Average of Rowe and Armitage 1987, and Carter and Kulhawy 1988
Rock	Eq. (2.30) by Horvath and Kenney: 1979 Section 2.3.2.4 Eq. (2.31) by Kulhawy et al.: 2005 Section 2.3.2.4	Rowe and Armitage 1987, Carter and Kulhawy 1988, O'Neill and Reese 1999, Sowers 1976, Average of Rowe and Armitage 1987, and Carter and Kulhawy 1988

The O'Neill and Reese (1999) β-method for skin friction prediction in sand is slightly modified in this study in order to increase its efficiency. In the original method, two different equations are proposed to estimate the depth dependent β coefficient for sandy soils and for gravelly soils with an SPT blow count greater than 15. The analyses herein show that the β coefficient equation for the gravelly soils produces resistance predictions that are generally much greater than the measured resistances, thus leading to a lower resistance factor and efficiency. Therefore in the context of depth dependent β-method, the following is proposed for cohesionless soils and IGM:

$$q_s = \beta\sigma'_V \tag{3.4}$$

where,

β = $1.5 - 0.135\sqrt{z}$ for all cohesionless soils with $N_{60} \geq 15$

β = $\frac{N_{60}}{15}\left(1.5 - 0.135\sqrt{z}\right)$ for all cohesionless soils with $N_{60} < 15$

N_{60} = Average SPT blow count in the design zone under consideration and corrected for hammer efficiency

z = Depth below ground surface at soil mid-depth (ft)

β values are limited to minimum and maximum values of 0.25 and 1.20, respectively.
Five end resistance prediction methods were considered. Application of the Carter and Kulhawy (1988) method was difficult because it required detailed description of certain rock mass features, which is not available in DSHAFT. Conservative estimates of the required parameters were made where necessary. Summaries of the various predicted resistances are presented in Appendix B.

CHAPTER 4. RESISTANCE FACTOR CALIBRATION

4.1. Resistance Bias Characterization

After sorting the database using the approach described in Section 3.2 and obtaining the necessary measured resistances using t-z analyses, the resistance bias was calculated for each shear zone and end bearing situation. In this process, two different methods were used in calculating the resistance bias for skin friction. Though a specific method of calculating the resistance bias has not been explicitly recommended in the resistance factor calibration framework, the resistance bias is commonly calculated as the ratio of total measured skin friction to total predicted skin friction. Because of the nature of the database used in this study, this typical approach cannot be used if resistance factors are to be calibrated for each geomaterial type. The load test schematic shown in Figure 4.1 is used to describe the two methods used to compute the resistance bias for skin friction.

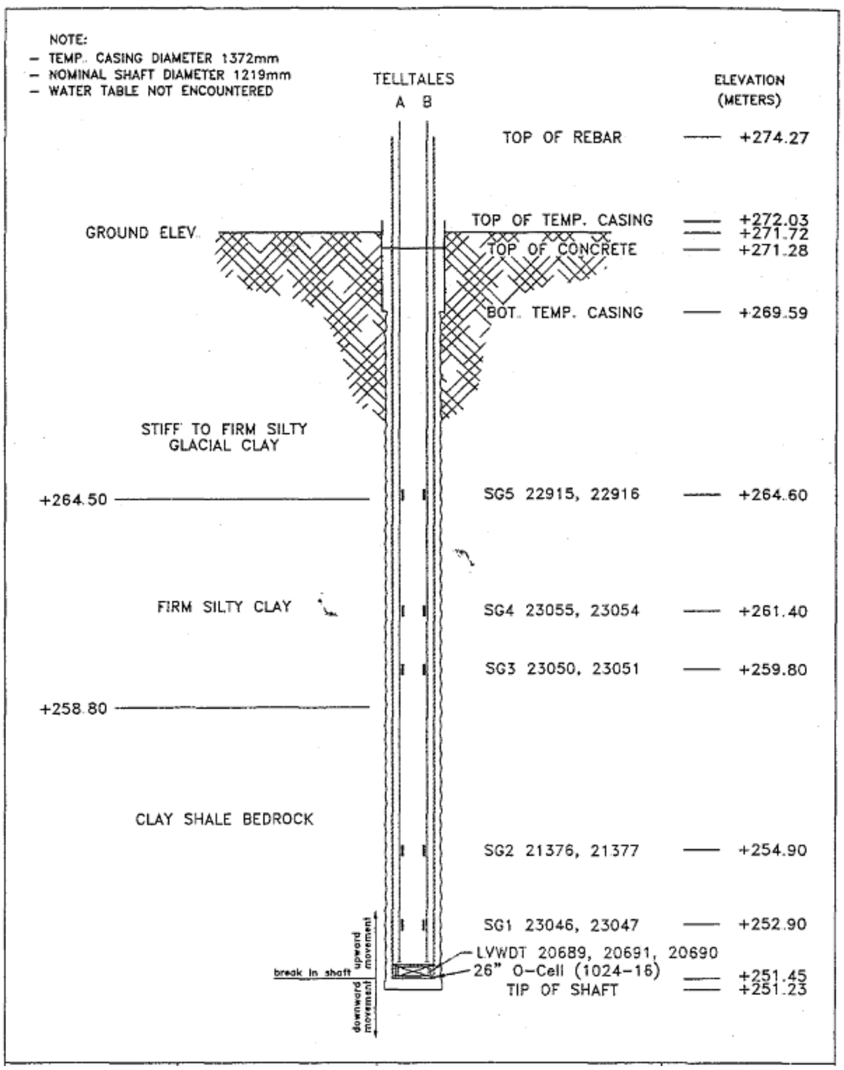

Figure 4.1. DST3 load test schematic

The soil profile shown in Figure 4.1 is composed of three clay shear zones and three cohesive IGM shear zones based on the soil classification and strength properties obtained from the boring log. In the first approach, the resistance bias is calculated for each individual shear zone. This procedure results in three different resistance bias values for the clay soil category and three values for the cohesive IGM category. The second approach follows the principle of total resistance commonly used in other calibration studies. It uses the sum of the resistance from shear zones of the same geomaterial category. For instance, instead of calculating three different bias values for the clay or IGM category shown in Figure 4.1, a single resistance bias can be calculated for each category as the sum of the measured skin friction to the predicted skin friction. The resistance bias datasets resulting from these two procedures are shown in Table 4.1 and Table 4.2 for Iowa usable load tests only and Table 4.3 and Table 4.4 for all usable load tests in the database. Presented are the number of observations, mean, standard deviation, and coefficient of variation for each geomaterial type and its corresponding design method.

Table 4.1. Skin friction statistical parameters from Approach I using Iowa usable load tests

	1 in. displacement				5% diameter displacement			
Design method	**Sample, N**	**Mean**	**Std dev**	**COV**	**Sample, N**	**Mean**	**Std dev**	**COV**
α-method	27	1.26	0.70	0.55	28	1.35	0.87	0.65
O'Neill and Reese 1999 β-Method	50	1.26	0.48	0.39	50	1.54	0.62	0.40
Brown et al. 2010 β-method	51	1.18	0.43	0.36	51	1.45	0.56	0.39
O'Neill and Reese 1999 modified α-method	11	2.09	1.43	0.68	11	2.46	1.65	0.67
Horvath and Kenney 1979	17	2.12	1.16	0.55	17	2.52	1.58	0.63
Kulhawy et al. 2005	18	1.17	0.67	0.57	18	1.36	0.84	0.62

Table 4.2. Skin friction statistical parameters from Approach II using Iowa usable load tests

	1 in. displacement				5% diameter displacement			
Design method	**Sample, N**	**Mean**	**Std dev**	**COV**	**Sample, N**	**Mean**	**Std dev**	**COV**
α-method	11	1.31	0.51	0.39	11	1.28	0.53	0.41
O'Neill and Reese 1999 β-Method	9	1.25	0.28	0.23	9	1.53	0.34	0.22
Brown et al. 2010 β-method	9	1.22	0.36	0.31	9	1.48	0.36	0.25
O'Neill and Reese 1999 modified α-method	5	1.88	0.81	0.43	5	2.50	1.63	0.65
Horvath and Kenney 1979	7	2.10	0.72	0.34	7	2.30	0.99	0.43
Kulhawy et al. 2005	7	1.06	0.23	0.22	7	1.17	0.40	0.34

Table 4.3. Skin friction statistical parameters from Approach I using all usable load tests

Design method	1 in. displacement				5% diameter displacement			
	Sample, N	Mean	Std dev	COV	Sample, N	Mean	Std dev	COV
α-method	27	1.26	0.70	0.55	28	1.35	0.87	0.65
O'Neill and Reese 1999 β-method	50	1.26	0.48	0.39	50	1.54	0.62	0.40
Brown et al. 2010 β-method	51	1.18	0.43	0.36	51	1.45	0.56	0.39
O'Neill and Reese 1999 modified α-method	25	2.58	1.57	0.61	26	2.85	1.62	0.57
Horvath and Kenney 1979	21	2.13	1.12	0.52	21	2.51	1.47	0.58
Kulhawy et al. 2005	21	1.11	0.63	0.57	22	1.29	0.78	0.61

Table 4.4. Skin friction statistical parameters from Approach II using all usable load tests

Design method	1 in. displacement				5% diameter displacement			
	Sample, N	Mean	Std dev	COV	Sample, N	Mean	Std dev	COV
α-method	11	1.31	0.51	0.39	11	1.28	0.53	0.41
O'Neill and Reese 1999 β-method	9	1.25	0.28	0.23	9	1.53	0.34	0.22
Brown et al. 2010 β-method	9	1.22	0.36	0.31	9	1.48	0.36	0.25
O'Neill and Reese 1999 modified α-method	10	2.26	1.15	0.51	11	2.94	1.59	0.54
Horvath and Kenney 1979	10	2.00	0.74	0.37	10	2.22	0.97	0.44
Kulhawy et al. 2005	10	0.94	0.30	0.32	10	1.05	0.42	0.40

A mean smaller than unity indicates a method that tends to under-predict the actual resistance, whereas a mean greater than unity indicates that the method has a tendency to over-predict the actual resistance. The COV indicates the accuracy of the method at predicting the actual resistance. The higher the COV the less accurate the method. Similarly to Paikowsky et al. (2004), data points that were two standard deviations away from the mean were discarded from the calibration.

A few observations can be made from the information presented in Table 4.1 through Table 4.4. The sample sizes resulting from Approach II are considerably smaller than those resulting from Approach I. Generally, the two different approaches to the resistance bias calculation lead to different statistical characteristics although identical values were obtained in a few cases. With the exception of a single case, all resistance bias means are greater than unity indicating the conservative nature of the design methods considered. The COV values tend to be moderately high to high illustrating a high variability in resistance prediction.

Resistance bias were also calculated for end bearing, and the resulting statistical parameters are presented in Table 4.5, Table 4.6, and Table 4.7.

Table 4.5. Statistical characteristics for end bearing in soil

Design method	1 in. displacement				5% diameter displacement			
	Sample, N	Mean	Std dev	COV	Sample, N	Mean	Std dev	COV
Cohesive soil, O'Neill and Reese 1999	2	0.80	1.11	1.38	2	1.08	1.44	1.34
Cohesionless soil, O'Neill and Reese 1999	3	0.86	0.23	0.26	2	1.54	0.56	0.36
Cohesionless soil with base grouting, O'Neill and Reese 1999	3	1.84	0.39	0.21	1	n/a	n/a	n/a

Table 4.6. Statistical characteristics for end bearing in rock

Design method	1 in. displacement				5% diameter displacement			
	Sample, N	Mean	Std dev	COV	Sample, N	Mean	Std dev	COV
Carter and Kulhawy 1988	6	7.92	10.79	1.36	6	37.17	68.48	1.84
Ng et al. 2014	6	0.33	0.19	0.58	6	0.67	0.37	0.55
O'Neill and Reese 1999	6	0.31	0.21	0.67	6	0.56	0.21	0.37
Rowe and Armitage 1987	6	0.26	0.21	0.83	6	0.44	0.20	0.46
Sowers 1979	6	0.39	0.20	0.52	6	0.83	0.46	0.57

Table 4.7. Statistical characteristics for end bearing in cohesive IGM

Design method	1 in. displacement				5% diameter displacement			
	Sample, N	Mean	Std dev	COV	Sample, N	Mean	Std dev	COV
Carter and Kulhawy 1988	6	24.60	36.49	1.48	6	32.23	45.10	1.40
Ng et al. 2014	6	1.92	2.15	1.12	6	2.76	2.46	0.89
O'Neill and Reese 1999	6	0.83	0.57	0.68	6	1.32	0.55	0.42
Rowe and Armitage 1987	6	1.12	1.10	0.98	6	1.62	1.23	0.76
Sowers 1979	6	2.79	2.74	0.98	6	4.06	3.06	0.76

For end bearing in soil, load tests were grouped in three different datasets including end bearing in clay, end bearing in sand without post-grouting, and end bearing in sand with post-grouting. The sample size is relatively small for all datasets and statistically insufficient for a reliable calibration. At the 1 in. top displacement criterion, there are two data points for end bearing in clay, three for end bearing in sand with no post-grouting, and three for end bearing in sand with post grouting.

At the AASHTO criterion, there are two data points for clay and for sand with no post-grouting, and only one for sand with post-grouting. Load tests with end bearing in cohesive IGM and rock are grouped into five datasets corresponding to five different design methods. As can be seen from Table 4.6 and Table 4.7, the sample size is relatively small similar to the case of end bearing in soil. With the exception of the Carter and Kulhawy (1988) method, all design methods for end bearing in rock are on the unconservative side with a large variability in resistance prediction as evidenced by the high COV values. In the case of end bearing in IGM, all methods under-predicted the tip resistance except for the O'Neill and Reese (1999) method at the Iowa DOT strength criterion. Similar to end bearing in rock, the COV values are high indicating a large scatter in tip resistance prediction. It should be noted that the uncertainty in resistance prediction at the AASHTO strength criterion is generally less than that associated with resistance prediction at 1 in. top displacement.

Various techniques were utilized to determine the distribution type that best suit the resistance bias for each data set. For each data set, histograms of observed values were generated and compared to theoretical normal and lognormal distribution fits. The first technique consisted in generating plots of the probability density functions (PDF) for the calculated resistance bias. An example of such a plot is presented in Figure 4.2 for resistance prediction in cohesive soils at the 1 in. strength criterion.

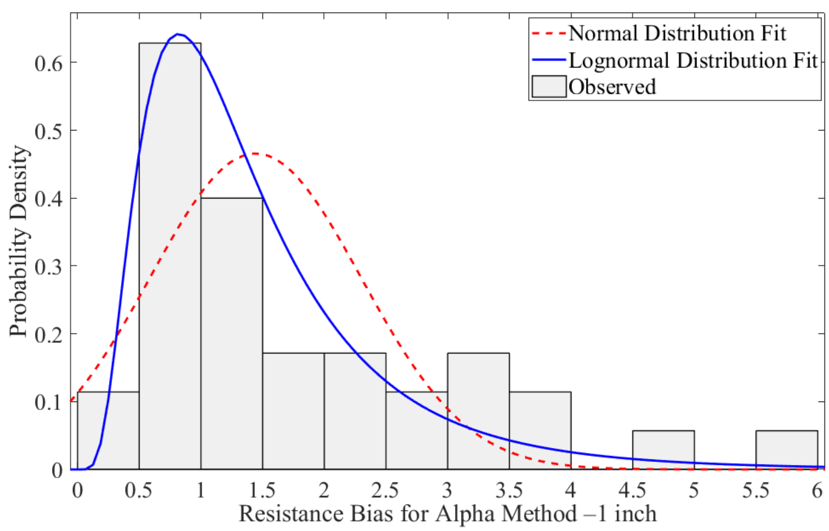

Figure 4.2. PDF for α-method at 1 in. strength criterion

The second technique consisted in generating plots of the cumulative distribution functions (CDF) for the calculated resistance bias as well as the theoretical normal and lognormal distribution fit corresponding to each data group. When plotted against the standard normal variable, a normal distribution follows a straight line while a lognormal distribution follows a curve. The most appropriate distribution can be visually determined from this technique. An example of CDF is shown in Figure 4.3 for resistance prediction in cohesive soils at the 1 in. strength criterion.

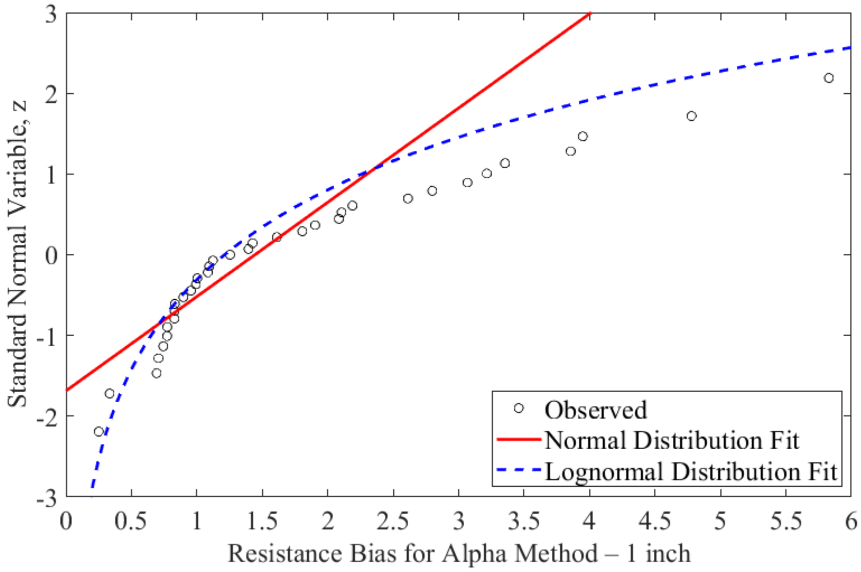

Figure 4.3. CDF for α-method at 1 in. strength criterion

All other PDF and CDF plots can be found Appendix C and Appendix D, respectively. Using these two techniques, the lognormal distribution was found to be the most suited distribution type in most cases.

4.2. Resistance Factors

The modified version of the FOSM reliability method detailed in Section 2.2 was used to calibrate the resistance factors presented in this study. Resistance factors were calibrated for the axial resistance of drilled shafts at Strength I limit state, which includes dead (Q_D) and live (Q_L) load only. The load and resistance random variables were assumed to follow a lognormal distribution, and the assumption associated with the resistance was verified using a combination of methods including histograms of the resistance bias and probability plots. The probability characteristics of the load variable given by Nowak (1999) and shown in Table 2.1 were adopted herein. Several values of the dead to live load ratio (Q_D/Q_L) were investigated and found to have negligible effect on the calibrated factors. Consistent with non-redundant foundations, the resistance factors were calibrated to achieve a reliability β_T of 3.0 approximately equivalent to a probability of failure (p_f) of 1/1,000.

4.2.1. Skin Friction

Table 4.8 presents resistance factors for skin friction calibrated using Approach I and considering load tests from the state of Iowa only.

Table 4.8. Summary of skin friction resistance factors from Approach I considering Iowa usable load tests

Design method	Geomaterial	Failure criteria	Resistance factors at $\beta_T = 3.00$, φ: NCHRP 343[e]	NCHRP 507[b]	NHI 05-052[a]	NHI 05-052[c]	AASHTO 2017[d]	Ng et al. 2014	This study	Efficiency, φ/λ: Ng et al. 2014	This study
O'Neill and Reese 1999 α-method	Cohesive Soil	1-in Δ	n/a	n/a	n/a	n/a	n/a	0.20	0.29	0.11	0.23
		5%D for Δ	0.65	0.36 (φ/λ: 0.41)	0.55	0.60	0.45	0.22	0.24	0.12	0.18
O'Neill and Reese 1999 β-method	Cohesionless soil	1-in Δ	n/a	n/a	n/a	n/a	n/a	0.48	0.48	0.54	0.38
		5%D for Δ	n/a	0.31 (φ/λ: 0.28)	0.52	n/a	n/a	0.47	0.55	0.53	0.36
Brown et al. 2010 β-method	Cohesionless soil	1-in Δ	n/a	n/a	n/a	n/a	n/a	n/a	0.48	n/a	0.41
		5%D for Δ	n/a	n/a	n/a	n/a	0.55	n/a	0.55	n/a	0.38
O'Neill and Reese 1999 modified α-method	Cohesive IGM	1-in Δ	n/a	n/a	n/a	n/a	n/a	0.63	0.34	0.30	0.16
		5%D for Δ	n/a	0.51 (φ/λ: 0.41)	0.55	n/a	0.60	0.69	0.41	0.32	0.17
Horvath and Kenney 1979	Rock	1-in Δ	n/a	n/a	n/a	n/a	n/a	0.55	0.50	0.49	0.24
		5%D for Δ	0.65	n/a	0.55	0.55	0.55	0.62	0.48	0.53	0.19
Kulhawy et al. 2005	Rock	1-in Δ	n/a	n/a	n/a	n/a	n/a	n/a	0.26	n/a	0.22
		5%D for Δ	n/a	n/a	n/a	n/a	0.55	n/a	0.26	n/a	0.19

[a] calibration by fitting to ASD; [b] calibration performed using reliability theory (FORM); [c] calibration performed using reliability theory (Monte Carlo method); [d] selected value among NCHRP 343(Barker et al. 1991), NCHRP 507 (Paikowsky et al. 2004), and Allen (2005); [e] recommended value; n/a = not available; Δ = shaft top displacement; D = shaft diameter

For skin friction in clay, the resistance factors were found to be 0.29 and 0.24 at the 1 in. top displacement criterion and the AASHTO criterion, respectively. Although a bit higher than the resistance factors established in the preliminary calibration by Ng et al. (2014), the newly calibrated factors do not show any improvements with regard to the code recommended value of 0.45. For skin friction in sand using O'Neill and Reese (1999) β-method, the calibrated factors were 0.48 and 0.55 for the 1 in. and 5% diameter top displacement criteria, respectively.

These values show an improvement compared to the value of 0.31 recommended in NCHRP 507 by Paikowsky et al. (2004), but they are lower than the resistance factors developed by Ng et al. (2014) in the preliminary calibration. This difference can be attributed to the difference in analysis procedures used. Resistance factors from Ng et al. (2014) were calibrated using the sum of the resistance approach, and the extrapolation technique used in that study differs from the one used in the study herein. For skin friction prediction in sand using the alternate β-method by Brown et al. (2010), the calibrated resistance factors were 0.48 and 0.55 for the Iowa DOT and AASHTO strength criteria, respectively. Compared to the AASHTO recommended value, which was established based on a calibration by fitting to a factor of safety of 2.5, the calibrated values in this study do not show any improvement. For skin friction in IGM, the calibrated factors of 0.34 and 0.41 show a decrease compared to values recommended by Paikowsky et al. (2004), Ng et al. (2014), and AASHTO. For skin friction in rock using Horvath and Kenney (1979), the calibrated factors were 0.50 for the Iowa DOT criterion and 0.48 for AASHTO criterion. These values are lower than the resistance factors recommended by all other studies considered. Resistance factors for skin friction in rock using Kulhawy et al. (2005) were found to be 0.26 at the Iowa DOT and AASHTO criteria. These resistance factors are considerably smaller than AASHTO recommended value of 0.55.

Considering the load tests from Iowa again, resistance factors were calibrated using Approach II, and the results are presented in Table 4.9.

Table 4.9. Summary of skin friction resistance factors from Approach II considering Iowa usable load tests

Design method	Geomaterial	Failure criteria	Resistance factors at $\beta_T = 3.00$, φ: NCHRP 343[e]	NCHRP 507[b]	NHI 05-052[a]	NHI 05-052[c]	AASHTO 2017[d]	Ng et al. 2014	This study	Efficiency, φ/λ: Ng et al. 2014	This study
O'Neill and Reese 1999 α-method	Cohesive Soil	1-in Δ	n/a	n/a	n/a	n/a	n/a	0.20	0.48	0.11	0.37
		5%D for Δ	0.65	0.36 (φ/λ: 0.41)	0.55	0.60	0.45	0.22	0.45	0.12	0.35
O'Neill and Reese 1999 β-method	Cohesionless soil	1-in Δ	n/a	n/a	n/a	n/a	n/a	0.48	0.76	0.54	0.61
		5%D for Δ	n/a	0.31 (φ/λ: 0.28)	0.52	n/a	0.55	0.47	0.94	0.53	0.62
Brown et al. 2010 β-method	Cohesionless soil	1-in Δ	n/a	n/a	n/a	n/a	n/a	n/a	0.61	n/a	0.49
		5%D for Δ	n/a	n/a	n/a	n/a	0.55	n/a	0.86	n/a	0.58
O'Neill and Reese 1999 modified α-method	Cohesive IGM	1-in Δ	n/a	n/a	n/a	n/a	n/a	0.63	0.62	0.30	0.33
		5%D for Δ	n/a	0.51 (φ/λ: 0.41)	0.55	n/a	0.60	0.69	0.44	0.32	0.18
Horvath and Kenney 1979	Rock	1-in Δ	n/a	n/a	n/a	n/a	n/a	0.55	0.91	0.49	0.43
		5%D for Δ	0.65	n/a	0.55	0.55	0.55	0.69	0.77	0.53	0.34
Kulhawy et al. 2005	Rock	1-in Δ	n/a	n/a	n/a	n/a	n/a	n/a	0.67	n/a	0.63
		5%D for Δ	n/a	n/a	n/a	n/a	0.55	n/a	0.51	n/a	0.43

[a] calibration by fitting to ASD; [b] calibration performed using reliability theory (FORM); [c] calibration performed using reliability theory (Monte Carlo method); [d] selected value among NCHRP 343 (Barker et al. 1991), NCHRP 507 (Paikowsky et al. 2004), and Allen (2005); [e] recommended value; n/a = not available; Δ = shaft top displacement; D = shaft diameter

Generally, the resistance factors calibrated in this manner are higher than those calibrated using Approach I, and they show some improvement compared to Paikowsky et al. (2004), Ng et al. (2014), and AASHTO, except for a few cases. For skin friction in clay using the α-method, the calibrated factors were 0.48 at the Iowa DOT strength criterion and 0.45 at the at the AASHTO criterion. While the calibrated factor at the AASHTO criterion was identical to the code recommended value of 0.45, the calibration achieved a 6.67% increase at the Iowa DOT 1 in. displacement criterion. For skin friction in sand using O'Neill and Reese (1999) β-method, the calibrated factors of 0.76 and 0.94 at the Iowa DOT and AASHTO criteria, respectively, corresponded to a 38.18% and 70.91% increase compared to the AASHTO value of 0.55. For skin friction in sand using Brown et al. (2010) β-method, the calibration resulted in a 10.91% increase at the Iowa DOT criterion and a 56.36% increase at the AASHTO criterion. In the case of skin friction in IGM, the calibrated factor of 0.62 at the Iowa DOT criterion was 3.33% greater than AASHTO value of 0.60 while no improvement was observed at the AASHTO criterion. For skin friction in rock using Horvath and Kenney (1979), the calibrated factors showed significant improvements compared to AASHTO value of 0.55. The resistance factor improved by 65.45% at the Iowa DOT criterion and by 40% at the AASHTO criterion. For skin friction in rock using Kulhawy et al. (2005), the calibration improved the resistance factor by 21.82% at the Iowa DOT criterion, but no improvement was observed at the AASHTO criterion.

After considering solely the load tests from Iowa, the resistance factors were recalibrated using all usable load tests in the database. The calibrated factors using Approach I and Approach II are shown in Table 4.10 and Table 4.11, respectively.

Table 4.10. Summary of skin friction resistance factors from Approach I considering all usable load tests

			Resistance factors at β_T = 3.00, φ							Efficiency, φ/λ	
Design method	**Geomaterial**	**Failure criteria**	**NCHRP 343[e]**	**NCHRP 507[b]**	**NHI 05-052[a]**	**NHI 05-052[c]**	**AASHTO 2017[d]**	**Ng et al. 2014**	**This study**	**Ng et al. 2014**	**This study**
O'Neill and Reese 1999 α-method	Cohesive Soil	1-in Δ	n/a	n/a	n/a	n/a	n/a	0.20	0.29	0.11	0.23
		5%D for Δ	0.65	0.36 (φ/λ: 0.41)	0.55	0.60	0.45	0.22	0.24	0.12	0.18
O'Neill and Reese 1999 β-method	Cohesionless soil	1-in Δ	n/a	n/a	n/a	n/a	n/a	0.48	0.48	0.54	0.38
		5%D for Δ	n/a	0.31 (φ/λ: 0.28)	0.52	n/a	n/a	0.47	0.55	0.53	0.36
Brown et al. 2010 β-method	Cohesionless soil	1-in Δ	n/a	n/a	n/a	n/a	n/a	n/a	0.48	n/a	0.41
		5%D for Δ	n/a	n/a	n/a	n/a	0.55	n/a	0.55	n/a	0.38
O'Neill and Reese 1999 modified α-method	Cohesive IGM	1-in Δ	n/a	n/a	n/a	n/a	n/a	0.63	0.51	0.30	0.20
		5%D for Δ	n/a	0.51 (φ/λ: 0.41)	0.55	n/a	0.60	0.69	0.64	0.32	0.22
Horvath and Kenney 1979	Rock	1-in Δ	n/a	n/a	n/a	n/a	n/a	0.55	0.54	0.49	0.25
		5%D for Δ	0.65	n/a	0.55	0.55	0.55	0.62	0.54	0.53	0.21
Kulhawy et al. 2005	Rock	1-in Δ	n/a	n/a	n/a	n/a	n/a	n/a	0.25	n/a	0.22
		5%D for Δ	n/a	n/a	n/a	n/a	0.55	n/a	0.26	n/a	0.20

[a] calibration by fitting to ASD; [b] calibration performed using reliability theory (FORM); [c] calibration performed using reliability theory (Monte Carlo method); [d] selected value among NCHRP 343 (Barker et al. 1991), NCHRP 507 (Paikowsky et al. 2004), and Allen (2005); [e] recommended value; n/a = not available; Δ = shaft top displacement; D = shaft diameter

Table 4.11. Summary of skin friction resistance factors from Approach II considering all usable load tests

			Resistance factors at $\beta_T = 3.00$, φ							Efficiency, φ/λ	
Design method	**Geomaterial**	**Failure criteria**	**NCHRP 343[e]**	**NCHRP 507[b]**	**NHI 05-052[a]**	**NHI 05-052[c]**	**AASHTO 2017[d]**	**Ng et al. 2014**	**This study**	**Ng et al. 2014**	**This study**
O'Neill and Reese 1999 α-method	Cohesive Soil	1-in Δ	n/a	n/a	n/a	n/a	n/a	0.20	0.48	0.11	0.37
		5%D for Δ	0.65	0.36 (φ/λ: 0.41)	0.55	0.60	0.45	0.22	0.45	0.12	0.35
O'Neill and Reese 1999 β-method	Cohesionless soil	1-in Δ	n/a	n/a	n/a	n/a	n/a	0.48	0.76	0.54	0.61
		5%D for Δ	n/a	0.31 (φ/λ: 0.28)	0.52	n/a	0.55	0.47	0.94	0.53	0.62
Brown et al. 2010 β-method	Cohesionless soil	1-in Δ	n/a	n/a	n/a	n/a	n/a	n/a	0.61	n/a	0.49
		5%D for Δ	n/a	n/a	n/a	n/a	0.55	n/a	0.86	n/a	0.58
O'Neill and Reese 1999 modified α-method	Cohesive IGM	1-in Δ	n/a	n/a	n/a	n/a	n/a	0.63	0.60	0.30	0.26
		5%D for Δ	n/a	0.51 (φ/λ: 0.41)	0.55	n/a	0.60	0.69	0.71	0.32	0.24
Horvath and Kenney 1979	Rock	1-in Δ	n/a	n/a	n/a	n/a	n/a	0.55	0.79	0.49	0.40
		5%D for Δ	0.65	n/a	0.55	0.55	0.55	0.69	0.73	0.53	0.33
Kulhawy et al. 2005	Rock	1-in Δ	n/a	n/a	n/a	n/a	n/a	n/a	0.44	n/a	0.46
		5%D for Δ	n/a	n/a	n/a	n/a	0.55	n/a	0.39	n/a	0.37

[a] calibration by fitting to ASD; [b] calibration performed using reliability theory (FORM); [c] calibration performed using reliability theory (Monte Carlo method); [d] selected value among NCHRP 343 (Barker et al. 1991), NCHRP 507 (Paikowsky et al. 2004), and Allen (2005); [e] recommended value; n/a = not available; Δ = shaft top displacement; D = shaft diameter

Since all usable load tests for the clay and sand categories came from Iowa, the resistance factors remain unchanged from the previous analyses; therefore, they will not be addressed in the following discussion. Following Approach I, the resistance factors obtained for skin friction in IGM were 0.51 and 0.64 at the Iowa DOT and AASHTO strength criteria, respectively, illustrating a 6.67% improvement at the AASHTO criterion. For skin friction in rock using Horvath and Kenney (1979) and Kulhawy et al. (2005), the calibrated factors did not show any improvements with respect to AASHTO recommendations.

All resistance factors calibrated using Approach I were lower than those obtained from the preliminary calibration by Ng. et al. (2014).

Similar to the calibration that considered Iowa load tests only, Approach II leads to higher resistance factors compared to Approach I. For skin friction in IGM, the calibrated factor was identical to AASHTO value at the Iowa DOT criterion and 18.33% greater than AASHTO value at AASHTO criterion. The calibrated factors associated with Horvath and Kenney (1979) were 43.63% and 32.73% greater than AASHTO value at the Iowa DOT and AASHTO criterion, respectively. No improvement was observed for Kulhawy et al. (2005).

4.2.2. End Bearing

Due to limited data available for end bearing in soil, reliable resistance factors could not be calibrated for tip resistance in clay and sand. Resistance factors for end bearing in cohesive IGM are presented in Table 4.12.

Table 4.12. Summary of resistance factors for end bearing in cohesive IGM

Design method	Failure criteria	Resistance factors at $\beta_T = 3.00$, φ					Efficiency, φ/λ	
		NCHRP 507 [(a)]	NHI 05-052[(b)]	AASHTO 2017 [(c)]	Ng et al. 2014	This study	Ng et al. 2014	This study
Carter and Kulhawy 1988	1-in Δ	n/a	n/a	n/a	1.71	0.69	0.22	0.03
	5%D for Δ	n/a	n/a	n/a	3.04	1.05	0.30	0.03
Ng et al. 2014	1-in Δ	n/a	n/a	n/a	0.64	0.11	0.58	0.06
	5%D for Δ	n/a	n/a	n/a	0.84	0.26	0.62	0.10
O'Neill and Reese 1999	1-in Δ	n/a	n/a	n/a	0.17	0.13	0.22	0.16
	5%D for Δ	0.57 to 0.65 (φ/λ: 0.44 to 0.48)	0.55	0.55	0.20	0.46	0.21	0.35
Rowe and Armitage 1987	1-in Δ	n/a	n/a	n/a	0.32	0.09	0.33	0.08
	5%D for Δ	n/a	n/a	n/a	0.44	0.22	0.36	0.13
Sowers 1976	1-in Δ	n/a	n/a	n/a	0.64	0.22	0.27	0.08
	5%D for Δ	n/a	n/a	n/a	1.06	0.54	0.33	0.13

(a) calibration performed using reliability theory (FORM); (b) calibration by fitting to ASD; (c) selected value among NCHRP 343 (Barker et al. 1991), NCHRP 507 (Paikowsky et al. 2004), and Allen (2005); LTR = load test report criterion; n/a = not available; Δ = shaft top displacement; D = shaft diameter

Generally, the resistance factors were considerably lower than those obtained in the preliminary calibration because of the differences in analyses and extrapolation procedures. Due to the overly conservative nature of the Carter and Kulhawy (1988) method, the calibration resulted in an unrealistic resistance factor greater than unity at the AASHTO strength criterion. The efficiencies of all methods are noticeably very low except for O'Neill and Reese (1999). A comparison of the efficiencies indicates that the O'Neill and Reese (1999) method would be the most economical design method with efficiencies of 0.16 and 0.35 at the Iowa DOT and AASHTO criterion, respectively. The resistance factor of 0.47 associated with this method at the AASHTO criterion is, however, lower than the values recommended by both AASHTO and Paikowsky et al. (2004).

Resistance factors for end bearing in rock are shown in Table 4.13.

Table 4.13. Summary of resistance factors for end bearing in rock

Design method	Failure criteria	Resistance factors at $\beta_T = 3.00$, φ					Efficiency, φ/λ	
		NCHRP 507 (a)	NHI 05-052(b)	AASHTO 2017 (c)	Ng et al. 2014	This study	Ng et al. 2014	This study
Carter and Kulhawy 1988	1-in Δ	n/a	n/a	n/a	0.22	0.28	0.04	0.03
	5%D for Δ	0.45 to 0.49 (φ/λ: 0.37 to 0.38)	0.55(d)	0.50(d)	0.31	0.36	0.04	0.04
Ng et al. 2014	1-in Δ	n/a	n/a	n/a	0.36	0.07	0.41	0.20
	5%D for Δ	n/a	n/a	n/a	0.71	0.16	0.68	0.24
O'Neill and Reese 1999	1-in Δ	n/a	n/a	n/a	0.22	0.05	0.29	0.15
	5%D for Δ	n/a	n/a	n/a	0.35	0.22	0.40	0.40
Rowe and Armitage 1987	1-in Δ	n/a	n/a	n/a	0.10	0.03	0.30	0.10
	5%D for Δ	n/a	n/a	n/a	0.44	0.14	0.38	0.31
Sowers 1976	1-in Δ	n/a	n/a	n/a	0.64	0.10	0.30	0.24
	5%D for Δ	n/a	n/a	n/a	1.06	0.19	0.38	0.23

(a) calibration performed using reliability theory (FORM); (b) calibration by fitting to ASD; (c) selected value among NCHRP 343 (Barker et al. 1991), NCHRP 507 (Paikowsky et al. 2004), and Allen (2005); (d) based on Canadian Geotechnical Society (1985); LTR = load test report criterion; n/a = not available; Δ = shaft top displacement; D = shaft diameter

Similar to end bearing in cohesive IGM, resistance factors and efficiencies in this study were generally much lower than those obtained in the preliminary calibration. Efficiency values indicates that Sowers (1976) and O'Neill and Reese (1999) would be the most efficient design methods at the Iowa DOT strength criterion and AASHTO criterion, respectively.

4.3. Summary and Recommendations

Following the LRFD resistance factor calibration framework, resistance factors were calibrated using an expanded version of DSHAFT. Eight additional load tests performed in Iowa have been included in the database so that a new calibration could be conducted in order to refine the preliminary values and recommend final values for implementation. The limitations of the analyses and extrapolation procedures developed and used in the preliminary calibration were highlighted, and a different approached based on t-z analysis was proposed and used in quantifying measured shaft resistances at target top displacements of 1 in. and 5% of the shaft diameter. Using the modified FOSM reliability method, resistance factors were calibrated at a target reliability of 3.0 for various skin friction and end bearing prediction methods recommended by O'Neill and Reese (1999), Brown et al. (2010), and several studies in the literature. Two different procedures i.e., Approach I and Approach II, were used in the calibration of skin friction resistance factors. The calibration initially considered load tests performed in Iowa only before including all usable load tests available in the database.

Following Approach I, the calibration generally led to resistance factors that were significantly lower than those obtained in the preliminary calibration as well as values recommended by other studies and AASHTO. The geographic location of the load tests used in the analyses (i.e., Iowa versus other states) had a noticeable effect on the resistance factors associated with O'Neill and Reese (1999) modified α-method and Horvath and Kenney (1979). Resistance factors calibrated using all load tests were greater than those calibrated using Iowa load tests only.

Resistance factors calibrated using Approach II, which was used in the preliminary calibration and is analogic to the total resistance procedure used in other calibration studies, showed some improvements compared to the preliminary calibrated resistance factors and AASHTO. With regard to the geographic location of the load tests used, resistance factors calibrated using Iowa load tests only were greater than those calibrated using all load tests for Horvath and Kenney (1979) and Kulhawy (2005) at both failure criteria considered. For O'Neill and Reese modified α-method, including load tests from other states in the calibration led to an increase of the resistance factor at the AASHTO criterion and a slight decrease at the Iowa DOT criterion.

The preceding discussion illustrates the importance of the procedure used in calibrating resistance factors. Lower resistance factors obtained from Approach I indicates that there is higher uncertainty associated with predicting skin friction locally as opposed to predicting the sum of the skin friction from several layers of the same geomaterial. The effect of the load tests geographic location is also highlighted. Load tests from other states have the general tendency of reducing the resistance factors in Approach I whereas the opposite can be observed in Approach II.

The lack of reliable data for end bearing in soil prevented the calibration of resistance factors for tip resistance in clay and sand. Furthermore, resistance factors could not be calibrated for Iowa load tests only due to limited load test data. Resistance factors for end bearing in cohesive IGM and rock did not show any improvement compared to the preliminary calibration results. Out of the five design methods investigated, the most efficient were O'Neill and Reese (1999) for end bearing in IGM, Sowers (1976) for end bearing in rock at the Iowa DOT criterion, and O'Neill and Reese (1999) for end bearing in rock at the AASHTO criterion.

Considering the calibration results discussed in Section 4.2, the resistance factors recommended for implementation are summarized in Table 4.14.

Table 4.14. Recommended Resistance Factors based on 1-in top displacement criterion

Resistance component	Geomaterial	Analytical method	Resistance factors for $\beta_T = 3.00$, $\varphi^{(c)}$
Side resistance	Cohesive soil	α-method by O'Neill and Reese 1999 (Eq. 2.15): Section 2.3.2.1	0.50
	Cohesionless soil and IGM	β-method O'Neill and Reese 1999 (Eq. 3.4): Section 3.4	0.75
	Cohesive IGM	O′Neill and Reese 1999 (Eq. 2.25): Section 2.3.2.3	0.60
	Rock	Kulhawy et al. 2005 (Eq. 2.31): Section 2.3.2.4	0.65
End bearing	Cohesive soil	Total stress method by O'Neill and Reese 1999: Section 2.3.3.1	$0.40^{(a)}$
	Cohesionless soil and IGM	Effective stress method by Reese and O'Neill 1989: Section 2.3.3.2	$0.50^{(a)}$
	Cohesive IGM	O'Neill and Reese 1999 (Eq. 2.38): Section 2.3.3.3	0.15
	Rock	Sowers 1976 (Eq. 2.39): Section 2.3.3.3	0.10
All	All	Static Load Test	$0.70^{(b)}$

$^{(a)}$ adopted from AASHTO (2017) corresponding to 5% of diameter for top displacement criterion; $^{(b)}$ maximum resistance factor recommended in AASHTO was adopted; $^{(c)}$ if a single-drilled shaft is used to support a bridge pier, the resistance factors should be reduced by 20%

The recommended factors were rounded to the nearest 0.05. With the exception of skin friction in cohesive IGM, all recommended resistance factors associated with skin friction show appreciable improvement compared to preliminary and AASHTO recommended values. The recommended regional factor of 0.60 for skin friction in IGM is the same as the preliminary calibrated value and AASHTO recommended value. The improvements achieved in this calibration stem from the fact that the measured shaft resistances needed in the calibration were determined from the actual strain gauge data of usable load tests along with conservative extrapolation as required rather than using the approximation procedure used by Ng et al. (2014). The measured shaft resistances determined from the approximation procedure included uncertainties associated with the static design methods that are part of the procedure. Thus, the resistance bias values calculated using these so determined measured shaft resistances are expected to be characterized by higher variability and lead to lower resistance factors compared to the approach adopted in the calibration presented in this report. Since there was insufficient data to calibrate resistance factors associated with end bearing prediction in clay and sand, AASHTO recommended values are recommended until regionally calibrated values can be established. As recommended by AASHTO, a maximum resistance factor of 0.70 should be used to account for variability in drilled shaft resistance obtained from static load tests. When a single shaft is used to support a bridge pier, all recommended factors should be reduced by 20% in accordance with AASHTO. The recommended resistance factors must be applied in accordance with the resistance components, geomaterials, and analytical methods used in the calibration to achieve the target reliability considered.

CHAPTER 5. SUMMARY AND FUTURE RESEARCH

5.1. Summary

Because of the numerous limitations associated with ASD, the FHWA has instigated a push for the adoption of LRFD procedures for foundations involved in all federally funded bridges. This transition would improve the assessment of the true level of risk associated with substructure design and lead to more consistent and uniform reliability across designs. While AASHTO has recommended resistance factors to be used in conjunction with particular drilled shaft design methods, states have been allowed the use of higher values at the regional level if they can be backed by sufficient statistical data. A regional calibration is necessary to overcome the major limitations associated with AASHTO recommended resistance factors. Due to the lack of sufficient load test data, all AASHTO resistance factors could not be recommended based solely on reliability analyses. Some factors were recommended based on calibration by fitting to ASD factor of safety, and others were recommended based on a combination of engineering judgment, calibration by fitting, and calibration using reliability theory.

Using a database of 41 load tests from Iowa and several other states, Ng et al. (2014) conducted a preliminary resistance factor calibration. Resistance factors were developed for drilled shaft static design methods recommended by O'Neill and Reese (1999) as well as various design methods for end bearing in rock and IGM available in the literature. A major challenge encountered in the study resided in the fact that the majority of the load tests in the database were terminated at relatively low displacements or before full mobilization of the shafts' resistance. Thus, measured resistances corresponding to the selected strength criteria could not be obtained without resorting to extrapolation. Three extrapolation procedures were developed by Ng et al. (2014) to overcome this challenge and estimate the necessary information. Resistance factors for each resistance component (i.e., side resistance, end bearing, and total resistance) and geomaterial were determined based on the following criteria: (1) maximum measured load reported in the load test reports; (2) 1-in. top displacement; and (3) 5% of shaft diameter for top displacement. The calibrated factors showed some improvements except for skin friction in clay and sand.

The overall goal of this research was to develop and recommend refined resistance factors for the design and construction of drilled shafts in axial compression for the state of Iowa. To achieve this objective, a thorough literature review on the LRFD calibration framework, reliability theory, drilled shaft design philosophy, design methods, construction methods, load testing methods, and the state of regional LRFD studies in various states was conducted in Chapter 2. The load test data available in the expanded DSHAFT were analyzed and the results are presented in Chapter 3 and the four appendices. The limitations of the analyses and extrapolation procedures used in the preliminary calibration were highlighted, and a different approach based on t-z analysis was proposed and used in quantifying measured shaft resistances at target top displacements of 1 in. and 5% of the shaft diameter. In Chapter 4, the drilled shaft resistance bias was statistically characterized and the resistance factors were determined. Using the modified FOSM reliability method, resistance factors were calibrated at a target reliability of 3.0 for various skin friction and end bearing prediction methods. Two different procedures, i.e., Approach I and Approach II, were used in the calibration of skin friction resistance factors. The calibration initially considered load tests performed in Iowa only before including all usable load tests available in the database.

5.2. Recommendations for Future Research

The resistance factors calibrated in this study show significant progress and represent a major step forward toward the development and implementation of complete LRFD guidelines for the design and construction of drilled shafts in Iowa. In light of the challenges encountered and to continuously refine the resistance factors and improve design efficiency, the following recommendations are made:

- Continuously increase the regional drilled shaft test data in DSHAFT.
- Conduct detailed soil and rock investigations at demonstration shafts' location beyond the typical SPT.
- Verify the recommended resistance factors by performing controlled O-cell load tests in Iowa and making appropriate revisions.
- Ensure that any future load tests are conducted to large displacements or complete geotechnical failure.
- Develop and recommend regional resistance factors for end bearing in cohesive and cohesionless soils as additional data become available.
- Using adequate data from load tests performed in Iowa, develop state-specific drilled shaft design methods that further increase drilled shaft design efficiency.

REFERENCES

Abu-Farsakh, M. Y., X. Yu, S. Yoon, and C. Tsai. 2010. *Calibration of Resistance Factors Needed in the LRFD Design of Drilled Shafts*. Louisiana Transportation Research Center, Baton Rouge, LA.

Abu-Farsakh, M., Q. Chen, and M. Haque. 2013. *Calibration of Resistance Factors of Drilled Shafts for the New FHWA Design Method*. Louisiana Transportation Research Center, Baton Rouge, LA.

Allen, T. M. 2005. *Development of Geotechnical Resistance Factors and Downdrag Load Factors for LRFD Foundation Strength Limit State Design*. FHWA-NHI-05-052. Federal Highway Administration and National Highway Institute, Washington, DC.

AASHTO. 2012. *AASHTO LRFD Bridge Design Specifications*. American Association of State Highway and Transportation Officials, Washington, DC.

AASHTO. 2017. *AASHTO LRFD Bridge Design Specifications*. Eighth Edition. American Association of State Highway and Transportation Officials, Washington, DC.

Anderson, T. W. and D. A. Darling. 1952. Asymptotic Theory of Certain "Goodness-Of-Fit" Criteria Based on Stochastic Processes. *Annals of Mathematical Statistics*, Vol. 23, No. 2, pp. 193–212. https://projecteuclid.org/download/pdf_1/euclid.aoms/1177729437.

Barker, R. M., J. M. Duncan|, K. B. Rojiani, P. S. K. Ooi, C. K. Tan, and S. G. Kim. 1991. *NCHRP Report 343: Manuals for the Design of Bridge Foundations*. National Cooperative Highway Research Program, Washington, DC. http://onlinepubs.trb.org/onlinepubs/nchrp/nchrp_rpt_343.pdf.

Bieniawski, Z. T. 1984. *Rock Mechanics Design in Mining and Tunneling*. A. A. Balkema, Rotterdam/Boston, MA. p. 272.

Bjerrum, L. 1972. Embankments on Soft Ground. *Performance of Earth and Earth-Supported Structures Conference Proceedings*, Vol. II, pp. 1−54.

Bloomquist, D., M. McVay, and Z. Hu. 2007. *Updating Florida Department of Transportation's (FDOT) Pile/Shaft Design Procedures Based on CPT & DTP Data*. Department of Civil and Coastal Engineering, University of Florida, Gainesville, FL. https://ftp.fdot.gov/file/d/FTP/FDOT%20LTS/CO/research/Completed_Proj/Summary_SMO/FDOT_BD545_43_rpt.pdf.

Bowles, E. J. 1982. *Foundation Analysis and Design*. The McGraw-Hill Companies, Inc.

Brown, D. A., J. P. Turner, and R. J. Castelli. 2010. *Drilled Shafts: Construction Procedures and LRFD Design Methods.* NHI Course No. 132014, Geotechnical Engineering Circular No. 10. National Highway Institute and Federal Highway Administration, Washington, DC.

Canadian Geotechnical Society. 1985. *Canadian Foundation Engineering Manual*. Second Edition. Canadian Geotechnical Society, Richmond, British Columbia, Canada.

Carter, J. P. and F. H. Kulhawy. 1988. *Analysis and Design of Drilled Shaft Foundations Socketed into Rock*. EL-5918. Electric Power Research Institute, Palo Alto, CA.

Chen, Y.-J. and F. H. Kulhawy. 2002. Evaluation of Drained Axial Capacity for Drilled Shafts. International Deep Foundations Congress 2002, February 14–16, Orlando, FL. pp. 1200–1214.

Chua, K. M., R. Meyers, and N. C. Samtani. 2000. Evolution of a Load Test and Finite Element Analysis of Drilled Shafts in Stiff Soils. GeoDenver, August 5–8, Denver, CO.

Fellenius, B. H. 2015. Using UniPile to Fit t-z or q-z Functions to Load-Movement Records. Second International Congress of Deep Foundations, May 12–15, Santa Cruz, Bolivia. https://www.fellenius.net/papers/347%20Fitting%20t-z%20q-z%20functions%20in%20UniPile%202nd%20CFPB.pdf.

Fortier, A. R. 2016. Calibration of Resistance Factors Needed in the LRFD Design of Drilled Shafts. Master's thesis, Louisiana State University and Agricultural and Mechanical College, Baton Rouge, LA.

Garder, J. A., K. W. Ng, S. Sritharan, and M. J. Roling. 2012. *Development of a Database for Drilled SHAft Foundation Testing (DSHAFT)*. Bridge Engineering Center, Iowa State University, Ames, IA. https://intrans.iastate.edu/app/uploads/2018/03/DSHAFT_Final_Report_June_2012.pdf.

Goodman, R. E. 1980. *Introduction to Rock Mechanics*. Wiley, New York, NY.

Hassan, K. M, M. W. O'Neill, S. A. Sheikh, and C. D. Ealy. 1997. Design method for Drilled Shafts in Soft Argillaceous Rock. *Journal of Geotechnical and Geoenvironmental Engineering*, Vol. 123, No.3, pp. 272−280.

Hoek, E. and E. T. Brown. 1988. The Hoek–Brown Failure Criterion—A 1988 Update. *Rock Engineering for Underground Excavations: Proceedings of the 15th Canadian Rock Mechanics Symposium*, Toronto, ON, Canada, pp. 31–38.

Horvath, R. G. and T. C. Kenney. 1979. Shaft Resistance of Rock Socketed Drilled Piers. *Proceedings of the Symposium on Deep Foundations*, pp. 182–214.

Horvath, R. G., T. C. Kenney, and P. Kozicki. 1983. Methods of Improving the Performance of Drilled Piers in Weak Rock. *Canadian Geotechnical Journal*, Vol. 20, No. pp. 758–772.

Iowa DOT. 2011. *LRFD Bridge Design Manual* – Section 6.3: Drilled Shafts. Iowa Department of Transportation, Ames, IA.

Kulhawy, F. H., S. O. Akbas, and W. A. Prakoso. 2005. Evaluation of Capacity of Rock Foundation Sockets. Alaska Rocks 2005, 40th U.S. Symposium on Rock Mechanics, June 25–29, Anchorage, AK.

Kulhawy, F. H. and K. K. Phoon. 2006. Some Critical Issues in Geo-RBD Calibrations for Foundations. GeoCongress 2006: Geotechnical Engineering in the Information Technology Age, February 26–March 1, Atlanta, GA.

Lee, J. S. and Y. H. Park. 2008. Equivalent Pile Load-Head Settlement Curve Using a Bi-Directional Pile Load Test. *Computers and Geotechnics*, Vol. 35, No. 2, pp. 124–133.

LOADTEST, Inc. 2010. *Report on Drilled Shaft Load Testing (Osterberg Method): Broadway Viaduct - Council Bluffs, IA-TS 3, Project Number - LT – 9640-2.* Longfellow Drilling, Clearfield, IA.

Meyer, P. C., D. V. Holmquist, and H. T. L. Matlock. 1975. Computer Predictions of Axially Loaded Piles with Non-Linear Supports. Offshore Technology Conference, May 5–8, Houston, TX.

Motamed, R., S. Elfass, and K. Stanton. 2016. *LRFD Resistance Factor Calibration for Axially Loaded Drilled Shafts in the Las Vegas Valley*. Nevada Department of Transportation, Carson City, NV. https://www.nevadadot.com/home/showdocument?id=3798.

Ng, T.-T. and S. Fazia. 2012. *Development and Validation of a Unified Equation for Drilled Shaft Foundation Design in New Mexico*. University of New Mexico, Civil Engineering Department, Albuquerque, NM.

Ng, K. W., S. Sritharan, and J. C. Ashlock. 2014. *Development of Preliminary Load and Resistance Factor Design of Drilled Shafts in Iowa*. Bridge Engineering Center, Institute of Transportation, Ames, IA. https://intrans.iastate.edu/app/uploads/2018/03/prelim_drilled_shaft_LRFD_w_cvr2-1.pdf.

Nowak, A. 1999. *Calibration of LRFD Bridge Design Code*. NCHRP Report 368, Transportation Research Board, Washington, DC.

O'Neill, M. W. and K. M. Hassan. 1994. Drilled Shafts: Effects of Construction on Performance and Design Criteria, *Proceedings: International Conference on Design and Construction of Deep Foundations*, December 6–8, Orlando, FL, pp. 137–187. https://ntrl.ntis.gov/NTRL/dashboard/searchResults/titleDetail/PB97103972.xhtml.

O'Neill, M. W. and L. C. Reese. 1999. *Drilled Shafts: Construction Procedures and Design Methods.* FHWA-IF-99-025. Federal Highway Administration, Washington, DC.

O'Neill, M. W., F. C. Townsend, K. M. Hassan, A. Buller, and P. S. Chan. 1996. *Load Transfer for Drilled Shafts in Intermediate Geomaterials*. FHWA-RD-95-171, Federal Highway Administration, McClean, VA.

Paikowsky, S. G. with contributions from B. Birgisson, M. McVay, T. Nguyen, C. Kuo, G. Baecher, B. Ayyab, K. Stenersen, K. O'Malley, L. Chernauskas, and M. O'Neill. 2004. *NCHRP Report 507: Load and Resistance Factor Design (LRFD) for Deep Foundations*. National Cooperative Highway Research Program, Washington, DC. http://140.112.12.21/issmge/missing/nchrp507.pdf.

Reese, L. C. and M. W. O'Neill. 1989. New Design Method for Drilled Shafts from Common Soil and Rock Tests. *Foundation Engineering: Current Principles and Practices Conference Proceedings*, Vol. 2, pp. 1026–1039.

Roling, M., S. Sritharan, and M. Suleiman. 2010. *Development of LRFD Procedures for Bridge Pile Foundations in Iowa – Volume I: An Electronic Database for PIle LOad Tests (PILOT)*. Bridge Engineering Center, Iowa State University, Ames, IA. https://intrans.iastate.edu/app/uploads/2018/03/tr-573_lrfd_vol_1_w_cvr.pdf.

Rowe, R. K. and H. H. Armitage. 1987. A Design Method for Drilled Piers in Soft Rock. *Canadian Geotechnical Journal*, Vol. 24, No. 1, pp. 126–142.

Sowers, G. F. 1976. Foundation Bearing in Weathered Rock. *Rock Engineering for Foundations and Slopes Conference Proceedings*, pp. 32–42.

Terzaghi, K. 1943. *Theoretical Soil Mechanics.* John Wiley and Sons, Inc., New York, NY.

Tomlinson, M. J. 1971. Some Effects of Pile Driving on Skin Friction. *Conference on Behavior of Piles Proceedings*, pp. 107−114.

U.S. Army Corps of Engineers. 1994. *Rock Foundations*. EM 1110-1-2908, Washington, DC.

Withiam, J. L., E. P. Voytko, R. M. Barker, J. M. Duncan, B. C. Kelly, S. C. Musser, and V. Elias. 1998. *Load and Resistance Factor Design (LRFD) for Highway Bridge Substructures*. FHWA HI-98-032. Federal Highway Administration, Washington, DC.

Yang, X., J. Han, and R. L. Parsons. 2010. *Development of Recommended Resistance Factors for Drilled Shafts in Weak Rocks Based on O-Cell Tests*. University of Kansas and Kansas Department of Transportation, Lawrence and Topeka, KS.

APPENDIX A. DSHAFT DATA

Table A.1. A summary of DSHAFT data

ID	State	Shaft diameter (ft)	Embedded length (ft)	Concrete f_c' (ksi)	Geomaterials		Rock/IGM socket	Construction method	Testing method	Usable data
					Shaft	Base				
1	IA	4	67.9	4.47	Clay	IGM[(a)]	Yes	Wet	Osterberg	No
2	IA	3	12.7	5.86	Rock	Rock	Yes	Wet	Osterberg	Yes
3	IA	4	65.8	3.8	Clay+Rock	Rock	Yes	Wet	Osterberg	Yes
4	IA	3.5	72.7	3.44	Mixed+IGM	IGM	Yes	Casing	Osterberg	Yes
5	IA	4	79.3	3.9	Clay+IGM+Rock	Rock	Yes	Wet	Osterberg	Yes
6	IA	2.5	64	3.48	Clay	Clay	No	Casing	Osterberg	Yes
7	IA	3	34	4.1	Clay+Rock	Rock	Yes	Wet	Osterberg	Yes
8	IA	5.5	105.2	3.8	Mixed+Rock	Rock	Yes	Casing	Osterberg	Yes
9	IA	5	66.25	5.78	Sand	Sand	No	Wet	Statnamic	Yes
10	IA	5	55.42	5.58	Mixed	Sand	No	Wet	Statnamic	Yes
11	IA	5	54.78	5.77	Mixed	Sand	No	Wet	Statnamic	Yes
12	MN	6.5	93.9	4.819	Sand+Rock[(a)]	Rock[(a)]	Yes	Wet	Osterberg	No
13	KS	6	49	6.011	IGM	IGM	Yes	Dry	Osterberg	Yes
14	MO	6	40.6	6	IGM+Rock	IGM	Yes	Dry	Osterberg	Yes
15	KS	3.5	19	4.55	IGM	IGM	Yes	Wet	Osterberg	Yes
16	KS	6	34	5.62	IGM	IGM	Yes	Dry	Osterberg	Yes
17	KY	8	105.2	n/a	IGM+Rock	Rock	Yes	Wet	Osterberg	Yes
18	MO	6.5	69.5	7.52	Sand+IGM[(a)]	IGM[(a)]	Yes	Wet	Osterberg	No
19	KS	6	26.24	5.419	IGM	IGM	Yes	Dry	Osterberg	Yes
20	MN	6	55.3	5.9	Sand	Sand	No	Casing	Osterberg	Yes
21	KS	5	93.99	6.47	Sand+IGM[(a)]	IGM[(a)]	Yes	Dry	Osterberg	No
22	MO	3.83	32	4.07	Mixed+Rock[(a)]	Rock[(a)]	Yes	Wet	Osterberg	No
23	MN	4	28	n/a	Sand+Rock[(a)]	Rock[(a)]	Yes	Casing	Osterberg	No
24	IL	5.17	75.112	5.28	IGM+Rock	Rock[(a)]	Yes	Dry	Osterberg	No
25	IL	3.5	37.5	4.1	Clay+IGM	Rock	Yes	Dry	Osterberg	Yes
26	IA	5	75.17	6.01	Sand	Sand	No	Wet	Osterberg	Yes
27	IA	5	75	5.63	Sand	Sand	No	Wet	Osterberg	Yes
28	TN	4	16	5.771	Rock	Rock	Yes	Dry	Osterberg	Yes
29	TN	4	23	5.9	Rock	Rock	Yes	Dry	Osterberg	Yes
30	NV	4	103	n/a	Mixed	Clay	No	Wet	Osterberg	No
31	NE	4	69.09	4.67	Mixed+IGM	IGM	Yes	Wet	Osterberg	No
32	SD	8	107.3	3.256	Sand+IGM[(a)]	IGM[(a)]	Yes	Wet	Osterberg	No

Table A.1. Summary of DSHAFT data (continued)

ID	State	Shaft diameter (ft)	Embedded length (ft)	Concrete f_c' (ksi)	Geomaterials		Rock/IGM socket	Construction method	Testing method	Usable data
					Shaft	Base				
33	CO	3.5	22.6	3.423	IGM	IGM	Yes	Dry	Osterberg	Yes
34	CO	3.5	16	3.193	Clay	IGM	Yes	Dry	Osterberg	Yes
35	CO	4	25.3	3.41	IGM	IGM	Yes	Casing	Osterberg	Yes
36	CO	3.5	40.6	3.936	Rock	Rock	Yes	Casing	Osterberg	Yes
37	CO	4.5	39.7	n/a	Sand+Rock[a]	Rock[a]	Yes	Dry	Osterberg	No
38	CO	3	11.25	4.88	Rock	Rock	Yes	Dry	Osterberg	Yes
39	CO	4	20	3.54	Rock	Rock	Yes	Casing	Osterberg	Yes
40	IA	4	59.5	3	Clay+IGM[a]	IGM[a]	Yes	Casing	Osterberg	No
41	MO	4.5	28.4	4.075	Rock[a]	Rock[a]	Yes	Casing	Osterberg	No
42	IA	6	87.4	5.341	Clay	Clay	No	Wet	Osterberg	Yes
43	IA	6	96.7	5.573	Mixed+Rock	Rock	Yes	Wet	Osterberg	Yes
44	IA	6.5	98.1	5.66	Mixed+Rock	Rock	Yes	Wet	Osterberg	Yes
45	IA	5.5	142.9	4.073	Sand+Rock[a]	Rock[a]	Yes	Wet	Osterberg	Yes
46	IA	5	77	4.825	Mixed+IGM+ Rock	Rock	Yes	Wet	Osterberg	Yes
47	IA	5	84.92	5.423	Sand+IGM+ Rock	Rock	Yes	Wet	Osterberg	Yes
48	IA	6.5	161.8	3.8	Mixed+IGM[a]	IGM[a]	Yes	Wet	Osterberg	Yes
49	IA	5	94.3	4.273	Mixed	Sand	No	Wet	Osterberg	Yes

ID = identification number, n/a = not available, IGM = intermediate geomaterial, f_c' = concrete compressive strength, [a] assumed geomaterials

Table A.2. Subsurface profile and material parameters for test ID No. 1

Soil layer	Material description	Embedded length (ft)	Material type	Measured parameters	Estimated parameters
1	Firm glacial clay	8.2	Cohesive soil	n/a	n/a
2	Firm silty glacial clay	7.9	Cohesive soil	n/a	n/a
3	Stiff silty clay	20	Cohesive soil	n/a	n/a
4	Firm glacial clay	12.1	Cohesive soil	n/a	n/a
5	Soft shale	16.4	Cohesive IGM or rock	n/a	n/a
6	Firm shale	3.3	Cohesive IGM or rock	n/a	n/a

Table A.3. Subsurface profile and material parameters for test ID No. 2

Soil layer	Material description	Embedded length (ft)	Material type	Measured parameters	Estimated parameters
1	Slightly weathered dolomite	12.7	Rock	q_u (shaft/toe) = 637.2 ksf; RQD = 90%	E_m/E_i = 0.90[(a)]; α_E = 0.96[(d)]; RMR = 81[(b)]; m = 2.035[(c)]; s = 0.0662[(c)]

[(a)] estimated from Table 2.7, [(b)] determined from Table 2.11, [(c)] determined from Table 2.10, [(d)] estimated from Table 2.6

Table A.4. Subsurface profile and material parameters for test ID No. 3

Soil layer	Material description	Embedded length (ft)	Material type	Measured parameters	Estimated parameters
1	Stiff to firm silty glacial clay	39	Clay	N_{60} = 11	S_u = 1.375 ksf[(a)]
2	Firm silty clay	4.92	Clay	N_{60} = 11	S_u = 1.375 ksf[(a)]
3	Clay shale	10.17	Clay	N_{60} = 41	S_u = 4 ksf[(a)]
4	Clay shale	3.61	Cohesive IGM	q_u (shaft) = 77.83 ksf; RQD = 46%	σ_n = 3.9[(b)]; α = 0.11[(c)]; ϕ = 0.58[(d)]
5	Clay shale	7.55	Cohesive IGM	q_u (shaft) = 77.83 ksf; RQD = 62%	σ_n = 3.9[(b)]; α = 0.11[(c)]
6	Clay shale	4.49	Cohesive IGM	q_u (shaft) = 24.37 ksf; q_u (toe) = 24.37 ksf; RQD = 70%	σ_n = 3.9[(b)]; α = 0.20[(c)]; RMR = 50[(e)]; m = 0.3653[(f)]; s = 0.0009[(f)]

[(a)] estimated from Table 2.2, [(b)] estimated using Eq. (2.27), [(c)] determined from Figure 2.3, [(d)] estimated from Table 2.5, [(e)] estimated from Table 2.11, [(f)] estimated from Table 2.10

Table A.5. Subsurface profile and material parameters for test ID No. 4

Soil layer	Material description	Embedded length (ft)	Material type	Measured parameters	Estimated parameters
1	Stiff sandy glacial clay	10.496	Clay	N_{60} = 22	
2	Fine to medium sand	32.5	Sand	N_{60} = 14	γ = 0.114 kcf[(a)]
3	Clay shale	5.51	Rock	q_u (shaft) = 126.41 ksf; RQD = 100%	α_E = 1.0[(g)]
4	Clay shale	6.56	Rock	q_u (shaft) = 101.45 ksf; RQD = 91%	α_E = 0.91[(g)]
5	Clay shale	8.63	Cohesive IGM	q_u (shaft) = 69.06 ksf; RQD = 86%	σ_n = 3.9[(b)]; α = 0.12[(c)]; ϕ = 0.94[(d)]
6	Clay shale	4.33	Cohesive IGM	q_u (shaft) = 70.22 ksf; RQD = 92%	σ_n = 3.9[(b)]; α = 0.11[(c)]; ϕ = 0.97[(d)]
7	Clay shale	4.56	Cohesive IGM	q_u (shaft) = 93.67 ksf; q_u (toe) = 191.81 ksf; RQD = 88%	σ_n = 3.9[(b)]; α = 0.10[(c)]; RMR = 83[(e)]; m = 3.1691[(f)]; s = 0.0741[(f)]

[(a)] estimated from Table 2.4, [(b)] estimated using Eq. (2.27), [(c)] determined from Figure 2.3, [(d)] estimated from Table 2.5, [(e)] estimated from Table 2.11, [(f)] estimated from Table 2.10, [(g)] estimated from Table 2.6

Table A.6. Subsurface profile and material parameters for test ID No. 5

Soil layer	Material description	Embedded length (ft)	Material type	Measured parameters	Estimated parameters
1	Silty sandy lean clay	7.9	Clay	$N_{60} = 5$	$S_u = 0.625$ ksf[(a)]; $\gamma = 0.115$ kcf[(h)]
2	Silty lean clay	4.9	Clay	$N_{60} = 11$	$S_u = 1.375$ ksf[(a)]; $\gamma = 0.127$ kcf[(h)]
3	Silty sandy lean clay	27.6	Clay	$N_{60} = 15$	$S_u = 1.875$ ksf[(a)]; $\gamma = 0.138$ kcf[(h)]
4	Gravel with sand	1.6	Sand	$N_{60} = 50$	$\gamma = 0.15$ kcf[(h)]
5	Black, carboniferous clay shale with traces of pyritization	7.9	Cohesive IGM	$q_u = 39.81$ ksf; RQD = 52%	$\sigma_n = 3.9$[(b)]; $\alpha = 0.16$[(c)]; $\phi = 0.63$[(d)]
6	Light gray, clay shale	15.4	Cohesive IGM	$q_u = 10.14$ ksf; RQD = 65%	$\sigma_n = 3.9$[(b)]; $\alpha = 0.28$[(c)]; $\phi = 0.83$[(d)]
6	Light gray, clay shale	3	Clay	$q_u = 3.76$ ksf; RQD = 42%	$S_u = 1.880$ ksf
7	Clay shale	8.3	Clay	$q_u = 5.80$ ksf; RQD = 23%	$S_u = 2.898$ ksf
8	Carboniferous clay shale	4.5	Rock	q_u (shaft) = 138.63 ksf; q_u (toe) = 191.81 ksf	$\alpha_E = 0.91$[(g)]; RMR = 32[(e)]; m = 0.10186[(f)]; s = 0.00004[(f)]

[(a)] estimated from Table 2.2, [(b)] estimated using Eq. (2.27), [(c)] determined from determined from Figure 2.3, [(d)] estimated from Table 2.5, [(e)] estimated from Table 2.11, [(f)] estimated from Table 2.10, [(g)] estimated from Table 2.6, [(h)] estimated from Table 2.3 and Table 2.4

Table A.7. Subsurface profile and material parameters for test ID No. 6

Soil layer	Material description	Embedded length (ft)	Material type	Measured parameters	Estimated parameters
1	Firm clay fill	5.9	Clay	$N_{60} = 10$	$S_u = 1.250$ ksf[(a)]
2	Stiff silty clay	21	Clay	$N_{60} = 5$	$S_u = 0.625$ ksf[(a)]
3	Firm glacial clay	18.7	Clay	$N_{60} = 13$	$S_u = 1.625$ ksf[(a)]
4	Very firm sandy glacial clay	10.5	Clay	$N_{60} = 24$	$S_u = 3.000$ ksf[(a)]
5	Very firm sandy glacial clay	10	Clay	$N_{60} = 23$	$S_u = 2.875$ ksf[(a)]

[(a)] estimated from Table 2.4

Table A.8. Subsurface profile and material parameters for test ID No. 7

Soil layer	Material description	Embedded length (ft)	Material Type	Measured parameters	Estimated parameters
1	Lean clay	4	Clay	N_{60} = 20	S_u = 2.500 ksf[(a)]; γ = 0.130 kcf[(b)]
2	Lean clay with sand	9	Clay	N_{60} = 10	S_u = 1.250 ksf[(a)]; γ = 0.122 kcf[(b)]
3	Mod weathered limestone	1.1	Rock	q_u = 555.84 ksf; RQD = 79%	α_E = 0.916[(c)]
4	Fresh limestone	2.3	Rock	q_u = 1388.16 ksf; RQD = 79%	α_E = 0.916[(c)]
5	Calcareous sandstone	4.3	Rock	q_u = 862.56 ksf; RQD = 83%	α_E = 0.932[(c)]
6	Fractured limestone with weathered shale	1.3	Rock	q_u = 1175.04 ksf; RQD = 83%	α_E = 0.932[(c)]
7	Fresh limestone	12	Rock	q_u (shaft) = 817.2 ksf; q_u (toe) = 635.04 ksf; RQD = 97%	α_E = 0.988[(c)]; RMR = 86[(d)]; m = 2.70667[(e)]; s = 0.14320[(e)]

[(a)] estimated from Table 2.2, [(b)] estimated from Table 2.4, [(c)] estimated from Table 2.6, [(d)] estimated from Table 2.11, [(e)] estimated from Table 2.10

Table A.9. Subsurface profile and material parameters for test ID No. 8

Soil layer	Material description	Embedded length (ft)	Material type	Measured parameters	Estimated parameters
1	Silty clay	10	Clay	N_{60} = 12	S_u = 1.572 ksf[(a)]; γ = 0.13 kcf[(b)]
2	Silt with minor sand	17	Sand	N_{60} = 2	γ = 0.085 kcf[(b)]
3	Fine to medium sand with fine gravel	42	Sand	N_{60} = 30	γ = 0.13 kcf[(b)]
4	Medium to coarse sand with gravel	21.5	Sand	N_{60} = 21	γ = 0.121 kcf[(b)]
5	Fresh limestone	14.7	Rock	q_u (shaft) = 510.34 ksf; q_u (toe) = 553.40 ksf; RQD = 73%	α_E = 0.892[(c)]; RMR = 86[(d)]; m = 2.70667[(e)]; s = 0.14320[(e)]

[(a)] estimated from Table 2.2, [(b)] estimated from Table 2.3 and Table 2.4, [(c)] estimated from Table 2.6, [(d)] estimated from Table 2.11, [(e)] estimated from Table 2.10

Table A.10. Subsurface profile and material parameters for test ID No. 9

Soil layer	Material description	Embedded length (ft)	Material type	Measured parameters	Estimated parameters
1	Stiff silty clay	10	Clay	N_{60} = 7; c = 0.875 ksf	S_u = 0.875 ksf[(a)]; γ = 0.125 kcf[(b)]
2	Soft to stiff silty clay	10	Clay	N_{60} = 4; c = 0.5 ksf	S_u = 0.5 ksf[(a)]; γ = 0.110 kcf[(b)]
3	Silty fine sand	10	Sand	N_{60} = 13; c = 1.715 ksf	γ = 0.113 kcf[(b)]
4	Fine sand	25	Sand	N_{60} = 20; c = 2.667 ksf	γ = 0.120 kcf[(b)]
5	Soft silty sand	5	Sand	N_{60} = 2; c = 0.25 ksf	γ = 0.085 kcf[(b)]
6	Coarse sand	6.25	Sand	N_{60} = 16; c = 2.134 ksf	γ = 0.116 kcf[(b)]

[(a)] estimated from Table 2.2, [(b)] estimated from Table 2.3 and Table 2.4

Table A.11. Subsurface profile and material parameters for test ID No. 10

Soil layer	Material description	Embedded length (ft)	Material type	Measured parameters	Estimated parameters
1	Stiff silty clay	5	Clay	N_{60} = 12; c = 1.572 ksf	S_u = 1.572 ksf[(a)]; γ = 0.130 kcf[(b)]
2	Soft to stiff silty clay	10	Clay	N_{60} = 7; c = 0.875 ksf	S_u = 0.875 ksf[(a)]; γ = 0.127 kcf[(b)]
3	Soft silty clay	5	Clay	N_{60} = 5; c = 0.625 ksf	S_u = 0.625 ksf[(a)]; γ = 0.122 kcf[(b)]
4	Fine sand	35	Sand	N_{60} = 15; c = 2 ksf	γ = 0.115 kcf[(b)]
5	Coarse sand with trace gravel	0.42	Sand	N_{60} = 18; c = 2.4 ksf	γ = 0.118 kcf[(b)]

[(a)] estimated from Table 2.2, [(b)] estimated from Table 2.3 and Table 2.4

Table A.12. Subsurface profile and material parameters for test ID No. 11

Soil layer	Material description	Embedded length (ft)	Material type	Measured parameters	Estimated parameters
1	Stiff silty clay	5	Clay	N_{60} = 14; c = 0.625 ksf	S_u = 0.625 ksf[(a)]; γ = 0.135 kcf[(b)]
2	Soft to stiff silty clay	15	Clay	N_{60} = 5; c = 1.857 ksf	S_u = 1.857 ksf[(a)]; γ = 0.115 kcf[(b)]
3	Fine sand	34.78	Sand	N_{60} = 17; c = 2.267 ksf	γ = 0.117 kcf[(b)]

[(a)] estimated from Table 2.2, [(b)] estimated from Table 2.3 and Table 2.4

Table A.13. Subsurface profile and material parameters for test ID No. 12

Soil layer	Material description	Embedded length (ft)	Material type	Measured parameters	Estimated parameters
1	Fill/Sand	10	Sand	N_{60} = 14	γ = 0.114 kcf[(a)]
2	Sand w/ gravel dense/ saturated	24	Sand	N_{60} = 57	γ = 0.15 kcf[(a)]
3	Fine sand w/ gravel	18	Sand	N_{60} = 32	γ = 0.112 kcf[(a)]
4	Sandstone	41.9	n/a	n/a	n/a

[(a)] estimated from Table 2.3

Table A.14. Subsurface profile and material parameters for test ID No. 13

Soil layer	Material description	Embedded length (ft)	Material type	Measured parameters	Estimated parameters
1	Fine grained silty sand	7	Sand	n/a	n/a
2	Medium to coarse grained silty sand	15	Sand	n/a	n/a
3	Shale	22	Cohesive IGM	q_u = 15.42 ksf; RQD = 47.5%	σ_n = 3.06[(a)]; α = 0.18[(b)]; ϕ = 0.583[(c)]
4	Sandstone	2	Clay	q_u = 4.15 ksf; RQD = 52%	
5	Shale	3	Clay	q_u (shaft) = 7.62 ksf; q_u (toe) = 7.62 ksf; RQD = 52%	

[(a)] estimated using Eq. (2.27), [(b)] determined from Figure 2.3, [(c)] estimated from Table 2.5

Table A.15. Subsurface profile and material parameters for test ID No. 14

Soil layer	Material description	Embedded length (ft)	Material type	Measured parameters	Estimated parameters
1	Weathered chanute shale	7	Cohesive IGM	q_u = 14.2 ksf	σ_n = 0.34[(a)]; α = 0.17[(b)]; ϕ = 0.45[(c)]
2	Unweathered chanute shale	11	Cohesive IGM	q_u = 19.6 ksf; RQD = 14%	σ_n = 1.22[(a)]; α = 0.15[(b)]; ϕ = 0.45[(c)]
3	Cement city limestone	5	Rock	q_u = 1334 ksf; RQD = 28%	α_E = 0.503[(d)]
4	Quivira shale	6	Cohesive IGM	q_u = 57.2 ksf; RQD = 14%	σ_n = 2.54[(a)]; α = 0.10[(b)]; ϕ = 0.45[(c)]
5	Westerville limestone	7	Rock	q_u = 1810 ksf; RQD = 58%	α_E = 0.735[(d)]
6	Weathered shale	4.6	Rock	q_u (shaft) = 102.4 ksf; q_u (toe) = 99.5 ksf; RQD = 30%	α_E = 0.517[(d)] ; RMR = 32[(e)]; m = 0.10186[(f)]; s = 0.000040[(f)]

[(a)] estimated using Eq. (2.27), [(b)] determined from Figure 2.3, [(c)] estimated from Table 2.5, [(d)] estimated from Table 2.11, [(e)] estimated from Table 2.10, [(f)] estimated from Table 2.6

Table A.16. Subsurface profile and material parameters for test ID No. 15

Soil layer	Material description	Embedded length (ft)	Material type	Measured parameters	Estimated parameters
1	Sandstone	4.86	n/a	q_u = 29.23 ksf; RQD = 20%	σ_n = 0.34[(a)]; α = 0.12[(b)]; ϕ = 0.45[(c)]
2	Competent shale	7.28	Cohesive IGM	q_u = 34.16 ksf; RQD = 35%	σ_n = 0.34[(a)]; α = 0.11[(b)]; ϕ = 0.55[(c)]
3	Shaley sandstone	6.86	Cohesive IGM	q_u (shaft) = 34.16 ksf; q_u (toe) = 34.16 ksf; RQD = 85%	σ_n = 0.34[(a)]; α = 0.11[(b)]; ϕ = 0.94[(c)]; RMR = 83[(d)]; m = 4.7491[(e)]; s = 0.07409[(e)]

[(a)] estimated using Eq. (2.27), [(b)] determined from Figure 2.3, [(c)] estimated from Table 2.5, [(d)] estimated from Table 2.10, [(e)] estimated from Table 2.6

Table A.17. Subsurface profile and material parameters for test ID No. 16

Soil layer	Material description	Embedded length (ft)	Material type	Measured parameters	Estimated parameters
1	Silty clay (with casing)	4.8	n/a	n/a	n/a
2	Shale (with casing)	6.42	n/a	n/a	n/a
3	Shale	22.78	Cohesive IGM	q_u (shaft) = 35.12 ksf; q_u (toe) = 49.1 ksf; RQD = 85%	σ_n = 2.69[a]; α = 0.113[b]; ϕ = 0.45[c]; RMR = 32[d]; m = 0.10186[e]; s = 0.000042[e]

[a] estimated using Eq. (2.27), [b] determined from Figure 2.3, [c] estimated from Table 2.5, [d] estimated from Table 2.10, [e] estimated from Table 2.6

Table A.18. Subsurface profile and material parameters for test ID No. 19

Soil layer	Material description	Embedded length (ft)	Material type	Measured parameters	Estimated parameters
1	Overburden soil	70.8	n/a	n/a	n/a
2	Shale soft to very soft	16	Cohesive IGM	q_u = 43.2 ksf; RQD = 53%	σ_n = 3.9[a]; α = 0.16[b]; ϕ = 0.649[c]
3	Coal	2	Cohesive IGM	q_u = 28.8 ksf; RQD = 60%	σ_n = 3.9[a]; α = 0.22[b]; ϕ = 0.763[c]
4	Gray shale—soft	7.9	Cohesive IGM	q_u = 43.2 ksf; RQD = 60%	σ_n = 3.9[a]; α = 0.16[b]; ϕ = 0.763[c]
5	Gray shale—medium hard to hard	1.6	Rock	q_u = 187.5 ksf; RQD = 60%	α_E = 0.763[d]
6	Gray shale—soft	2.3	Rock	q_u = 144 ksf; RQD = 60%	α_E = 0.763[d]
7	Gray sandy shale—soft	4.6	Cohesive IGM	q_u = 72 ksf; RQD = 58%	σ_n = 3.9[a]; α = 0.14[b]; ϕ = 0.735[c]
8	Gray shale—medium hard to hard	0	Rock	q_u (toe) = 93.5 ksf; RQD = 75%	RMR = 73[e]; m = 1.865[f]; s = 0.0346[f]

[a] estimated using Eq. (2.27), [b] determined from Figure 2.3, [c] estimated from Table 2.5, [d] estimated from Table 2.11, [e] estimated from Table 2.10, [f] estimated from Table 2.6

Table A.19. Subsurface profile and material parameters for test ID No. 18

Soil layer	Material description	Embedded length (ft)	Material type	Measured parameters	Estimated parameters
1	Medium and coarse dense sand	18.5	Sand	n/a	n/a
2	Clay shale	51	n/a	n/a	n/a

Table A.20. Subsurface profile and material parameters for test ID No. 19

Soil layer	Material description	Embedded length (ft)	Material type	Measured parameters	Estimated parameters
1	Overburden alluvium soil	0	n/a	n/a	n/a
2	Shale	10.7	Cohesive IGM	q_u = 25.8 ksf; RQD = 39.33%	σ_n = 0.63[(a)]; α = 0.13[(b)]; ϕ = 0.545[(c)]
3	Shale	9.5	Cohesive IGM	N_{60} = 86; q_u = 17.11 ksf; RQD = 74%	σ_n = 1.73[(a)]; α = 0.21[(b)]; ϕ = 0.87[(c)]
4	Sandstone	6.04	Clay	q_u = 4.24 ksf; RQD = 47%	

[(a)] estimated using Eq. (2.27), [(b)] determined from Figure 2.3, [(c)] estimated from Table 2.5

Table A.21. Subsurface profile and material parameters for test ID No. 20

Soil layer	Material description	Embedded length (ft)	Material type	Measured parameters	Estimated parameters
1	Loamy sand	6	Sand	N_{60} = 8	γ = 0.105 kcf[(a)]
2	Sand with organic matter	3	Sand	N_{60} = 10	γ = 0.115 kcf[(a)]
3	Sandy loam	2	Sand	N_{60} = 8	γ = 0.107 kcf[(a)]
4	Sand	5	Sand	N_{60} = 19	γ = 0.119 kcf[(a)]
5	Sand	9	Sand	N_{60} = 32	γ = 0.112 kcf[(a)]
6	Sand w/ gravel	4	Sand	N_{60} = 30	γ = 0.130 kcf[(a)]
7	sand and gravel	6	Sand	N_{60} = 25	γ = 0.125 kcf[(a)]
8	Loamy fine sand	5	Sand	N_{60} = 37	γ = 0.121 kcf[(a)]
9	Sand w/ gravel	5	Sand	N_{60} = 60	γ = 0.150 kcf[(a)]
10	Loamy sand	5	Sand	N_{60} = 39	γ = 0.124 kcf[(a)]
11	Loamy sand	5.3	Sand	N_{60} = 46	γ = 0.134 kcf[(a)]

[(a)] estimated from Table 2.3

Table A.22. Subsurface profile and material parameters for test ID No. 21

Soil layer	Material description	Embedded length (ft)	Material type	Measured parameters	Estimated parameters
1	Silty shale	93.99	n/a	n/a	n/a

Table A.23. Subsurface profile and material parameters for test ID No. 22

Soil layer	Material description	Embedded length (ft)	Material type	Measured parameters	Estimated parameters
1	Weathered shaley limestone	4.9	n/a	n/a	n/a
2	Fine grained sandstone	14.8	n/a	n/a	n/a
3	Moderately hard shale	12.3	n/a	n/a	n/a

Table A.24. Subsurface profile and material parameters for test ID No. 23

Soil layer	Material description	Embedded length (ft)	Material type	Measured parameters	Estimated parameters
1	Friable sandstone	28	n/a	n/a	n/a

Table A.25. Subsurface profile and material parameters for test ID No. 24

Soil layer	Material description	Embedded length (ft)	Material type	Measured parameters	Estimated parameters
1	Sandstone	0.72	n/a	n/a	n/a
2	GR laminated shale	17.32	Cohesive IGM	q_u = 16.71 ksf; RQD = 50%	$\alpha = 0.16$[(a)]; $\phi = 0.6$[(b)]
3	GR to GRN GR massive shale	2	Cohesive IGM	q_u = 8.35 ksf; RQD = 63%	$\alpha = 0.2$[(a)]; $\phi = 0.7625$[(b)]
4	LT GR to GRN GR laminated shale	3	Cohesive IGM	q_u = 16.71 ksf; RQD = 71%	$\alpha = 0.16$[(a)]; $\phi = 0.85$[(b)]
5	Massive silty shale	17	Rock	q_u = 223.47 ksf; RQD = 75%	$\alpha_E = 0.613$[(c)]
6	Francis Creek shale	35.136	Rock	q_u (shaft) = 223.4 ksf; RQD (shaft) = 75%; (No geomaterial information beneath the shaft base)	$\alpha_E = 0.613$[(c)]

(a) determined from Figure 2.3, (b) estimated from Table 2.5, (c) estimated from Table 2.11

Table A.26. Subsurface profile and material parameters for test ID No. 25

Soil layer	Material description	Embedded length (ft)	Material type	Measured parameters	Estimated parameters
1	Sandy loam and shaley clay	9.84	Clay	$N_{60} = 5$	$S_u = 0.625$ ksf[d]
2	Very dense shale	3.5	Clay	$N_{60} = 27$; $q_u = 5.64$ ksf; RQD = 0%	$S_u = 3.375$ ksf
3	Shale	17.5	Clay	$q_u = 5.64$ ksf; RQD = 0%	$S_u = 2.820$ ksf
4	Sandstone	6.65	Cohesive IGM	$q_u = 50.4$ ksf; RQD = 35%	$\sigma_n = 3.33$ [a]; $\alpha = 0.14$[b]; $\phi = 0.525$[c]
5	Sandstone (toe)	0	Rock	q_u (toe) = 231.3 ksf; RQD (toe) = 60%	RMR = 54[e]; m = 0.73024[f]; s = 0.00144[f]

[a] estimated using Eq. (2.27), [b] determined from Figure 2.3, [c] estimated from Table 2.5, [d] estimated from Table 2.2, [e] estimated from Table 2.11, [f] estimated from Table 2.10

Table A.27. Subsurface profile and material parameters for test ID No. 26

Soil layer	Material description	Embedded length (ft)	Material type	Measured parameters	Estimated parameters
1	Lean clay	10	Clay	$N_{60} = 7$	$S_u = 0.875$ ksf[a]; $\gamma = 0.120$ kcf[b]
2	Fine sand	8.5	Sand	$N_{60} = 4$	$\gamma = 0.090$ kcf[b]
3	Silty clay	5	Clay	$N_{60} = 3$	$S_u = 0.375$ ksf[a]; $\gamma = 0.110$ kcf[b]
4	Fine sand	10	Sand	$N_{60} = 9$	$\gamma = 0.111$ kcf[b]
5	Fine sand	10	Sand	$N_{60} = 6$	$\gamma = 0.098$ kcf[b]
6	Fine sand	11.5	Sand	$N_{60} = 12$	$\gamma = 0.112$ kcf[b]
7	Fine sand	20.2	Sand	$N_{60} = 11$	$\gamma = 0.111$ kcf[b]

[a] estimated from Table 2.2, [b] estimated from Table 2.3 and Table 2.4

Table A.28. Subsurface profile and material parameters for test ID No. 27

Soil layer	Material description	Embedded length (ft)	Material type	Measured parameters	Estimated parameters
1	Lean clay	10	Clay	$N_{60} = 7$	$S_u = 0.875$ ksf[(a)]; $\gamma = 0.125$ kcf[(b)]
2	Fine sand	8.5	Sand	$N_{60} = 5$	$\gamma = 0.094$ kcf[(b)]
3	Silty clay	5	Clay	$N_{60} = 5$	$S_u = 0.625$ ksf[(a)]; $\gamma = 0.115$ kcf[(b)]
4	Fine sand	2.5	Sand	$N_{60} = 4$	$\gamma = 0.090$ kcf[(b)]
5	Fine sand	15	Sand	$N_{60} = 11$	$\gamma = 0.111$ kcf[(b)]
6	Fine sand	5	Sand	$N_{60} = 6$	$\gamma = 0.098$ kcf[(b)]
7	Fine sand	5	Sand	$N_{60} = 14$	$\gamma = 0.114$ kcf[(b)]
8	Fine sand	4	Sand	$N_{60} = 38$	$\gamma = 0.122$ kcf[(b)]
9	Fine sand	20	Sand	$N_{60} = 19$	$\gamma = 0.119$ kcf[(b)]

(a) estimated from Table 2.2, (b) estimated from Table 2.3 and Table 2.4

Table A.29. Subsurface profile and material parameters for test ID No. 28

Soil layer	Material description	Embedded length (ft)	Material type	Measured parameters	Estimated parameters
1	Limestone	2.5	Rock	$q_u = 1744.63$ ksf; RQD = 26%	$\alpha_E = 0.49$[(a)]
2	Limestone	5	Rock	$q_u = 904.56$ ksf; RQD = 26%	$\alpha_E = 0.49$[(a)]
3	Limestone	5	Rock	$q_u = 1218.43$ ksf; RQD = 38%	$\alpha_E = 0.558$[(a)]
4	Limestone	3.5	Rock	q_u (shaft) = 775.44 ksf; RQD (shaft) = 37%; q_u (toe) = 775.44 ksf; RQD (toe) = 53%	$\alpha_E = 0.555$[(a)]; RMR = 59[(b)]; m = 0.44729[(c)]; s = 0.00212[(c)]

(a) estimated from Table 2.6, (b) estimated from Table 2.11, (c) estimated from Table 2.10

Table A.30. Subsurface profile and material parameters for test ID No. 29

Soil layer	Material description	Embedded length (ft)	Material type	Measured parameters	Estimated parameters
1	Limestone	6	Rock	n/a	
2	Limestone	5	Rock	q_u = 1080 ksf; RQD = 19%	α_E = 0.45[a]
3	Limestone	5	Rock	q_u = 2934 ksf; RQD = 42%	α_E = 0.568[a]
4	Limestone	5	Rock	q_u = 1720.8 ksf; RQD = 52%	α_E = 0.629[a]
5	Limestone	2	Rock	q_u (shaft) = 3024 ksf; RQD (shaft) = 54%; q_u (toe) = 2966.4 ksf; RQD (toe) = 60%	α_E = 0.670[a]; RMR = 67[b]; m = 0.75750[c]; s = 0.01084[c]

[a] estimated from Table 2.6, [b] estimated from Table 2.11, [c] estimated from Table 2.10

Table A.31. Subsurface profile and material parameters for test ID No. 30

Soil layer	Material description	Embedded length (ft)	Material type	Measured parameters	Estimated parameters
1	Caliche	3	Sand	N_{60} = 50	γ = 0.15 kcf[a]
2	Clayey sand	8	Sand	N_{60} = 29	γ = 0.129 kcf[a]
3	Caliche	6.5	Sand	N_{60} = 200	γ = 0.15 kcf[a]
4	Clay w/ sand	5.5	Clay	N_{60} = 6	γ = 0.12 kcf[a]; S_u = 0.636 ksf
5	Silty, clayey sand	5	Sand	N_{60} = 16	γ = 0.116 kcf[a]
6	Clayey sand	10	Sand	N_{60} = 15	γ = 0.115 kcf[a]
7	Sandy clay	3	Clay	N_{60} = 60	γ = 0.14 kcf[a]; S_u = 6.36 ksf
8	Caliche	2	Sand	N_{60} = 50	γ = 0.15 kcf[a]
9	Clayey sand	6	Sand	N_{60} = 24	γ = 0.124 kcf[a]
10	Caliche	1.5	Sand	N_{60} = 150	γ = 0.15 kcf[a]
11	Sandy clay	5	Clay	N_{60} = 19	γ = 0.124 kcf[a]; S_u = 2.014 ksf
12	Silty clay	5	Clay	N_{60} = 18	γ = 0.124 kcf[a]; S_u = 1.908 ksf
13	Sandy clay	6.5	Clay	N_{60} = 40	γ = 0.14 kcf[a]; S_u = 4.24 ksf
14	Silty sand	4	Sand	N_{60} = 11	γ = 0.111 kcf[a]
15	Sandy clay	7	Clay	N_{60} = 25	γ = 0.131 kcf[a]; S_u = 2.65 ksf
16	Silty sand	3	Sand	N_{60} = 8	γ = 0.107 kcf[a]
17	Sandy clay	22	Clay	n/a	n/a)

[a] estimated from Table 2.3 and Table 2.4

Table A.32. Subsurface profile and material parameters for test ID No. 31

Soil layer	Material description	Embedded length (ft)	Material type	Measured parameters	Estimated parameters
1	Fine to medium sand	35	Sand	N_{60} = 17	n/a
2	Fat clay	6	Clay	N_{60} = 12; q_u = 1 ksf	n/a
3	Sandy lean clay	9	Clay	N_{60} = 13	n/a
4	Fine to medium sand-weathered sandstone	11	Sand	N_{60} = 47	n/a
5	Lean clay-weathered shale	8.9	Cohesive IGM	q_u = 7.5 ksf	n/a

Table A.33. Subsurface profile and material parameters for test ID No. 32

Soil layer	Material description	Embedded length (ft)	Material type	Measured parameters	Estimated parameters
1	Loose to medium dense sand	21	Sand	N_{60} = 11	n/a
2	Medium dense fine grained sand	11.5	Sand	N_{60} = 20	n/a
3	Hard shale	74.8	n/a	N_{60} = 48	n/a

Table A.34. Subsurface profile and material parameters for test ID No. 33

Soil layer	Material description	Embedded length (ft)	Material type	Measured parameters	Estimated parameters
1	Firm to medium claystone bedrock	10	Cohesive IGM	N_{60} = 32; q_u = 8.3 ksf; RQD = 50%	$\alpha = 0.2^{(a)}$; $\phi = 0.6^{(b)}$
2	Medium hard to hard brown claystone w/ sandstone	6.1	Cohesive IGM	N_{60} = 55; q_u = 12.3 ksf; RQD = 50%	$\alpha = 0.22^{(a)}$; $\phi = 0.6^{(b)}$
3	Medium hard to hard brown claystone w/ sandstone	0	Cohesionless IGM	N_{60} = 58; q_u = 13.1 ksf; RQD = 50%	n/a

(a) determined from Figure 2.3, (b) determined from Table 2.5

Table A.35. Subsurface profile and material parameters for test ID No. 34

Soil layer	Material description	Embedded length (ft)	Material type	Measured parameters	Estimated parameters
1	Medium hard brown silty and very weak sandstone bedrock	2	Sand	N_{60} = 30	γ = 0.12 kcf[(a)]
2	Medium hard claystone bedrock layer (olive to light gray)	14	Clay	N_{60} = 37; q_u = 6.05 ksf; RQD = 50%	γ = 0.106 kcf[(a)]; S_u = 3.024 ksf
3	Hard claystone bedrock (toe)	0	Cohesive IGM	N_{60} (toe) = 61; q_u (toe) = 16.85 ksf; RQD (toe) = 50%	γ = 0.111 kcf[(a)]

[(a)] estimated from Table 2.3 and Table 2.4

Table A.36. Subsurface profile and material parameters for test ID No. 35

Soil layer	Material description	Embedded length (ft)	Material type	Measured parameters	Estimated parameters
1	Sandy and clayey sand soils	4.5	Sand	n/a	n/a
2	Very hard sandy to very sandy claystone w/ very clayey sandstone interbeds	20.8	Cohesive IGM	N_{60} = 150; q_u = 63.94 ksf; RQD = 80%	α = 0.1[(a)]; ϕ = 0.9[(b)]
3	Very hard dark gray and very sandy claystone	0	Cohesive IGM	N_{60} = 120; q_u = 71 ksf; RQD = 80%	n/a

[(a)] determined from Figure 2.3, [(b)] determined from Table 2.5

Table A.37. Subsurface profile and material parameters for test ID No. 36

Soil layer	Material description	Embedded length (ft)	Material type	Measured parameters	Estimated parameters
1	Light brown claystone	3	Rock	N_{60} = 200; q_u = 97.056 ksf; RQD = 75%	α_E = 0.90[a]
2	Very clayey, fine to medium grained, well cemented sandstone	15	Rock	N_{60} = 218; q_u = 293.04 ksf; RQD = 85%	α_E = 0.94[a]
3	Blue clayey to very clayey sandstone bedrock	12.1	Rock	N_{60} = 166; q_u (shaft) = 219.024 ksf; q_u (toe) = 219.024 ksf; RQD = 75%	α_E = 0.90[a]; RMR = 58[b]; m = 0.396[c]; s = 0.001577[c]

[a] determined from Table 2.6, [b] determined from Table 2.11, [c] determined from Table 2.10

Table A.38. Subsurface profile and material parameters for test ID No. 37

Soil layer	Material description	Embedded length (ft)	Material type	Measured parameters	Estimated parameters
1	Silty sandy gravel-overburden	5.9	n/a	n/a	n/a
2	Weathered shale bedrock	3.60	n/a	n/a	n/a
3	Shale bedrock	41.50	n/a	RQD = 89%	n/a

Table A.39. Subsurface profile and material parameters for test ID No. 38

Soil layer	Material description	Embedded length (ft)	Material type	Measured parameters	Estimated parameters
1	Pierre shale bedrock	11.25	Rock	q_u (shaft) = 373.104 ksf; q_u (toe) = 346.34 ksf; RQD = 94%	α_E = 0.976[a]; RMR = 48[b]; m = 0.699[c]; s = 0.002543[c]

[a] determined from Table 2.6, [b] determined from Table 2.11, [c] determined from Table 2.10

Table A.40. Subsurface profile and material parameters for test ID No. 39

Soil layer	Material description	Embedded length (ft)	Material type	Measured parameters	Estimated parameters
1	Pierre shale bedrock	20	Rock	q_u (shaft) = 406.46 ksf; RQD (shaft) = 75.5%; q_u (toe) = 335.98 ksf; RQD (toe) = 88%	α_E = 0.902[(a)]; RMR = 48[(b)]; m = 0.699[(c)]; s = 0.002447[(c)]

[(a)] determined from Table 2.6, [(b)] determined from Table 2.11, [(c)] determined from Table 2.10

Table A.41. Subsurface profile and material parameters for test ID No. 40

Soil layer	Material description	Embedded length (ft)	Material type	Measured parameters	Estimated parameters
1	Hard shale	32.5	Rock	N_{60} > 100	n/a

Table A.42. Subsurface profile and material parameters for test ID No. 41

Soil layer	Material description	Embedded length (ft)	Material type	Measured parameters	Estimated parameters
1	Clay shale, moderately hard	0.77	Clay	q_u = 7.056 ksf; RQD = 100%	n/a
2	Fine grained limestone, hard	1.18	n/a	RQD = 100%	n/a
3	Clay shale, moderately hard	0.2	n/a	RQD = 100%	n/a
4	Clay shale and coal	2.39	n/a	n/a	n/a
5	Clay shale, soft	0.36	n/a	n/a	n/a
6	Clay shale, hard and brittle	0.59	n/a	n/a	n/a
7	Fine grained limestone, very hard	0.33	n/a	n/a	n/a
8	Clay shale, soft	8.86	Cohesive IGM	q_u = 35.42 ksf	n/a
9	Shaley limestone, very hard	1.12	n/a	n/a	n/a
10	Clay shale, moderately hard but brittle	7.68	Cohesive IGM	q_u = 16.416 ksf	n/a
11	Silt shale, hard	2.79	n/a	n/a	n/a
12	Clay shale, moderately hard	0.66	n/a	n/a	n/a
13	Shale to coal, moderately hard	0.13	n/a	n/a	n/a
14	soft clay shale	1.34	Cohesive IGM	q_u = 19 ksf	n/a

Table A.43. Subsurface profile and material parameters for test ID No. 42

Soil layer	Material description	Embedded length (ft)	Material type	Measured parameters	Estimated parameters
1	Soft silty clay	4.04	Clay	S_u = 2.278 ksf	n/a
2	Stiff silty clay	4.5	Clay	S_u = 2.278 ksf	n/a
3	Stiff silty clay w/ sand	15	Clay	S_u = 2.727 ksf	n/a
4	Very firm glacial clay	15	Clay	N_{60} = 28 S_u = 2.567 ksf	n/a
5	Very firm sandy glacial clay	46	Clay	N_{60} = 30 S_u = 2.014 ksf	n/a
6	Very firm glacial clay	6.26	Clay	N_{60} = 22 S_u = 2.014 ksf	n/a

Table A.44. Subsurface profile and material parameters for test ID No. 43

Soil layer	Material description	Embedded length (ft)	Material type	Measured parameters	Estimated parameters
1	Stiff silty clay	28	Clay	N_{60} = 6	S_u = 0.75ksf [(b)]; γ = 0.12 kcf[(a)]
2	Silty fine sand, loose to medium dense	15	Sand	N_{60} = 6	S_u = 0.75 ksf[(b)]; γ = 0.12 kcf[(a)]
3	Fine sand, medium dense	25	Sand	N_{60} = 9	γ = 0.113 kcf[(a)]
4	Fine to medium sand, medium dense	5	Sand	N_{60} = 12	γ = 0.112 kcf[(a)]
5	Silty fine sand, trace gravel, medium dense	5	Sand	N_{60} = 19	γ = 0.119 kcf[(a)]
6	Fine to medium sand, trace gravel, medium dense	8	Sand	N_{60} = 18	γ = 0.118 kcf[(a)]
7	Weathered shale	3.5	Clay	N_{60} = 50	S_u = 4.99 ksf[(b)]
8	Weathered shale	7.2	Rock	q_u (shaft) = 129.6 ksf; RQD (shaft) = 59%; q_u (toe) = 895.2 ksf; RQD (toe) = 100%	α_E = 0.749[(c)]; RMR = 86[(d)]; m = 2.70667[(e)]; s = 0.14320[(e)]

[(a)] estimated from Table 2.3 and Table 2.4, [(b)] estimated from Table 2.2, [(c)] estimated from Table 2.6, [(d)] estimated from Table 2.11, [(e)] estimated from Table 2.10

Table A.45. Subsurface profile and material parameters for test ID No. 44

Soil layer	Material description	Embedded length (ft)	Material type	Measured parameters	Estimated parameters
1	Stiff silty clay	12	Clay	N_{60} = 8	S_u = 1.0 ksf[(b)]; γ = 0.12 kcf[(a)]
2	Stiff silty clay	3	Clay	N_{60} = 5	S_u = 0.625 ksf[(b)]; γ = 0.115 kcf[(a)]
3	Soft silty clay	12.5	Clay	N_{60} = 2	S_u = 0.25 ksf[(b)]; ksf; γ = 0.110 kcf[(a)]
4	Fine to medium sand, medium dense	17.5	Sand	N_{60} = 11	γ = 0.111 kcf[(a)]
5	Fine to medium sand, medium dense	15	Sand	N_{60} = 13	γ = 0.113 kcf[(a)]
6	Coarse sand, medium dense	10	Sand	N_{60} = 27	γ = 0.127 kcf[(a)]
7	Coarse sand, medium dense	10	Sand	N_{60} = 16	γ = 0.116 kcf[(a)]
8	Fine to coarse sand, w/ clay and gravel, very dense	5	Sand	N_{60} = 63	γ = 0.140 kcf[(a)]
9	Sand with boulders	1.5	Sand	N_{60} = 50	γ = 0.140 kcf[(a)]
10	Medium hard limestone	16	Rock	q_u (shaft) = 792.29 ksf; RQD (shaft) = 86%; q_u (toe) = 279.36 ksf; RQD (toe) = 88%	α_E = 0.944[(c)]; RMR = 74[(d)]; m = 1.49635[(e)]; s = 0.03851[(e)]

[(a)] estimated from Table 2.3 and Table 2.4, [(b)] estimated from Table 2.2, [(c)] estimated from Table 2.6, [(d)] estimated from Table 2.11, [(e)] estimated from Table 2.10

Table A.46. Subsurface profile and material parameters for test ID No. 45

Soil layer	Material description	Embedded length (ft)	Material type	Measured parameters	Estimated parameters
1	Fine sand, loose	13	Clay	$N_{60} = 4$	$\gamma = 0.110$ kcf[(a)]
2	Silty sand, fine grained, very loose to loose	15	Clay	$N_{60} = 7$	$\gamma = 0.103$ kcf[(a)]
3	Fine sand, trace gravel, medium dense	10	Clay	$N_{60} = 13$	$\gamma = 0.113$ kcf[(a)]
4	Fine sand, trace gravel, medium dense	10	Sand	$N_{60} = 25$	$\gamma = 0.125$ kcf[(a)]
5	Fine sand, trace gravel, medium dense	25	Sand	$N_{60} = 29$	$\gamma = 0.129$ kcf[(a)]
6	Fine sand, trace gravel, medium dense	25	Sand	$N_{60} = 15$	$\gamma = 0.115$ kcf[(a)]
7	Fine to medium sand, trace gravel, medium dense	10	Sand	$N_{60} = 25$	$\gamma = 0.125$ kcf[(a)]
8	Gravel, very dense	5	Cohesionless IGM	$N_{60} = 50$	$\gamma = 0.140$ kcf[(a)]
9	Fine sand, trace gravel, dense	5	Sand	$N_{60} = 40$	$\gamma = 0.125$ kcf[(a)]
10	Fine to medium sand, trace gravel, medium dense	5	Sand	$N_{60} = 18$	$\gamma = 0.118$ kcf[(a)]
11	Gravelly sand, medium dense	5	Sand	$N_{60} = 26$	$\gamma = 0.126$ kcf[(a)]
12	Fine sand w/ gravel, very dense	5	Cohesionless IGM	$N_{60} = 55$	$\gamma = 0.140$ kcf[(a)]
13	Weathered shale	12.9			

[(a)] estimated from Table 2.3 and Table 2.4

Table A.47. Subsurface profile and material parameters for test ID No. 46

Soil layer	Material description	Embedded length (ft)	Material type	Measured parameters	Estimated parameters
1	Stiff sandy fat clay, medium stiff to stiff	12	Cohesive soil	N_{60} = 8	S_u = 1.0 ksf[h]; γ = 0.12 kcf[g]
2	Firm fat clay, very stiff	6	Cohesive soil	N_{60} = 14	S_u = 1.75 ksf[h]; γ = 0.125 kcf[g]
3	Stiff silty clay, stiff	5	Cohesive soil	N_{60} = 7	S_u = 0.875 ksf[h]; γ = 0.120 kcf[g]
4	Silty sand w/ dark gray silt lenses, loose	3	Cohesionless soil	N_{60} = 4	γ = 0.095 kcf[g]
5	Silty sand w/ dark gray silt lenses, medium dense	6	Cohesionless soil	N_{60} = 12	γ = 0.112 kcf[g]
6	Gravelly sand, medium dense	11	Cohesionless soil	N_{60} = 18	γ = 0.118 kcf[g]
7	Coarse sand, medium dense	17.5	Cohesionless soil	N_{60} = 24	γ = 0.124 kcf[g]
8	Fresh sandstone w/ gray shale seams	6	Cohesive IGM	q_u = 48.67 ksf; RQD = 21%	σ_n = 3.9[a]; α = 0.14[b]; ϕ = 0.457[c]
9	Fresh sandstone w/ carbonaceous shale seams	18.5	Rock	q_u = 128.59 ksf; RQD = 6%	α_E = 0.45[d]
10	Fresh limestone	1.5	Rock	q_u = 996.91 ksf; RQD = 29%	α_E = 0.51[d]
11	Fresh sandstone w/ carbonaceous shale seams	4.5	Rock	q_u (shaft) = 128.59 ksf; RQD (shaft) = 6%; q_u (toe) = 128.59; RQD (toe) = 0%	α_E = 0.45[d]; RMR = 16[e]; m = 0.04490[f]; s = 0.000002[f]

[a] estimated using Eq. (2.27), [b] determined from Figure 2.3, [c] estimated from Table 2.5, [d] estimated from Table 2.6, [e] estimated from Table 2.11, [f] estimated from Table 2.10, [g] estimated from Table 2.3 and Table 2.4, [h] estimated using Table 2.2

Table A.48. Subsurface profile and material parameters for test ID No. 47

Soil layer	Material description	Embedded length (ft)	Material type	Measured parameters	Estimated parameters
1	Firm silty clay	7	Cohesive soil	N_{60} = 13	S_u = 1.625 ksf[h]; γ = 0.124 kcf[g]
2	Stiff sandy clay	4	Cohesive soil	N_{60} = 6	S_u = 0.75 ksf[h]; γ = 0.120 kcf[g]
3	Stiff silty clay	5	Cohesive soil	N_{60} = 6	S_u = 0.75 ksf[h]; γ = 0.120 kcf[g]
4	Coarse sand	4	Cohesionless soil	N_{60} = 11	γ = 0.111 kcf[g]
5	Coarse sand	2	Cohesionless soil	N_{60} = 16	γ = 0.116 kcf[g]
6	Coarse sand	15	Cohesionless soil	N_{60} = 27	γ = 0.127 kcf[g]
7	Gravelly sand	2	Cohesionless soil	N_{60} = 12	γ = 0.112 kcf[g]
8	Gravelly sand	18	Cohesionless soil	N_{60} = 26	γ = 0.126 kcf[g]
9	Weathered clay shale	9	Cohesive soil	q_u = 3.63 ksf; RQD = 16%	S_u = 1.81 ksf
10	Weathered limestone	6	Cohesive IGM	q_u = 15.89 ksf; RQD = 99%	σ_n = 3.9[a]; α = 0.24[b]; ϕ = 0.996[c]
11	Fresh sandy limestone	3	Cohesive IGM	q_u = 41.33 ksf; RQD = 99%	σ_n = 3.9[a]; α = 0.16[b]; ϕ = 0.996[c]
12	Weathered clay shale	3	Cohesive soil	q_u = 6.62 ksf; RQD= 90%	S_u = 3.31 ksf
13	Fresh fine grained calcareous sandstone	5	Rock	q_u = 381.53 ksf; RQD = 64%	α_E = 0.88[d]
14	Fresh clay shale	8	Cohesive soil	q_u = 8.50 ksf; RQD = 73%	S_u = 4.25 ksf
15	Fresh fine grained sandstone w/ thin shale seams	6.97	Rock	q_u (shaft) = 109.4 ksf; RQD (shaft) = 54%; q_u (toe) = 200.23; RQD (toe) = 41%	α_E = 0.67[d]; RMR = 32[e]; m = 0.15271[f]; s = 0.000040[f]

[a] estimated using Eq. (2.27), [b] determined from Figure 2.3, [c] estimated from Table 2.5, [d] estimated from Table 2.6, [e] estimated from Table 2.11, [f] estimated from Table 2.10, [g] estimated from Table 2.3 and Table 2.4, [h] estimated using Table 2.2

Table A.49. Subsurface profile and material parameters for test ID No. 48

Soil layer	Material description	Embedded length (ft)	Material type	Measured parameters	Estimated parameters
1	Sandy lean clay, trace organics	4	Cohesive soil	$N_{60} = 4$	$S_u = 0.50$ ksf[(b)]; $\gamma = 0.110$ kcf[(a)]
2	Lean clay, moist, rather soft	3	Cohesive soil	$N_{60} = 4$	$S_u = 0.50$ ksf[(b)]; $\gamma = 0.110$ kcf[(a)]
3	Poorly graded sand	15	Cohesionless soil	$N_{60} = 7$	$\gamma = 0.103$ kcf[(a)]
4	Lean clay, wet, very stiff	5.5	Cohesive soil	$N_{60} = 22$	$S_u = 2.75$ ksf[(b)]; $\gamma = 0.116$ kcf[(a)]
5	Gravelly poorly graded sand w/ silt	30	Cohesionless soil	$N_{60} = 22$	$\gamma = 0.122$ kcf[(a)]
6	Gravelly poorly graded sand w/ silt	15.5	Cohesionless soil	$N_{60} = 32$	$\gamma = 0.132$ kcf[(a)]
7	Poorly graded sand w/ silt w/ gravel	29	Cohesionless soil	$N_{60} = 28$	$\gamma = 0.128$ kcf[(a)]
8	Silty sand w/ gravel	10.5	Cohesionless soil	$N_{60} = 26$	$\gamma = 0.126$ kcf[(a)]
9	Poorly graded sand, trace gravel	18.5	Cohesionless IGM	$N_{60} = 66$	$\gamma = 0.140$ kcf[(a)]
10	Clayey sand, residuum	6.5	Cohesionless IGM	$N_{60} = 50$	$\gamma = 0.140$ kcf[(a)]
11	Poorly graded sand w/ silt	10.5	Cohesionless IGM	$N_{60} = 50$	$\gamma = 0.140$ kcf[(a)]
12	Clayey sand, residuum	5.5	Cohesionless IGM	$N_{60} = 50$	$\gamma = 0.140$ kcf[(a)]
13	Clayey sand, residuum	7.5	Cohesionless IGM	$N_{60} = 50$	$\gamma = 0.140$ kcf[(a)]

[(a)] estimated from Table 2.3 and Table 2.4, [(b)] estimated using Table 2.2

Table A.50. Subsurface profile and material parameters for test ID No. 49

Soil layer	Material description	Embedded length (ft)	Material type	Measured parameters	Estimated parameters
1	Fill—lean clay, trace sand, dark brown	5.1	Cohesive soil	$N_{60} = 5$	$S_u = 0.625$ ksf[(b)]; $\gamma = 0.110$ kcf[(a)]
2	Fat clay, trace sand, grayish brown	8	Cohesive soil	$N_{60} = 4$	$S_u = 0.50$ ksf[(b)]; $\gamma = 0.110$ kcf[(a)]
3	Lean clay, trace sand, gray, brown	5	Cohesive soil	$N_{60} = 4$	$S_u = 0.50$ ksf[(b)]; $\gamma = 0.110$ kcf[(a]
4	Fine to medium sand, brown	7	Cohesionless soil	$N_{60} = 2$	$S_u = 2.75$ ksf[(b)]; $\gamma = 0.085$ kcf[(a)]
5	Fine Sand, trace gravel, gray	33	Cohesionless soil	$N_{60} = 15$	$\gamma = 0.115$ kcf[(a)]
6	Fine to coarse sand, trace gravel, gray	10	Cohesionless soil	$N_{60} = 10$	$\gamma = 0.110$ kcf[(a)]
7	Fine Sand, trace gravel, gray	5	Cohesionless IGM	$N_{60} = 53$	$\gamma = 0.140$ kcf[(a)]
8	Gravel, w/ sand, gray and brown	5	Cohesionless soil	$N_{60} = 17$	$\gamma = 0.117$ kcf[(a)]
9	Fine to coarse sand, w/ gravel, brown and gray	5	Cohesionless soil	$N_{60} = 8$	$\gamma = 0.107$ kcf[(a)]
10	Fine to medium sand, trace gravel brown	10	Cohesionless soil	$N_{60} = 19$	$\gamma = 0.119$ kcf[(a)]
11	Gravel, w/ sand, gray and brown	5	Cohesionless soil	$N_{60} = 17$	$\gamma = 0.117$ kcf[(a)]
12	Fine to coarse sand, trace gravel, brown and gray	5	Cohesionless soil	$N_{60} = 19$	$\gamma = 0.119$ kcf[(a)]
13	Gravel, gray and brown	11.5	Cohesionless soil	$N_{60} = 17$	$\gamma = 0.117$ kcf[(a)]

[(a)] estimated from Table 2.3 and Table 2.4, [(b)] estimated using Table 2.2

APPENDIX B. SUMMARY OF ESTIMATED SHAFT RESISTANCES

Table B.1. Estimated shaft resistances for data point ID No. 1

Shaft segment	Geomaterial	Unit side resistance (ksf)	Unit end bearing (ksf)
1	Cohesive soil	n/a	n/a
2	Cohesive soil	n/a	n/a
3	Cohesive soil	n/a	n/a
4	Cohesive soil	n/a	n/a
5	Cohesive IGM or rock	n/a	n/a
6	Cohesive IGM or rock	n/a	n/a

Table B.2. Estimated shaft resistances for data point ID No. 2

		O'Neill and Reese 1999		Brown et al. 2010	
Shaft segment	Geomaterial	Unit side resistance (ksf)	Side resistance (kips)	Unit side resistance (ksf)	Side resistance (kips)
DST2 TOS-SG3	Rock	22.93	911	36.75	1,460
DST2 SG3-SG2	Rock	22.93	333	36.75	534
DST2 SG2-SG1	Rock	22.93	444	36.75	712
DST2 SG1-Tip	Rock	22.93	1,133	36.75	1,815

Table B.3. Estimated shaft resistances for data point ID No. 3

Shaft segment	Geomaterial	O'Neill and Reese 1999 Unit side resistance (ksf)	O'Neill and Reese 1999 Side resistance (kips)	Brown et al. 2010 Unit side resistance (ksf)	Brown et al. 2010 Side resistance (kips)
DST3 TOS-SG5	Cohesive soil	0.76	188	0.76	188
DST3 SG5-SG4	Cohesive soil	0.76	100	0.76	100
DST3 SG4-SG3	Cohesive soil	0.76	50	0.76	50
DST3 SG3-SG2	Cohesive IGM	2.51	507	2.51	507
DST3 SG2-SG1	Cohesive IGM	6.76	558	6.76	558
DST3 SG1-Tip	Cohesive IGM	4.80	326	4.80	326

Table B.4. Estimated shaft resistances for data point ID No. 4

Shaft segment	Geomaterial	O'Neill and Reese 1999 Unit side resistance (ksf)	O'Neill and Reese 1999 Side resistance (kips)	Brown et al. 2010 Unit side resistance (ksf)	Brown et al. 2010 Side resistance (kips)
DST4 BOC-Tip	Cohesive IGM	8.80	3,068	11.08	3,301

Table B.5. Estimated shaft resistances for data point ID No. 5

Shaft segment	Geomaterial	O'Neill and Reese 1999 Unit side resistance (ksf)	O'Neill and Reese 1999 Side resistance (kips)	Brown et al. 2010 Unit side resistance (ksf)	Brown et al. 2010 Side resistance (kips)
DST5 TOS-SG5	Cohesive soil	0.74	281	0.74	281
DST5 SG5-SG4	Cohesive soil	1.56	257	1.42	234
DST5 SG4-SG3	Cohesive IGM	3.32	548	3.32	548
DST5 SG3-SG2	Cohesive IGM	2.34	232	2.34	232
DST5 SG2-SG1	Cohesive IGM	1.96	73	1.96	73
DST5 SG1-Tip	Cohesive IGM	1.87	253	2.80	386

Table B.6. Estimated shaft resistances for data point ID No. 6

		O'Neill and Reese 1999		Brown et al. 2010	
Shaft segment	Geomaterial	Unit side resistance (ksf)	Side resistance (kips)	Unit side resistance (ksf)	Side resistance (kips)
DST6 TOS-SG4	Cohesive soil	0.50	128	0.50	128
DST6 SG4-SG3	Cohesive soil	0.89	46	0.89	46
DST6 SG3-SG2	Cohesive soil	1.05	54	1.05	54
DST6 SG2-O-CELL	Cohesive soil	1.64	131	1.64	131
DST6 O-CELL-TIP	Cohesive soil	1.58	112	1.58	112

Table B.7. Estimated shaft resistances for data point ID No. 7

		O'Neill and Reese 1999		Brown et al. 2010	
Shaft segment	Geomaterial	Unit side resistance (ksf)	Side resistance (kips)	Unit side resistance (ksf)	Side resistance (kips)
DST7 TOS-SG5	Cohesive soil	0.55	95	0.55	95
DST7 SG5-SG4	Rock	18.10	188	30.35	315
DST7 SG4-SG3	Rock	21.03	456	35.32	766
DST7 SG3-SG2	Rock	21.42	868	35.38	1,434
DST7 SG2-SG1	Rock	22.30	925	35.38	1,467
DST7 SG1-Tip	Rock	22.72	1,306	35.38	2,034

Table B.8. Estimated shaft resistances for data point ID No. 8

Shaft segment	Geomaterial	O'Neill and Reese 1999 Unit side resistance (ksf)	O'Neill and Reese 1999 Side resistance (kips)	Brown et al. 2010 Unit side resistance (ksf)	Brown et al. 2010 Side resistance (kips)
DST8 BOC-SG2	Rock	20.63	318	34.06	524
DST8 SG2-SG1	Rock	19.75	1,811	34.06	3,123
DST8 SG1-Tip	Rock	16.35	2,118	28.94	3,750

Table B.9. Estimated shaft resistances for data point ID No. 9

Shaft segment	Geomaterial	O'Neill and Reese 1999 Unit side resistance (ksf)	O'Neill and Reese 1999 Side resistance (kips)	Brown et al. 2010 Unit side resistance (ksf)	Brown et al. 2010 Side resistance (kips)
DST9 TOS-SG2	Cohesive soil	n/a	n/a	n/a	n/a
DST9 SG2-SG3	Cohesionless soil	n/a	n/a	n/a	n/a
DST9 SG3-SG4	Cohesionless soil	n/a	n/a	n/a	n/a

Table B.10. Estimated shaft resistances for data point ID No. 10

Shaft segment	Geomaterial	O'Neill and Reese 1999 Unit side resistance (ksf)	O'Neill and Reese 1999 Side resistance (kips)	Brown et al. 2010 Unit side resistance (ksf)	Brown et al. 2010 Side resistance (kips)
DST10 TOS-SG2	Cohesive soil	n/a	n/a	n/a	n/a
DST10 SG2-SG3	Cohesionless soil	n/a	n/a	n/a	n/a
DST10 SG3-SG4	Cohesionless soil	n/a	n/a	n/a	n/a

Table B.11. Estimated shaft resistances for data point ID No. 11

		O'Neill and Reese 1999		Brown et al. 2010	
Shaft segment	**Geomaterial**	**Unit side resistance (ksf)**	**Side resistance (kips)**	**Unit side resistance (ksf)**	**Side resistance (kips)**
DST11 TOS-SG2	Cohesive soil	n/a	n/a	n/a	n/a
DST11 SG2-SG3	Cohesionless soil	n/a	n/a	n/a	n/a
DST11 SG3-SG4	Cohesionless soil	n/a	n/a	n/a	n/a

Table B.12. Estimated shaft resistances for data point ID No. 12

Soil layer	Geomaterial	Unit side resistance (ksf)	Side resistance (kips)	Unit end bearing (ksf)	End bearing (kip)	Total resistance (kip)
1	Sand	1.03	211	n/a	n/a	n/a
2	Sand	10.96	5,371	n/a	n/a	
3	Sand	6.55	2,409	n/a	n/a	
4	n/a	n/a	n/a	n/a	n/a	

Table B.13. Estimated shaft resistances for data point ID No. 13

		O'Neill and Reese 1999		Brown et al. 2010	
Shaft segment	**Geomaterial**	**Unit side resistance (ksf)**	**Side resistance (kips)**	**Unit side resistance (ksf)**	**Side resistance (kips)**
DST13 BOC-SG2	Cohesive IGM	2.20	154	2.20	154
DST13 SG2-SG1	Cohesive IGM	1.83	345	1.83	345
DST13 SG1-Tip	Cohesive IGM	2.30	550	2.30	550

Table B.14. Estimated shaft resistances for data point ID No. 14

		O'Neill and Reese 1999		Brown et al. 2010	
Shaft segment	Geomaterial	Unit side resistance (ksf)	Side resistance (kips)	Unit side resistance (ksf)	Side resistance (kips)
DST14 TOS-SG6	Cohesive IGM	1.32	189	1.32	189
DST14 SG6-SG5	Cohesive IGM	1.10	135	1.10	135
DST14 SG5-SG4	Cohesive IGM	1.10	123	1.10	123
DST14 SG4-OCELL	Rock	10.95	2,342	29.17	6,239
DST14 OCELL-SG1	Rock	15.93	2,227	42.80	5,984
DST14 SG1-Tip	Cohesive IGM	3.04	264	3.04	264

Table B.15. Estimated shaft resistances for data point ID No. 15

		O'Neill and Reese 1999		Brown et al. 2010	
Shaft segment	Geomaterial	Unit side resistance (ksf)	Side resistance (kips)	Unit side resistance (ksf)	Side resistance (kips)
DST15 TOS-O-Cell	Cohesive IGM	1.97	738	1.97	738

Table B.16. Estimated shaft resistances for data point ID No. 16

		O'Neill and Reese 1999		Brown et al. 2010	
Shaft segment	Geomaterial	Unit side resistance (ksf)	Side resistance (kips)	Unit side resistance (ksf)	Side resistance (kips)
DST16 BOC-SG2	Cohesive IGM	1.42	243	1.42	243
DST16 SG2-SG1	Cohesive IGM	1.69	191	1.69	191
DST16 SG1-Tip	Cohesive IGM	2.07	318	2.07	318

Table B.17. Estimated shaft resistances for data point ID No. 17

Shaft segment	Geomaterial	O'Neill and Reese 1999 Unit side resistance (ksf)	O'Neill and Reese 1999 Side resistance (kips)	Brown et al. 2010 Unit side resistance (ksf)	Brown et al. 2010 Side resistance (kips)
DST17 BOC-ECT4	-	-	-	-	-
DST17 ECT4-ECT3	Cohesive IGM	2.35	591	2.35	591
DST17 ECT3.-ECT2	Cohesive IGM	4.30	918	4.30	918
DST17 ECT2-Tip	Rock	8.26	3,198	16.89	6,537

Table B.18. Estimated shaft resistances for data point ID No. 18

Shaft segment	Geomaterial	O'Neill and Reese 1999 Unit side resistance (ksf)	O'Neill and Reese 1999 Side resistance (kips)	Brown et al. 2010 Unit side resistance (ksf)	Brown et al. 2010 Side resistance (kips)
DST18	n/a	n/a	n/a	n/a	n/a

Table B.19. Estimated shaft resistances for data point ID No. 19

Shaft segment	Geomaterial	O'Neill and Reese 1999 Unit side resistance (ksf)	O'Neill and Reese 1999 Side resistance (kips)	Brown et al. 2010 Unit side resistance (ksf)	Brown et al. 2010 Side resistance (kips)
DST19 TOS-SG2	Cohesive IGM	1.80	149	1.80	149
DST19 SG2-SG1	Cohesive IGM	1.80	340	1.80	340
DST19 SG1-TIP	Cohesive IGM	1.76	343	1.76	343

Table B.20. Estimated shaft resistances for data point ID No. 20

		O'Neill and Reese 1999		Brown et al. 2010	
Shaft segment	Geomaterial	Unit side resistance (ksf)	Side resistance (kips)	Unit side resistance (ksf)	Side resistance (kips)
DST20	n/a	n/a	n/a	n/a	n/a

Table B.21. Estimated shaft resistances for data point ID No. 21

		O'Neill and Reese 1999		Brown et al. 2010	
Shaft segment	Geomaterial	Unit side resistance (ksf)	Side resistance (kips)	Unit side resistance (ksf)	Side resistance (kips)
DST21	n/a	n/a	n/a	n/a	n/a

Table B.22. Estimated shaft resistances for data point ID No. 22

		O'Neill and Reese 1999		Brown et al. 2010	
Shaft segment	Geomaterial	Unit side resistance (ksf)	Side resistance (kips)	Unit side resistance (ksf)	Side resistance (kips)
DST22	n/a	n/a	n/a	n/a	n/a

Table B.23. Estimated shaft resistances for data point ID No. 23

		O'Neill and Reese 1999		Brown et al. 2010	
Shaft segment	Geomaterial	Unit side resistance (ksf)	Side resistance (kips)	Unit side resistance (ksf)	Side resistance (kips)
DST23	n/a	n/a	n/a	n/a	n/a

Table B.24. Estimated shaft resistances for data point ID No. 24

		O'Neill and Reese 1999		Brown et al. 2010	
Shaft segment	Geomaterial	Unit side resistance (ksf)	Side resistance (kips)	Unit side resistance (ksf)	Side resistance (kips)
DST25	n/a	n/a	n/a	n/a	n/a

Table B.25. Estimated shaft resistances for data point ID No. 25

Shaft segment	Geomaterial	O'Neill and Reese 1999		Brown et al. 2010	
		Unit side resistance (ksf)	Side resistance (kips)	Unit side resistance (ksf)	Side resistance (kips)
DST25 TOS-SG3	Cohesive soil	n/a	n/a	n/a	n/a
DST25 SG3-SG2	Cohesive soil	84	1.21	1.21	84
DST25 SG2-SG1	Cohesive soil	80	1.21	1.21	80
DST25 SG1-Tip	Cohesive soil	354	2.50	2.50	354

Table B.26. Estimated shaft resistances for data point ID No. 26

Shaft segment	Geomaterial	O'Neill and Reese 1999		Brown et al. 2010	
		Unit side resistance (ksf)	Side resistance (kips)	Unit side resistance (ksf)	Side resistance (kips)
DST26 TOS-SG7	Cohesive soil	0.25	45	0.26	45
DST26 SG7-SG6	Mixed	0.44	104	0.55	131
DST26 SG6-SG5	Cohesionless soil	1.01	162	0.91	142
DST26 SG5-SG4	Cohesionless soil	0.91	146	0.93	149
DST26 SG4-SG3	Cohesionless soil	1.41	217	1.16	179
DST26 SG3-O-CELL	Cohesionless soil	1.69	134	1.71	134
DST26 O-CELL-SG2	Cohesionless soil	1.69	131	1.71	132
DST26 SG2-Tip	Cohesionless soil	1.69	261	1.71	311

Table B.27. Estimated shaft resistances for data point ID No. 27

Shaft segment	Geomaterial	O'Neill and Reese 1999 Unit side resistance (ksf)	O'Neill and Reese 1999 Side resistance (kips)	Brown et al. 2010 Unit side resistance (ksf)	Brown et al. 2010 Side resistance (kips)
DST27 TOS-SG7	Cohesive soil	0.25	45	0.26	45
DST27 SG7-SG6	Mixed	0.47	104	0.61	131
DST27 SG6-SG5	Cohesionless soil	1.31	203	1.01	142
DST27 SG5-SG4	Cohesionless soil	1.10	174	0.97	149
DST27 SG4-SG3	Cohesionless soil	1.67	263	1.49	179
DST27 SG3-O-CELL	Cohesionless soil	1.38	107	1.30	134
DST27 O-CELL-SG2	Cohesionless soil	1.38	108	1.30	132
DST27 SG2-Tip	Cohesionless soil	1.38	212	1.30	311

Table B.28. Estimated shaft resistances for data point ID No. 28

Shaft segment	Geomaterial	O'Neill and Reese 1999 Unit side resistance (ksf)	O'Neill and Reese 1999 Side resistance (kips)	Brown et al. 2010 Unit side resistance (ksf)	Brown et al. 2010 Side resistance (kips)
DST28 TOS-SG1	Rock	12.82	1,506	41.97	4,928
DST28 SG1-Tip	Rock	15.41	1,650	41.97	4,494

Table B.29. Estimated shaft resistances for data point ID No. 29

Shaft segment	Geomaterial	O'Neill and Reese 1999 Unit side resistance (ksf)	O'Neill and Reese 1999 Side resistance (kips)	Brown et al. 2010 Unit side resistance (ksf)	Brown et al. 2010 Side resistance (kips)
DST29	n/a	n/a	n/a	n/a	n/a

Table B.30. Estimated shaft resistances for data point ID No. 30

Shaft segment	Geomaterial	O'Neill and Reese 1999 Unit side resistance (ksf)	O'Neill and Reese 1999 Side resistance (kips)	Brown et al. 2010 Unit side resistance (ksf)	Brown et al. 2010 Side resistance (kips)
DST30	n/a	n/a	n/a	n/a	n/a

Table B.31. Estimated shaft resistances for data point ID No. 31

Shaft segment	Geomaterial	O'Neill and Reese 1999 Unit side resistance (ksf)	O'Neill and Reese 1999 Side resistance (kips)	Brown et al. 2010 Unit side resistance (ksf)	Brown et al. 2010 Side resistance (kips)
DST31	n/a	n/a	n/a	n/a	n/a

Table B.32. Estimated shaft resistances for data point ID No. 32

Shaft segment	Geomaterial	O'Neill and Reese 1999 Unit side resistance (ksf)	O'Neill and Reese 1999 Side resistance (kips)	Brown et al. 2010 Unit Side resistance (ksf)	Brown et al. 2010 Side resistance (kips)
DST32	n/a	n/a	n/a	n/a	n/a

Table B.33. Estimated shaft resistances for data point ID No. 33

Shaft segment	Geomaterial	O'Neill and Reese 1999 Unit side resistance (ksf)	O'Neill and Reese 1999 Side resistance (kips)	Brown et al. 2010 Unit side resistance (ksf)	Brown et al. 2010 Side resistance (kips)
DST33	n/a	n/a	n/a	n/a	n/a

Table B.34. Estimated shaft resistances for data point ID No. 34

Shaft segment	Geomaterial	O'Neill and Reese 1999 Unit side resistance (ksf)	O'Neill and Reese 1999 Side resistance (kips)	Brown et al. 2010 Unit side resistance (ksf)	Brown et al. 2010 Side resistance (kips)
DST34	n/a	n/a	n/a	n/a	n/a

Table B.35. Estimated shaft resistances for data point ID No. 35

		O'Neill and Reese 1999		Brown et al. 2010	
Shaft segment	Geomaterial	Unit side resistance (ksf)	Side resistance (kips)	Unit side resistance (ksf)	Side resistance (kips)
DST35	n/a	n/a	n/a	n/a	n/a

Table B.36. Estimated shaft resistances for data point ID No. 36

		O'Neill and Reese 1999		Brown et al. 2010	
Shaft segment	Geomaterial	Unit side resistance (ksf)	Side resistance (kips)	Unit side resistance (ksf)	Side resistance (kips)
DST36	n/a	n/a	n/a	n/a	n/a

Table B.37. Estimated shaft resistances for data point ID No. 37

		O'Neill and Reese 1999		Brown et al. 2010	
Shaft segment	Geomaterial	Unit side resistance (ksf)	Side resistance (kips)	Unit side resistance (ksf)	Side resistance (kips)
DST37	n/a	n/a	n/a	n/a	n/a

Table B.38. Estimated shaft resistances for data point ID No. 38

		O'Neill and Reese 1999		Brown et al. 2010	
Shaft segment	Geomaterial	Unit side resistance (ksf)	Side resistance (kips)	Unit side resistance (ksf)	Side resistance (kips)
DST38	n/a	n/a	n/a	n/a	n/a

Table B.39. Estimated shaft resistances for data point ID No. 39

		O'Neill and Reese 1999		Brown et al. 2010	
Shaft segment	Geomaterial	Unit side resistance (ksf)	Side resistance (kips)	Unit side resistance (ksf)	Side resistance (kips)
DST39	n/a	n/a	n/a	n/a	n/a

Table B.40. Estimated shaft resistances for data point ID No. 40

		O'Neill and Reese 1999		Brown et al. 2010	
Shaft segment	Geomaterial	Unit side resistance (ksf)	Side resistance (kips)	Unit side resistance (ksf)	Side resistance (kips)
DST40	n/a	n/a	n/a	n/a	n/a

Table B.41. Estimated shaft resistances for data point ID No. 41

		O'Neill and Reese 1999		Brown et al. 2010	
Shaft segment	Geomaterial	Unit side resistance (ksf)	Side resistance (kips)	Unit side resistance (ksf)	Side resistance (kips)
DST41	n/a	n/a	n/a	n/a	n/a

Table B.42. Estimated shaft resistances for data point ID No. 42

		O'Neill and Reese 1999		Brown et al. 2010	
Shaft segment	Geomaterial	Unit side resistance (ksf)	Side resistance (kips)	Unit side resistance (ksf)	Side resistance (kips)
DST42 TOS-SG8	Cohesive soil	1.43	419	1.43	419
DST42 SG8-SG7	Cohesive soil	1.50	185	1.50	185
DST42 SG7-SG6	Cohesive soil	1.41	216	1.41	216
DST42 SG6-SG5	Cohesive soil	1.41	214	1.41	214
DST42 SG5-SG4	Cohesive soil	1.11	281	1.11	281
DST42 SG4-O-CELL	Cohesive soil	1.11	423	1.11	423
DST42 O-CELL-Tip	Cohesive soil	1.11	473	1.11	473

Table B.43. Estimated shaft resistances for data point ID No. 43

Shaft segment	Geomaterial	O'Neill and Reese 1999 Unit side resistance (ksf)	O'Neill and Reese 1999 Side resistance (kips)	Brown et al. 2010 Unit side resistance (ksf)	Brown et al. 2010 Side resistance (kips)
DST43 TOS-SG9	Cohesive soil	0.41	160	0.41	160
DST43 SG9-SG8	Cohesive soil	0.41	42	0.41	42
DST43 SG8-SG7	Cohesionless soil	1.18	260	1.29	285
DST43 SG7-SG6	Cohesionless soil	1.40	338	1.26	304
DST43 SG6-SG5	Cohesionless soil	1.51	363	1.25	300
DST43 SG5-SG4	Cohesionless soil	1.57	376	1.56	374
DST43 SG4-SG3	Cohesionless soil	1.45	316	1.79	390
DST43 SG3-SG2	Cohesive soil	2.32	160	2.32	160
DST43 SG2-Tip	Rock	8.07	1,103	16.58	2,266

Table B.44. Estimated shaft resistances for data point ID No. 44

Shaft segment	Geomaterial	O'Neill and Reese 1999 Unit side resistance (ksf)	O'Neill and Reese 1999 Side resistance (kips)	Brown et al. 2010 Unit side resistance (ksf)	Brown et al. 2010 Side resistance (kips)
DST44 TOS-SG9	Cohesive soil	0.32	107	0.32	107
DST44 SG9-SG8	Cohesive soil	0.14	18	0.14	18
DST44 SG8-SG7	Cohesive soil	0.14	18	0.14	18
DST44 SG7-SG6	Cohesionless soil	1.21	347	1.01	290
DST44 SG6-SG5	Cohesionless soil	1.40	383	1.10	302
DST44 SG5-SG4	Cohesionless soil	1.56	429	1.32	363
DST44 SG4-SG3	Cohesionless soil	1.53	421	1.35	370
DST44 SG3-SG2	Cohesionless IGM	1.36	192	3.15	434
DST44 SG2-Tip	Rock	24.67	5,850	40.81	9,679

Table B.45. Estimated shaft resistances for data point ID No. 45

		O'Neill and Reese 1999		Brown et al. 2010	
Shaft segment	**Geomaterial**	**Unit side resistance (ksf)**	**Side resistance (kips)**	**Unit side resistance (ksf)**	**Side resistance (kips)**
DST45 TOS-SG7	Cohesionless soil	0.36	129	.59	216
DST45 SG7-SG6	Cohesionless soil	1.20	518	1.11	483
DST45 SG6-SG5	Cohesionless soil	1.66	741	1.71	764
DST45 SG5-SG4	Cohesionless soil	1.35	583	1.50	649
DST45 SG4-SG3	Cohesionless soil	1.52	394	2.43	630
DST45 SG3-SG2	Cohesionless soil	1.76	395	2.25	504
DST45 SG2-O-Cell	Cohesionless IGM	1.91	231	3.41	413
DST 45 O-CELL-Tip	n/a	n/a	n/a	n/a	n/a

Table B.46. Estimated shaft resistances for data point ID No. 46

Shaft segment	Geomaterial	O'Neill and Reese 1999 Unit side resistance (ksf)	O'Neill and Reese 1999 Side resistance (kips)	Brown et al. 2010 Unit side resistance (ksf)	Brown et al. 2010 Side resistance (kips)
DST46 TOS-SG11	Cohesive soil	0.18	28	0.18	28
DST46 SG11-SG10	Cohesionless soil	0.44	37	0.62	52
DST46 SG10-SG9	Cohesionless soil	1.01	77	1.09	84
DST46 SG9-SG8	Cohesionless soil	0.93	75	0.94	77
DST46 SG8-SG7	Cohesionless soil	0.91	89	0.91	89
DST46 SG7-SG6	Cohesionless soil	1.25	176	1.76	248
DST46 SG6-SG5	Cohesionless IGM	1.29	186	1.86	269
DST46 SG5-SG4	Cohesive IGM	3.11	315	3.11	315
DST46 SG4-SG3	Rock	4.83	643	16.51	2,200
DST46 SG3-O-Cell	Rock	4.83	401	16.51	1,370
DST46 O-Cell-SG2	Rock	4.83	464	16.51	1,585
DST46 SG2-Tip	Rock	6.55	766	21.26	2,489

Table B.47. Estimated shaft resistances for data point ID No. 47

Shaft segment	Geomaterial	O'Neill and Reese 1999 Unit side resistance (ksf)	O'Neill and Reese 1999 Side resistance (kips)	Brown et al. 2010 Unit side resistance (ksf)	Brown et al. 2010 Side resistance (kips)
DST47 TOS-SG11	Mixed	0.44	87	0.31	61
DST47 SG11-SG10	Cohesionless soil	1.21	147	0.92	111
DST47 SG10-SG9	Cohesionless soil	1.21	145	0.92	110
DST47 SG9-SG8	Cohesionless soil	1.64	277	1.26	213
DST47 SG8-SG7	Cohesionless soil	1.76	289	1.40	231
DST47 SG7-SG6	Cohesive soil	1.02	148	1.01	147
DST47 SG6-SG5	Cohesive IGM	3.69	357	3.69	357
DST47 SG5-SG4	Cohesive IGM	6.36	308	6.36	308
DST47 SG4-SG3	Cohesive soil	2.18	106	2.18	106
DST47 SG3-O-Cell	Rock	12.05	1,379	20.70	2,367
DST47 O-Cell-SG2	Cohesive soil	2.12	222	2.12	222
DST47 SG2-Tip	Rock	6.53	837	14.94	1,914

Table B.48. Estimated shaft resistances for data point ID No. 48

Shaft segment	Geomaterial	O'Neill and Reese 1999 Unit side resistance (ksf)	O'Neill and Reese 1999 Side resistance (kips)	Brown et al. 2010 Unit side resistance (ksf)	Brown et al. 2010 Side resistance (kips)
DST48 TOS-SG8	Mixed	1.13	888	0.92	720
DST48 SG8-SG7	Cohesionless soil	3.02	635	635	388
DST48 SG7-SG6	Cohesionless soil	2.77	1,781	2.19	1,412
DST48 SG6-SG5	Cohesionless soil	1.88	1,145	2.50	1,523
DST48 SG5-SG4	Cohesionless soil	2.19	496	2.54	577
DST48 SG4-SG3	Cohesionless IGM	2.46	988	3.40	1,365
DST48 SG3-O-CELL	Cohesionless IGM	2.75	561	5.23	1,066
DST48 O-CELL-SG2	Cohesionless IGM	2.87	405	5.34	754
DST48 SG2-Tip	Cohesionless IGM	2.58	719	3.54	985

Table B.49. Estimated shaft resistances for data point ID No. 49

		O'Neill and Reese 1999		Brown et al. 2010	
Shaft segment	Geomaterial	Unit side resistance (ksf)	Side resistance (kips)	Unit side resistance (ksf)	Side resistance (kips)
DST49 TOS-SG11	Cohesive soil	0.34	26	0.34	26
DST49 SG11-SG10	Cohesive soil	0.28	37	0.28	37
DST49 SG10-SG9	Cohesive soil	0.28	23	0.28	23
DST49 SG9-SG8	Cohesionless soil	0.40	46	0.49	56
DST49 SG8-SG7	Cohesionless soil	1.58	281	1.17	209
DST49 SG7-SG6	Cohesionless soil	1.58	279	1.17	207
DST49 SG6-SG5	Cohesionless soil	1.58	293	1.17	217
DST49 SG5-OCELL	Cohesionless soil	0.99	172	1.13	196
DST49 OCELL-SG4	Cohesionless IGM	1.50	130	2.34	203
DST49 SG4-SG3	Cohesionless soil	1.46	126	1.51	130
DST49 SG3-SG2	Cohesionless soil	1.18	102	1.18	102
DST49 SG2-Tip	Cohesionless soil	1.28	254	1.65	323

Table B.50. Estimated tip resistances

Load test ID	Geomaterial	Rowe and Armitage 1987 (ksf)	Carter and Kulhawy 1988 (ksf)	Proposed method (ksf)	O'Neill and Reese 1999 (ksf)	Sowers 1976 (ksf)	Brown et al. 2010
DST1	n/a	n/a	n/a	n/a	n/a	n/a	n/a
DST2	n/a						
DST3	Cohesive IGM	60.93	3.39	32.16	109.13	24.37	n/a
DST4	Cohesive IGM	234.18	116.15	175.16	216.86	93.67	n/a
DST5	Rock	479.53	6.24	242.89	312.56	191.81	n/a

Load test ID	Geomaterial	Rowe and Armitage 1987 (ksf)	Carter and Kulhawy 1988 (ksf)	Proposed method (ksf)	O'Neill and Reese 1999 (ksf)	Sowers 1976 (ksf)	Brown et al. 2010
DST6	Cohesive soil	n/a	n/a	n/a	25.88	n/a	25.88
DST7	Rock	1,587.60	926.46	1,257.03	575.56	635.04	n/a
DST8	Rock	1,383.60	807.42	1,095.51	536.57	553.44	n/a
DST9	Cohesionless soil	n/a	n/a	n/a	19.20	n/a	19.20
DST10	Cohesionless soil	n/a	n/a	n/a	21.60	n/a	21.60
DST11	Cohesionless soil	n/a	n/a	n/a	18.00	n/a	18.00
DST12	n/a	n/a	n/a	n/a	n/a	n/a	n/a
DST13	Cohesive soil	n/a	n/a	n/a	34.29	n/a	34.29
DST14	Cohesive IGM	248.75	3.24	125.99	223.64	99.50	n/a
DST15	Cohesive IGM	85.41	49.24	67.33	129.65	34.16	n/a
DST16	Cohesive IGM	122.75	1.62	62.18	156.00	49.10	n/a
DST17	Cohesive IGM	233.64	75.07	154.36	216.61	93	n/a
DST18	n/a	n/a	n/a	n/a	n/a	n/a	n/a
DST19	Cohesive soil	n/a	n/a	n/a	60.00	n/a	60.00
DST20	n/a	n/a	n/a	n/a	n/a	n/a	n/a
DST21	n/a	n/a	n/a	n/a	n/a	n/a	n/a
DST22	n/a	n/a	n/a	n/a	n/a	n/a	n/a
DST23	n/a	n/a	n/a	n/a	n/a	n/a	n/a
DST24	n/a	n/a	n/a	n/a	n/a	n/a	n/a
DST25	IGM	578.25	48.29	313.27	343.87	231.3	n/a
DST26	Cohesionless soil	n/a	n/a	n/a	16.00	n/a	16.00
DST27	Cohesionless soil	n/a	n/a	n/a	16.00	n/a	16.00
DST28	Rock	1,938.60	152.54	1,045.57	637.28	775.44	n/a
DST29	Rock	7,416.00	1197.21	4,306.60	1,263.27	2,966.40	n/a
DST30	n/a	n/a	n/a	n/a	n/a	n/a	n/a
DST31	n/a	n/a	n/a	n/a	n/a	n/a	n/a
DST32	n/a	n/a	n/a	n/a	n/a	n/a	n/a
DST33	IGM	123.75	n/a	n/a	156.64	49.50	n/a
DST34	IGM	42.13	n/a	n/a	90.41	16.85	n/a
DST35	IGM	78.13	n/a	n/a	123.89	31.25	n/a
DST36	n/a	n/a	n/a	n/a	n/a	n/a	n/a
DST37	n/a	n/a	n/a	n/a	n/a	n/a	n/a
DST38	Rock	865.85	83.17	474.51	422.48	346.34	n/a
DST39	Rock	839.95	77.92	458.93	415.99	335.98	n/a
DST40	n/a	n/a	n/a	n/a	n/a	n/a	n/a
DST41	n/a	n/a	n/a	n/a	n/a	n/a	n/a

Load test ID	Geomaterial	Rowe and Armitage 1987 (ksf)	Carter and Kulhawy 1988 (ksf)	Proposed method (ksf)	O'Neill and Reese 1999 (ksf)	Sowers 1976 (ksf)	Brown et al. 2010
DST42	Cohesive soil	n/a	n/a	n/a	18.12	n/a	18.12
DST43	Rock	2,238.00	1,306.01	1,772.01	685.71	895.20	n/a
DST44	Rock	698.40	215.83	457.11	378.62	279.36	n/a
DST45	n/a	n/a	n/a	n/a	n/a	n/a	n/a
DST46	Rock	321.48	1.22	161.35	254.89	128.59	n/a
DST47	Rock	500.58	7.63	254.11	319.48	200.23	n/a
DST48	n/a	n/a	n/a	n/a	n/a	n/a	n/a
DST49	Cohesionless soil	n/a	n/a	n/a	22.00	n/a	22.00

APPENDIX C. PROBABILITY DENSITY FUNCTIONS

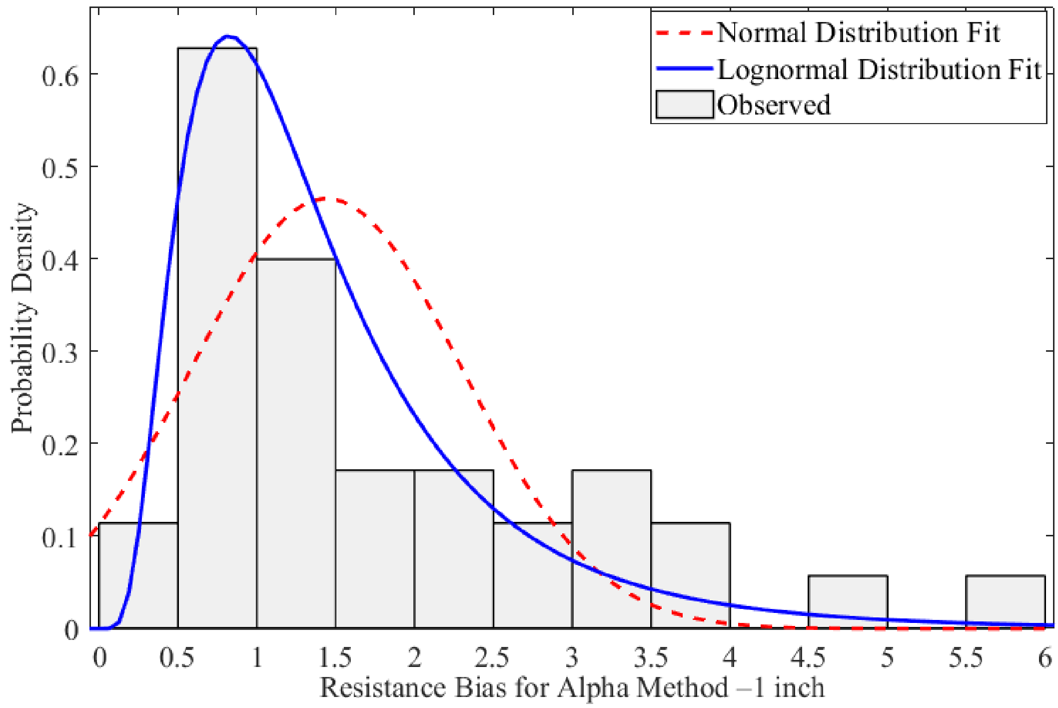

Figure C.1. PDF for α-method at 1 in. – Approach I

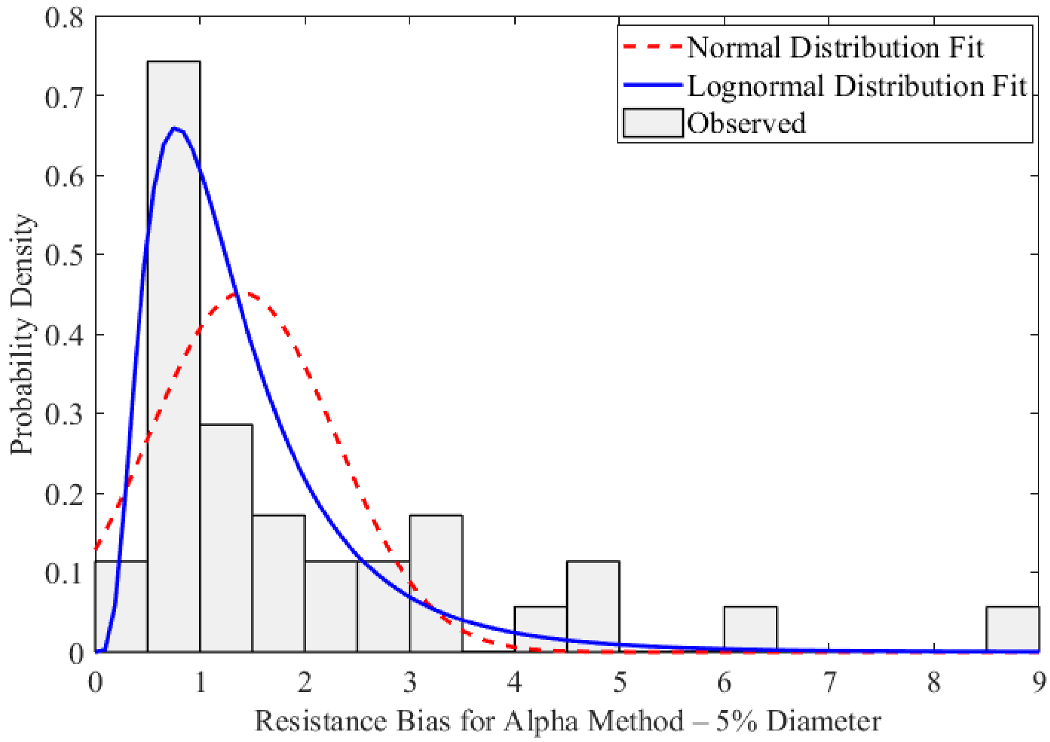

Figure C.2. PDF for α-method at 5%B – Approach I

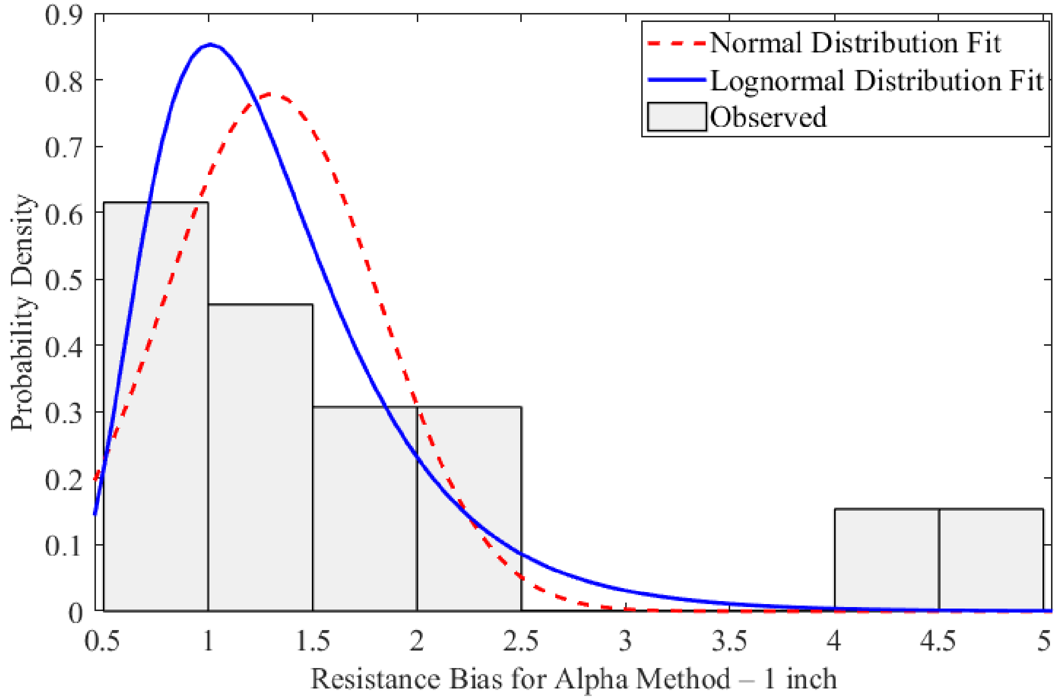

Figure C.3. PDF for α-method at 1 in. – Approach II

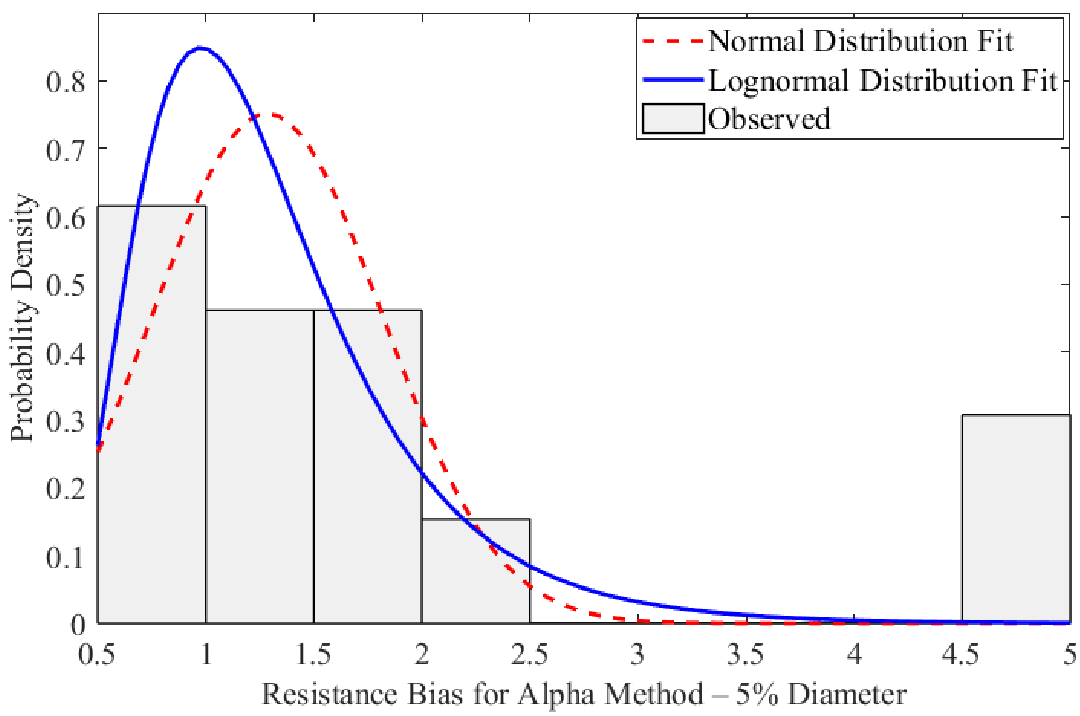

Figure C.4. PDF for α-method at 5%B – Approach II

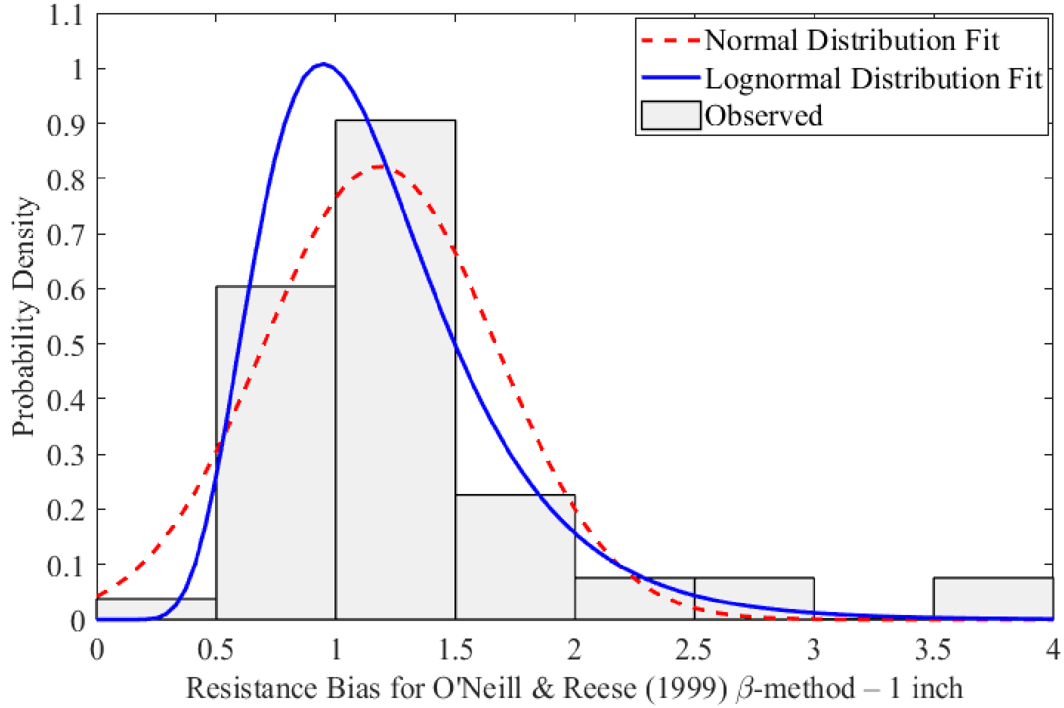

Figure C.5. PDF for O'Neill and Reese (1999) β-method at 1 in. – Approach I

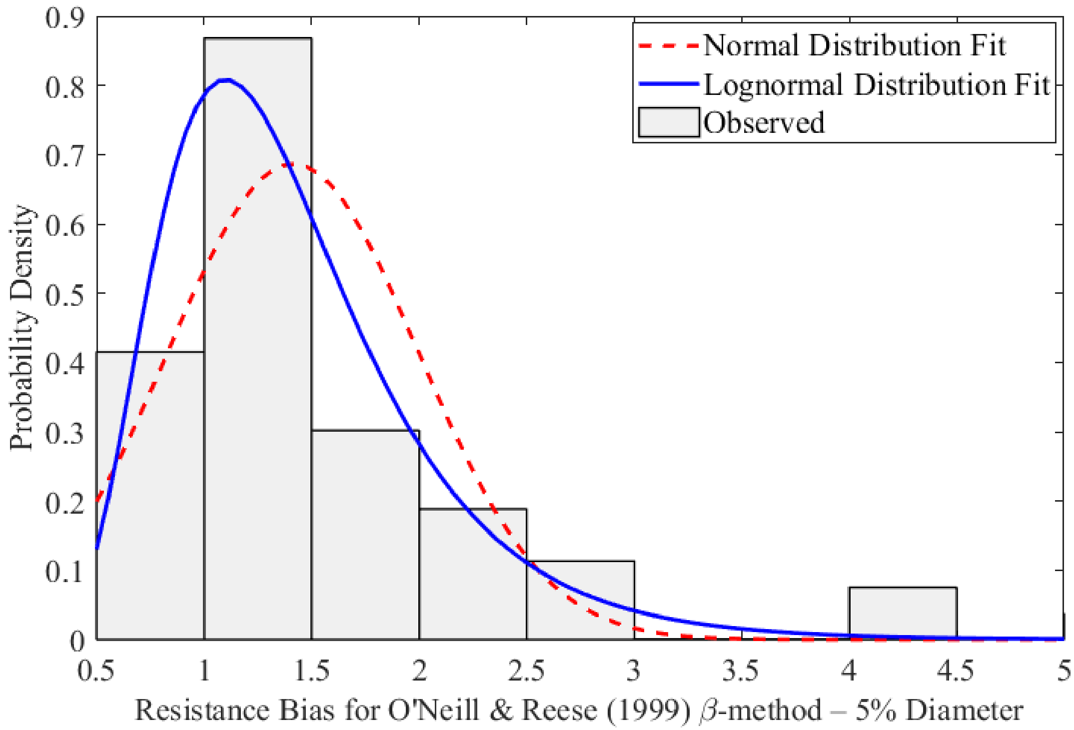

Figure C.6. PDF for O'Neill and Reese (1999) β-method at 5%B – Approach I

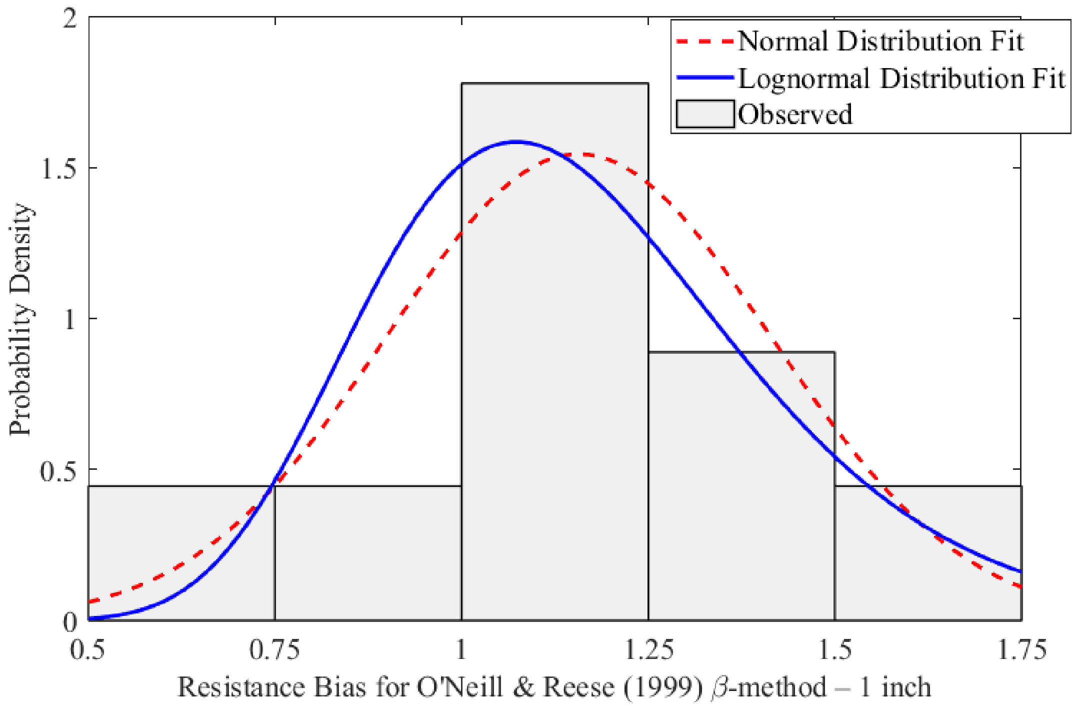

Figure C.7. PDF for O'Neill and Reese (1999) β-method at 1 in. – Approach II

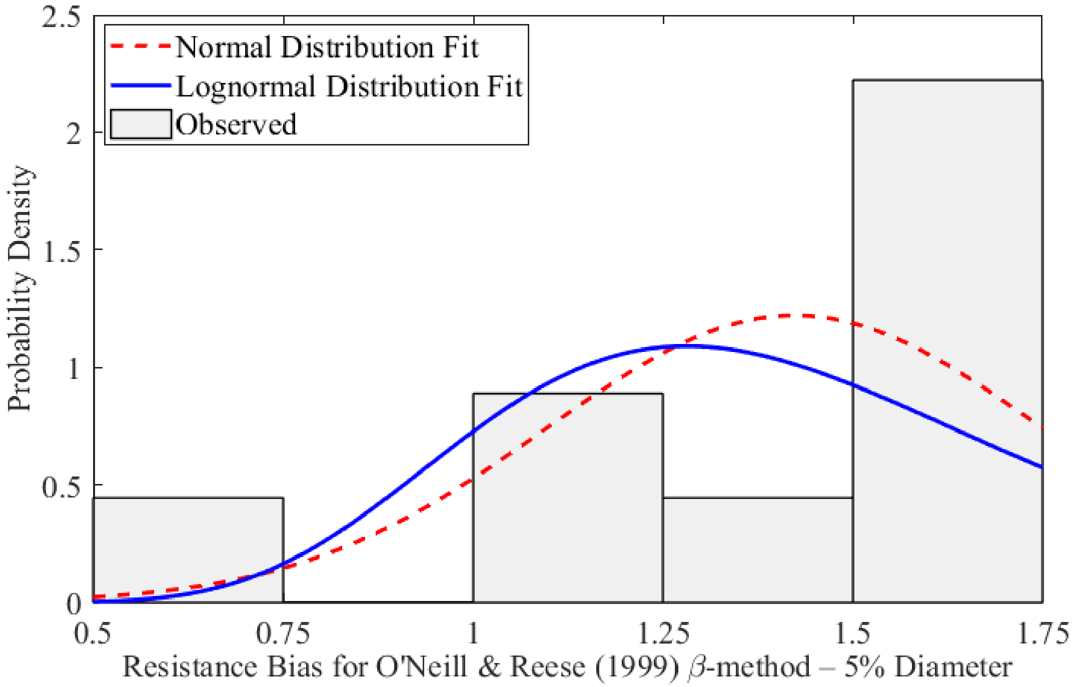

Figure C.8. PDF for O'Neill and Reese (1999) β-method at 5%B – Approach II

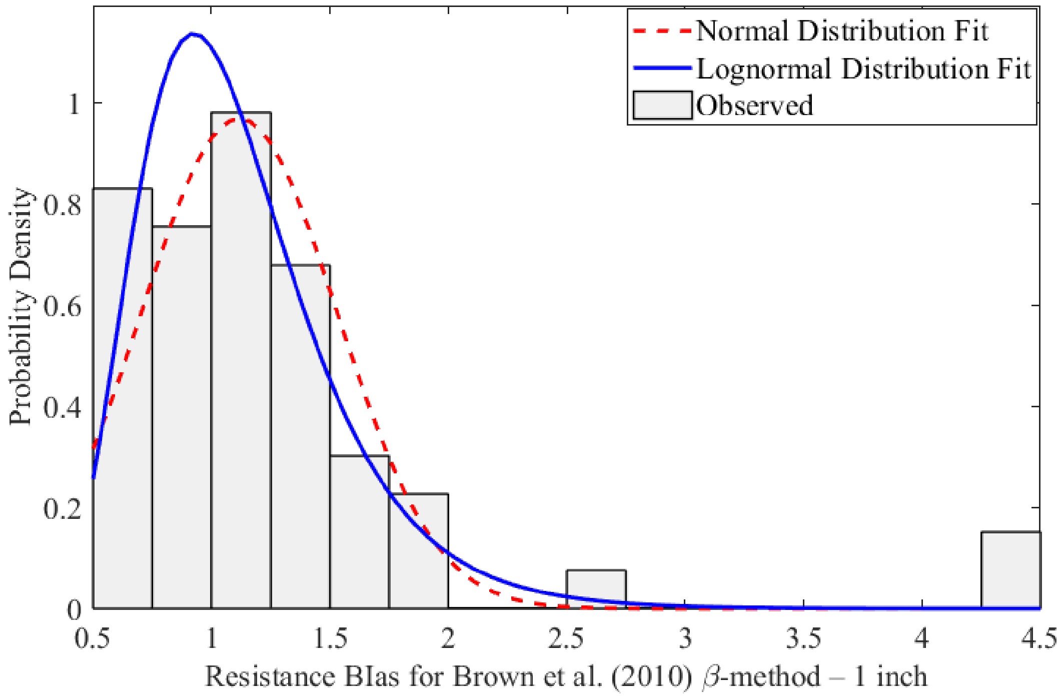

Figure C.9. PDF for Brown et al. (2010) β-method at 1 in. – Approach I

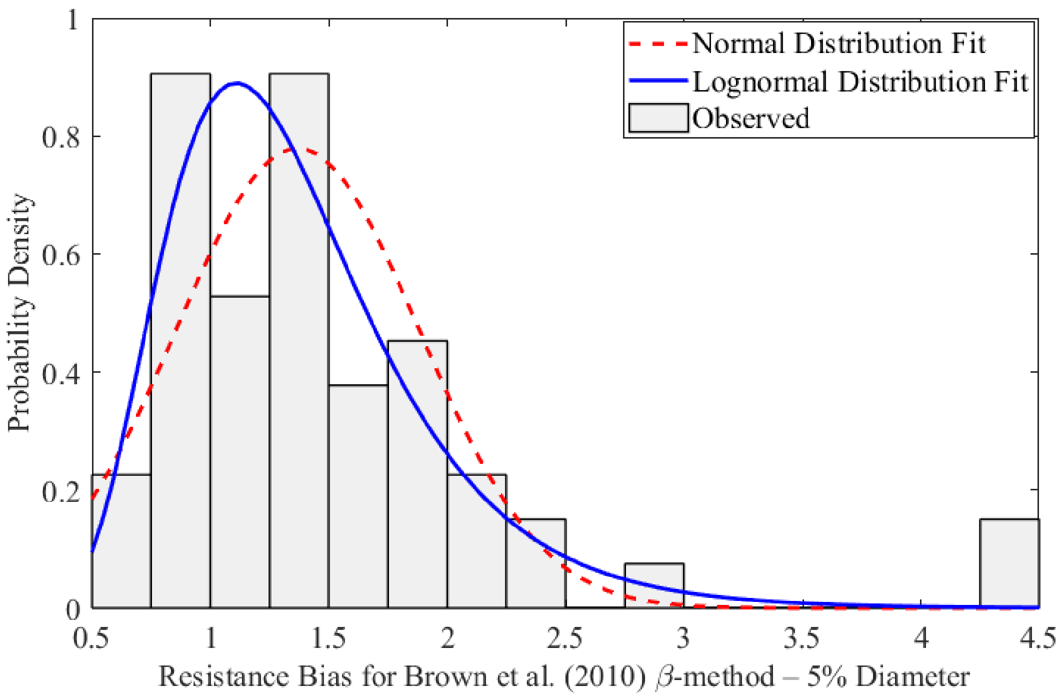

Figure C.10. PDF for Brown et al. (2010) β-method at 5%B – Approach I

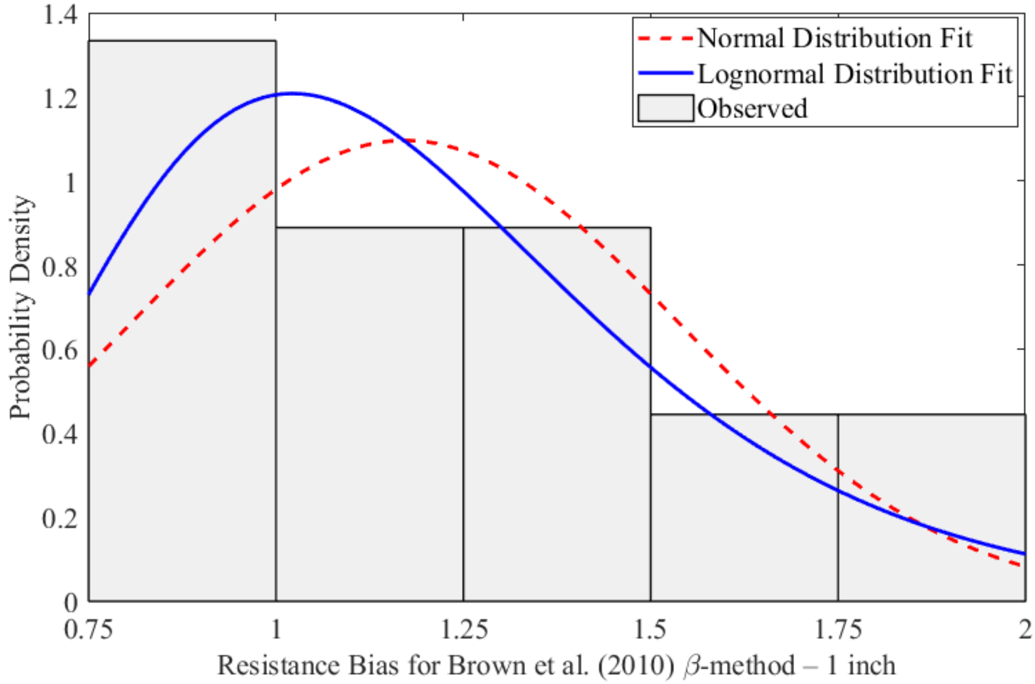

Figure C.11. PDF for Brown et al. (2010) β-method at 1 in. – Approach II

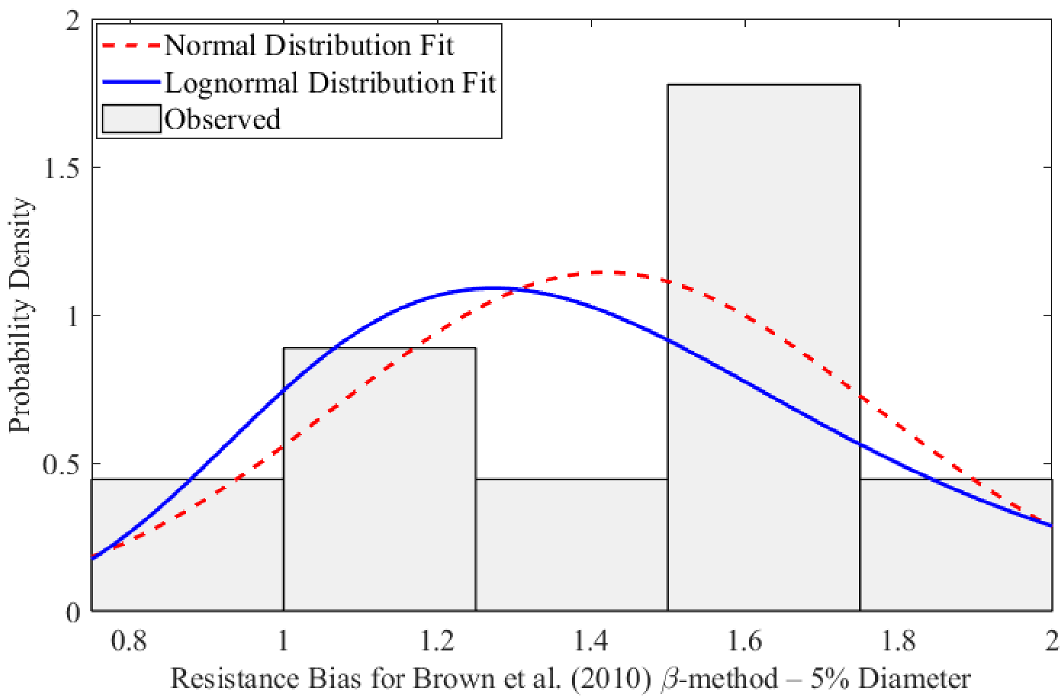

Figure C.12. PDF for Brown et al. (2010) β-method at 5%B – Approach II

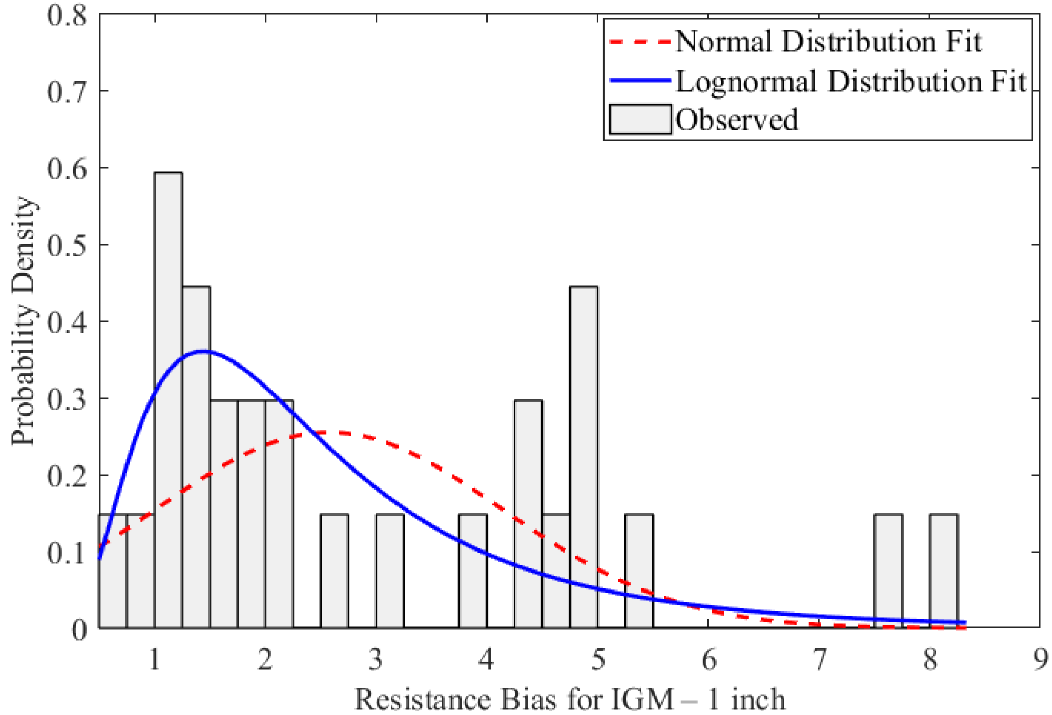

Figure C.13. PDF for skin friction in IGM at 1 in. – Approach I

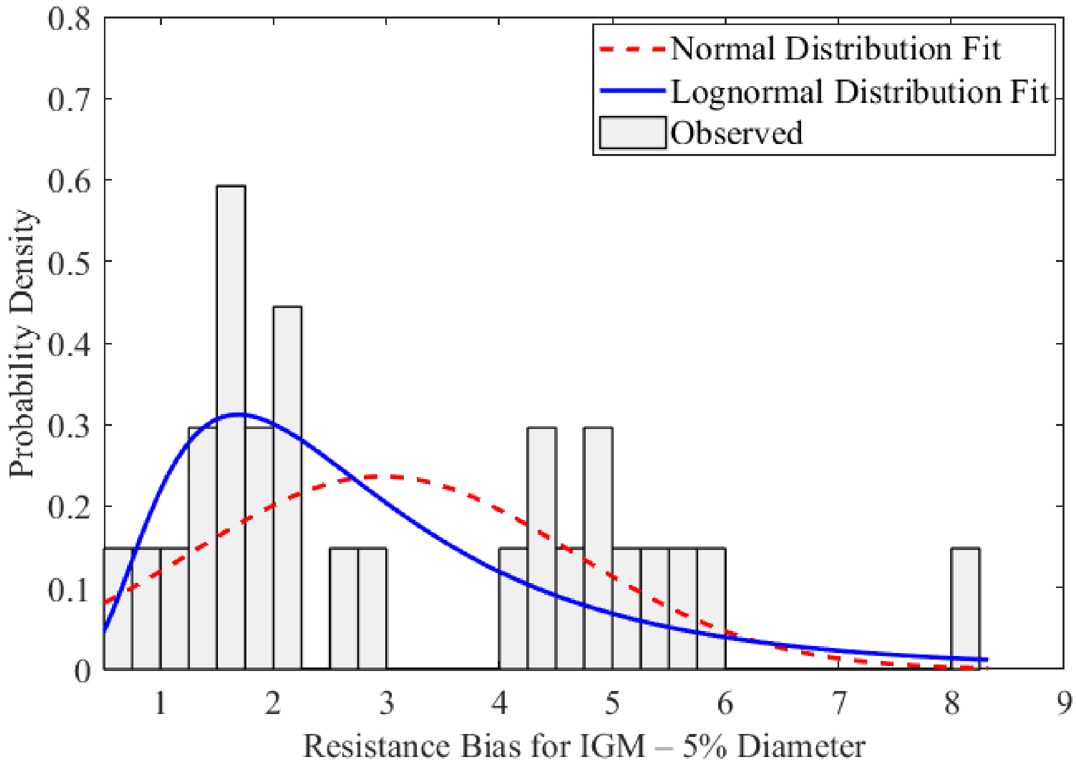

Figure C.14. PDF for skin friction in IGM at 5%B – Approach I

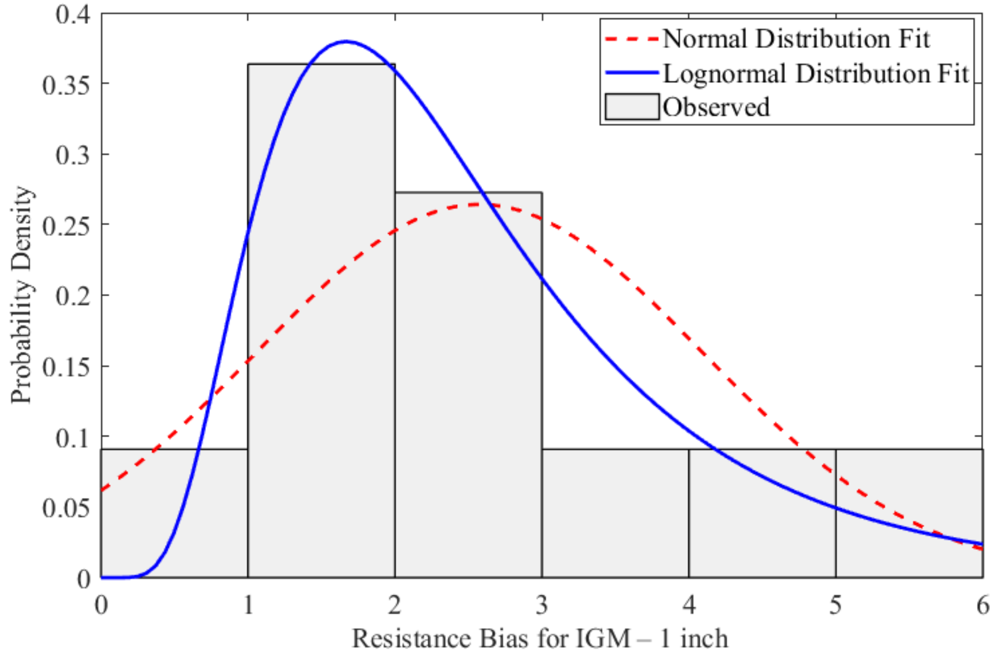

Figure C.15. PDF for skin friction in IGM at 1 in. – Approach II

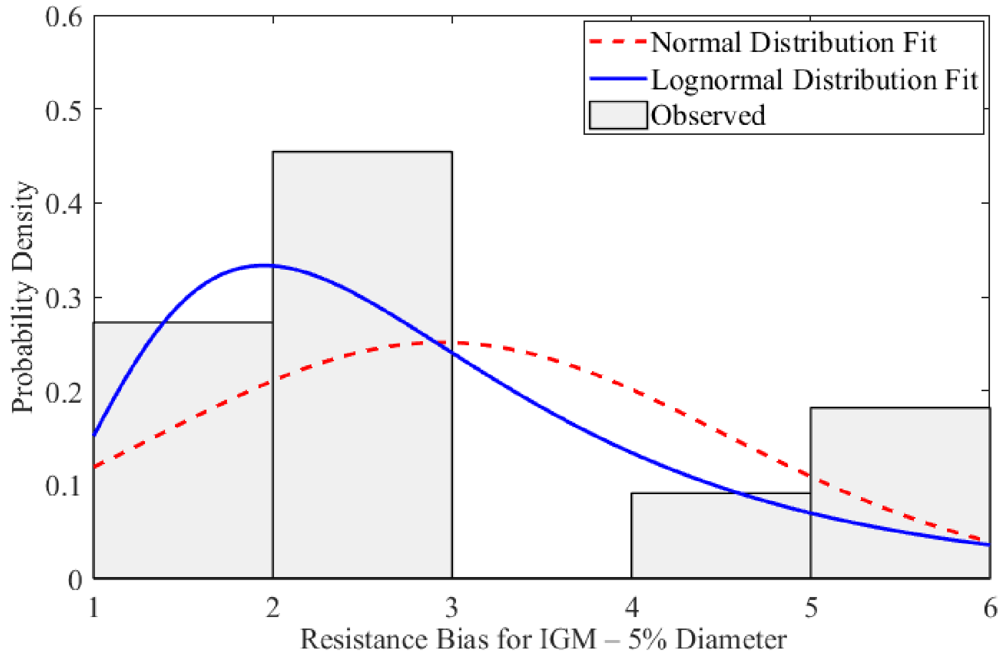

Figure C.16. PDF for skin friction in IGM at 5%B – Approach II

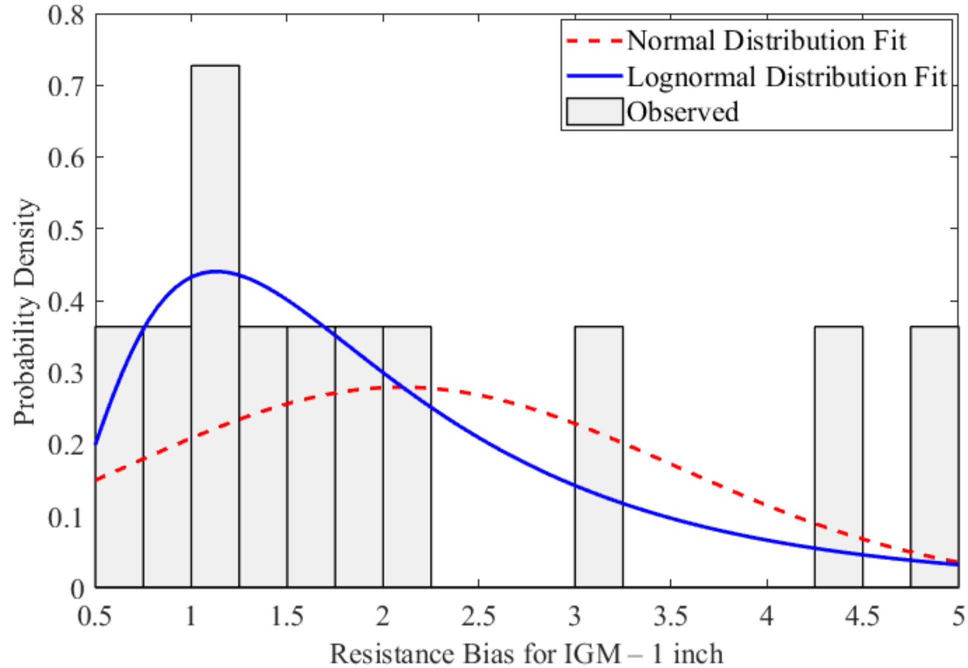

Figure C.17. PDF for skin friction in IGM at 1 in., Iowa data only – Approach I

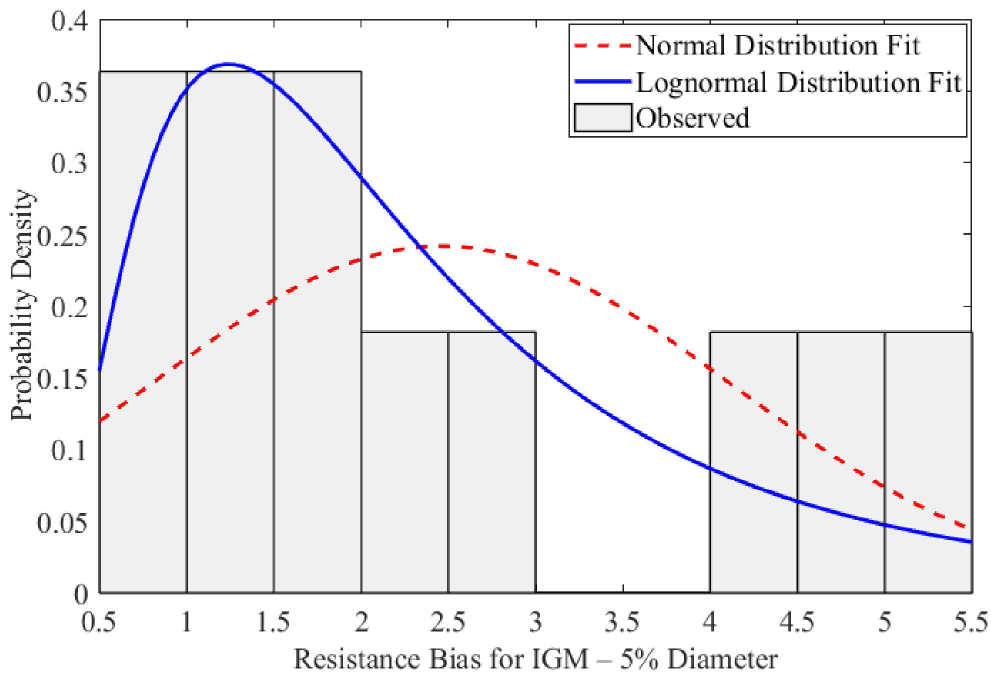

Figure C.18. PDF for skin friction in IGM at 5%B, Iowa data only – Approach I

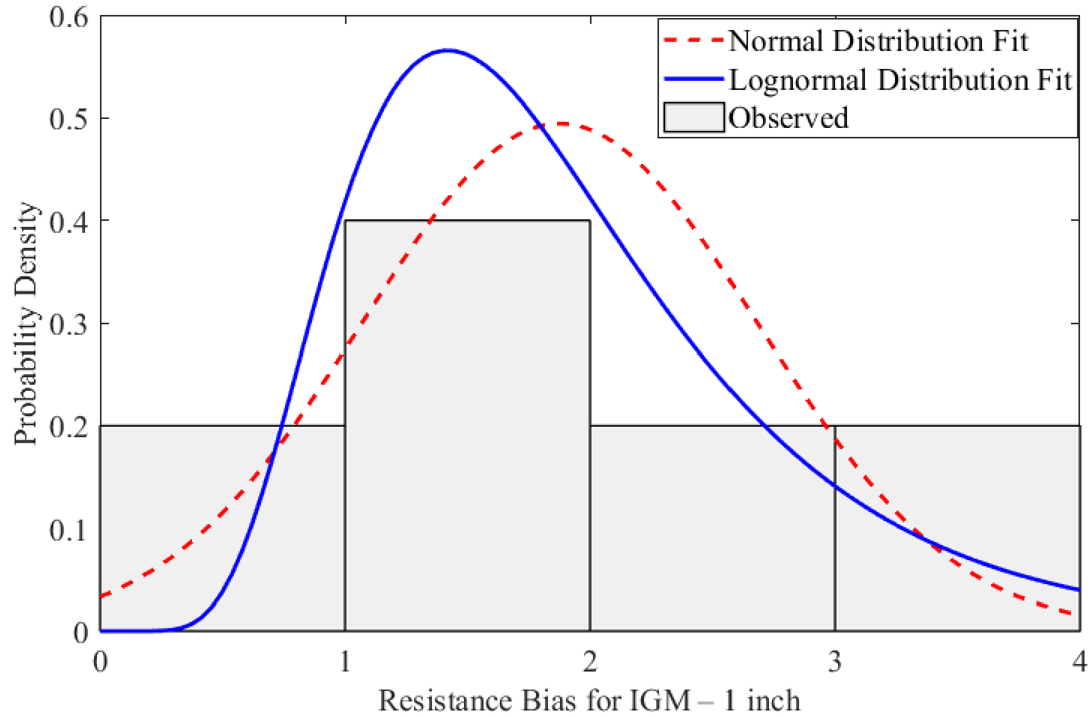

Figure C.19. PDF for skin friction in IGM at 1 in., Iowa data only – Approach II

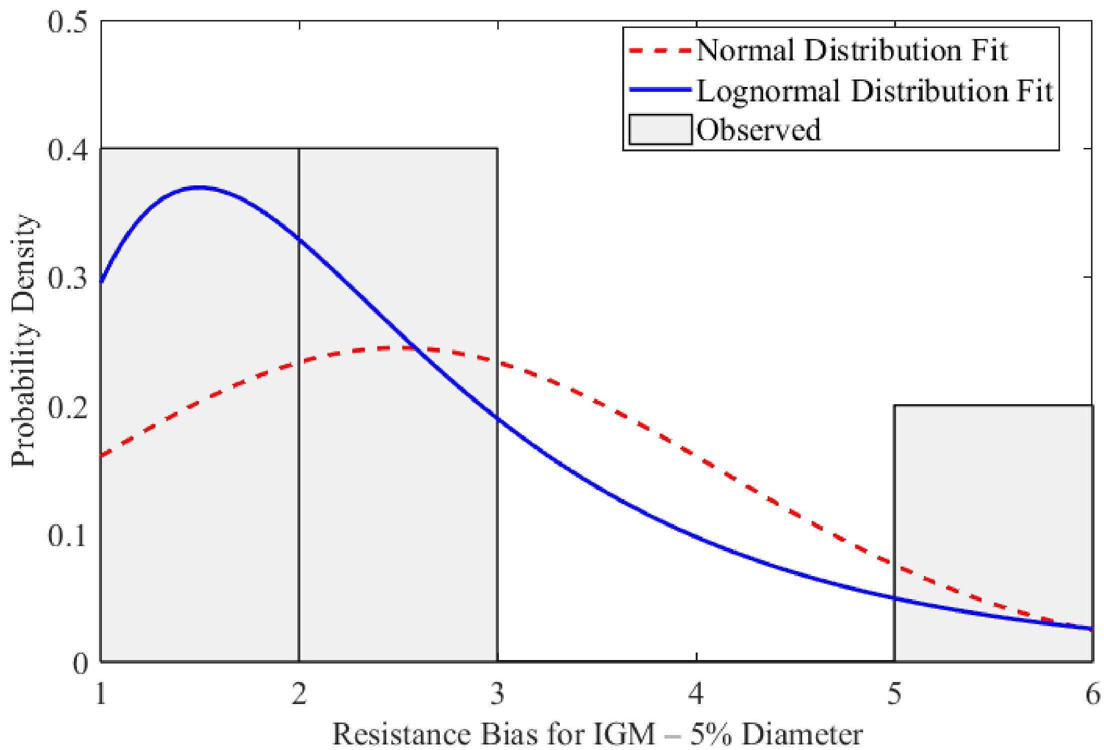

Figure C.20. PDF for skin friction in IGM at 5%B, Iowa data only – Approach II

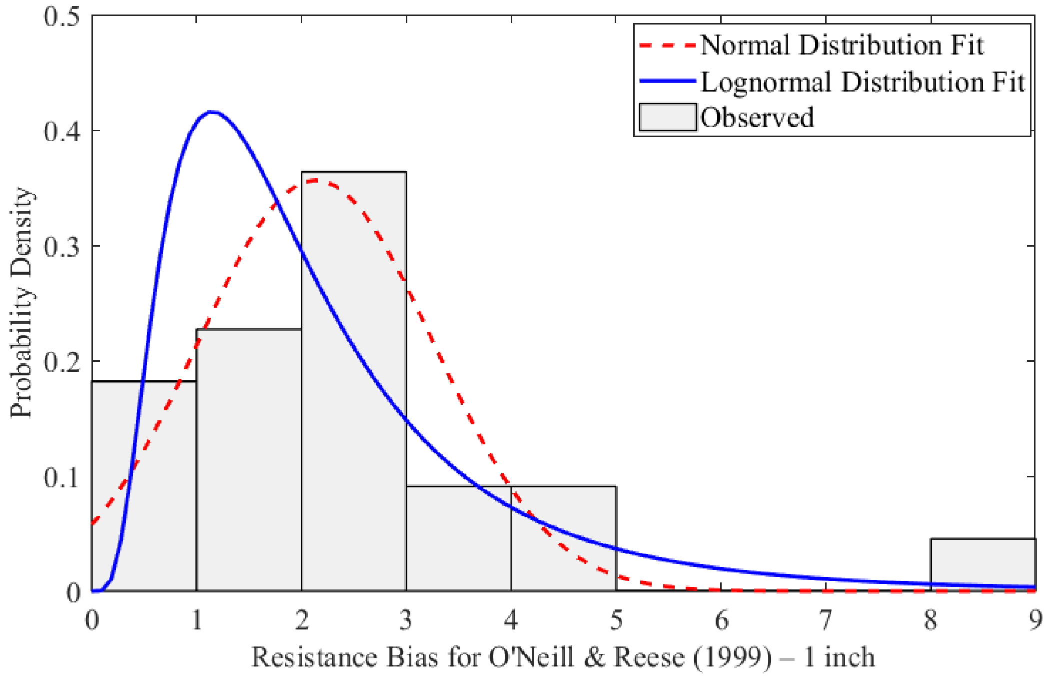

Figure C.21. PDF for skin friction in rock at 1 in. using O'Neill and Reese (1999) – Approach I

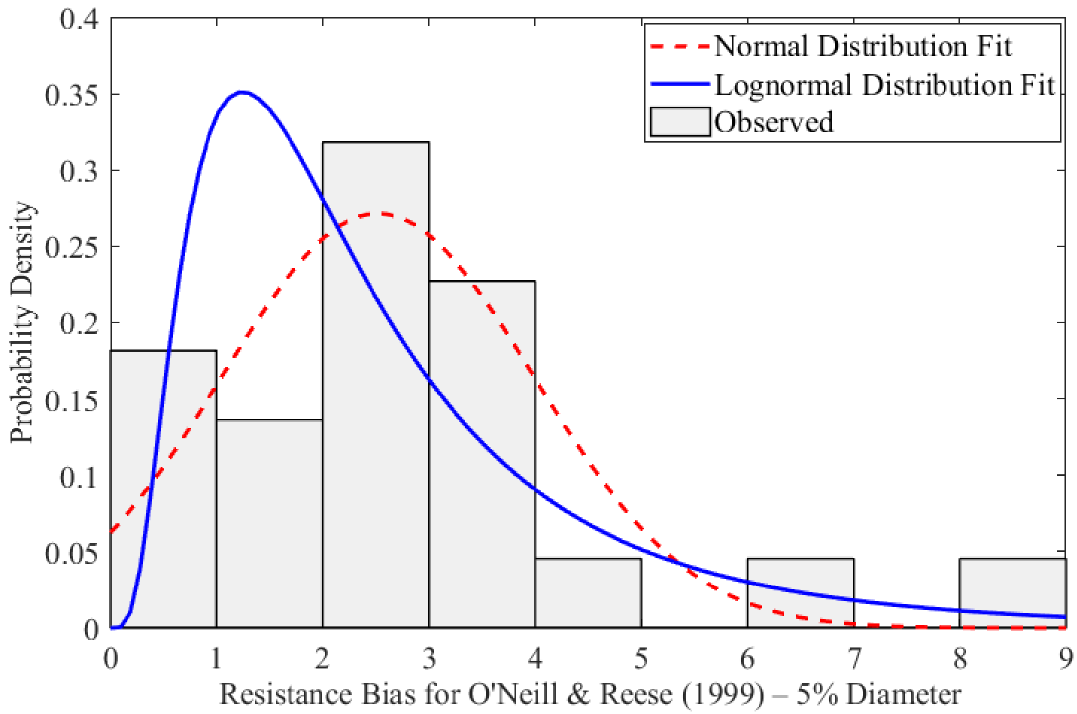

Figure C.22. PDF for skin friction in rock at 5%B using O'Neill and Reese (1999) – Approach I

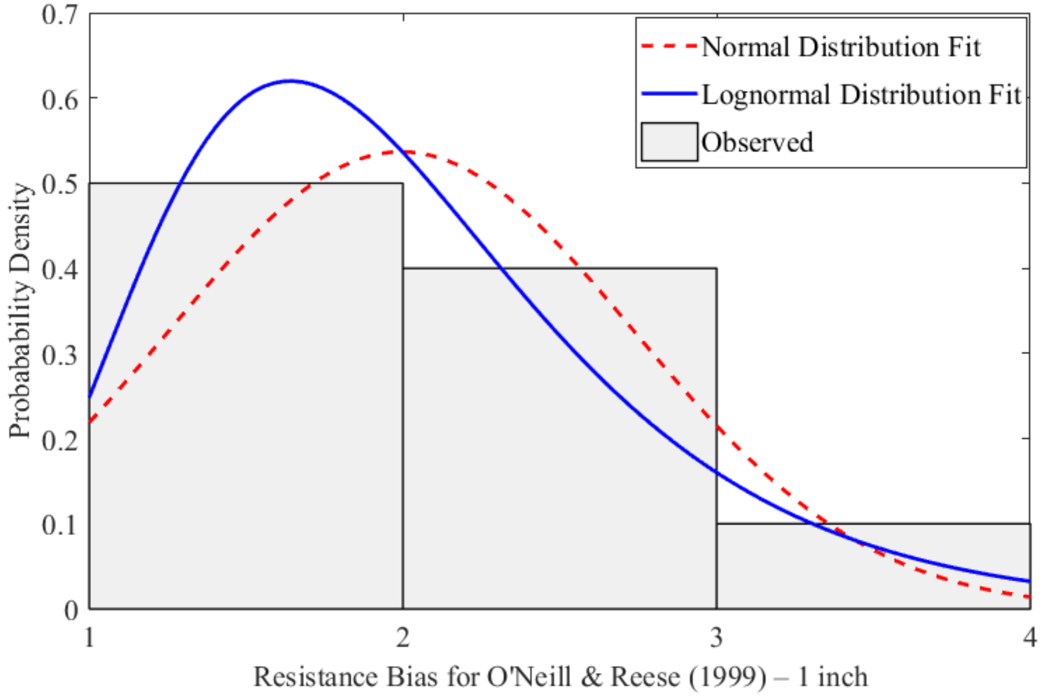

Figure C.23. PDF for skin friction in rock at 1 in. using O’Neill and Reese (1999) – Approach II

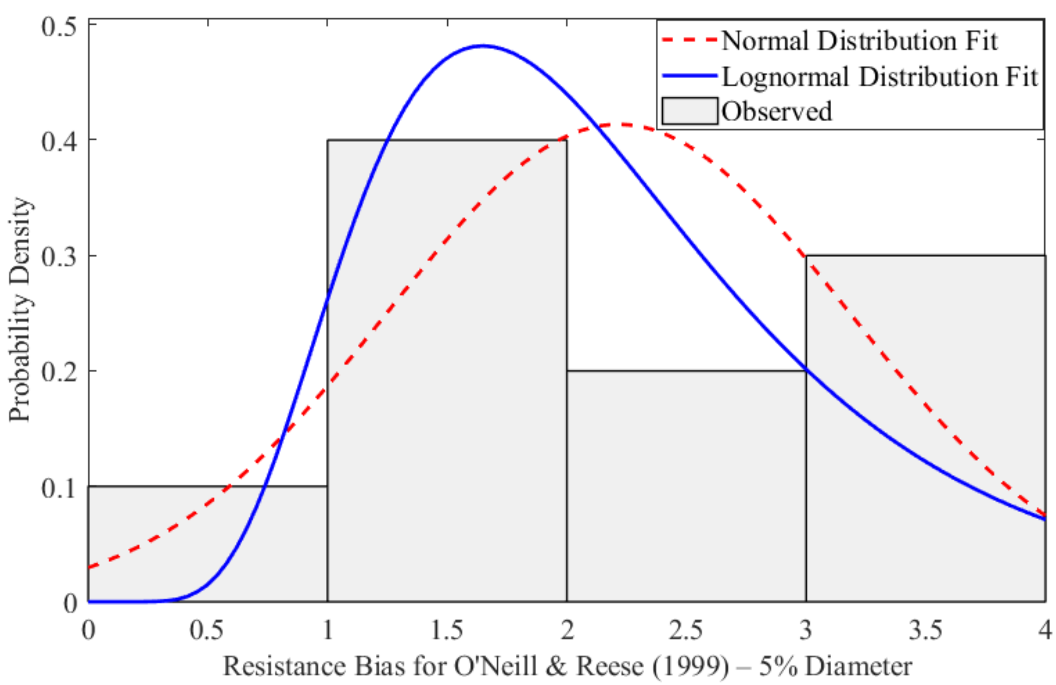

Figure C.24. PDF for skin friction in rock at 5%B using O’Neill and Reese (1999) – Approach II

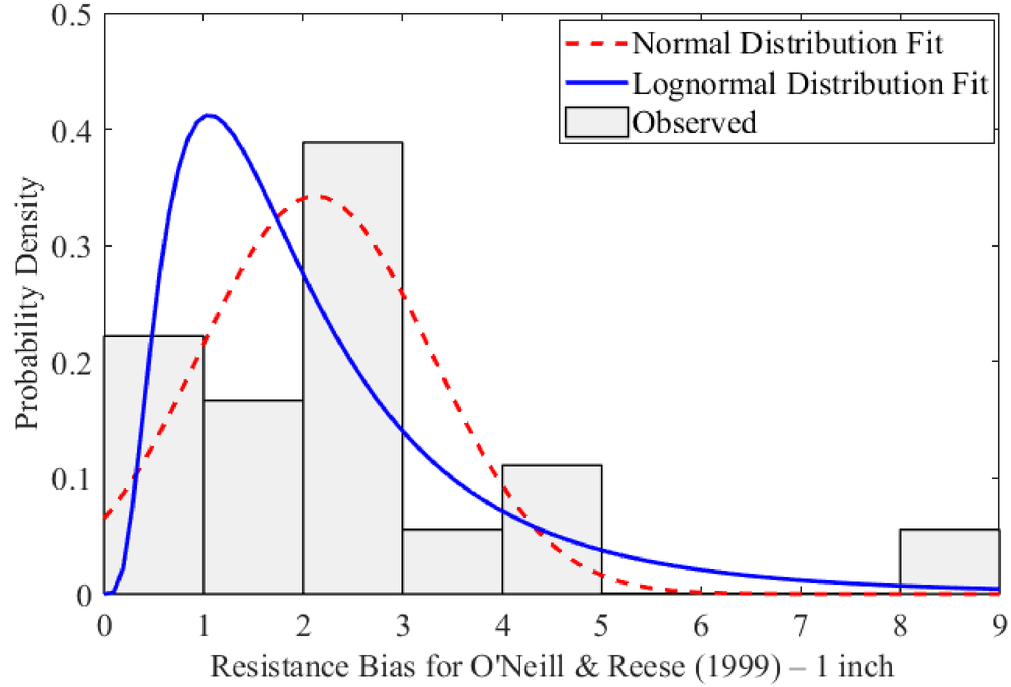

Figure C.25. PDF for skin friction in rock at 1 in. using O'Neill and Reese (1999), Iowa data only – Approach I

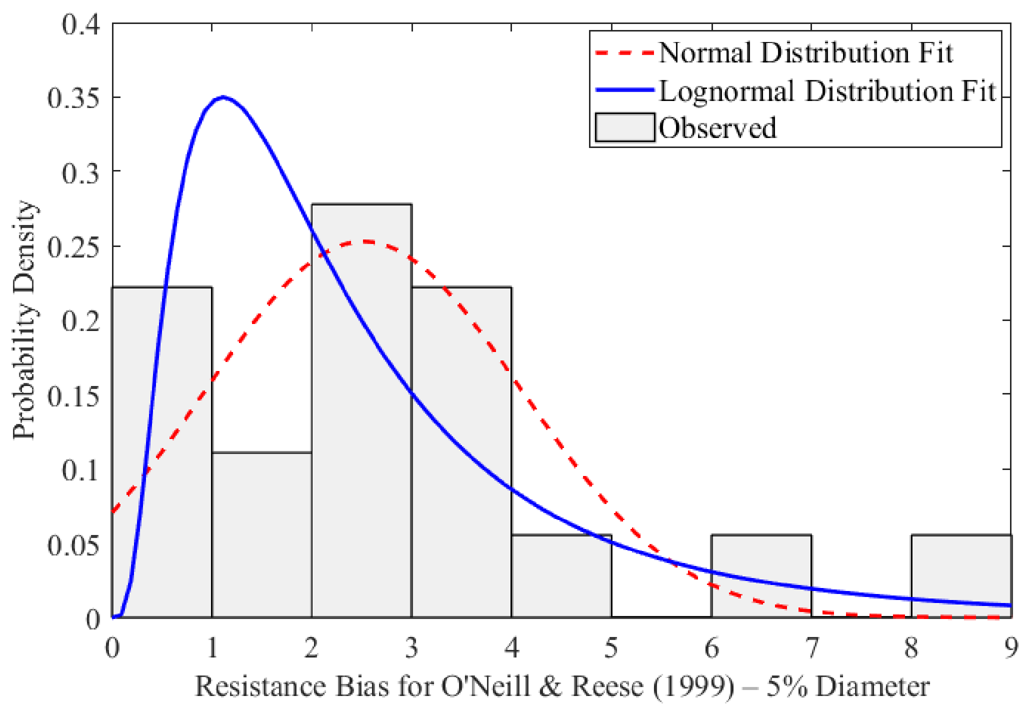

Figure C.26. PDF for skin friction in rock at 5%B using O'Neill and Reese (1999), Iowa data only – Approach I

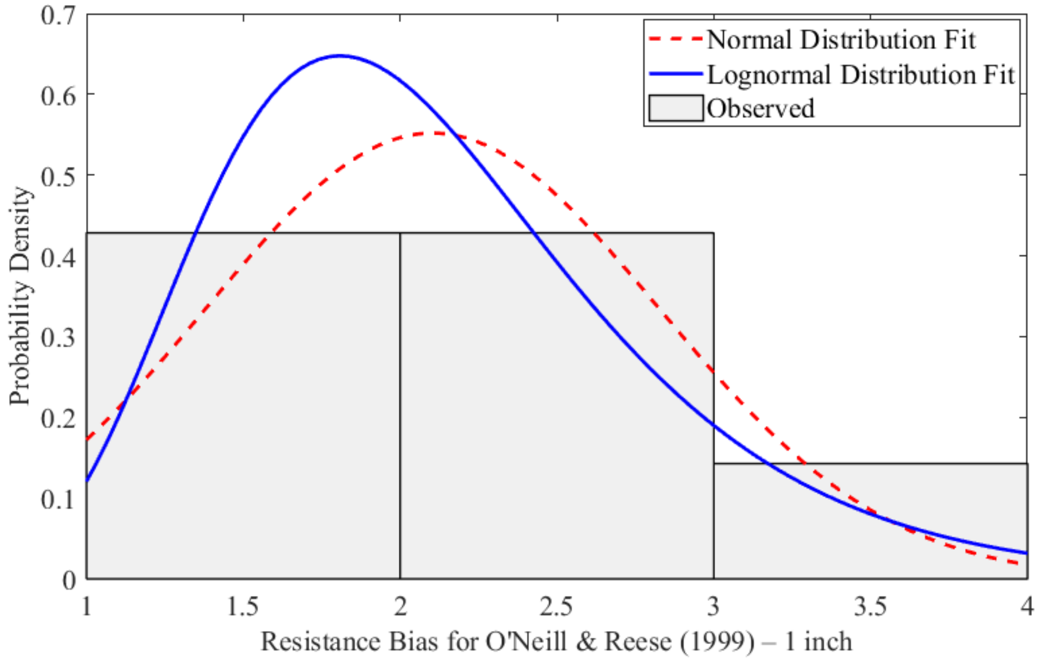

Figure C.27. PDF for skin friction in rock at 1 in. using O'Neill and Reese (1999), Iowa data only – Approach II

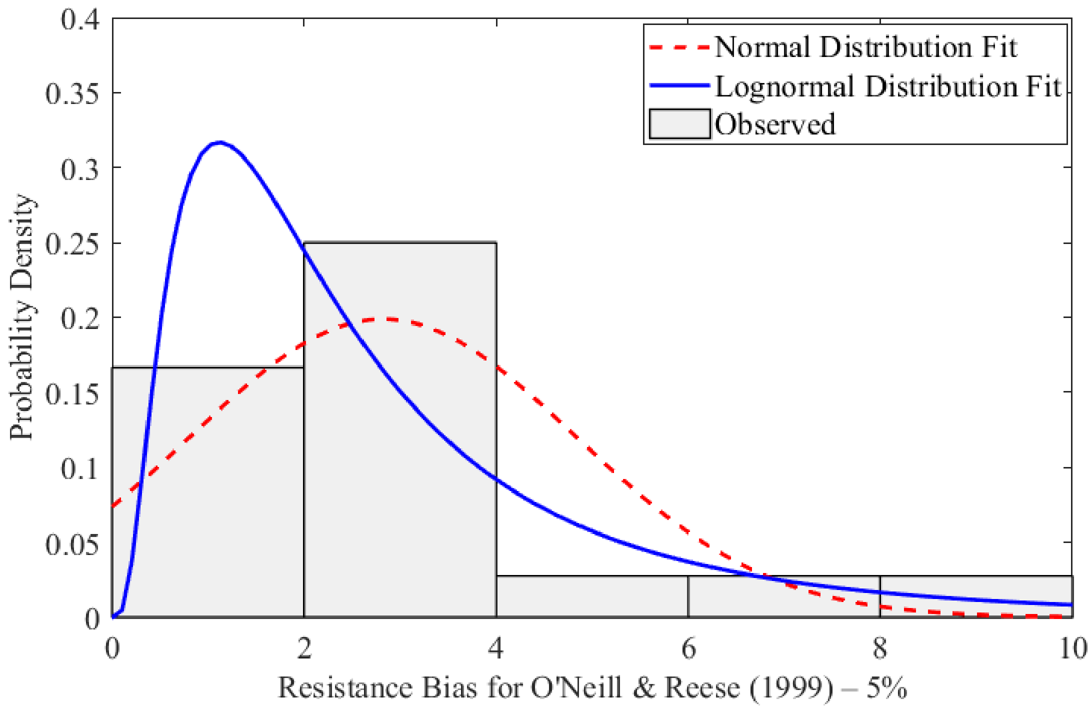

Figure C.28. PDF for skin friction in rock at 5%B using O'Neill and Reese (1999), Iowa data – Approach II

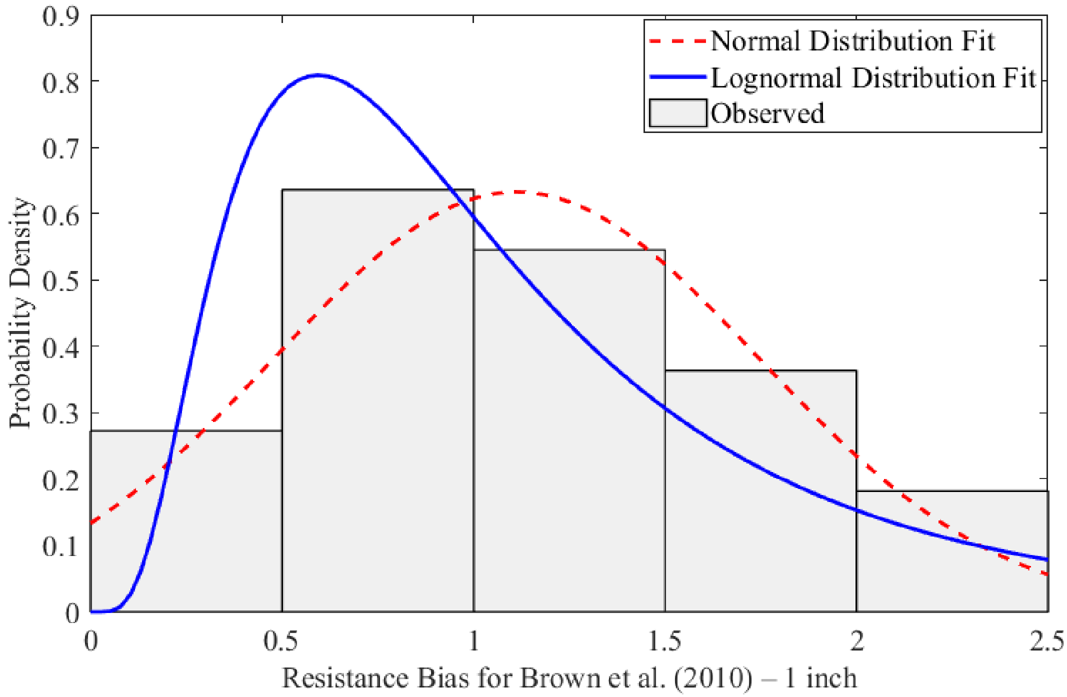

Figure C.29. PDF for skin friction in rock at 1 in. using Brown et al. (2010) – Approach I

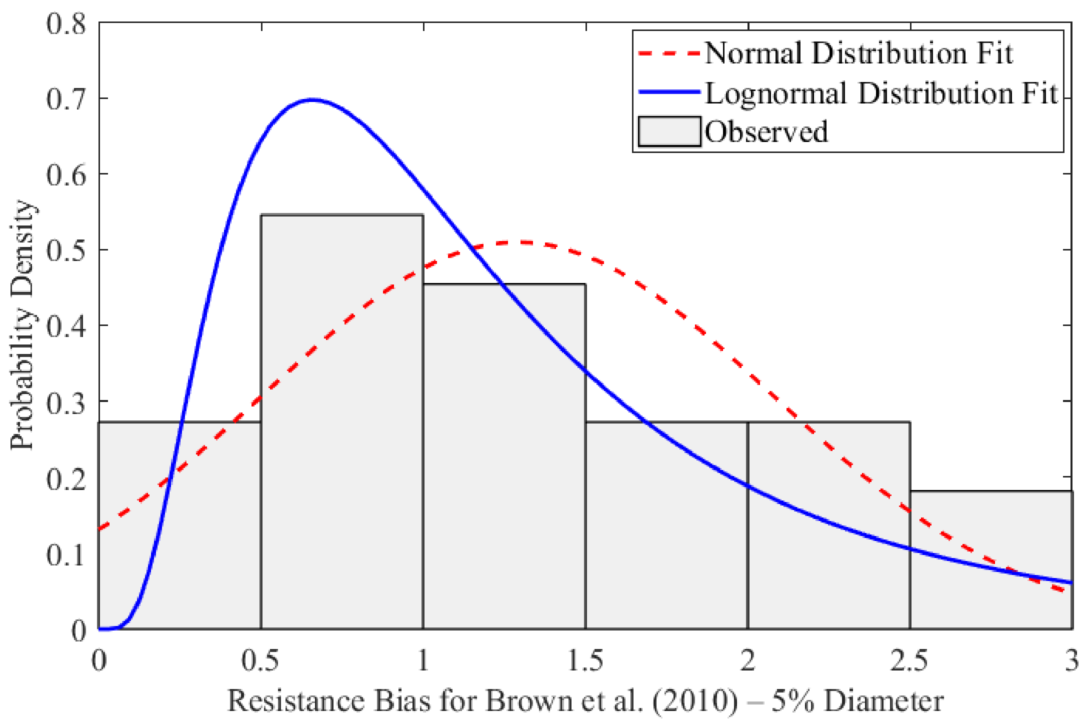

Figure C.30. PDF for skin friction in rock at 5%B using Brown et al. (2010) – Approach I

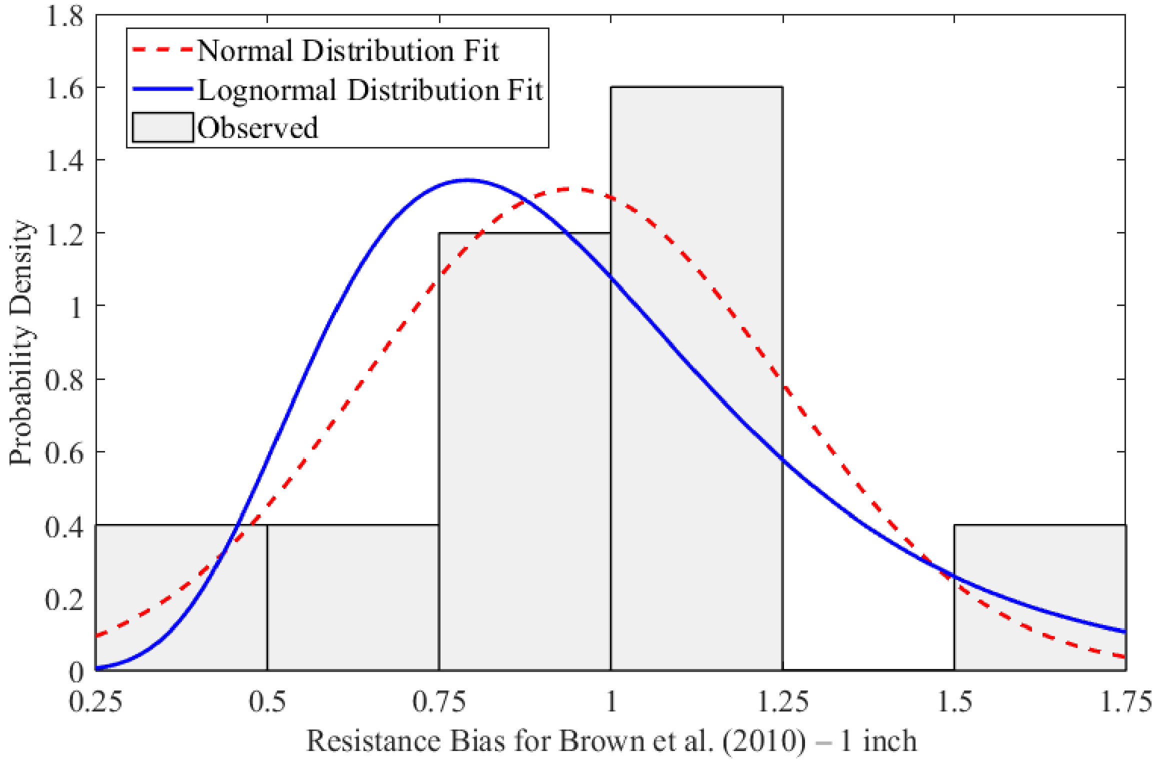

Figure C.31. PDF for skin friction in rock at 1 in. using Brown et al. (2010) – Approach II

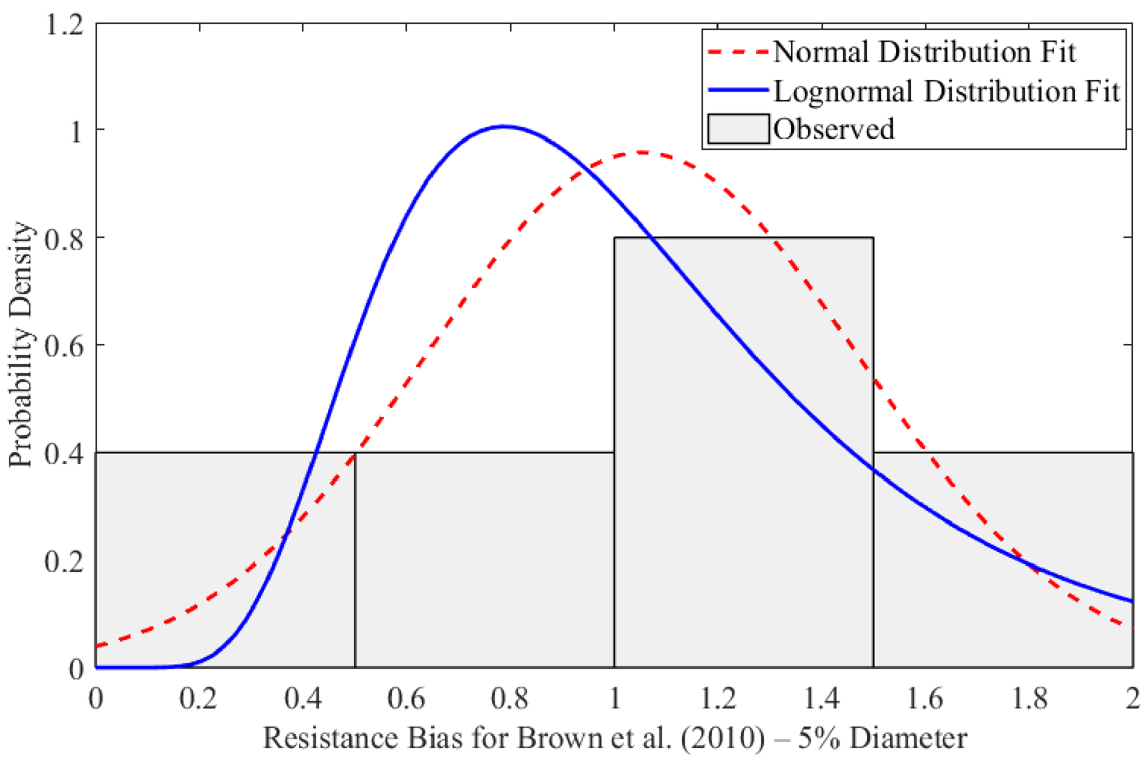

Figure C.32. PDF for skin friction in rock at 5%B using Brown et al. (2010) – Approach II

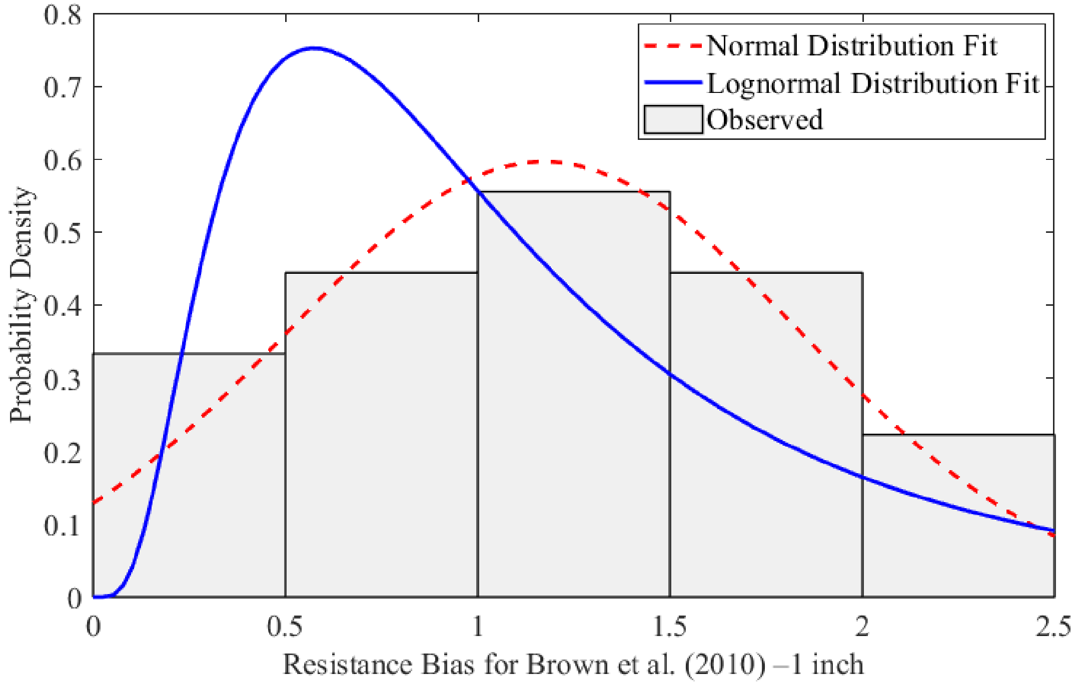

Figure C.33. PDF for skin friction in rock at 1 in. using Brown et al. (2010), Iowa data – Approach I

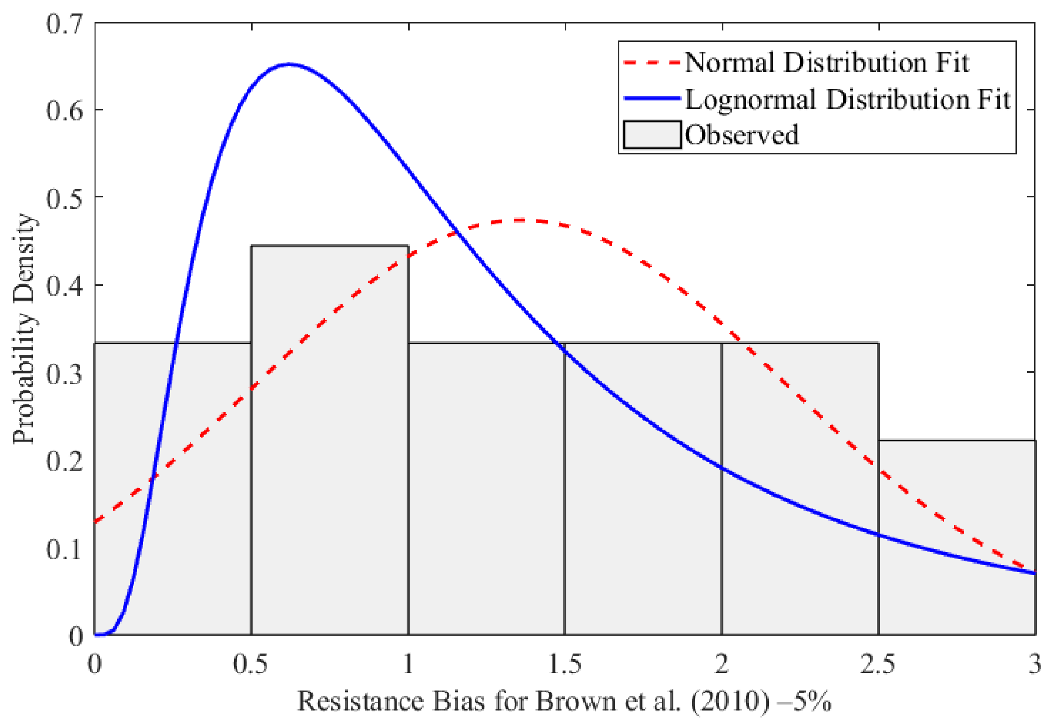

Figure C.34. PDF for skin friction in rock at 5%B using Brown et al. (2010), Iowa data – Approach I

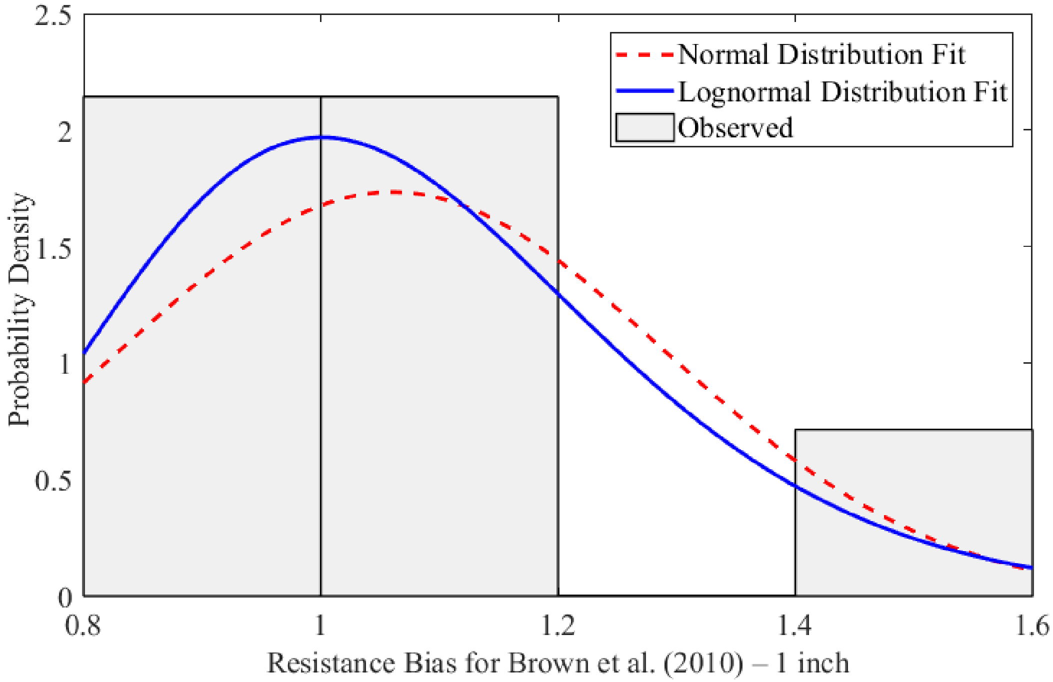

Figure C.35. PDF for skin friction in rock at 1 in. using Brown et al. (2010), Iowa data – Approach II

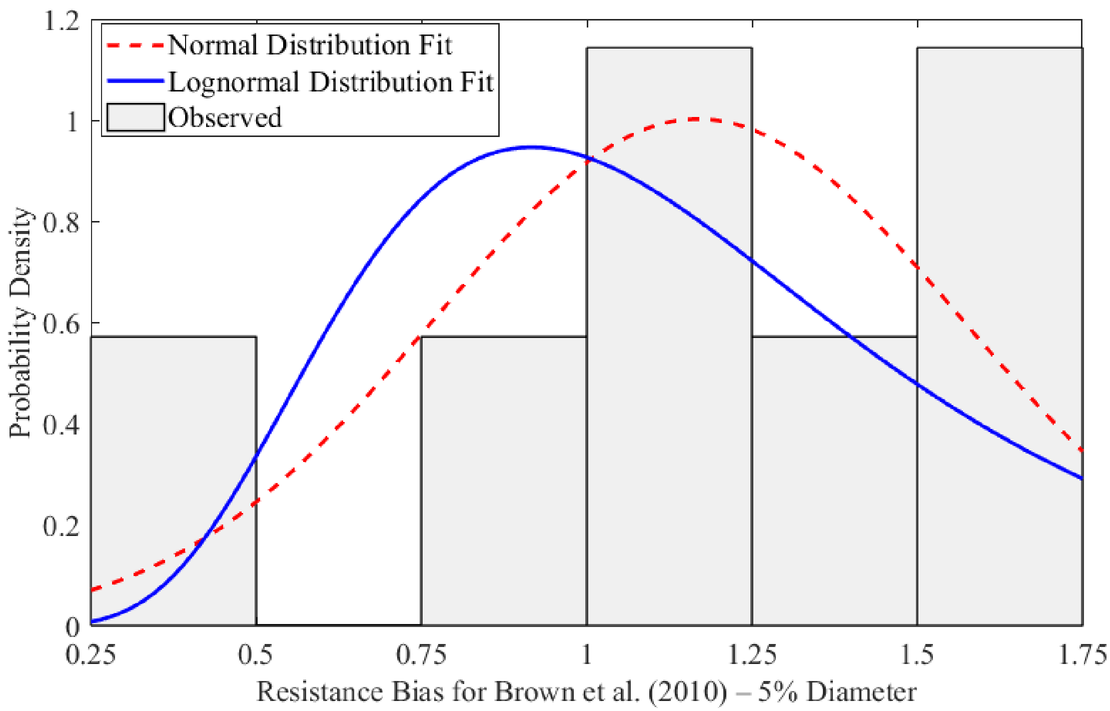

Figure C.36. PDF for skin friction in rock at 5%B using Brown et al. (2010), Iowa data – Approach II

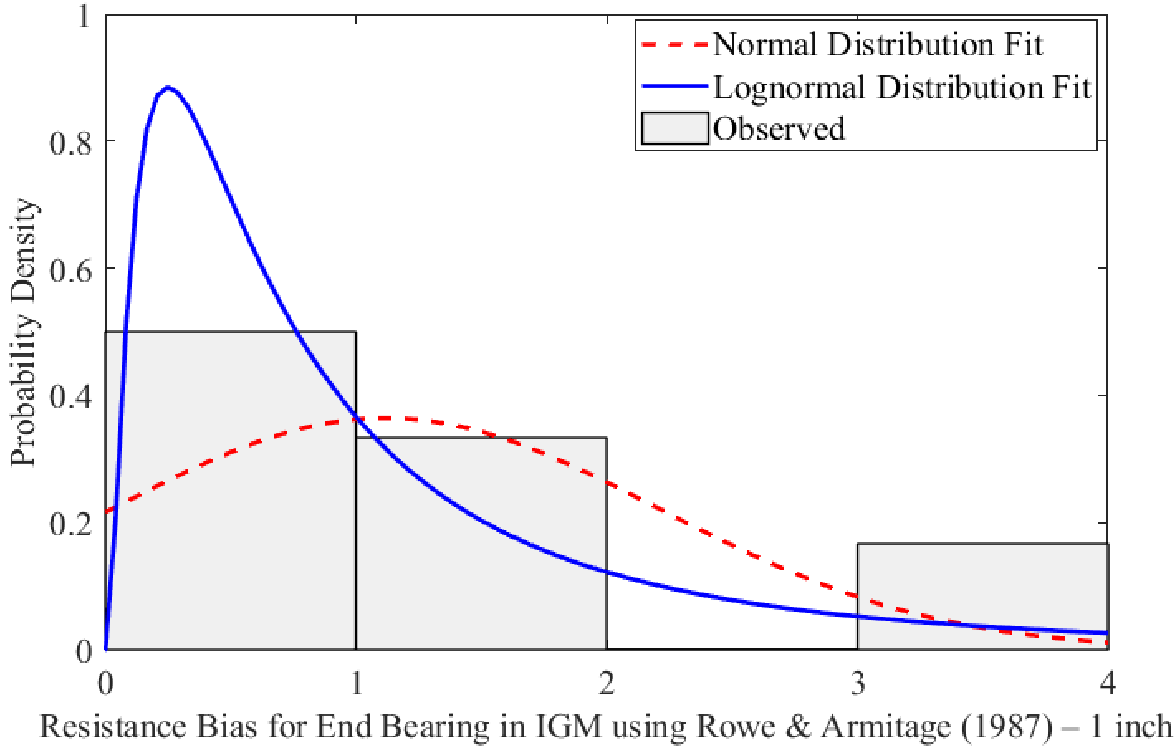

Figure C.37. PDF for end bearing in IGM at 1 in. using Rowe and Armitage (1987)

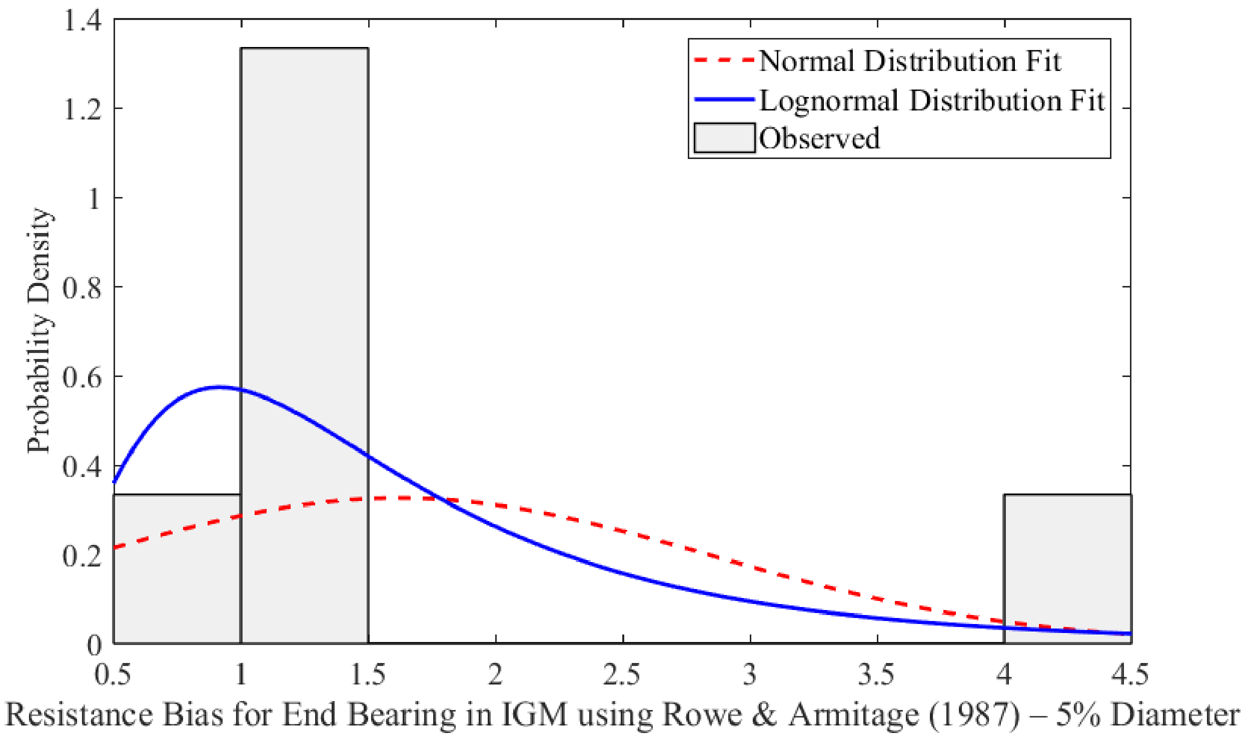

Figure C.38. PDF for end bearing in IGM at 5%B using Rowe and Armitage (1987)

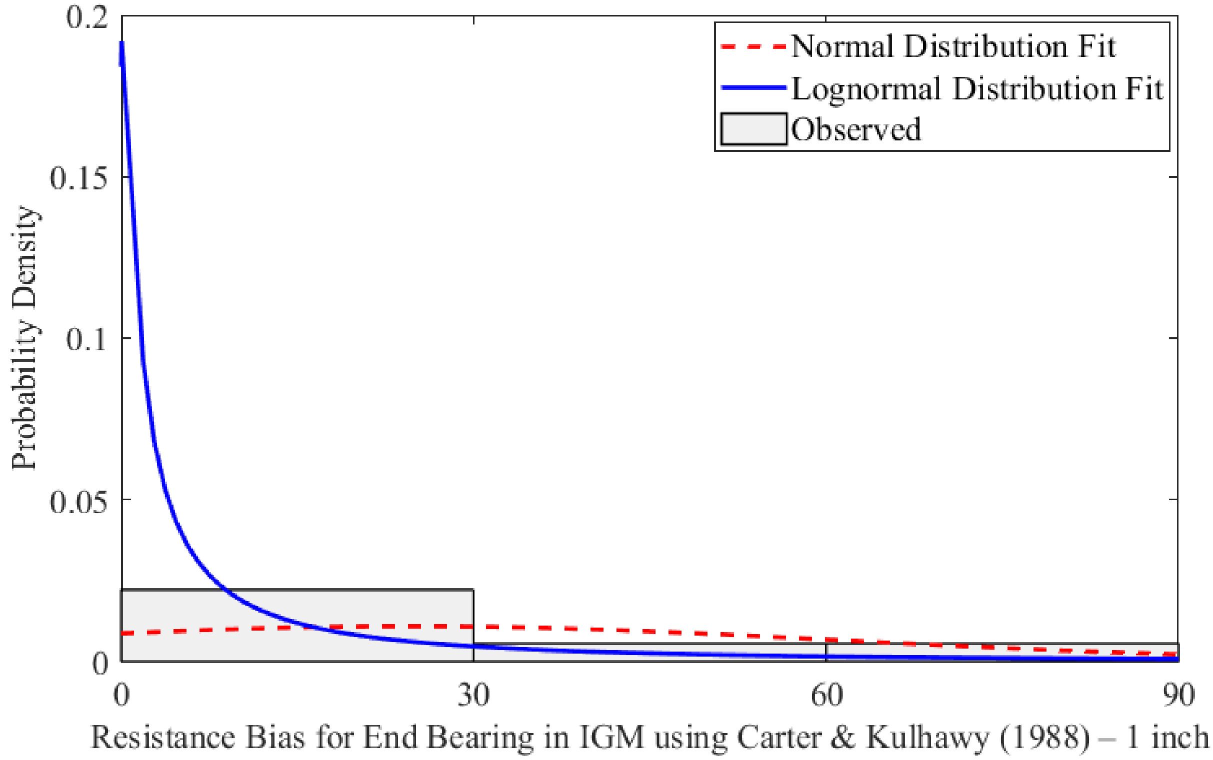

Figure C.39. PDF for end bearing in IGM at 1 in. using Carter and Kulhawy (1988)

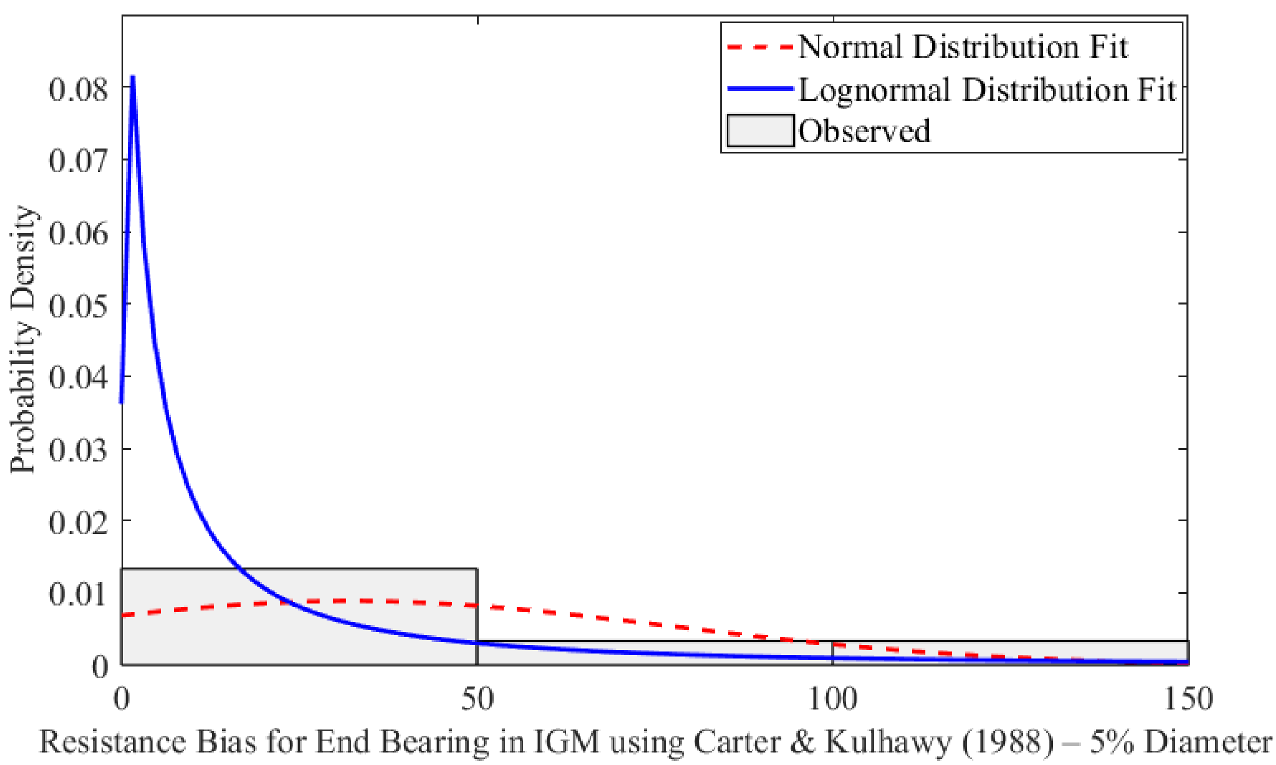

Figure C.40. PDF for end bearing in IGM at 5%B using Carter and Kulhawy (1988)

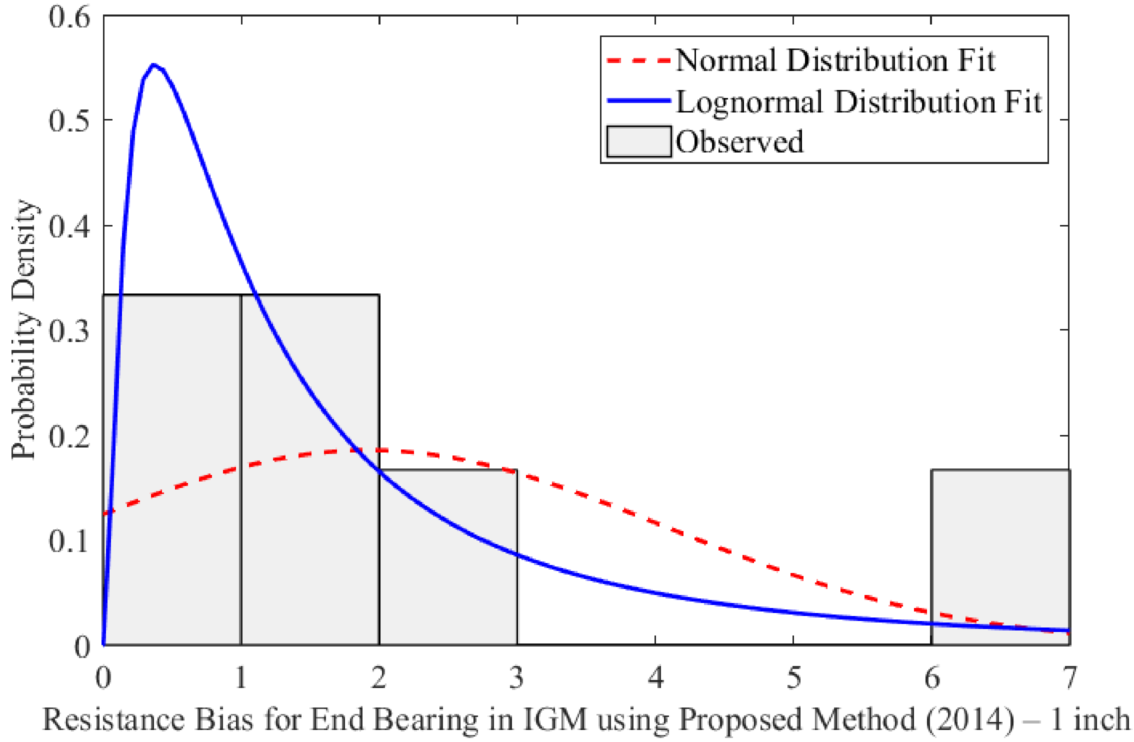

Figure C.41. PDF for end bearing in IGM at 1 in. using proposed method (2014)

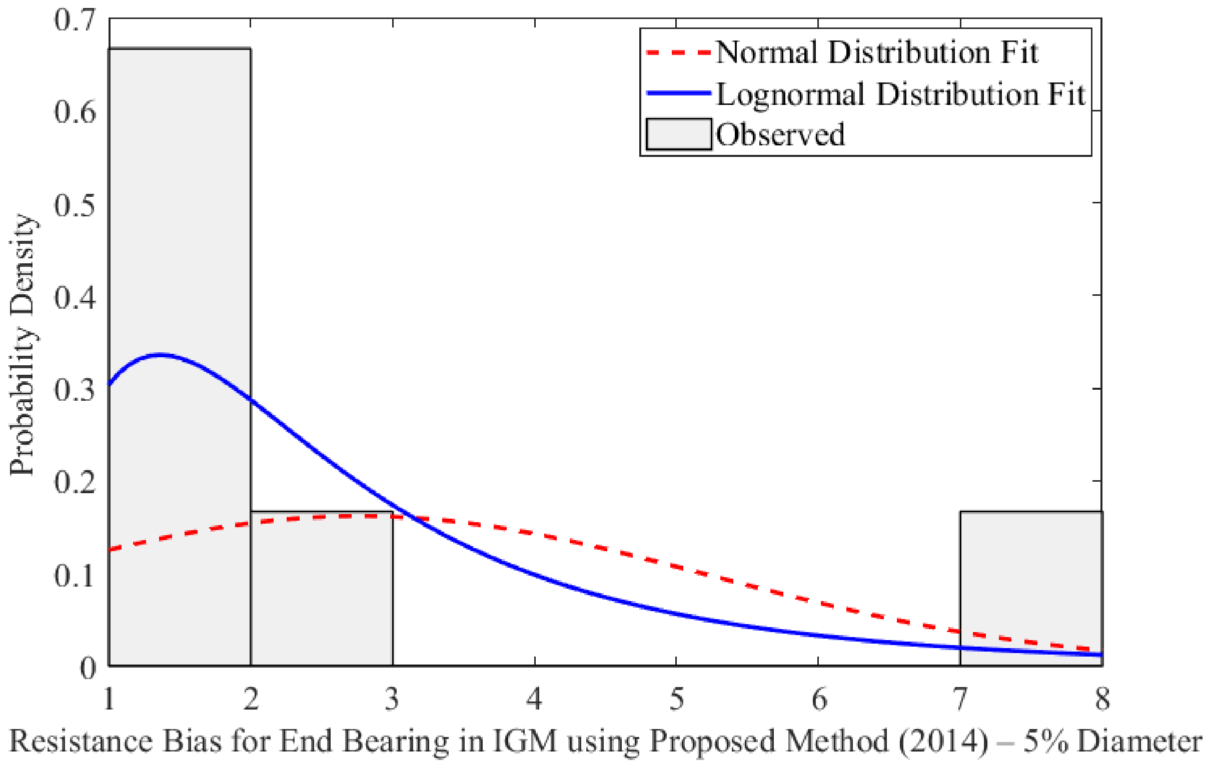

Figure C.42. PDF for end bearing in IGM at 5%B using proposed method (2014)

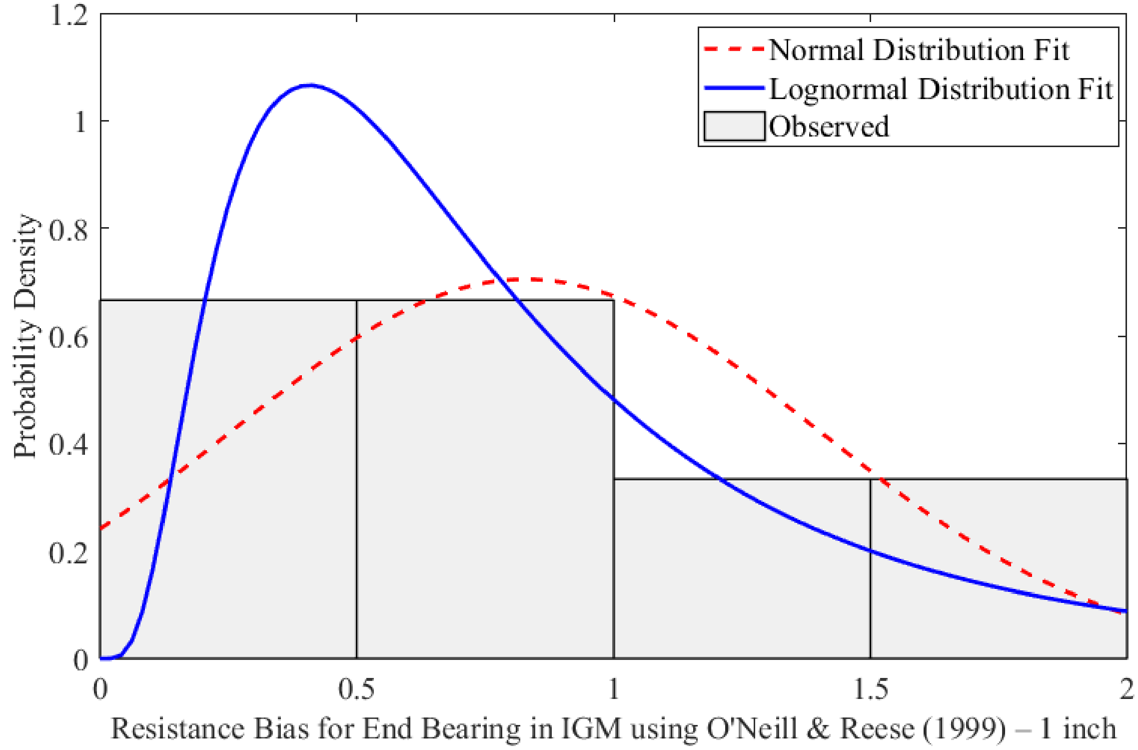

Figure C.43. PDF for end bearing in IGM at 1 in. using O'Neill and Reese (1999)

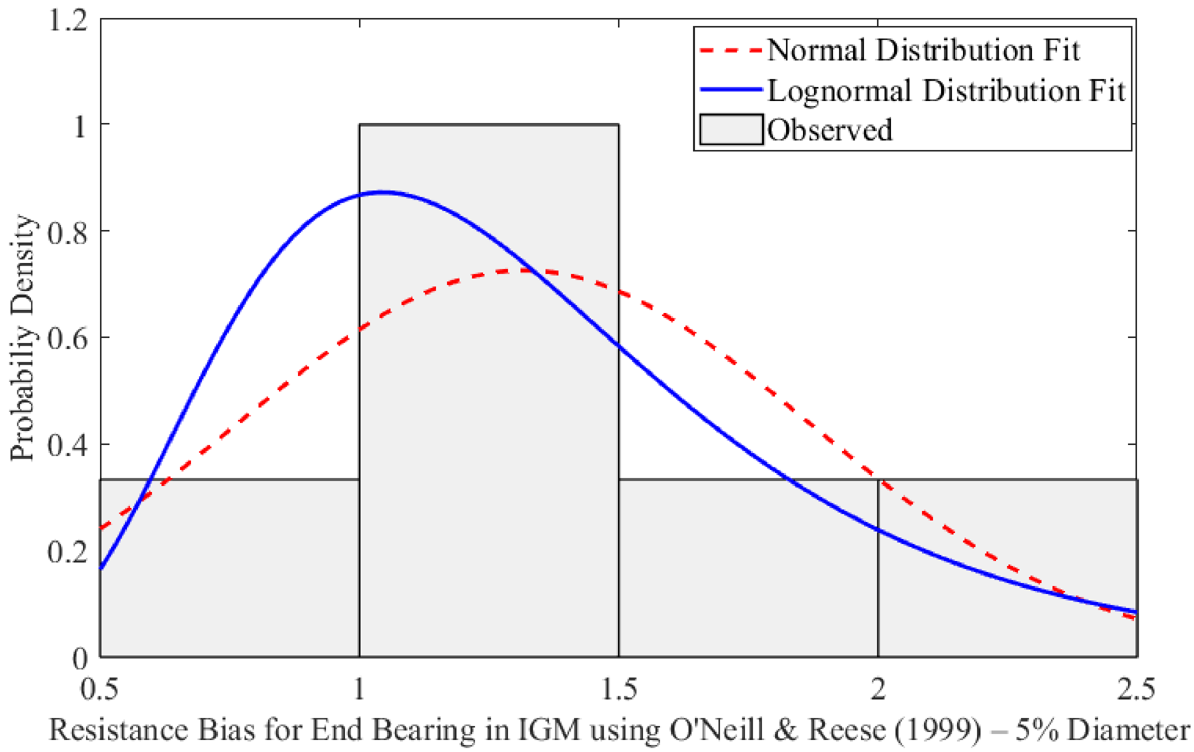

Figure C.44. PDF for end bearing in IGM at 5%B using O'Neill and Reese (1999)

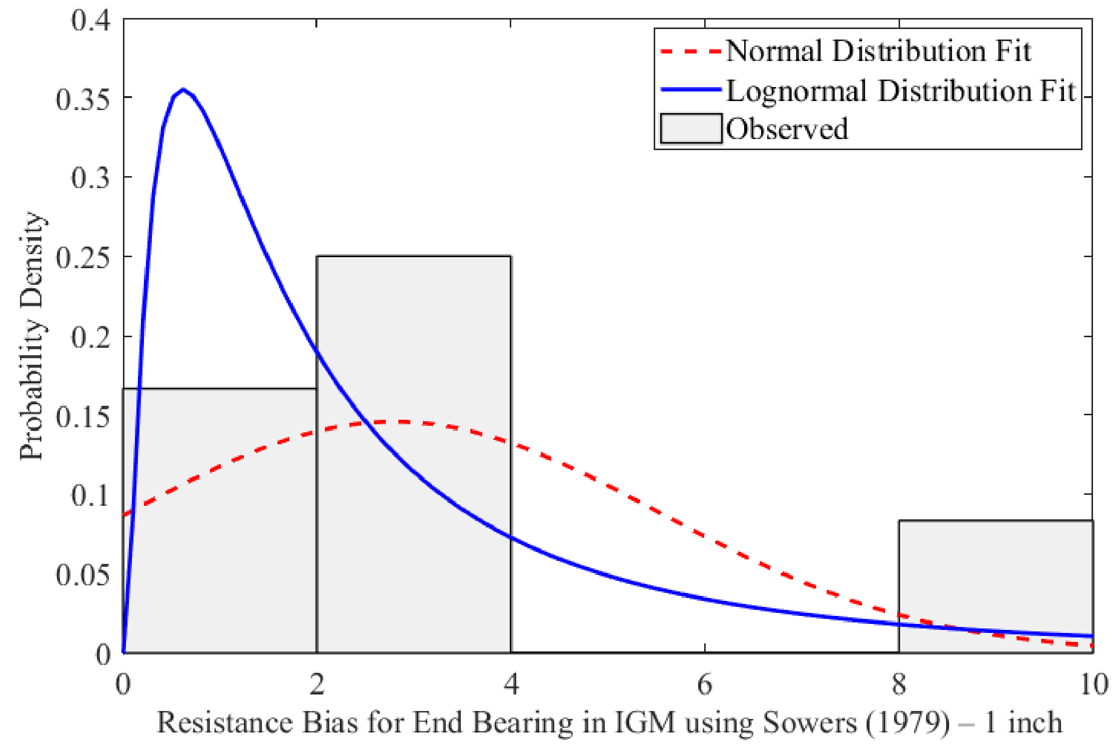

Figure C.45. PDF for end bearing in IGM at 1 in. using Sowers (1976)

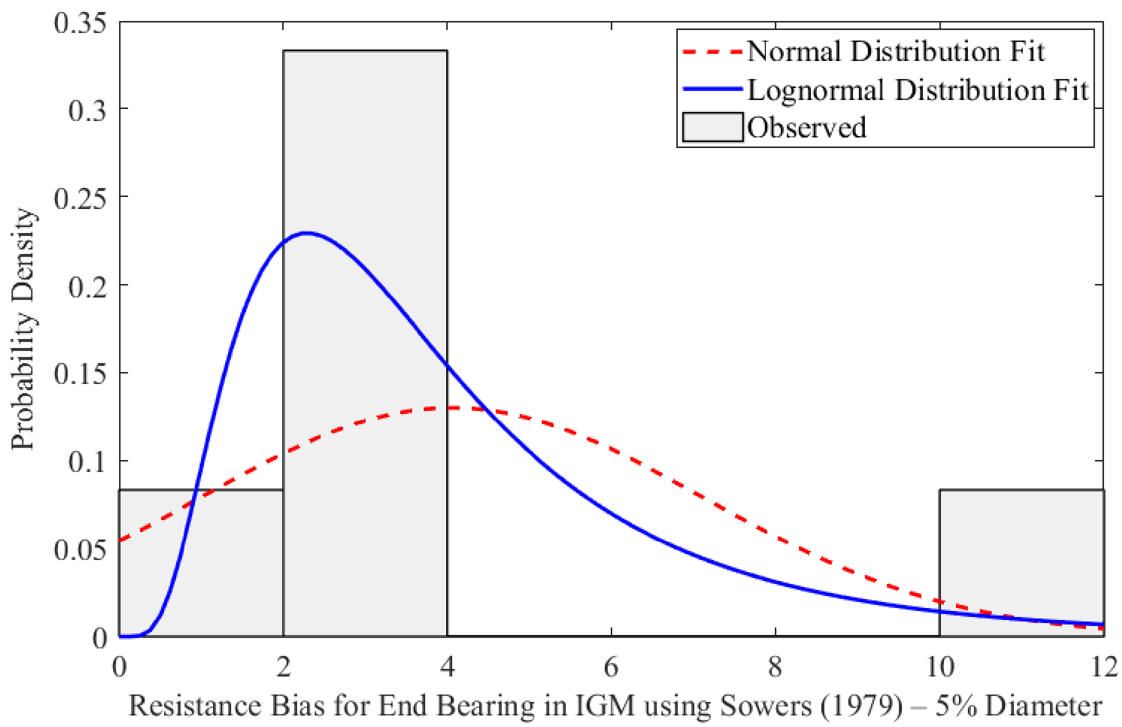

Figure C.46. PDF for end bearing in IGM at 5%B using Sowers (1976)

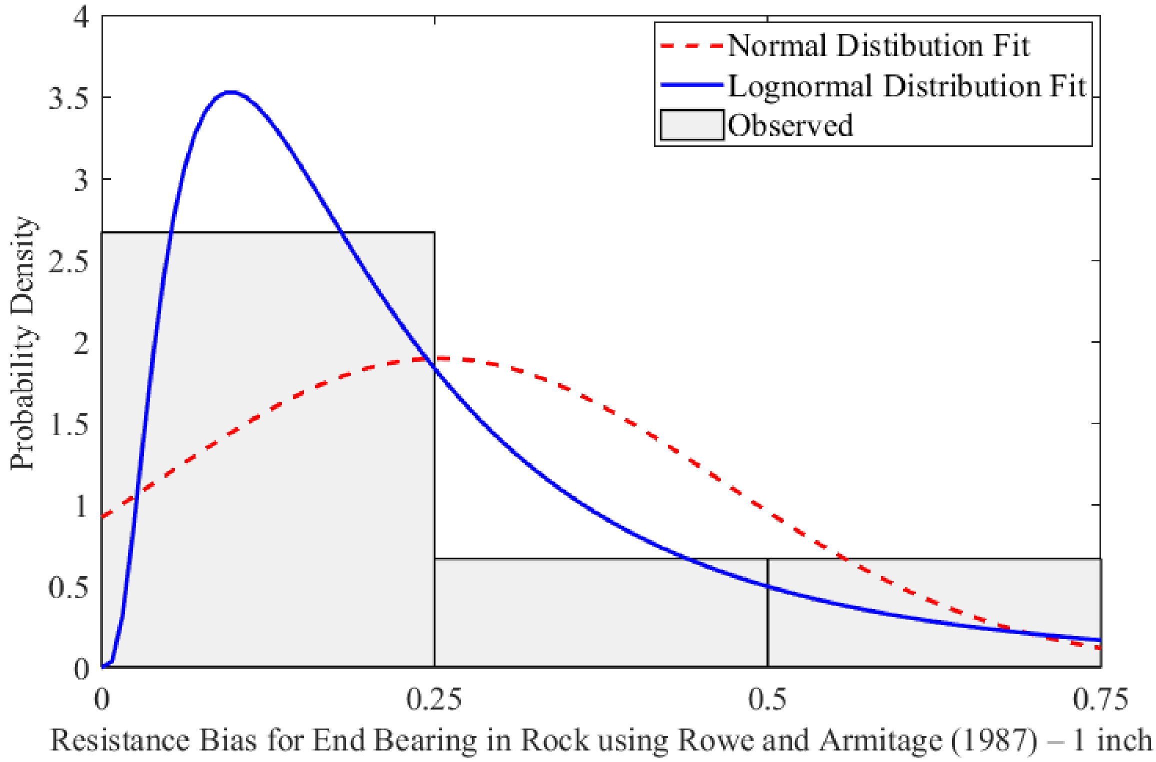

Figure C.47. PDF for end bearing in rock at 1 in. using Rowe and Armitage (1987)

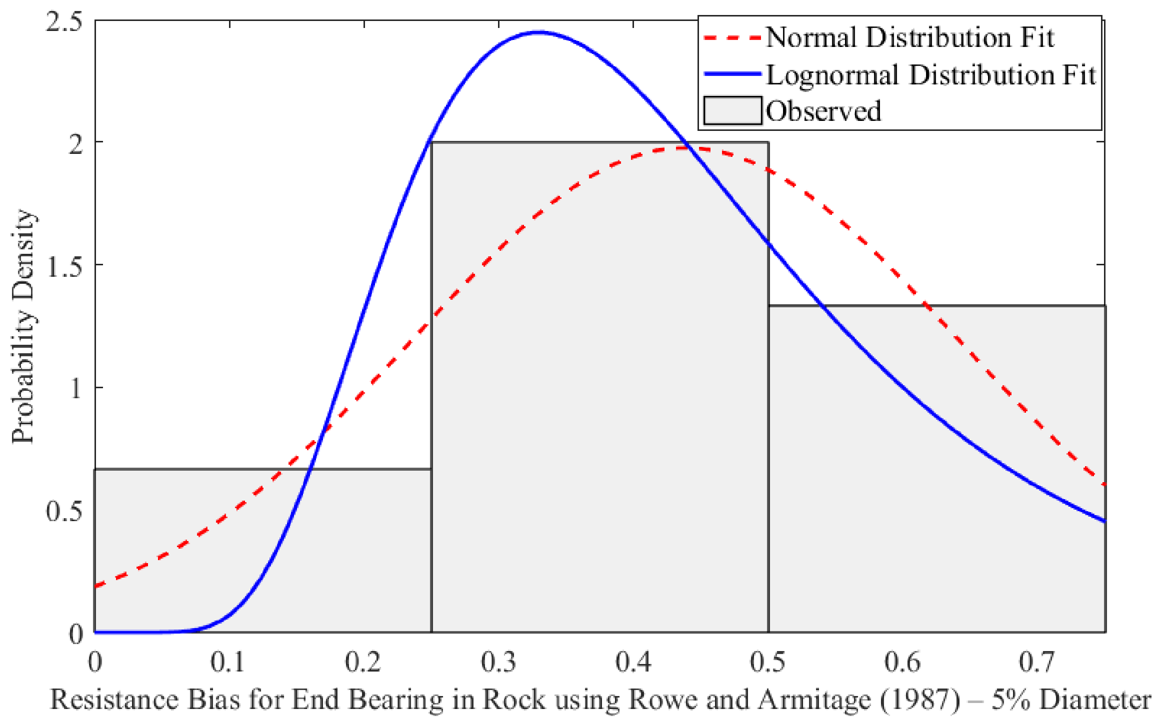

Figure C.48. PDF for end bearing in rock at 5%B using Rowe and Armitage (1987)

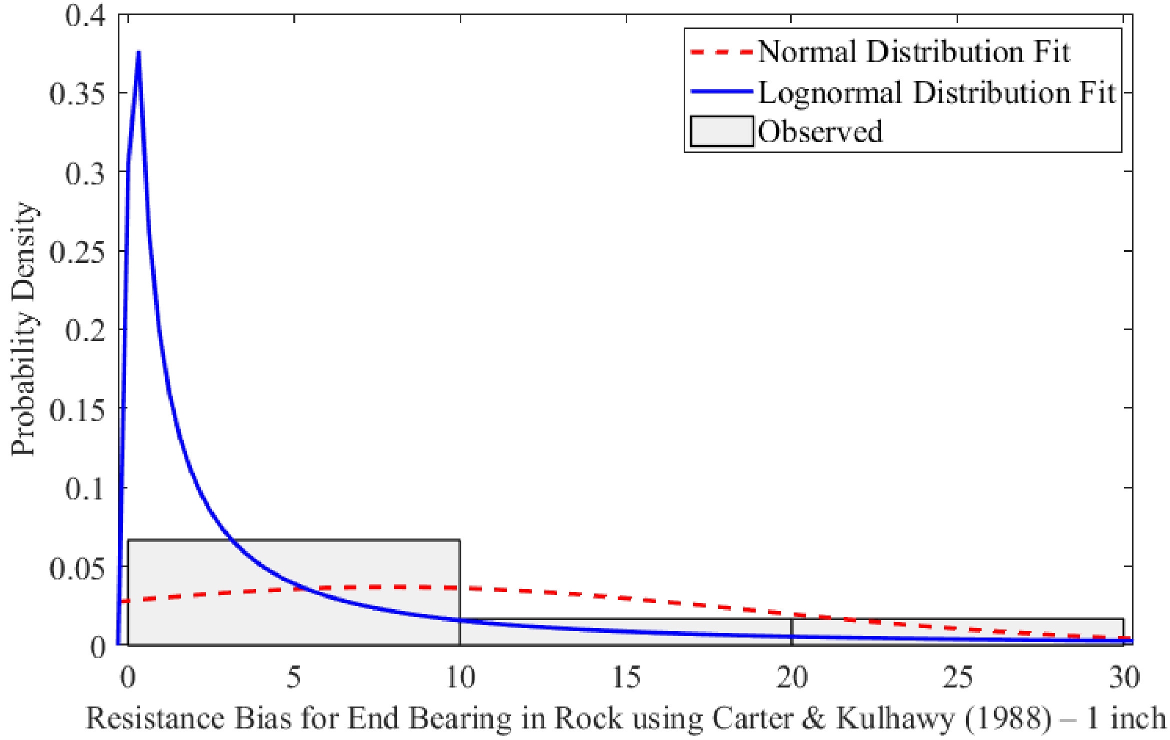

Figure C.49. PDF for end bearing in rock at 1 in. using Carter and Kulhawy (1988)

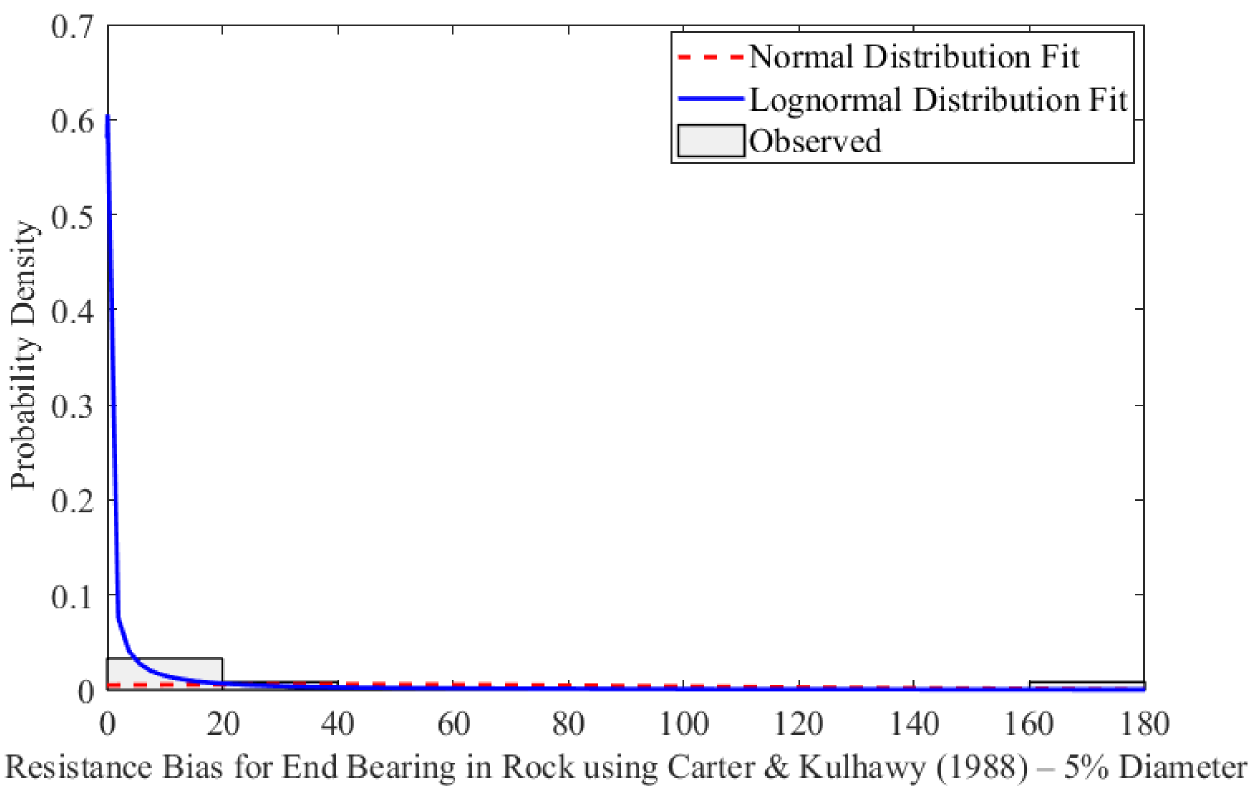

Figure C.50. PDF for end bearing in rock at 5%B using Carter and Kulhawy (1988)

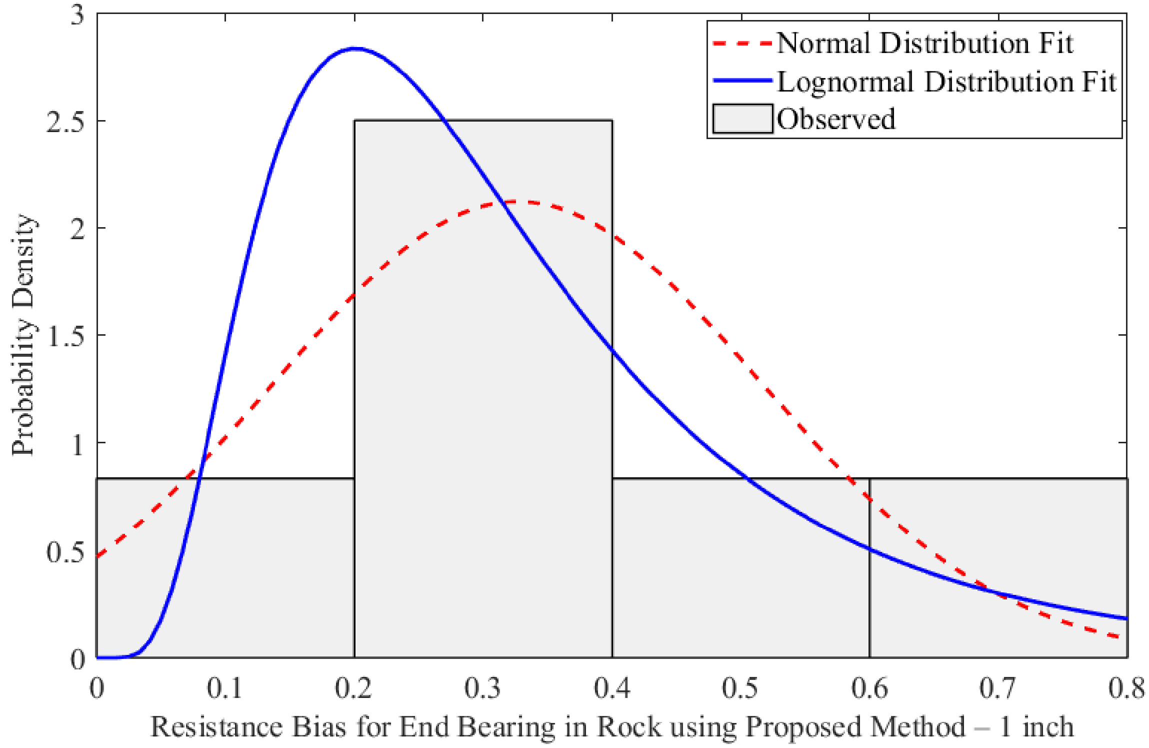

Figure C.51. PDF for end bearing in rock at 1 in. using proposed method (2014)

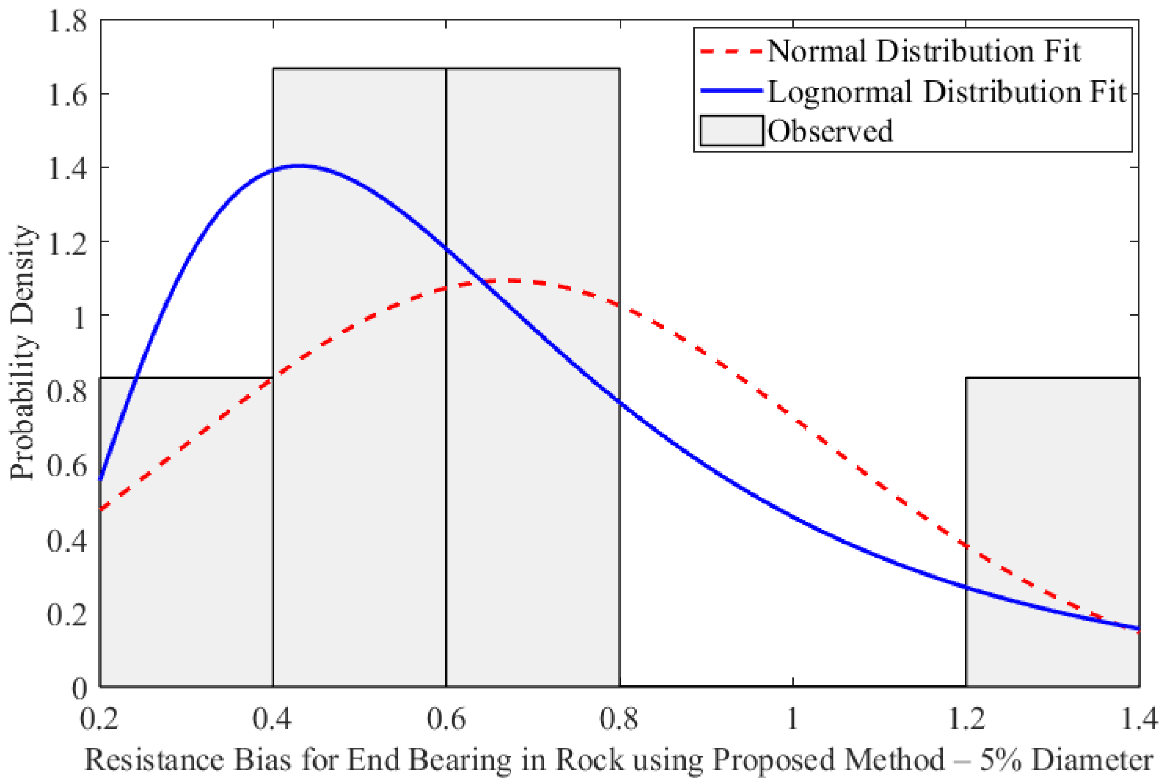

Figure C.52. PDF for end bearing in rock at 5%B using proposed method (2014)

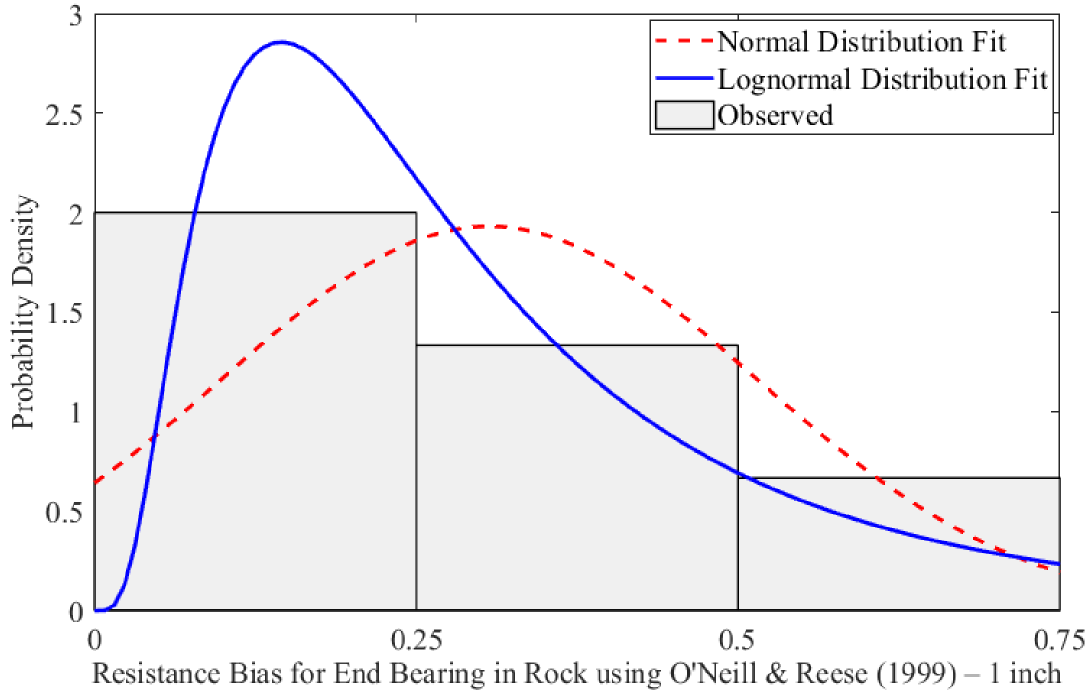

Figure C.53. PDF for end bearing in rock at 1 in. using O'Neill and Reese (1999)

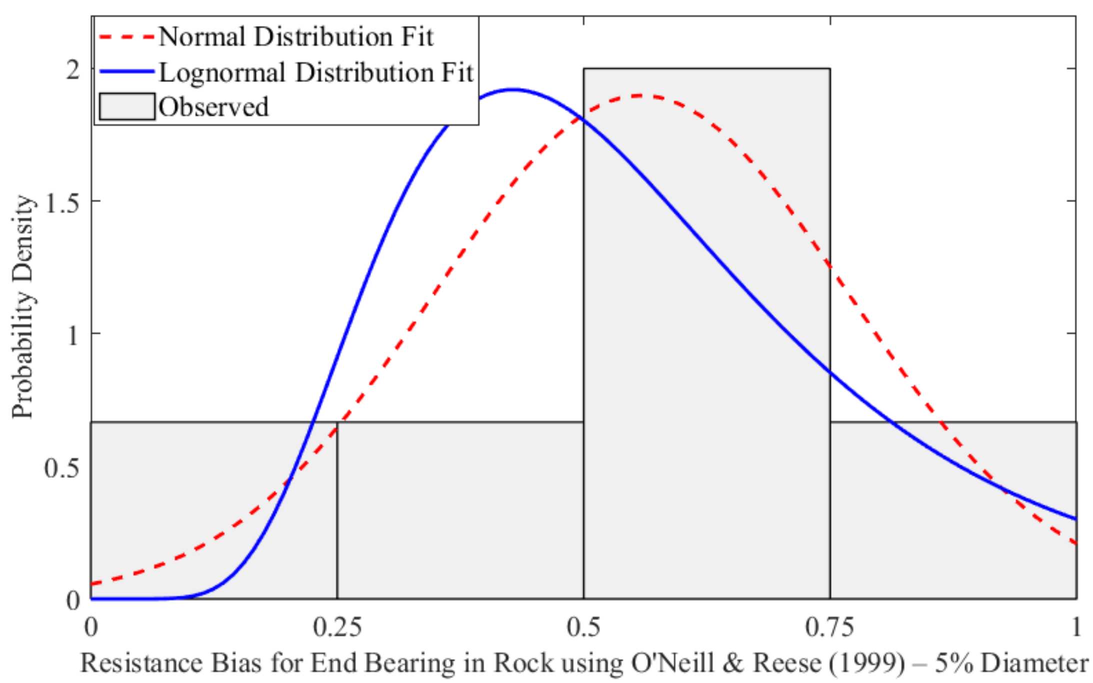

Figure C.54. PDF for end bearing in rock at 5%B using O'Neill and Reese (1999)

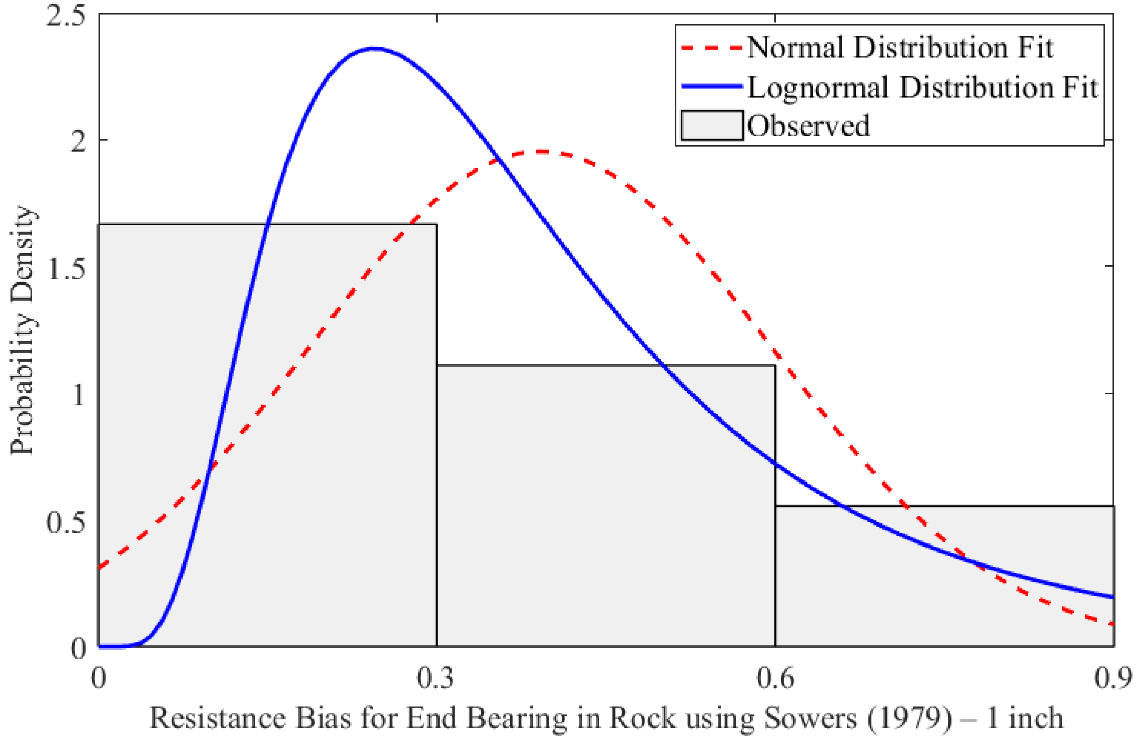

Figure C.55. PDF for end bearing in rock at 1 in. using Sowers (1976)

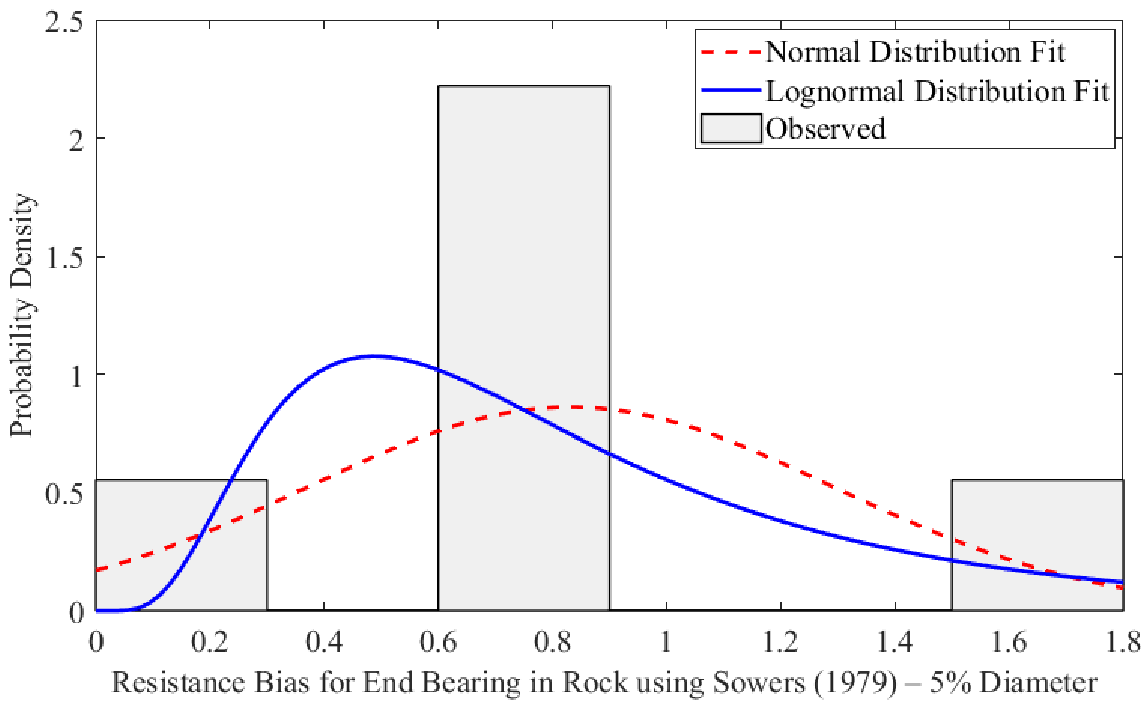

Figure C.56. PDF for end bearing in rock at 5%B using Sowers (1976)

APPENDIX D. CUMULATIVE DISTRIBUTION FUNCTIONS

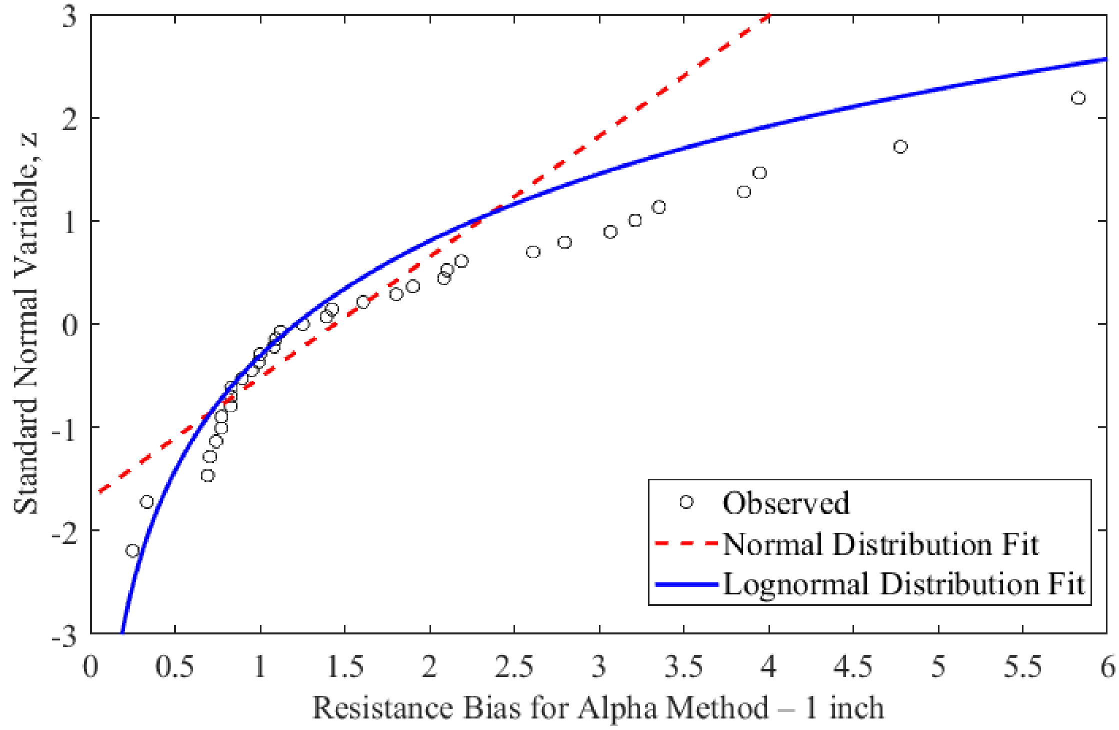

Figure D.1. CDF for α-method at 1 in. – Approach I

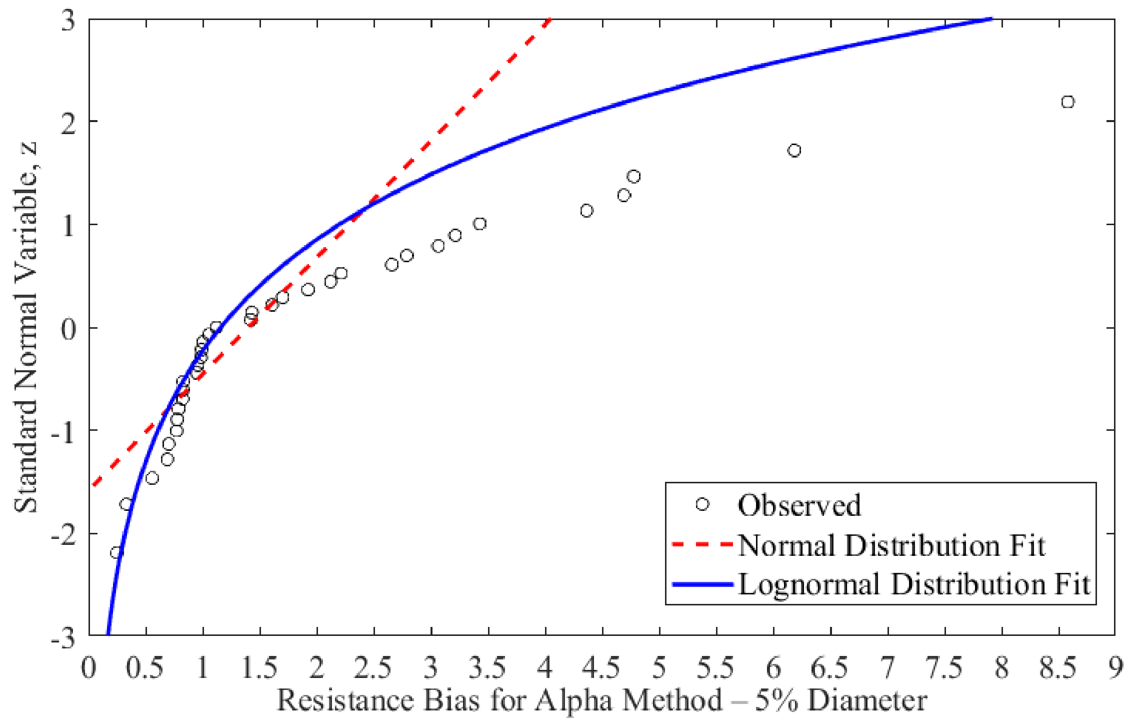

Figure D.2. CDF for α-method at 5%B in. – Approach I

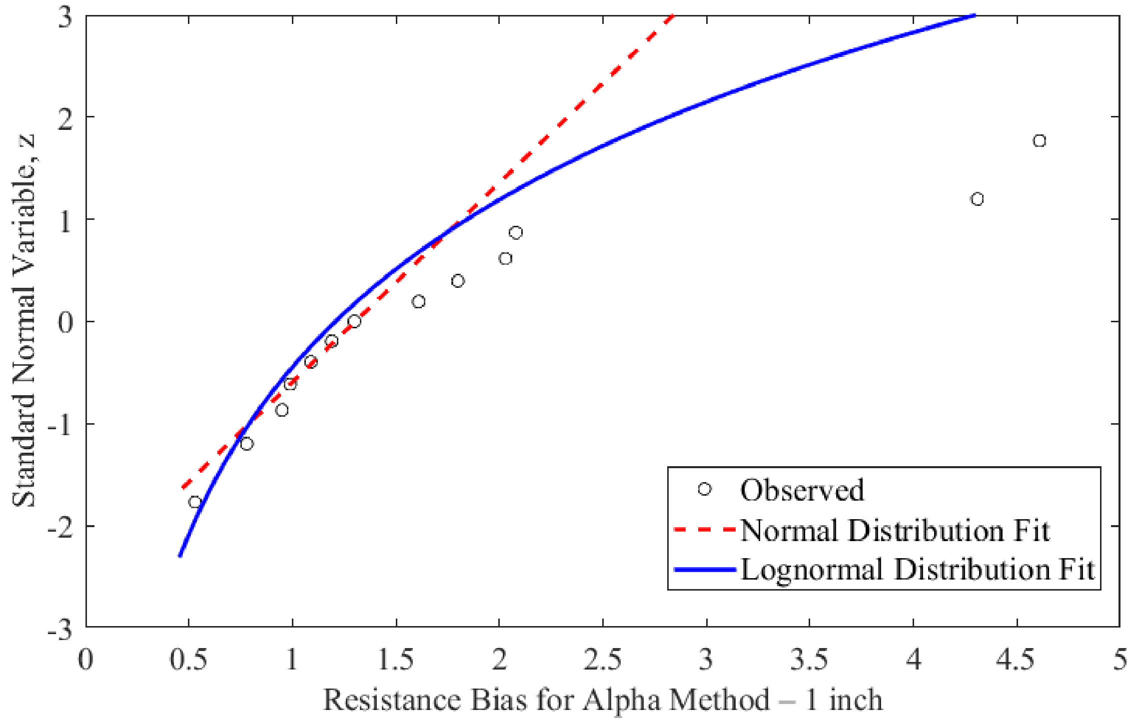

Figure D.3. CDF for α-method at 1 in. – Approach II

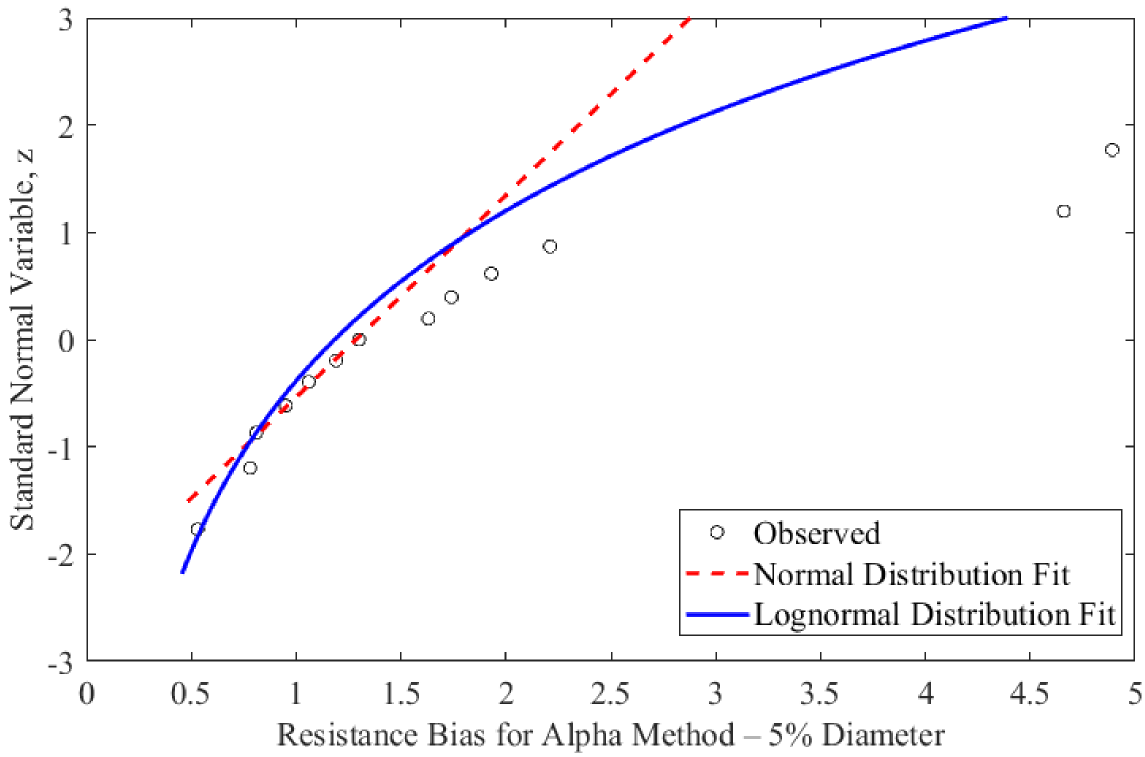

Figure D.4. CDF for α-method at 5%B – Approach II

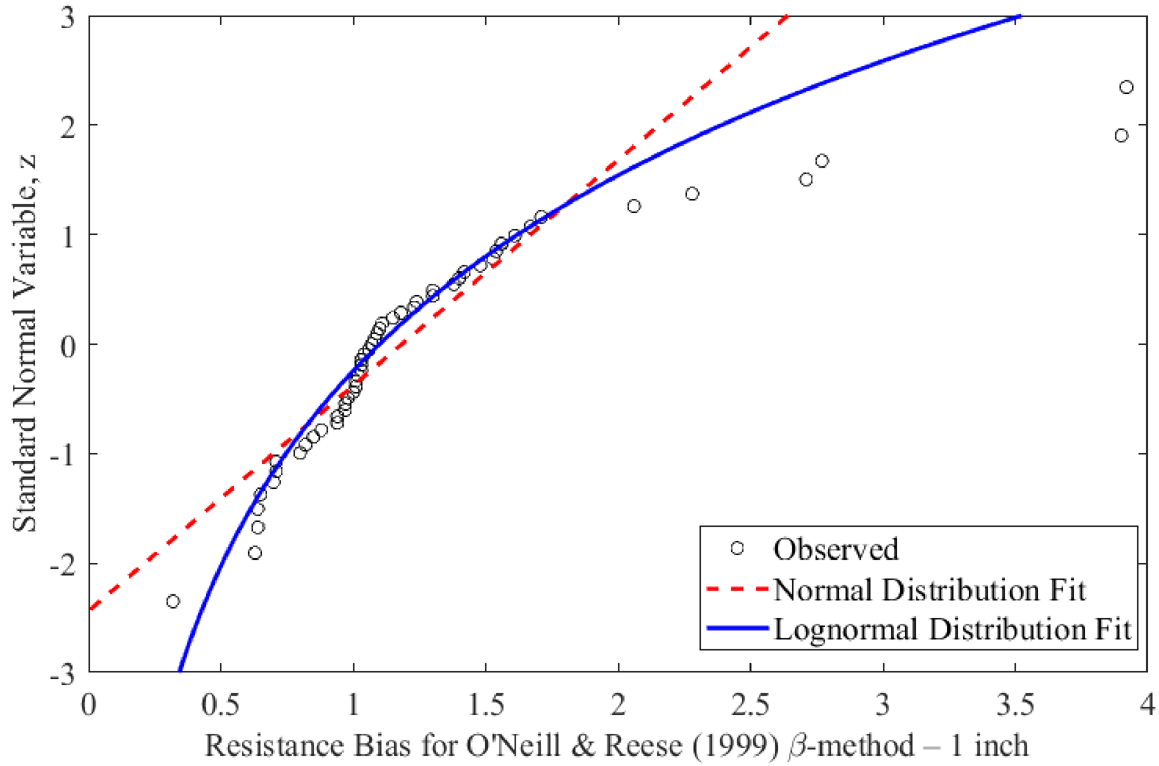

Figure D.5. CDF for O'Neill and Reese (1999) β-method at 1 in. – Approach I

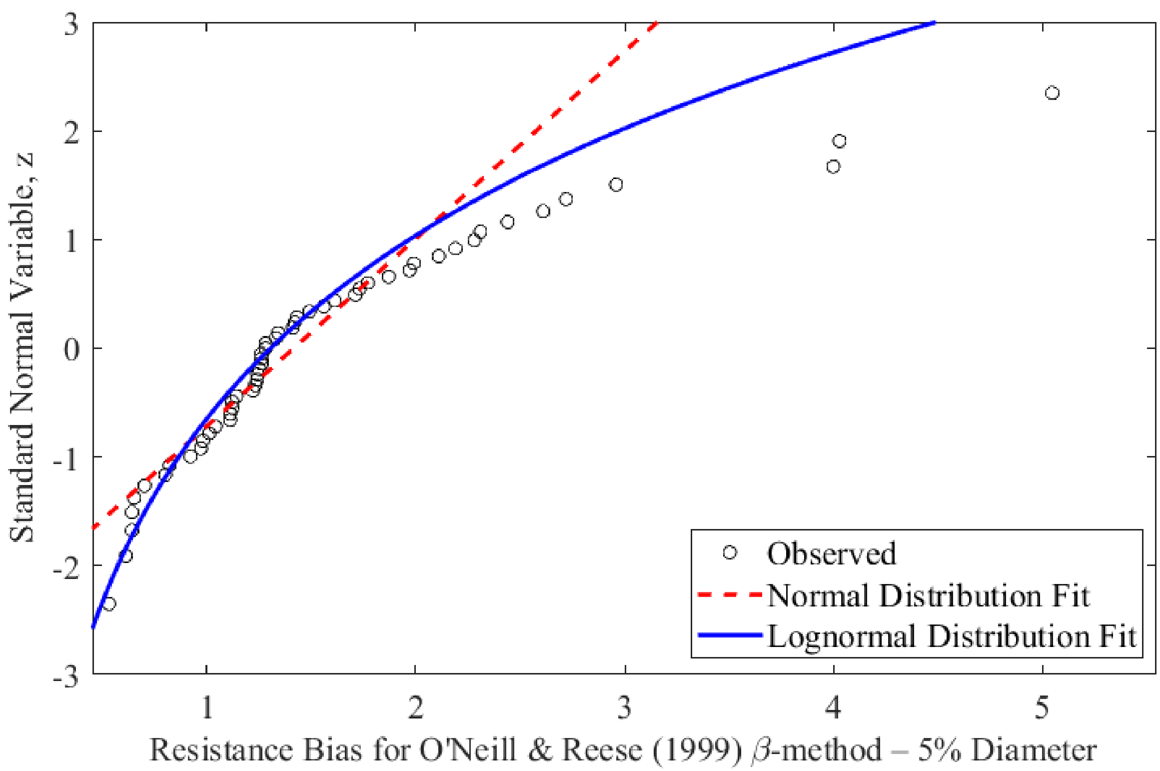

Figure D.6. CDF for O'Neill and Reese (1999) β-method at 5%B – Approach I

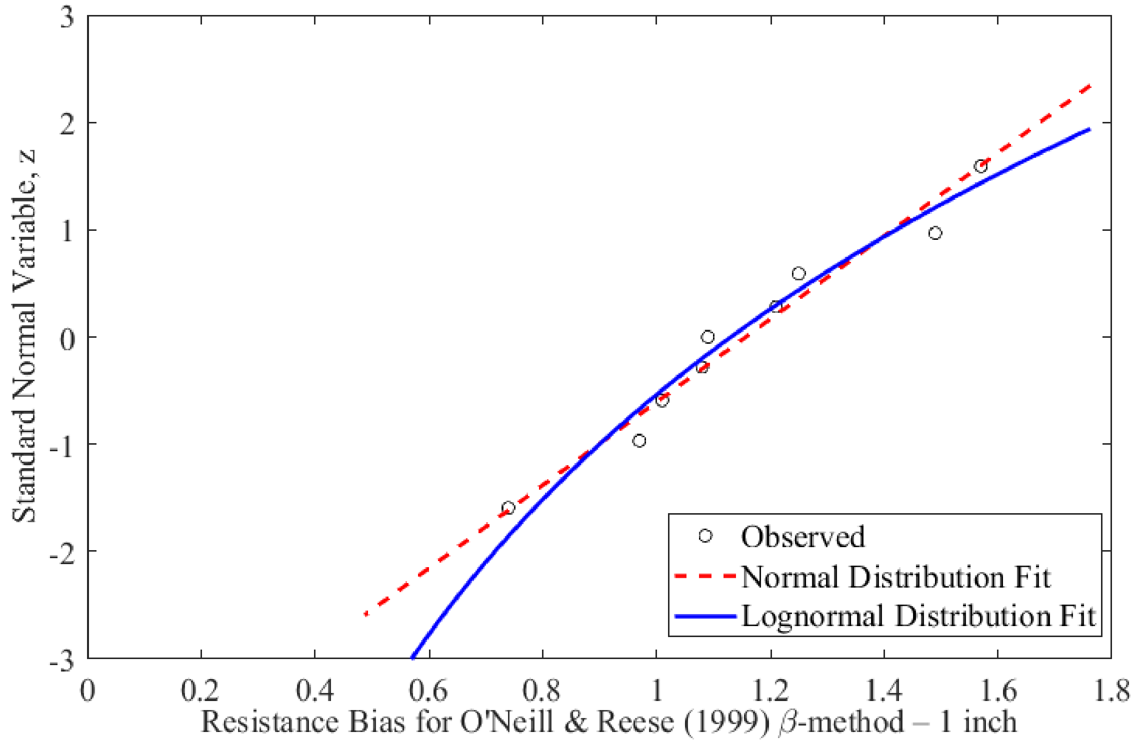

Figure D.7. CDF for O'Neill and Reese (1999) β-method at 1 in. – Approach II

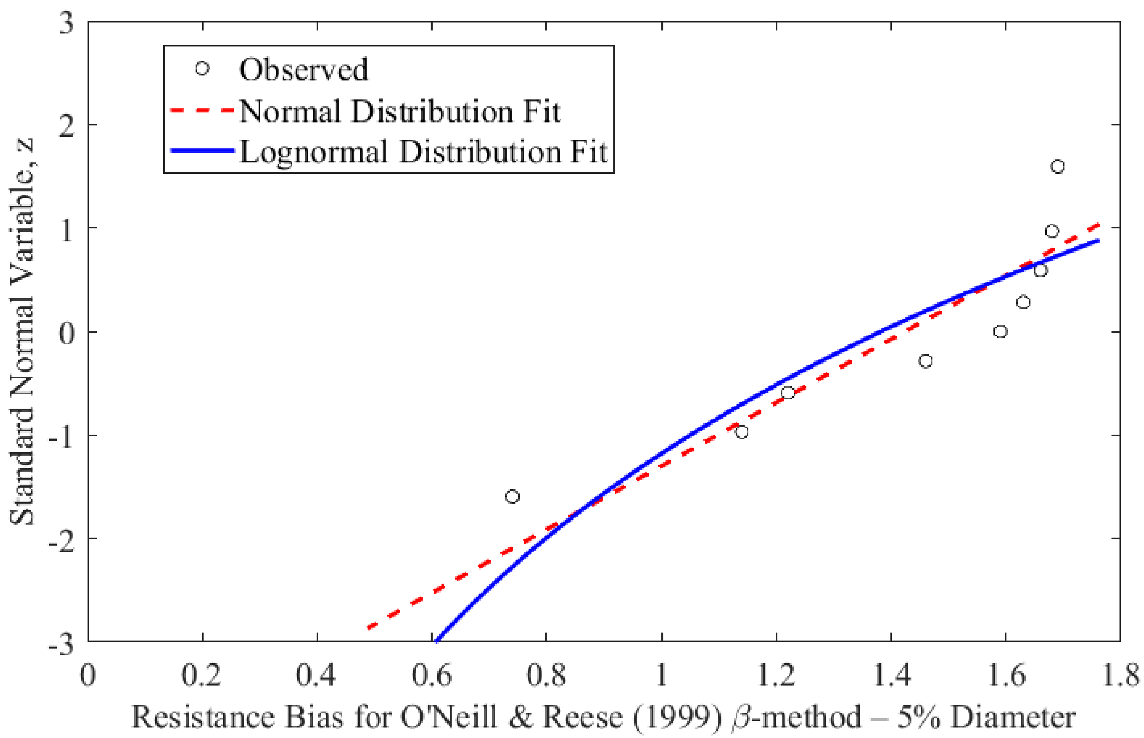

Figure D.8. CDF for O'Neill and Reese (1999) β-method at 5%B – Approach II

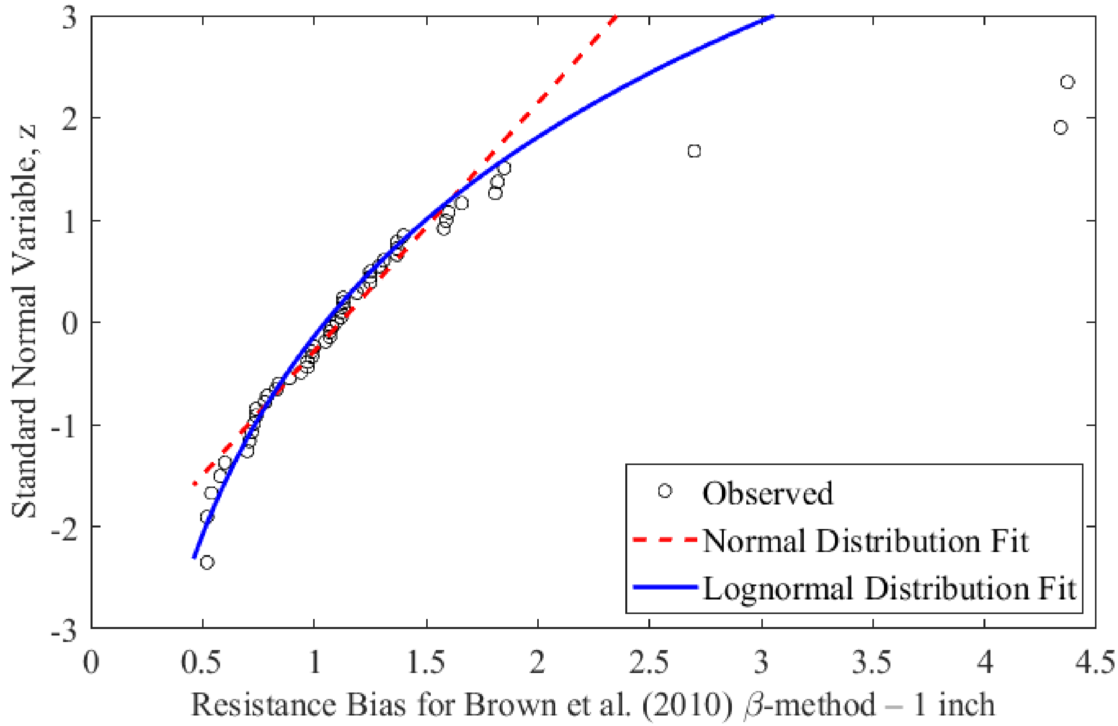

Figure D.9. CDF for Brown et al. (2010) β-method at 1 in. – Approach I

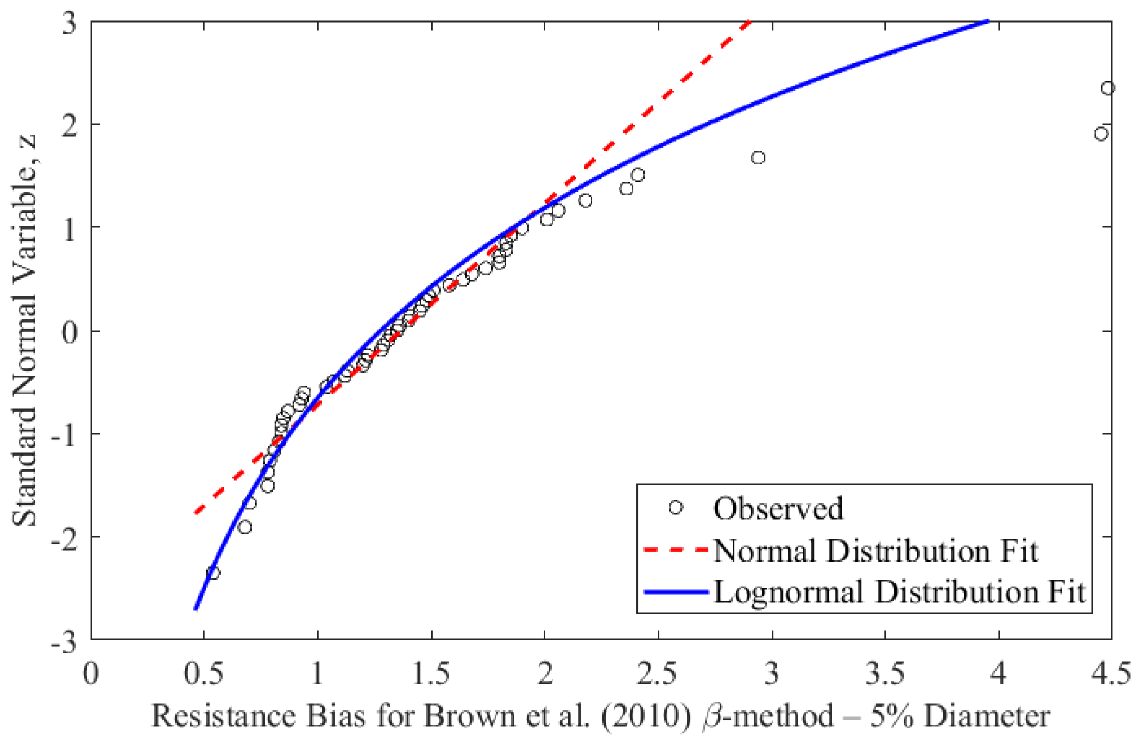

Figure D.10. CDF for Brown et al. (2010) β-method at 5%B – Approach I

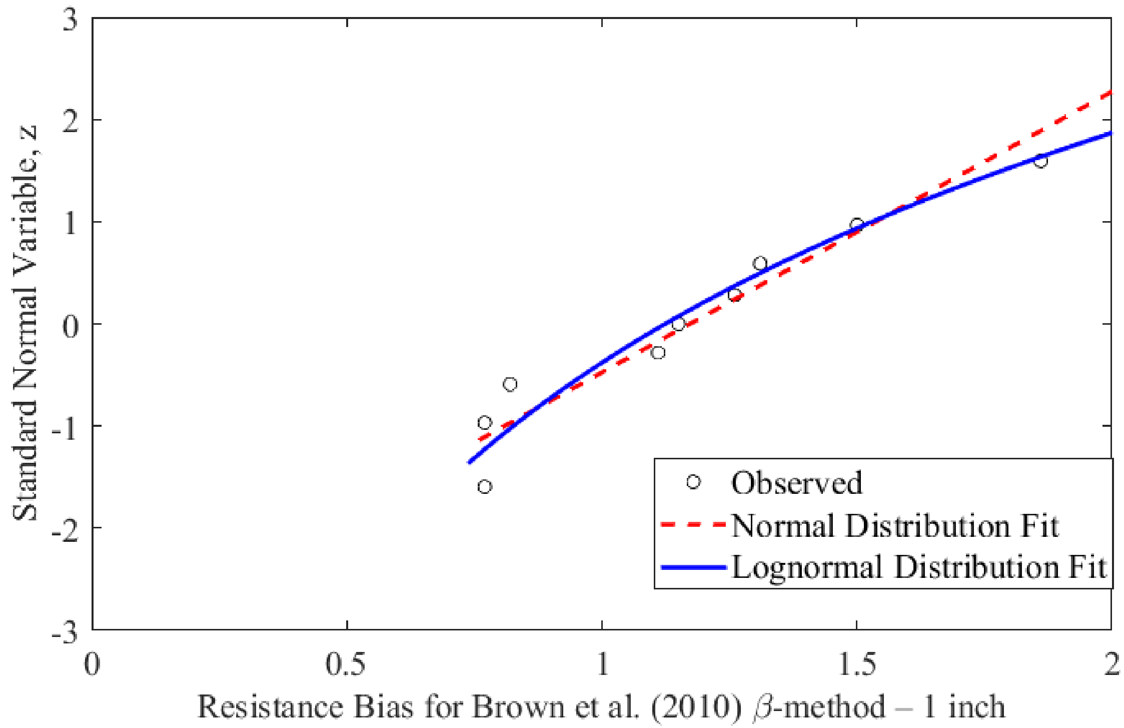

Figure D.11. CDF for Brown et al. (2010) β-method at 1 in. – Approach II

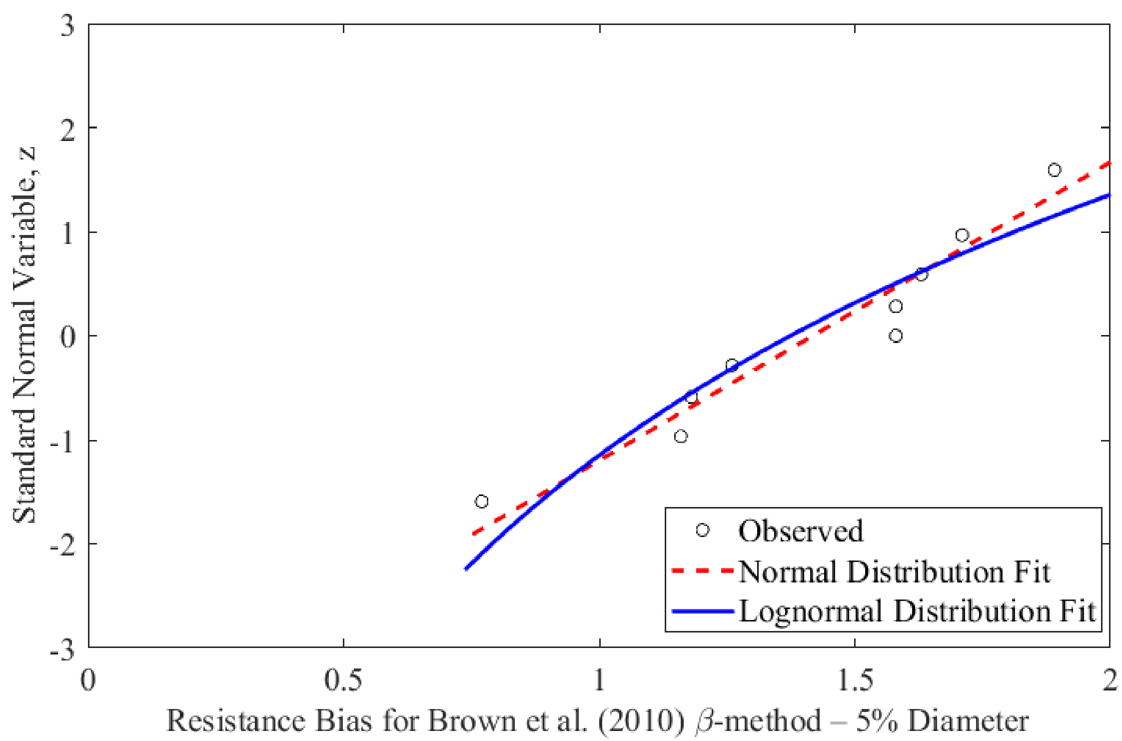

Figure D.12. CDF for Brown et al. (2010) β-method at 5%B – Approach II

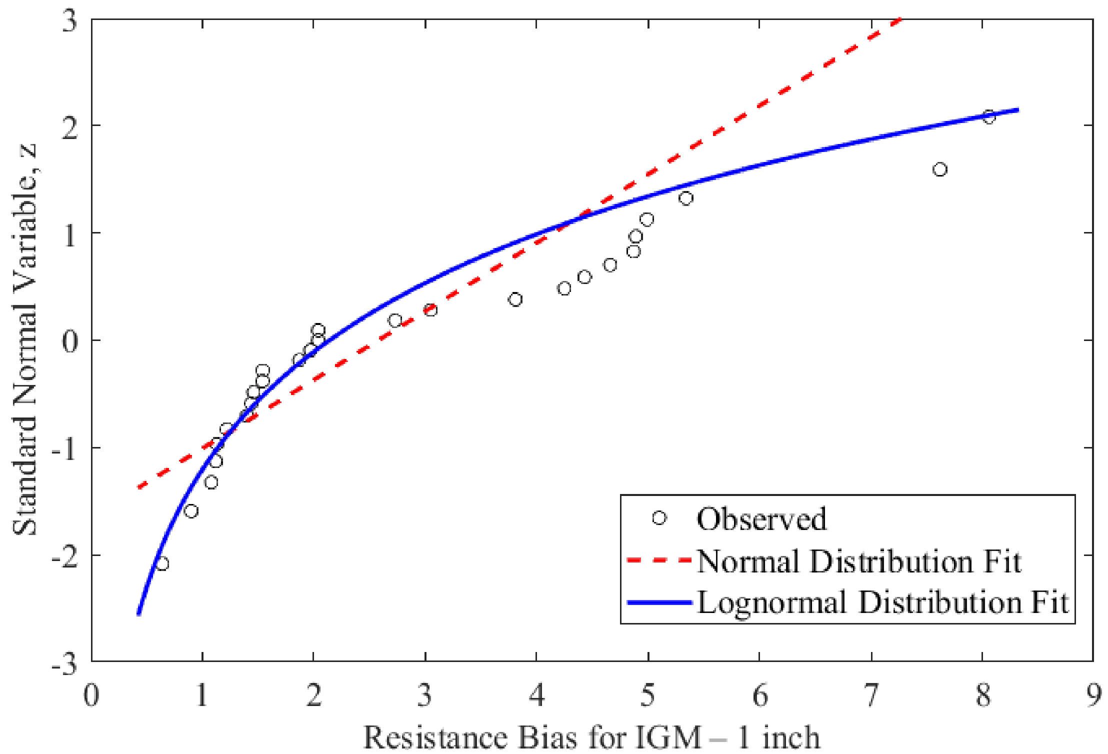

Figure D.13. CDF for skin friction in IGM at 1 in. – Approach I

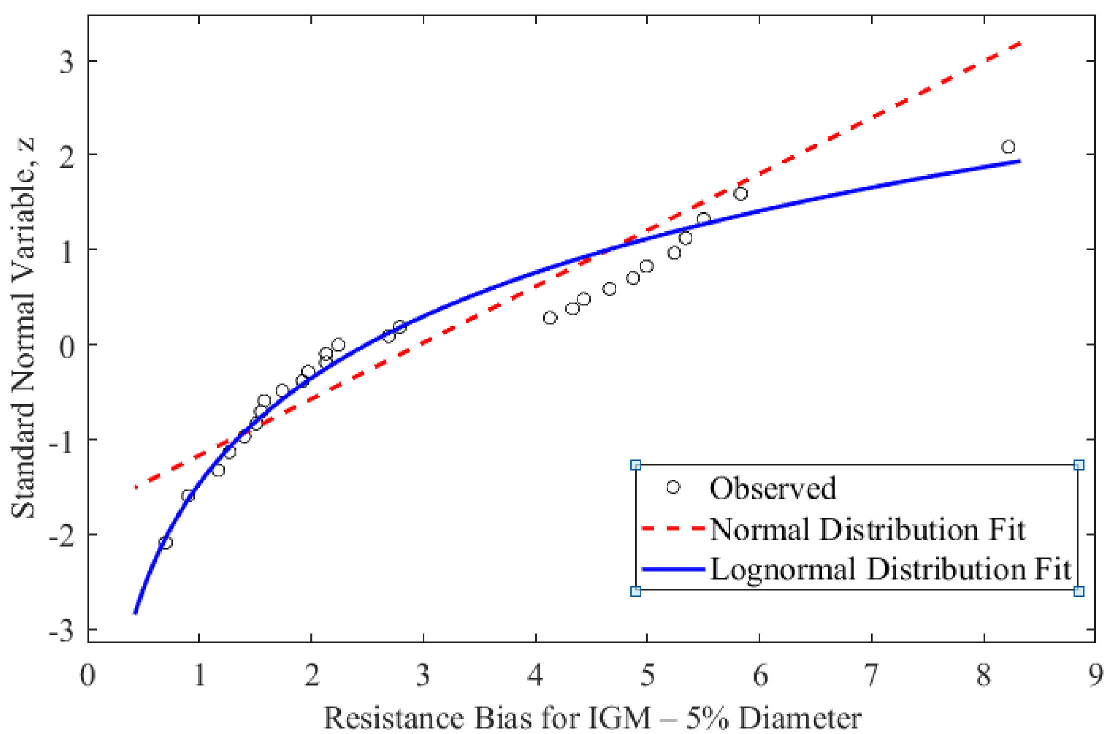

Figure D.14. CDF for skin friction in IGM at 5%B – Approach I

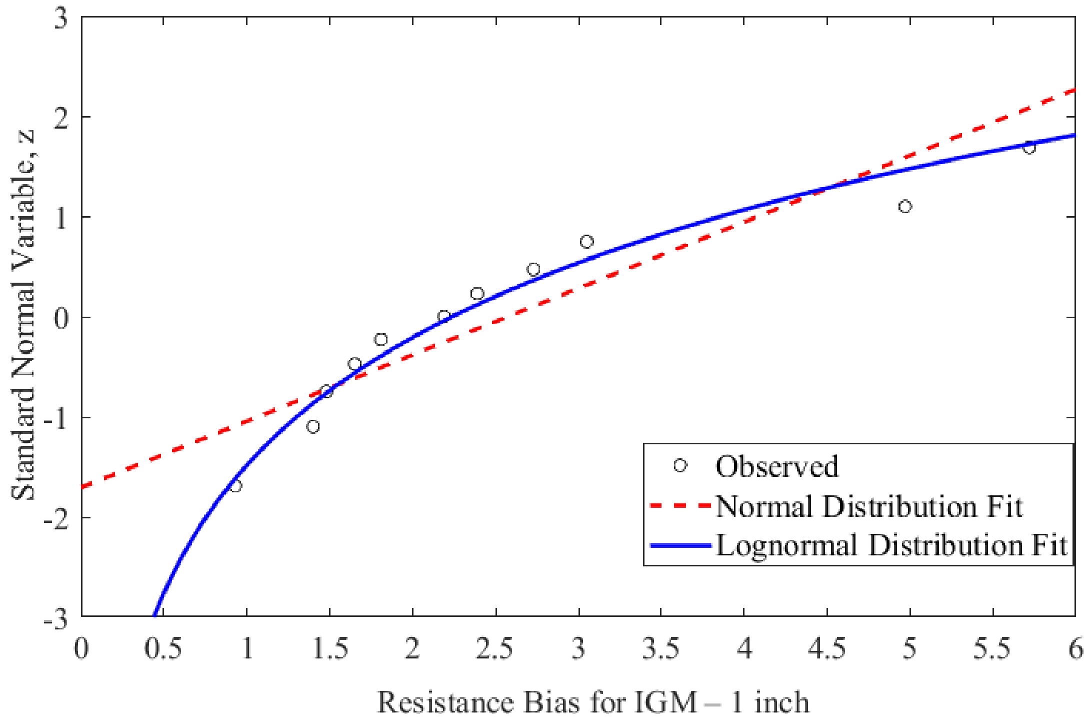

Figure D.15. CDF for skin friction in IGM at 1 in. – Approach II

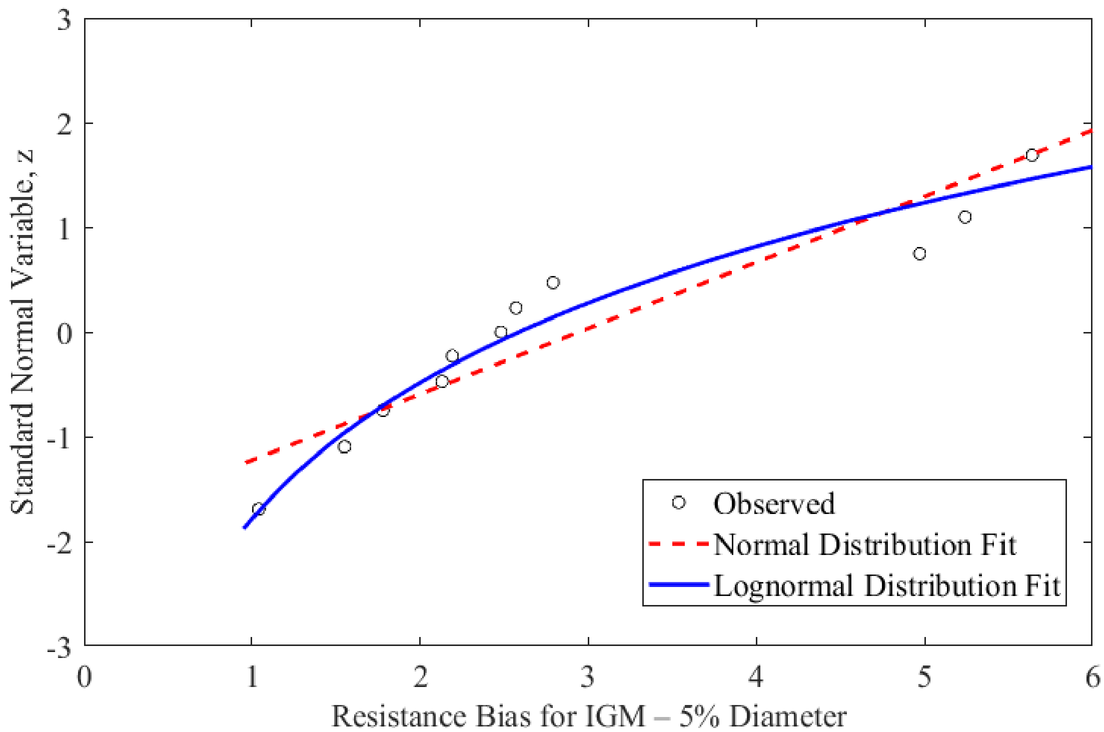

Figure D.16. CDF for skin friction in IGM at 5%B – Approach II

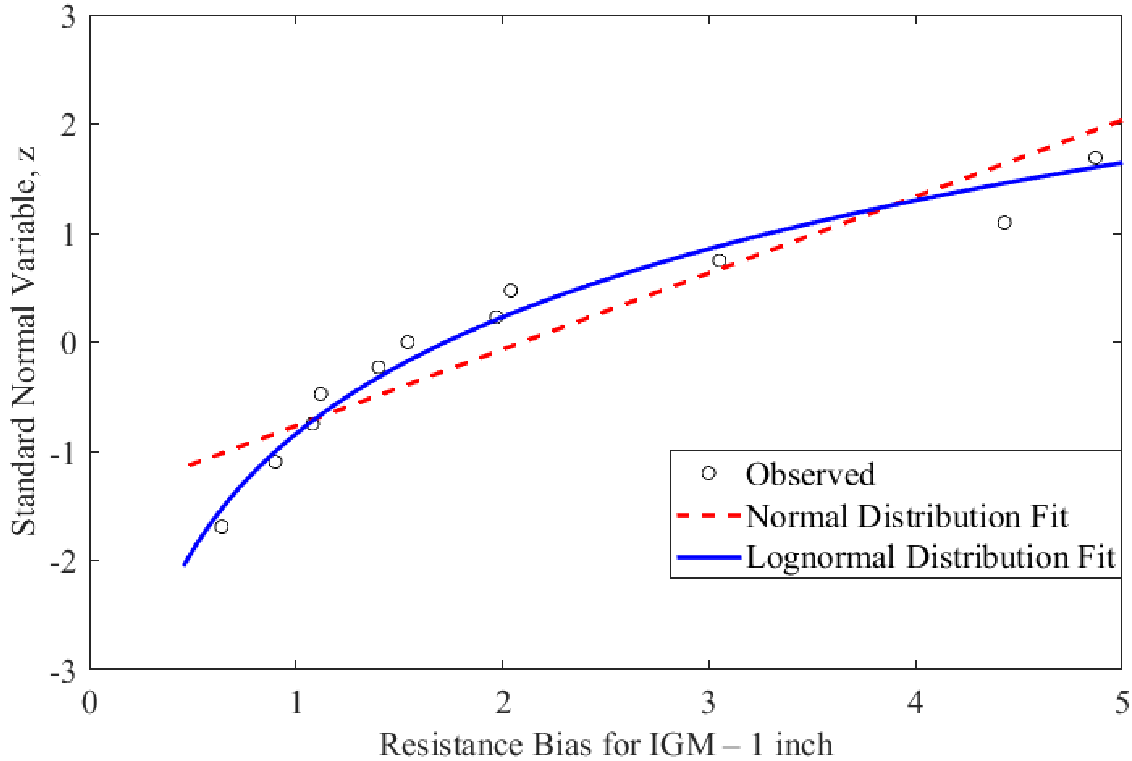

Figure D.17. CDF for skin friction in IGM at 1 in., Iowa data – Approach I

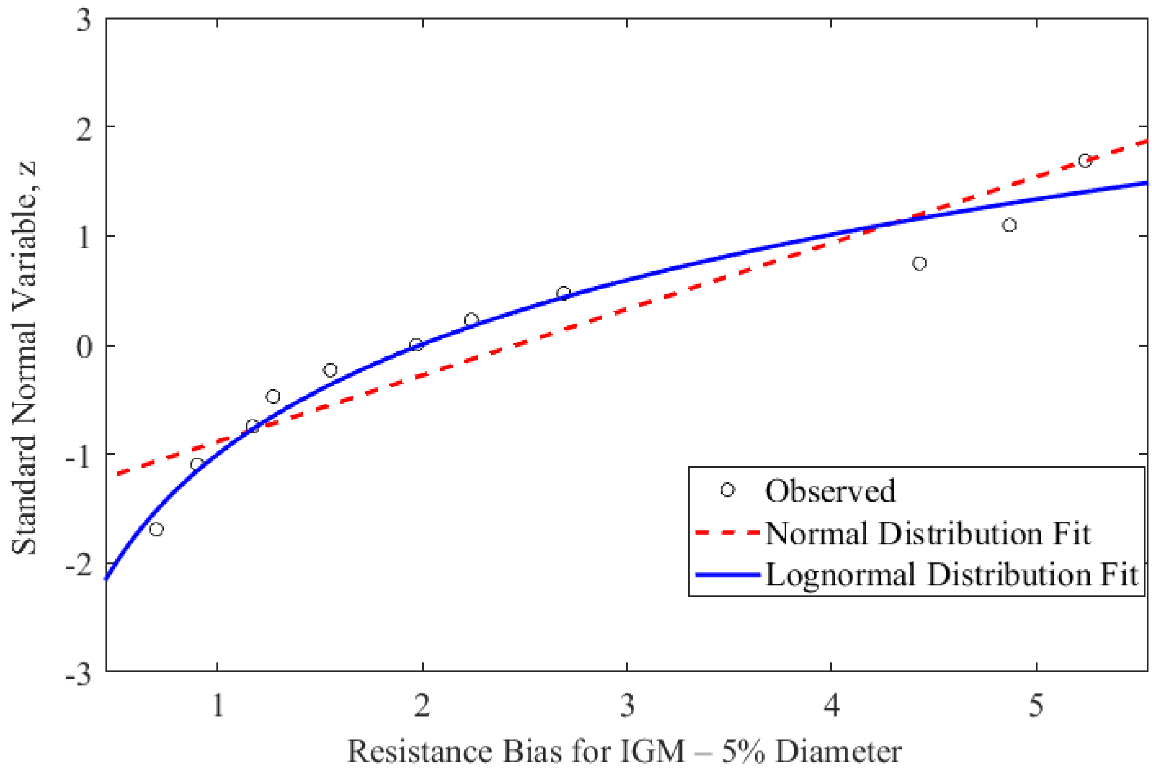

Figure D.18. CDF for skin friction in IGM at 5%B, Iowa data – Approach I

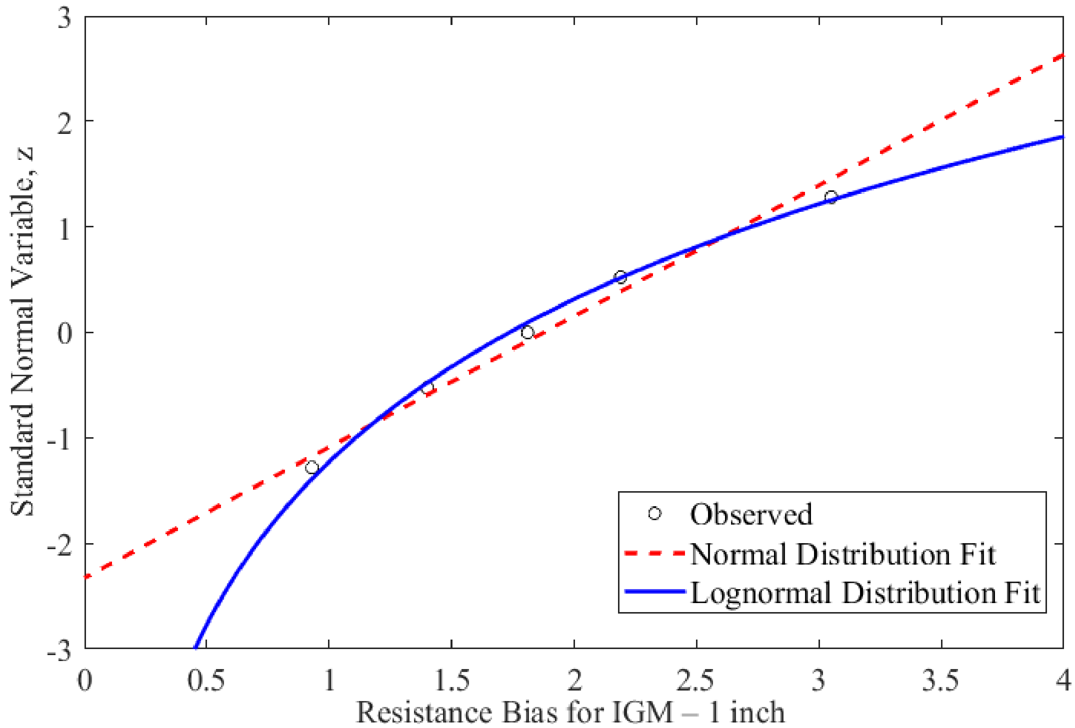

Figure D.19. CDF for skin friction in IGM at 1 in., Iowa data – Approach II

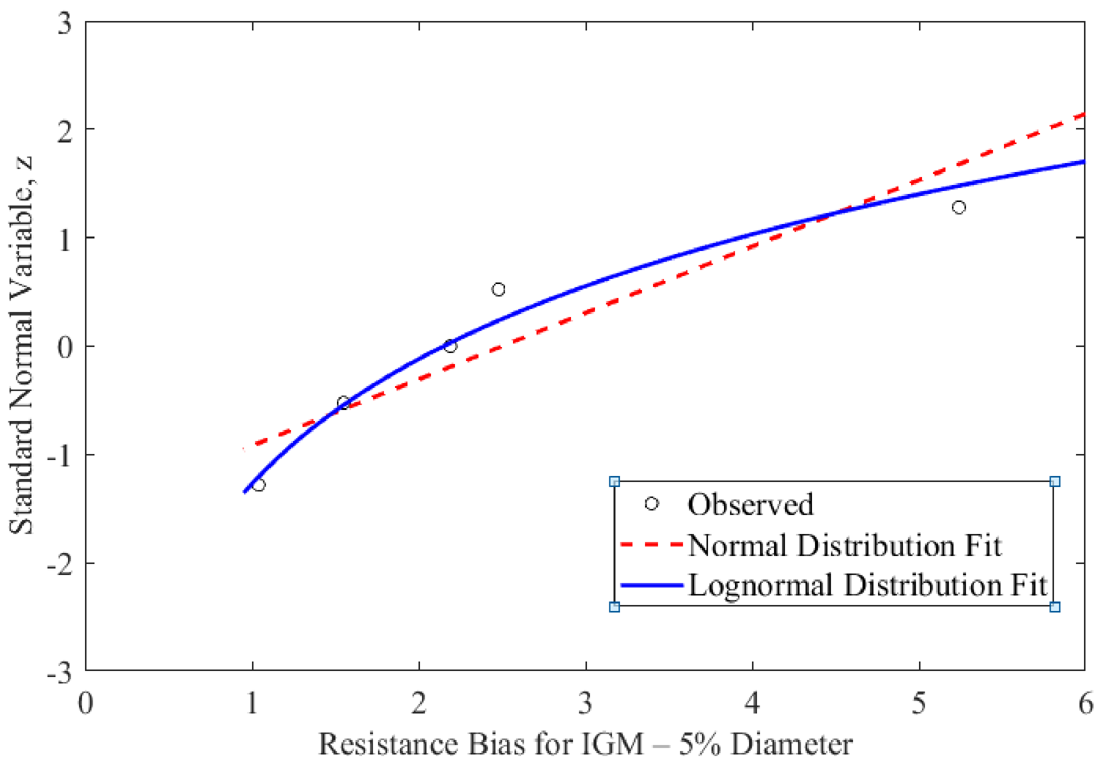

Figure D.20. CDF for skin friction in IGM at 5%B, Iowa data – Approach II

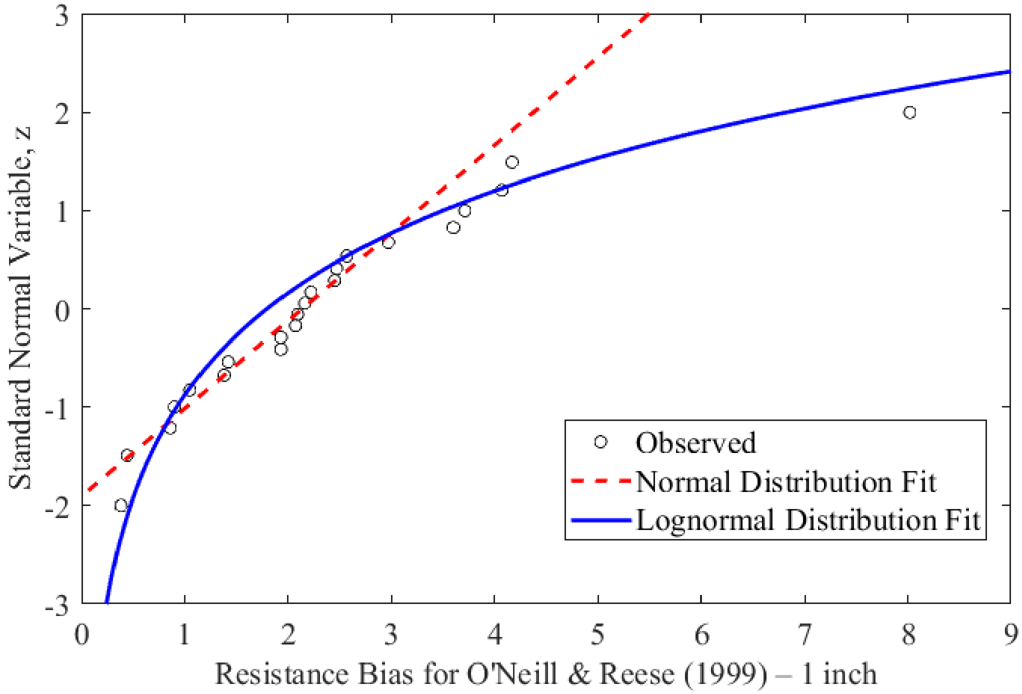

Figure D.21. CDF for skin friction in rock at 1 in. using O'Neill and Reese (1999) – Approach I

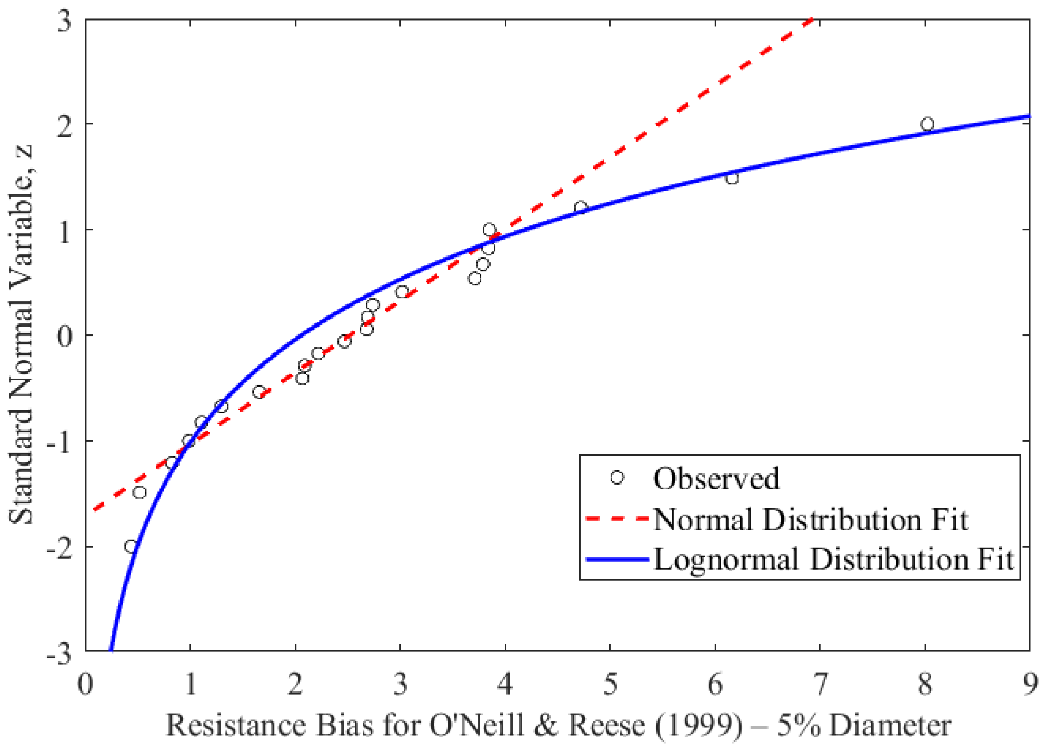

Figure D.22. CDF for skin friction in rock at 5%B using O'Neill and Reese (1999) – Approach I

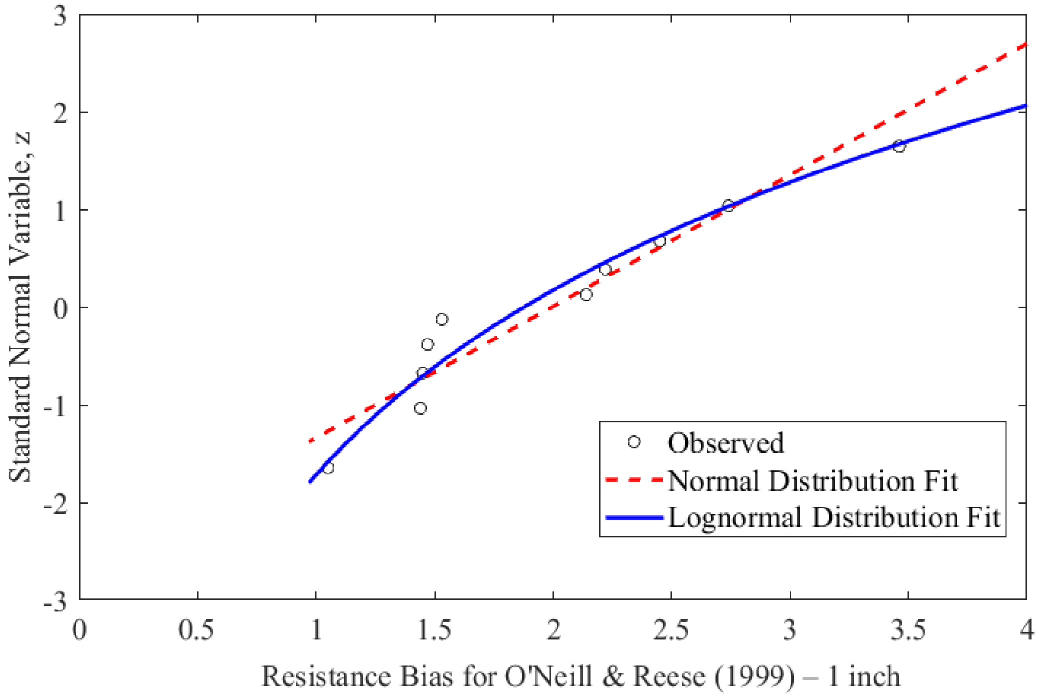

Figure D.23. CDF for skin friction in rock at 1 in. using O'Neill and Reese (1999) – Approach II

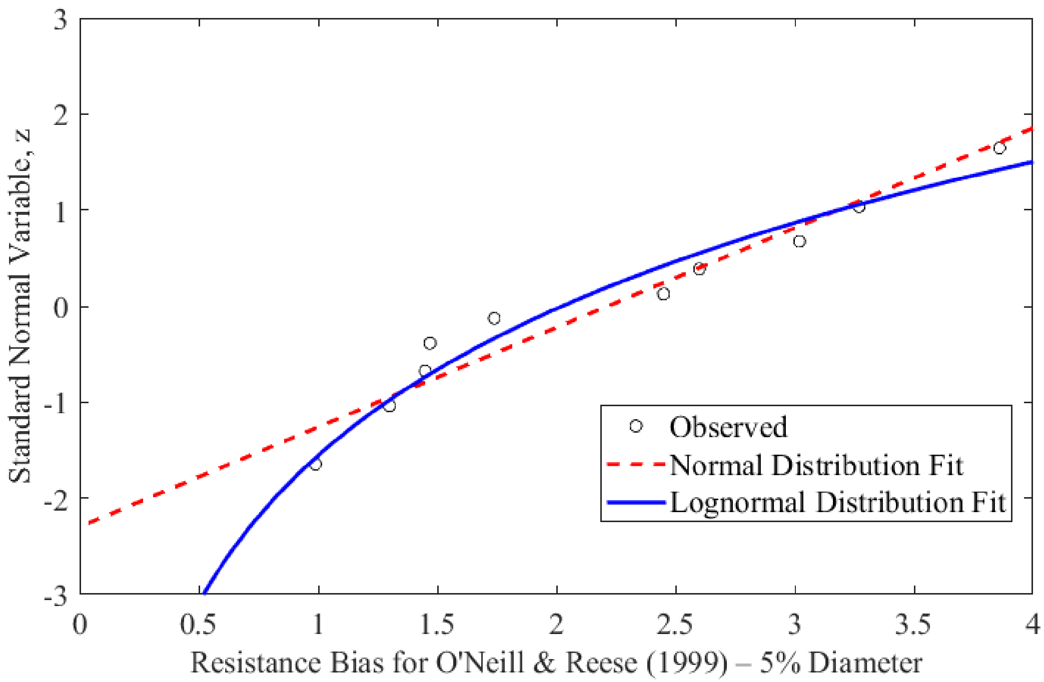

Figure D.24. CDF for skin friction in rock at 5%B using O'Neill and Reese (1999) – Approach II

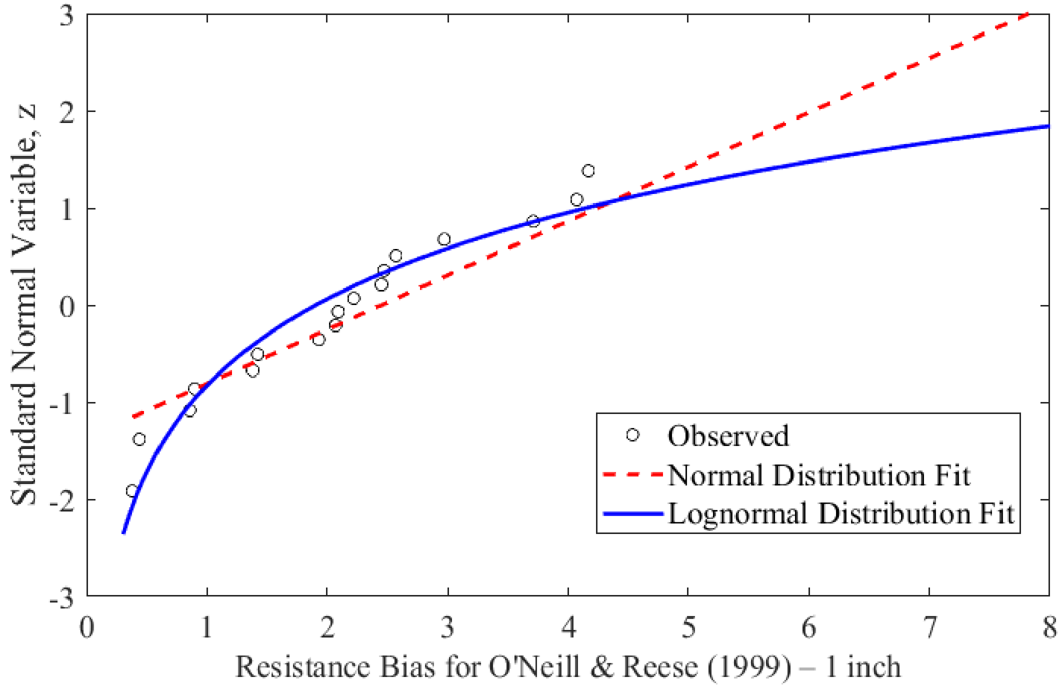

Figure D.25. CDF for skin friction in rock at 1 in. using O'Neill and Reese (1999), Iowa data – Approach I

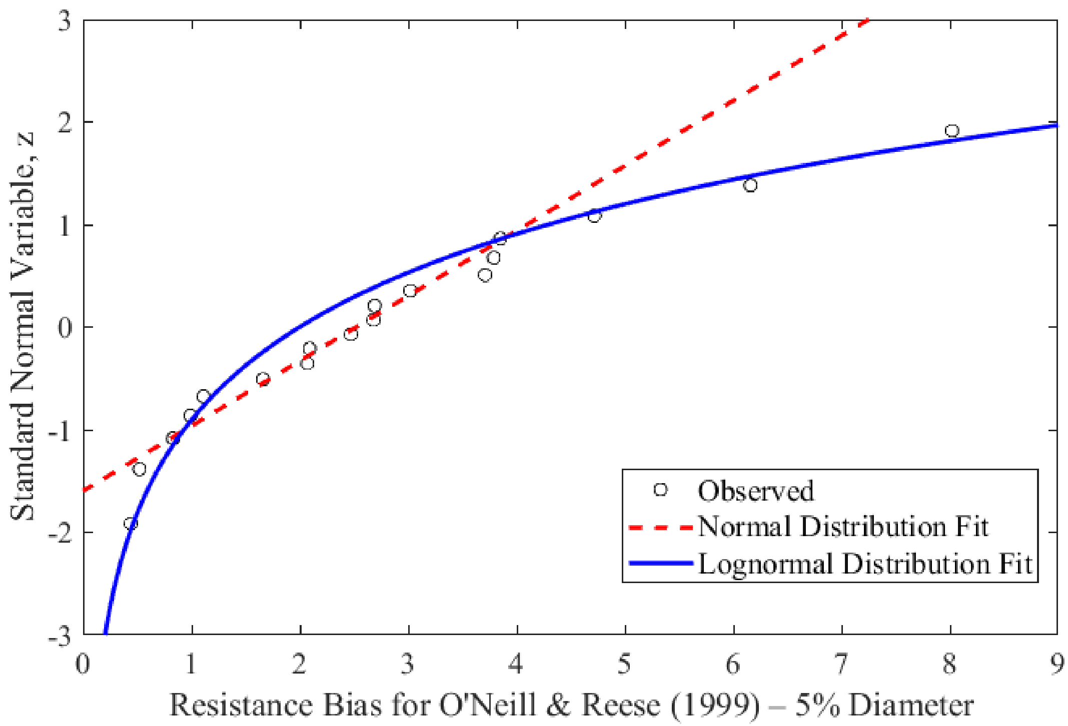

Figure D.26. CDF for skin friction in rock at 5%B using O'Neill and Reese (1999), Iowa data – Approach I

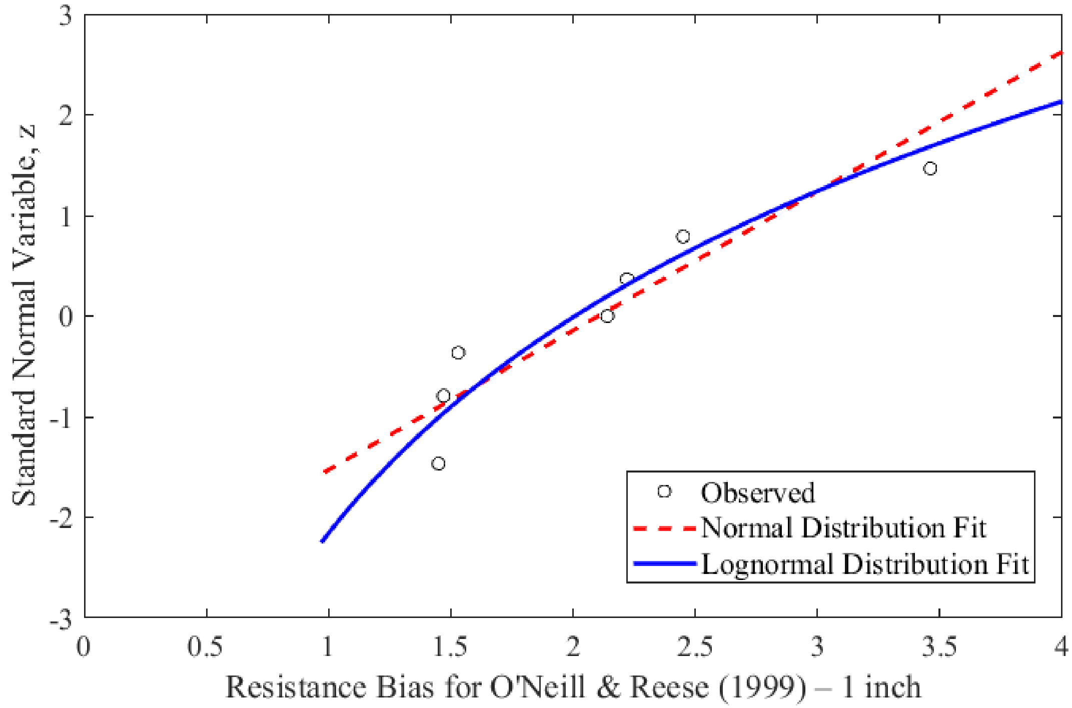

Figure D.27. CDF for skin friction in rock at 1 in. using O'Neill and Reese (1999), Iowa data – Approach II

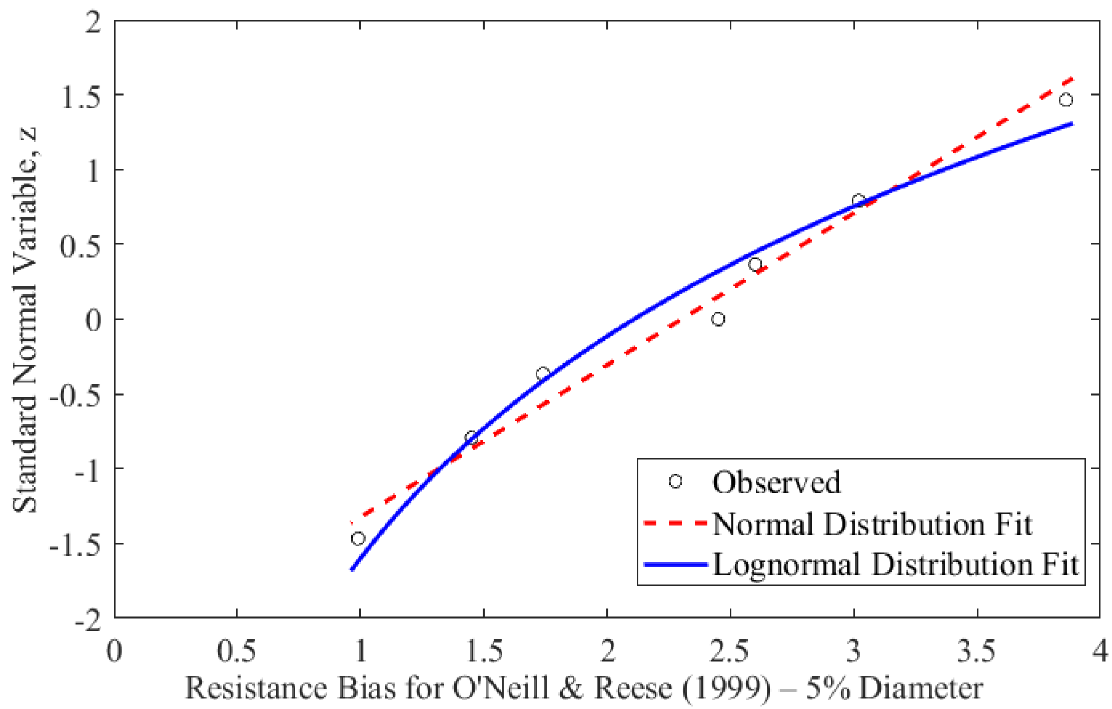

Figure D.28. CDF for skin friction in rock at 5%B using O'Neill and Reese (1999), Iowa data – Approach II

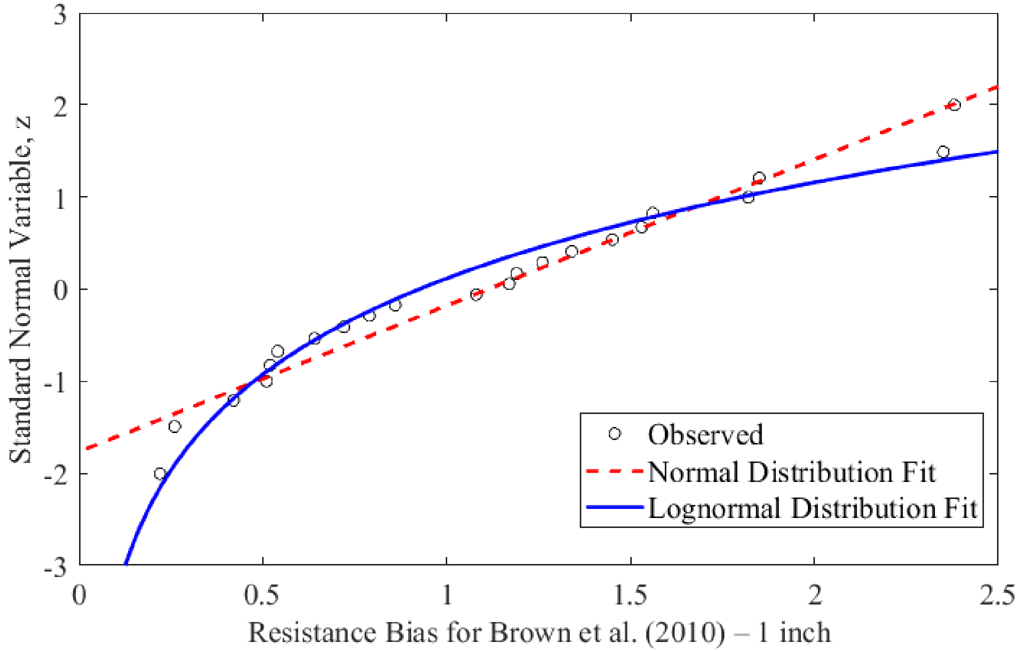

Figure D.29. CDF for skin friction in rock at 1 in. using Brown et al. (2010) – Approach I

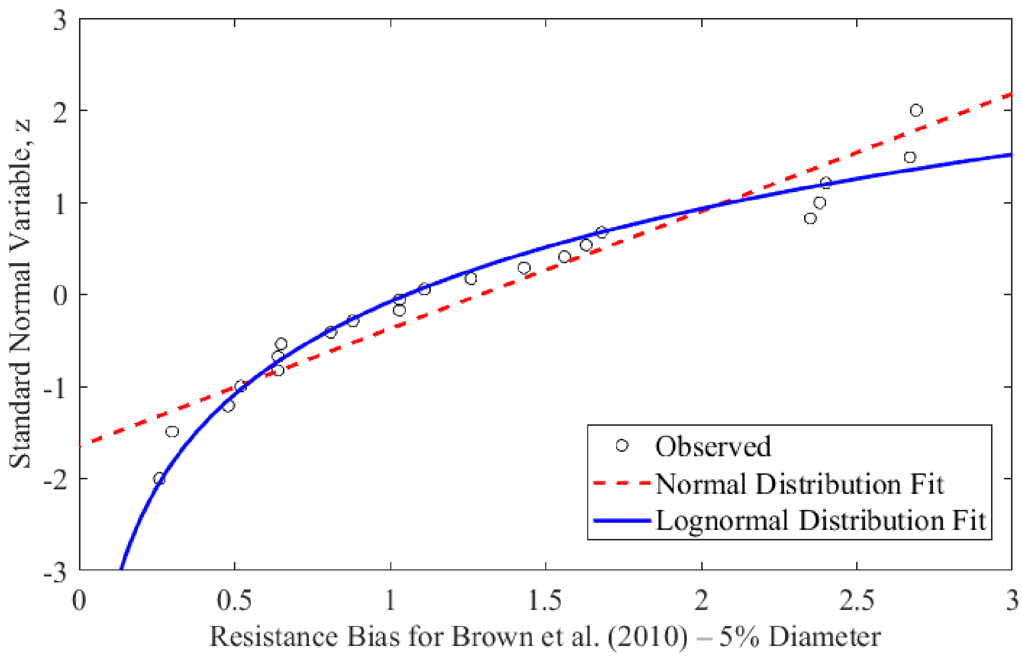

Figure D.30. CDF for skin friction in rock at 5%B using Brown et al. (2010) – Approach I

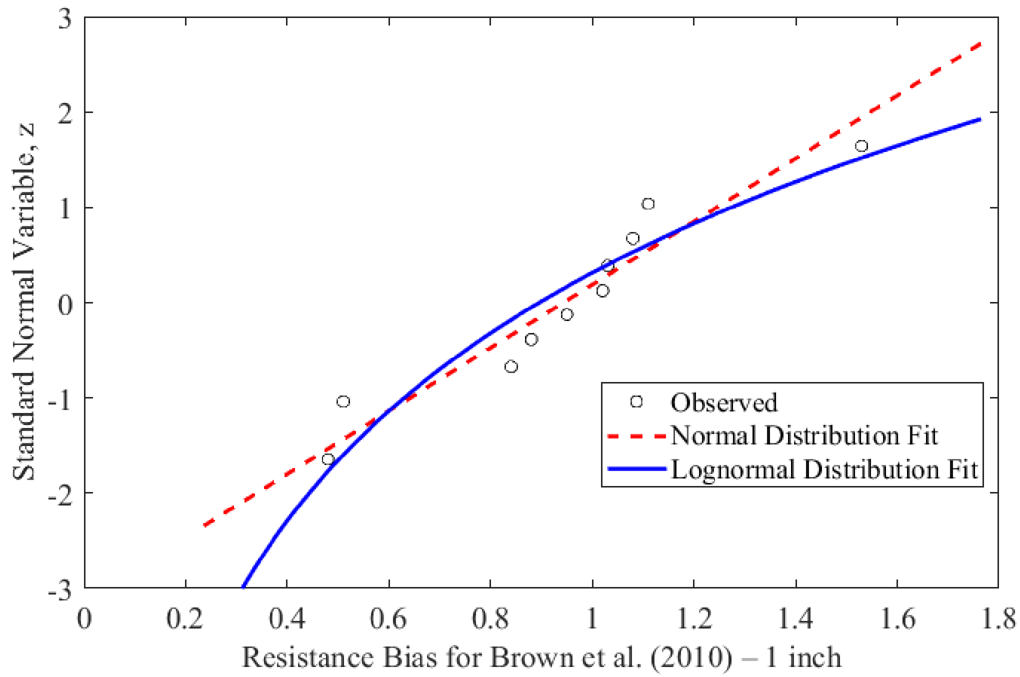

Figure D.31. CDF for skin friction in rock at 1 in. using Brown et al. (2010) – Approach II

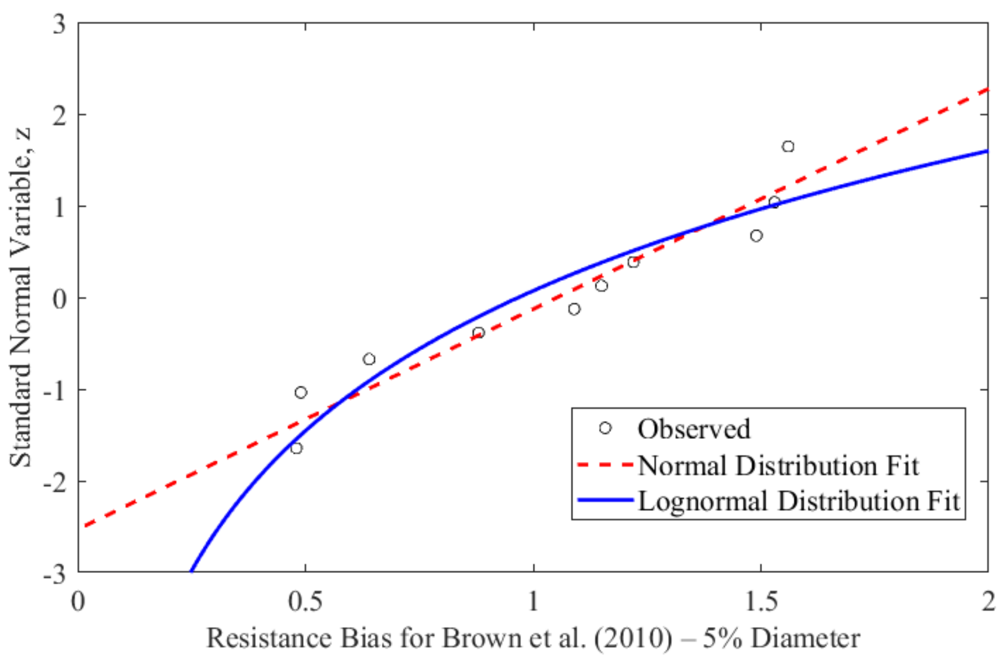

Figure D.32. CDF for skin friction in rock at 5%B using Brown et al. (2010) – Approach II

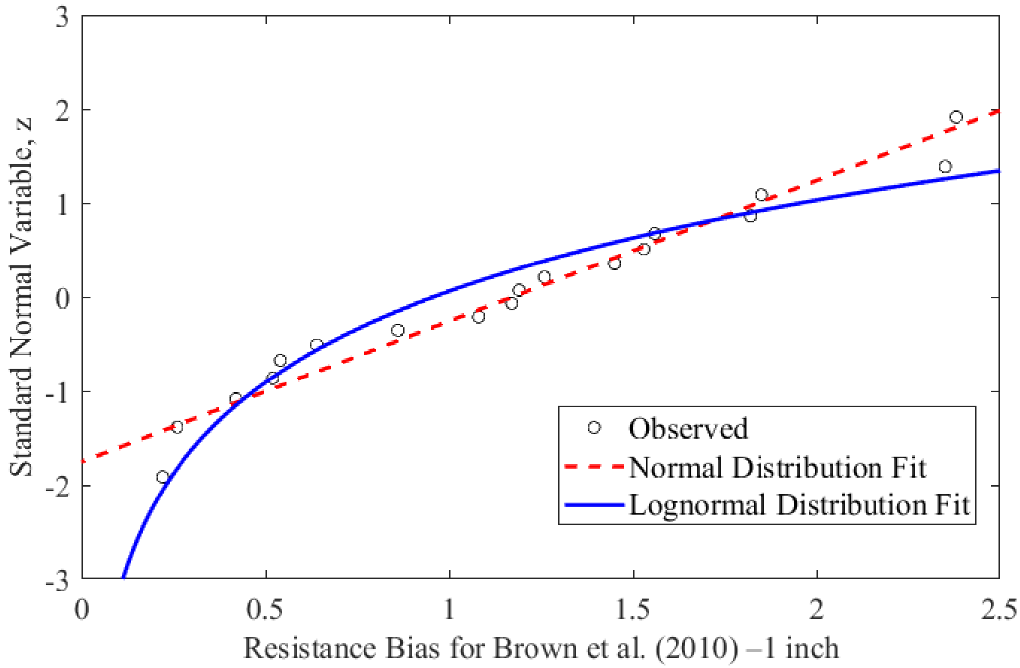

Figure D.33. CDF for skin friction in rock at 1 in. using Brown et al. (2010), Iowa data – Approach I

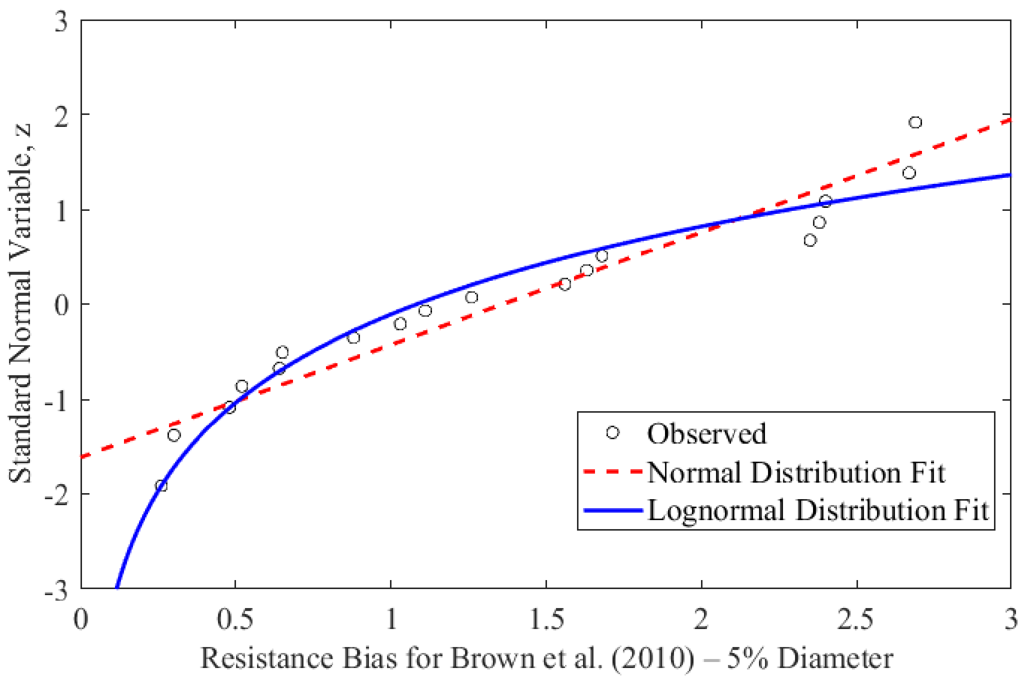

Figure D.34. CDF for skin friction in rock at 5%B using Brown et al. (2010), Iowa data – Approach I

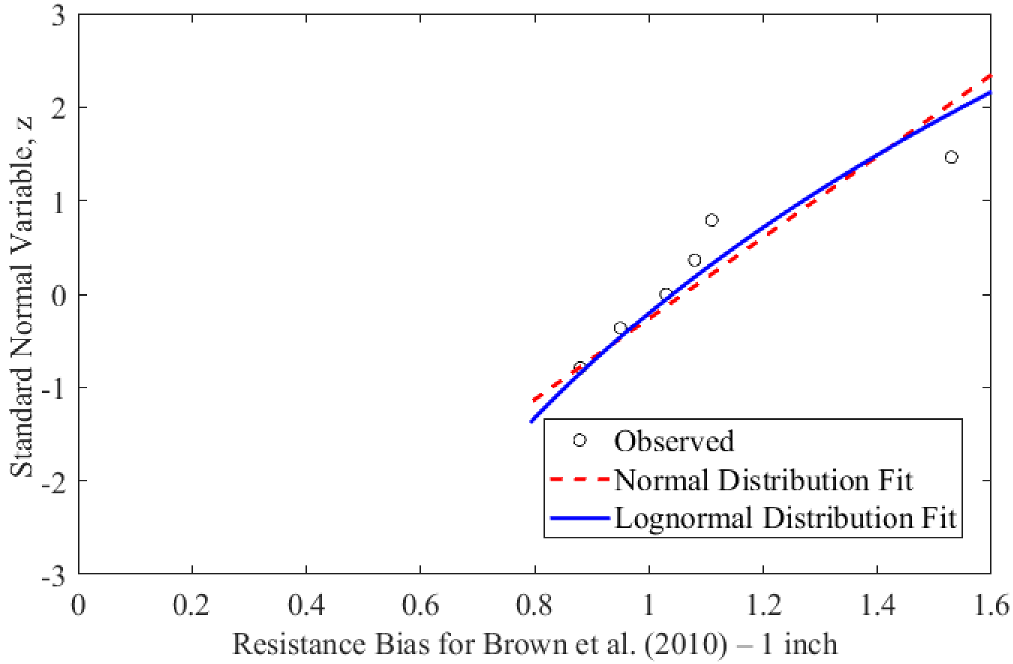

Figure D.35. CDF for skin friction in rock at 1 in. using Brown et al. (2010), Iowa data – Approach II

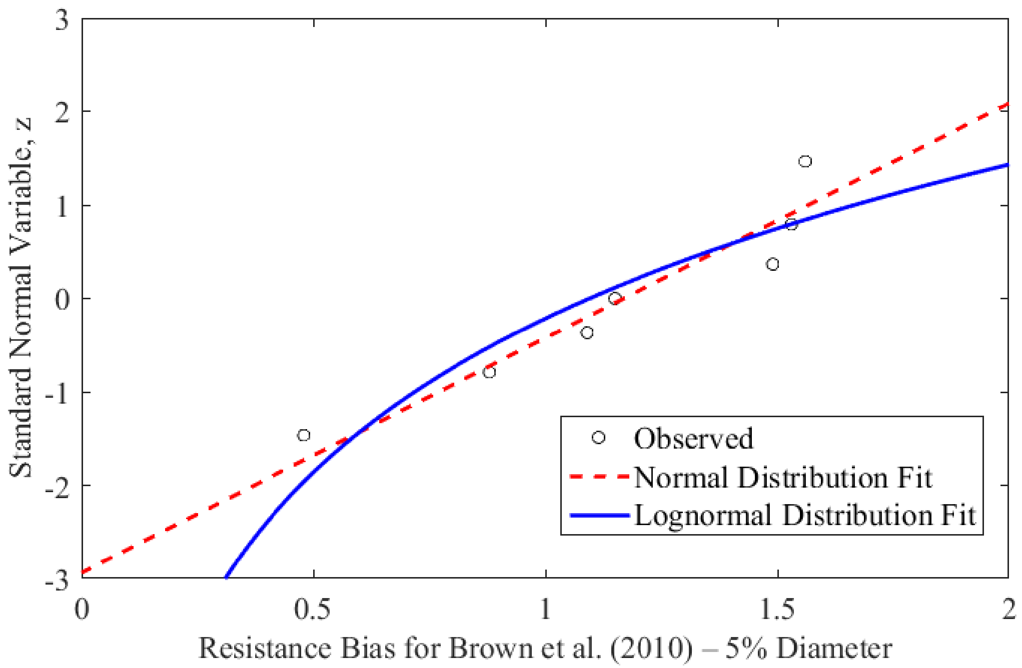

Figure D.36. CDF for skin friction in rock at 5%B using Brown et al. (2010), Iowa data – Approach II

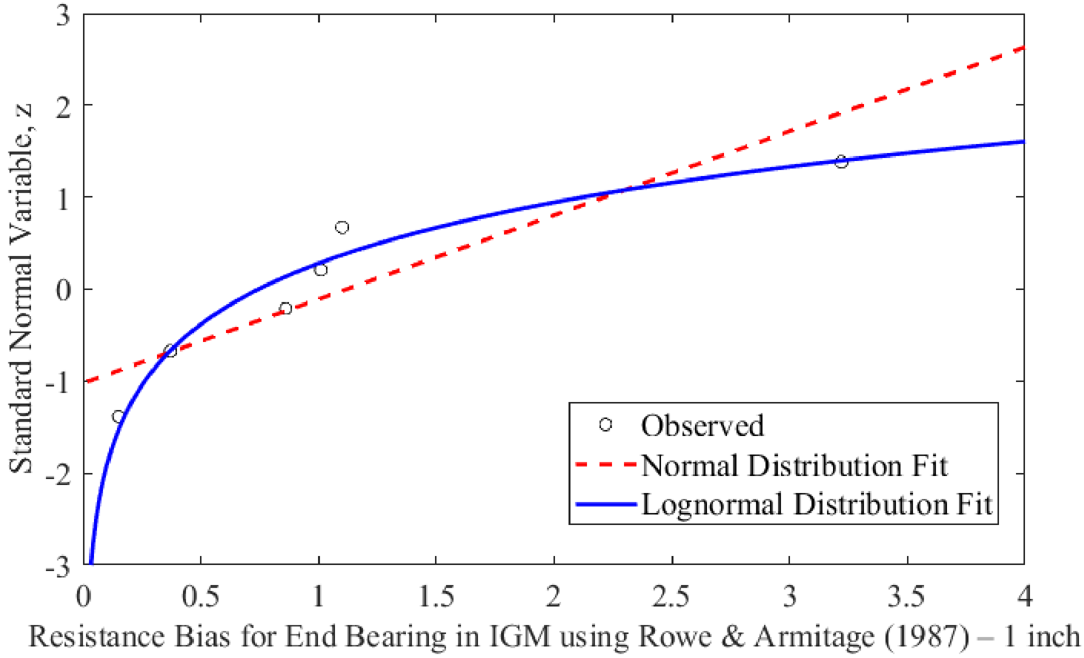

Figure D.37. CDF for end bearing in IGM at 1 in. using Rowe and Armitage (1987)

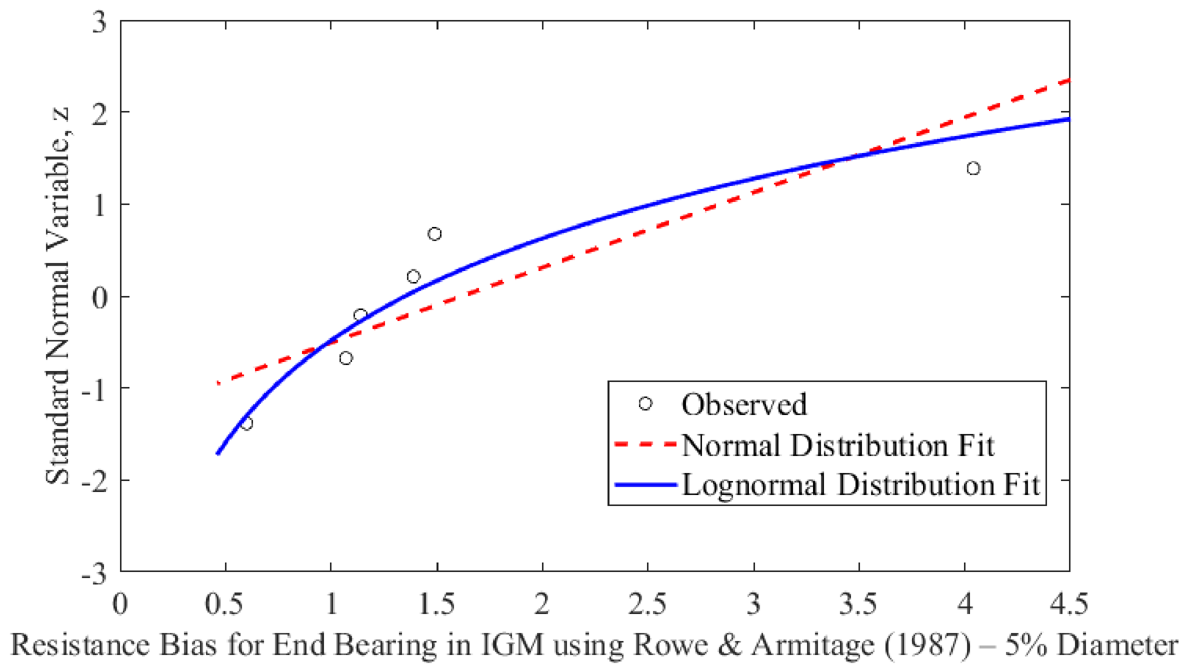

Figure D.38. CDF for end bearing in IGM at 1 in. using Rowe and Armitage (1987)

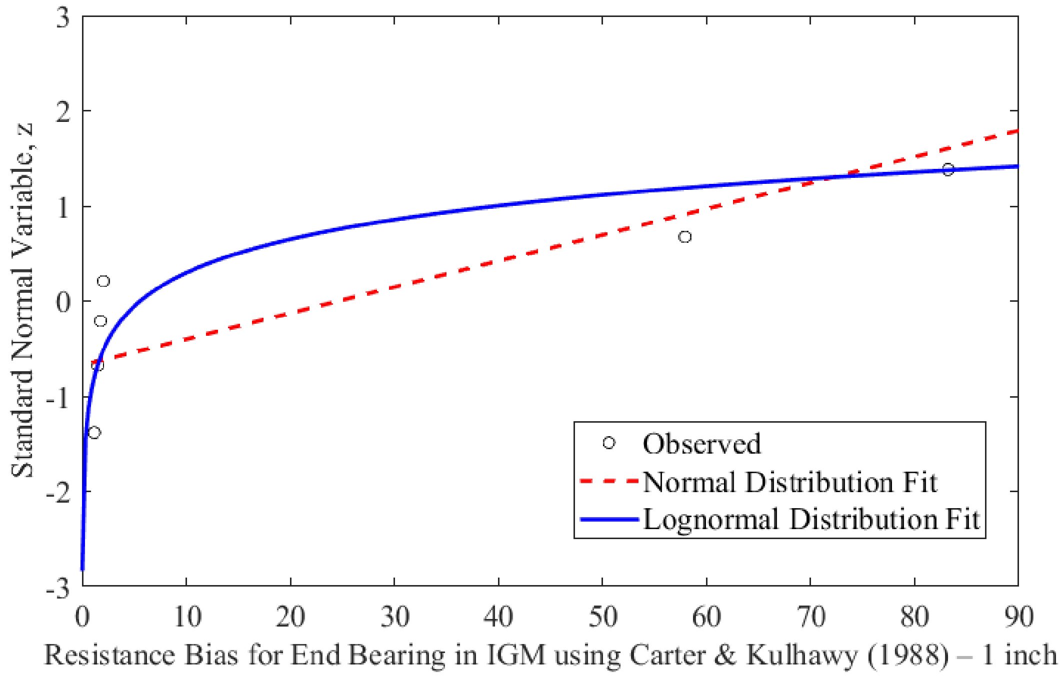

Figure D.39. CDF for end bearing in IGM at 1 in. using Carter and Kulhawy (1988)

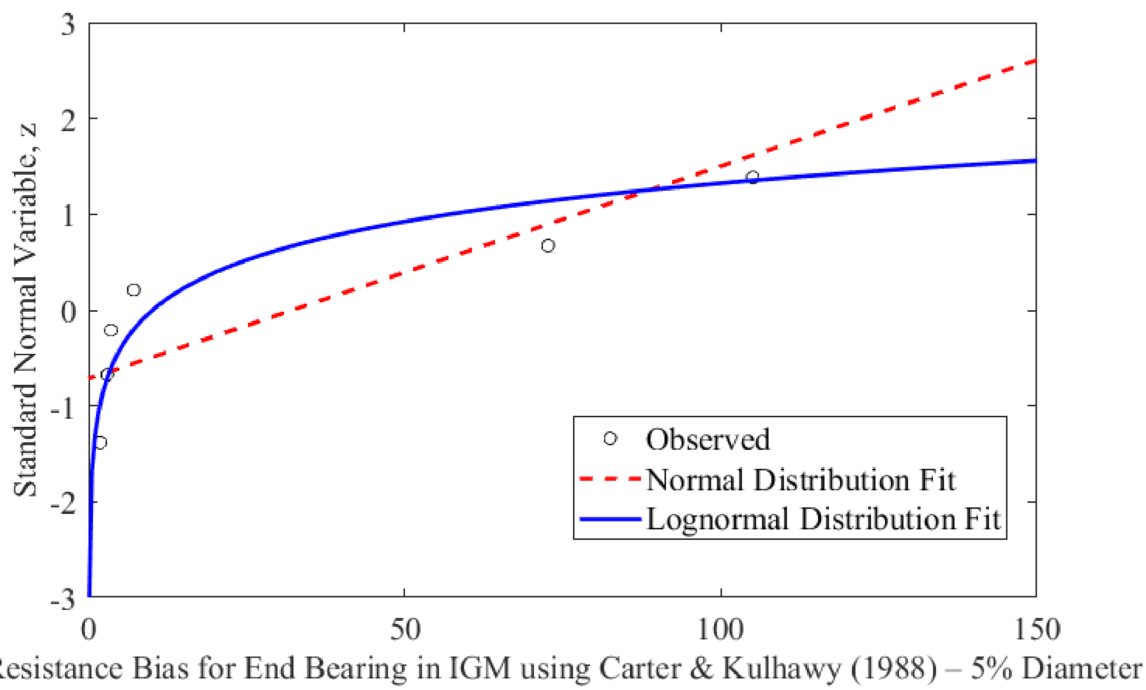

Figure D.40. CDF for end bearing in IGM at 5%B using Carter and Kulhawy (1988)

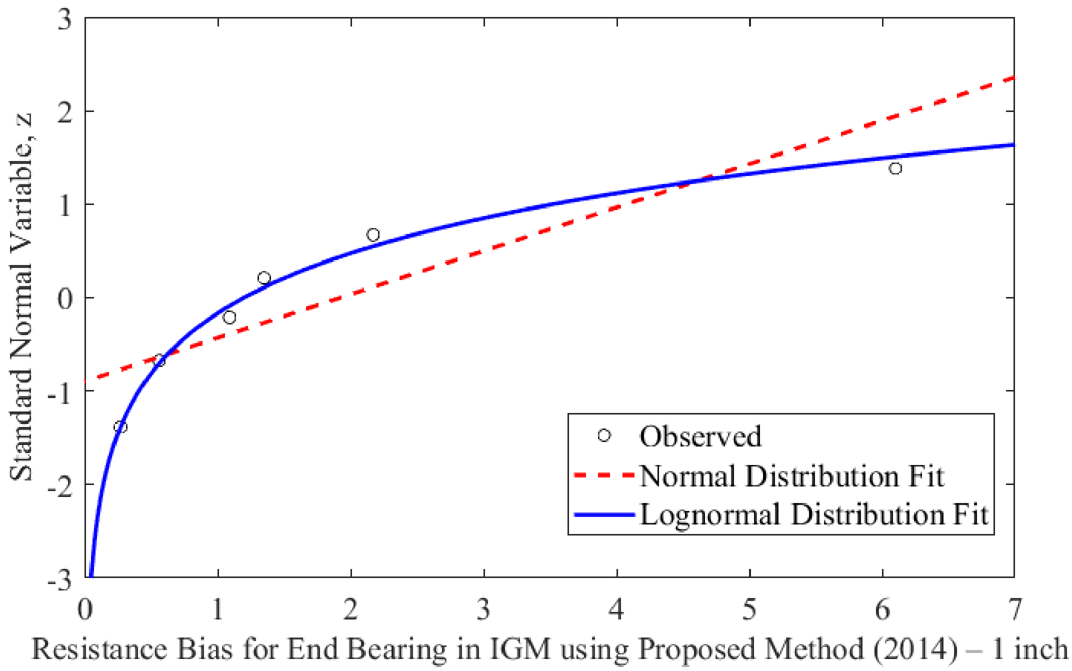

Figure D.41. CDF for end bearing in IGM at 1 in. using proposed method (2014)

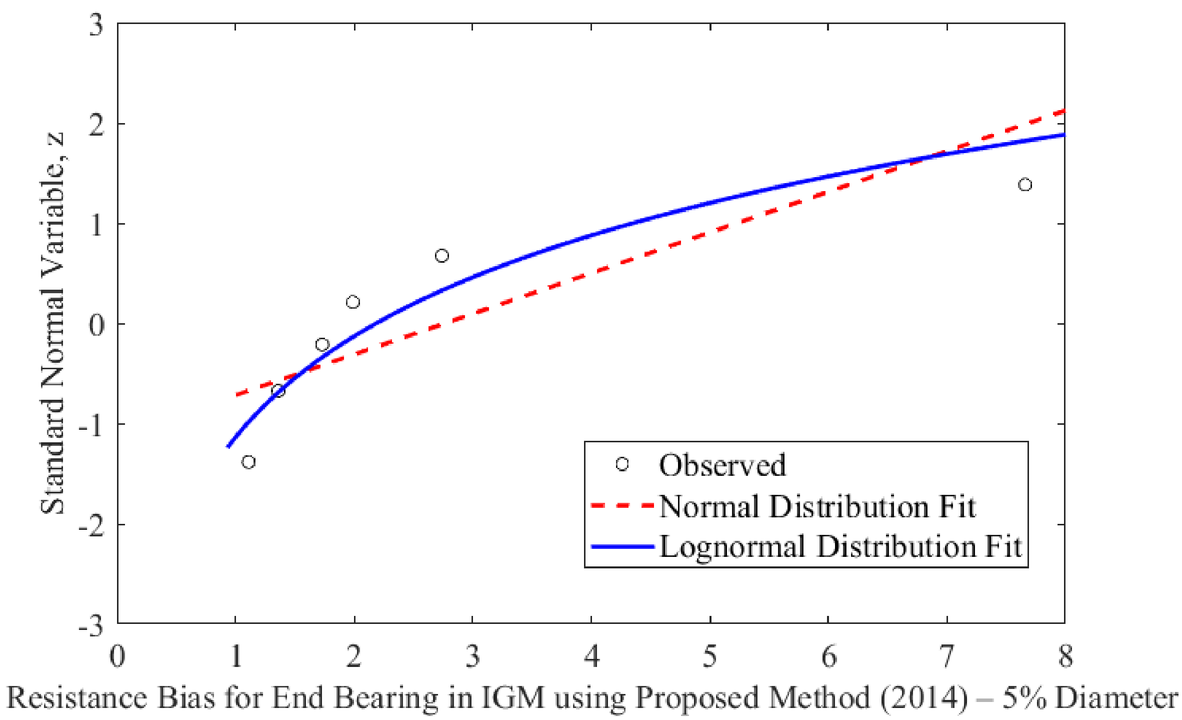

Figure D.42. CDF for end bearing in IGM at 5%B using proposed method (2014)

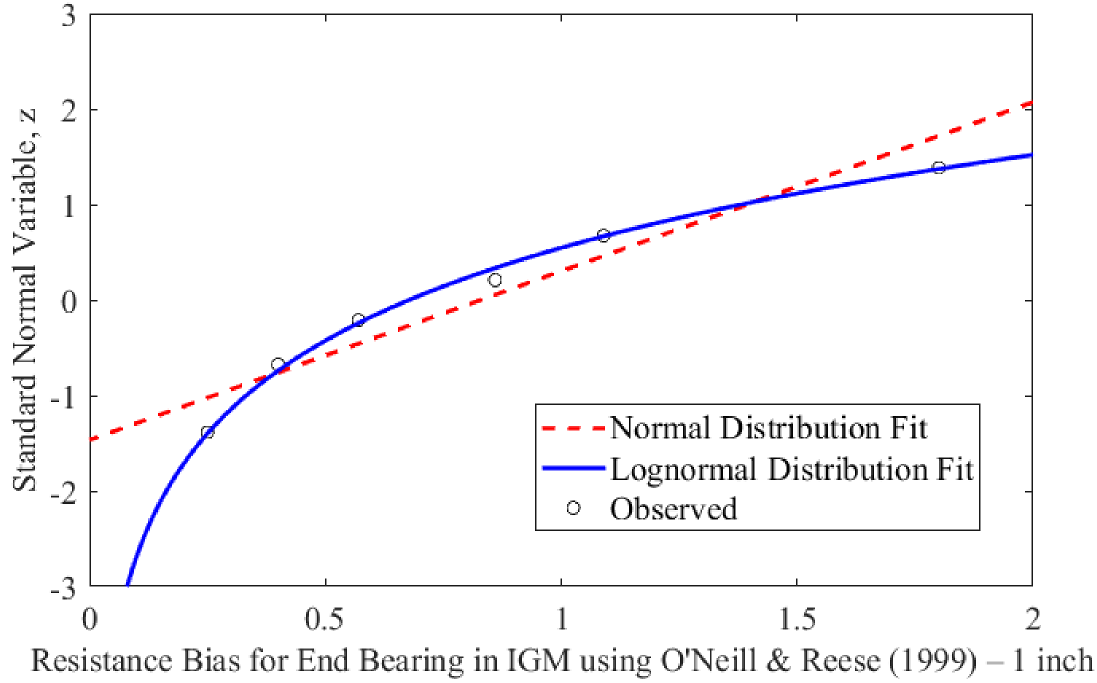

Figure D.43. CDF for end bearing in IGM at 1 in. using O'Neill and Reese (1999)

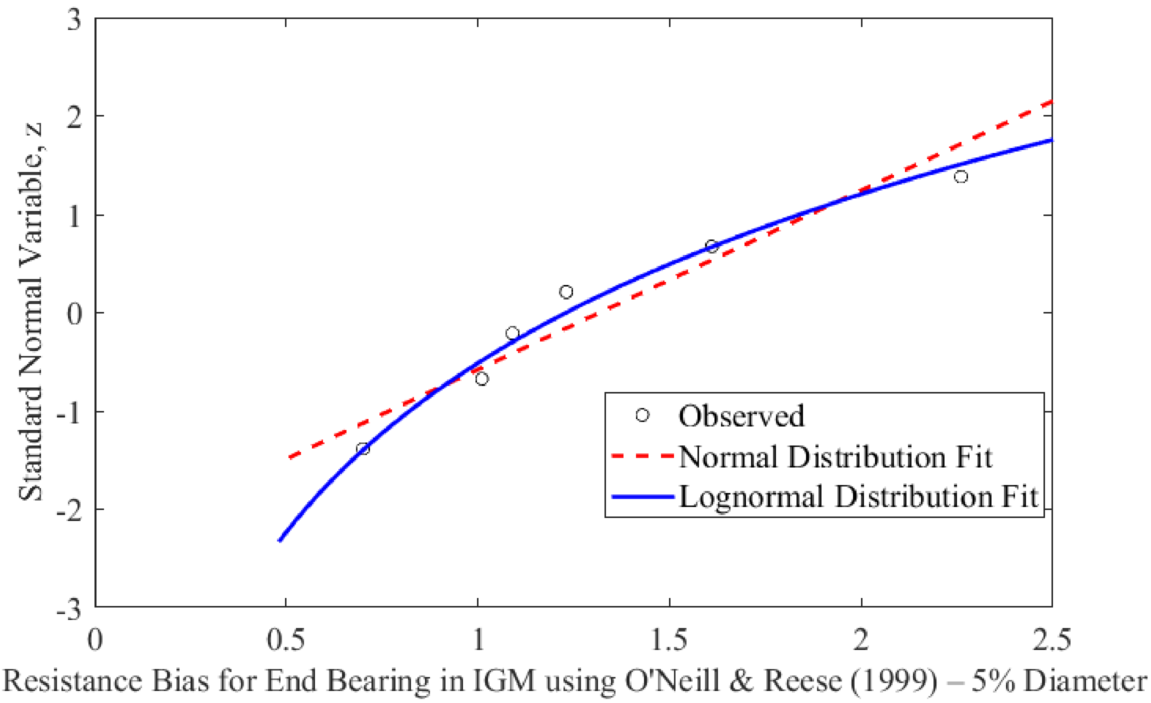

Figure D.44. CDF for end bearing in IGM at 5%B using O'Neill and Reese (1999)

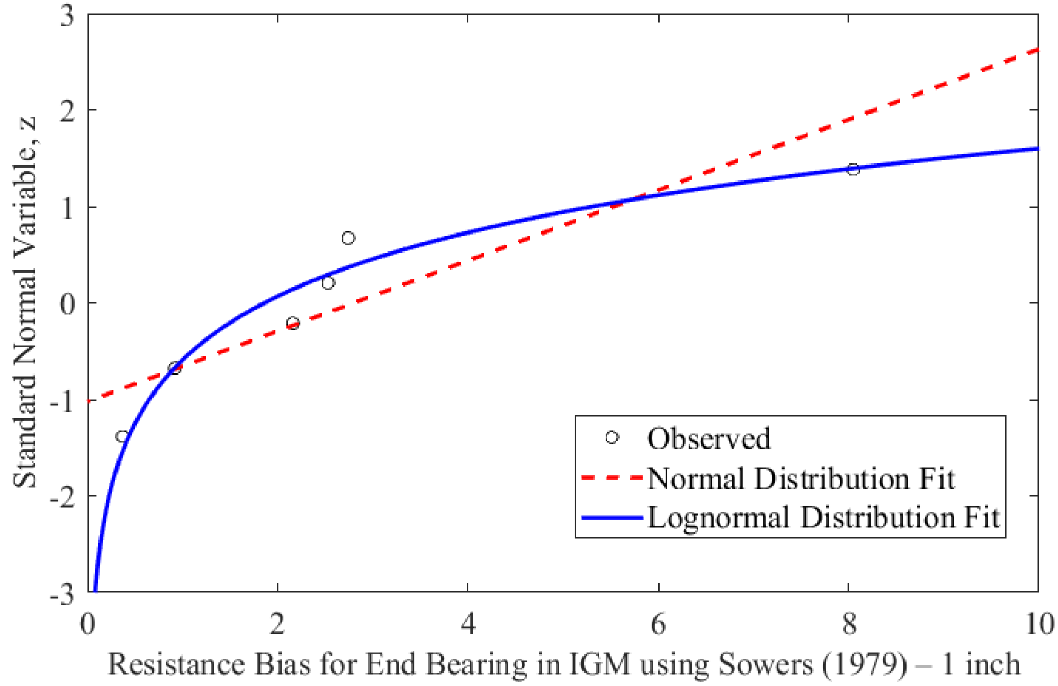

Figure D.45. CDF for end bearing in IGM at 1 in. using Sowers (1976)

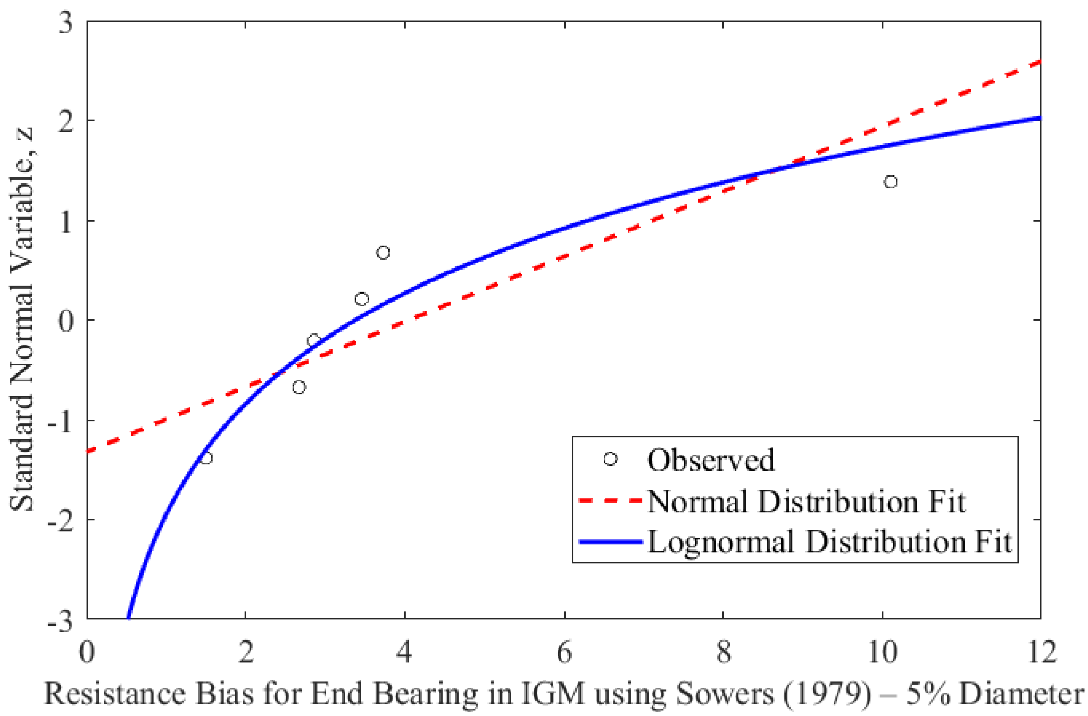

Figure D.46. CDF for end bearing in IGM at 5%B using Sowers (1976)

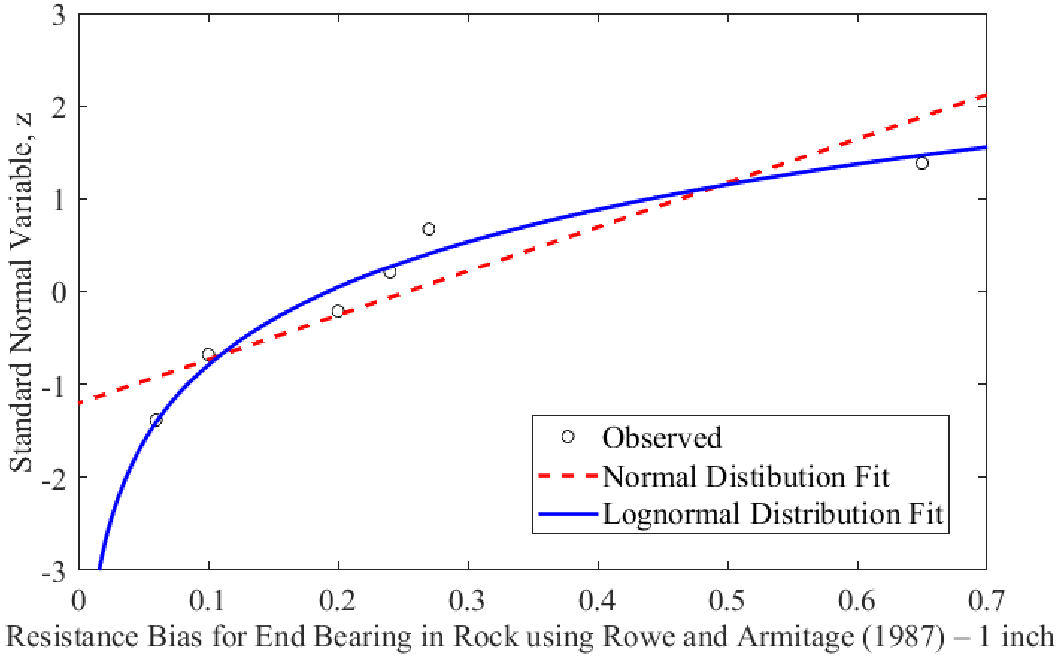

Figure D.47. CDF for end bearing in rock at 1 in. using Rowe and Armitage (1987)

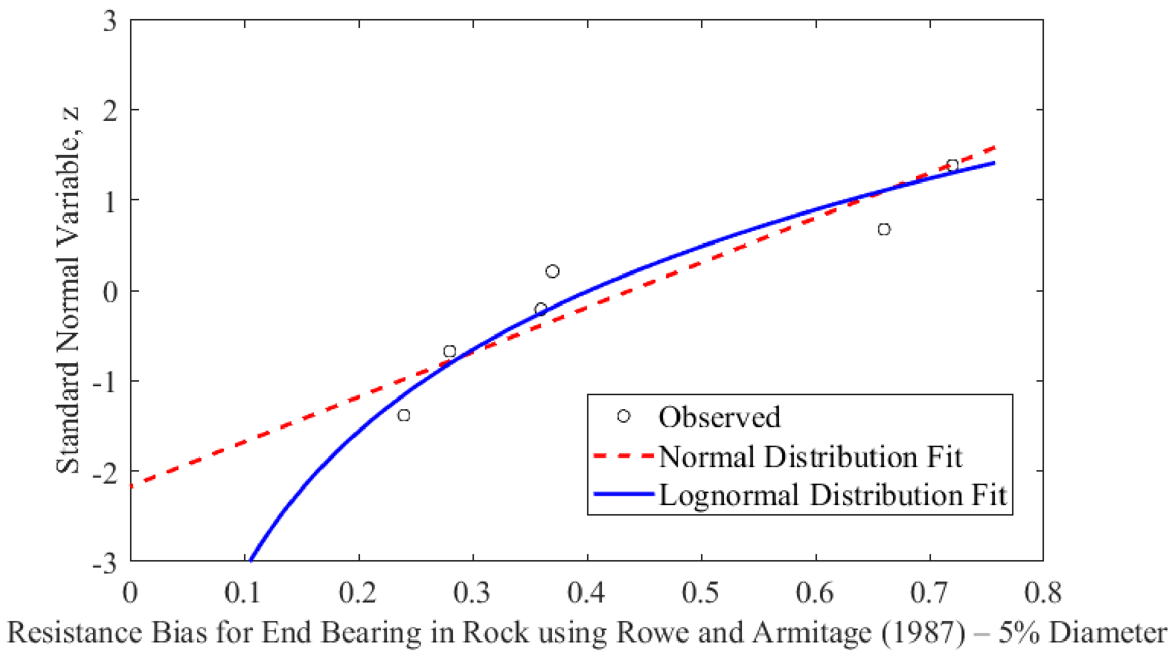

Figure D.48. CDF for end bearing in rock at 5%B using Rowe and Armitage (1987)

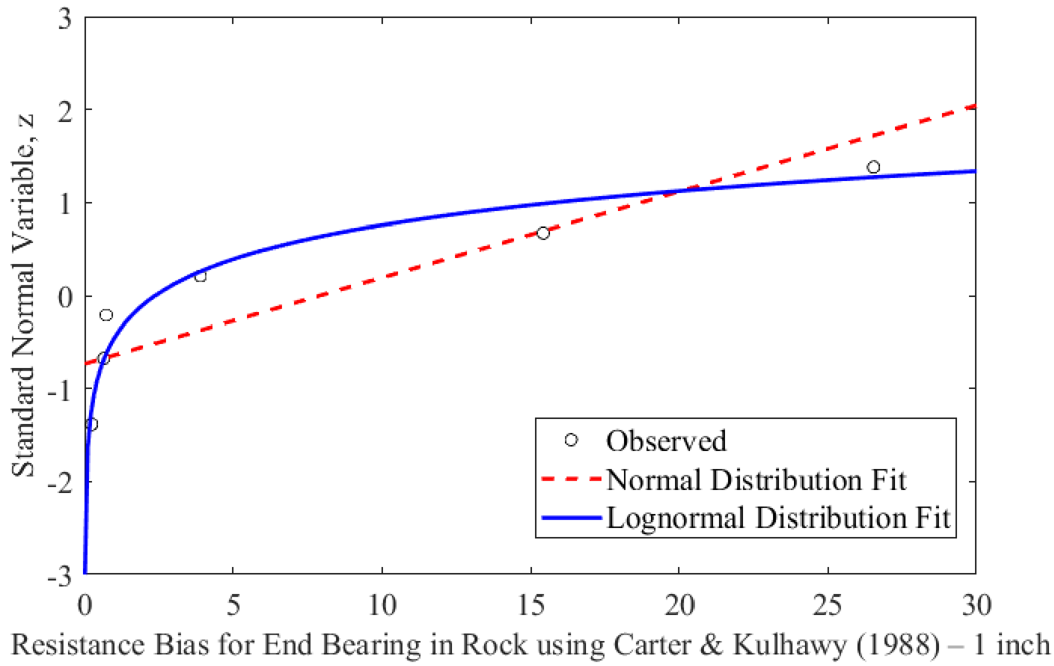

Figure D.49. CDF for end bearing in rock at 1 in. using Carter and Kulhawy (1988)

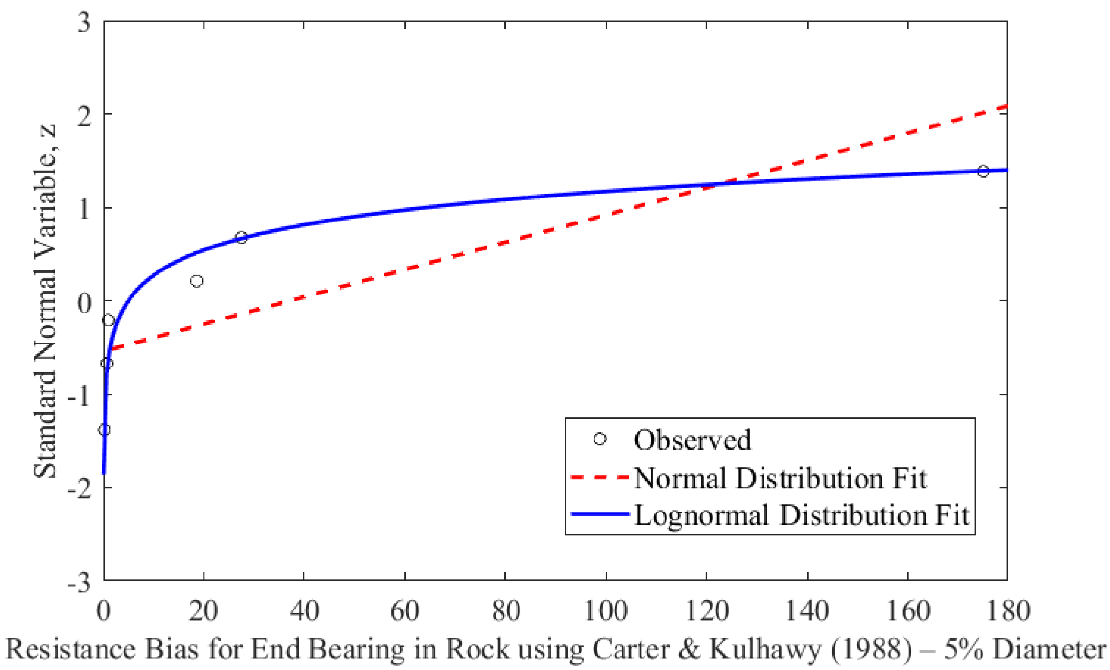

Figure D.50. CDF for end bearing in rock at 5%B using Carter and Kulhawy (1988)

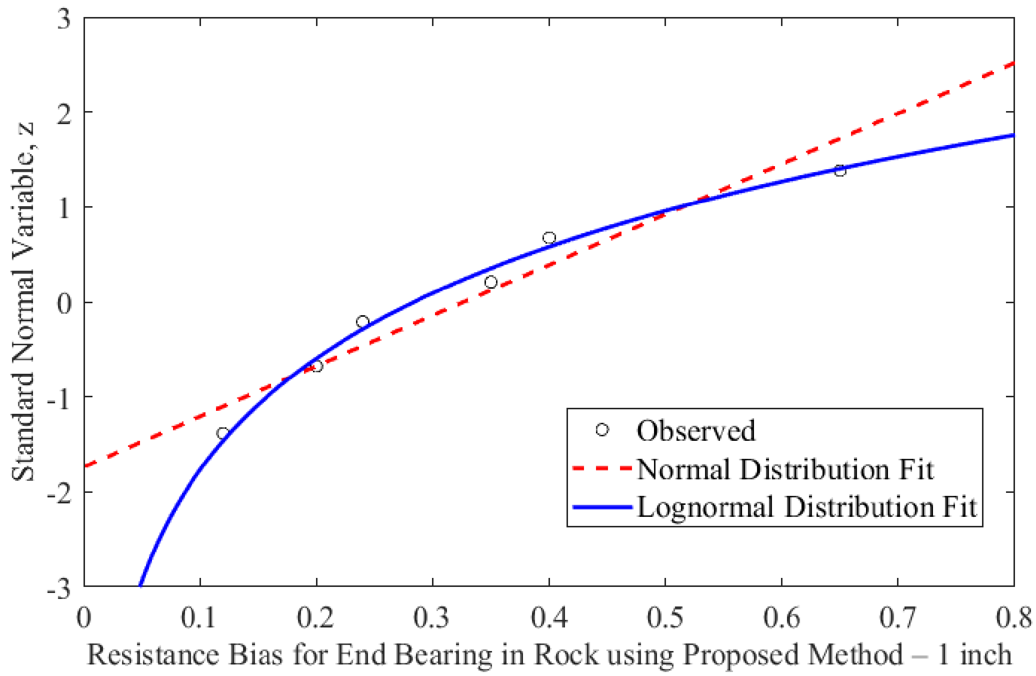

Figure D.51. CDF for end bearing in rock at 1 in. using proposed method (2014)

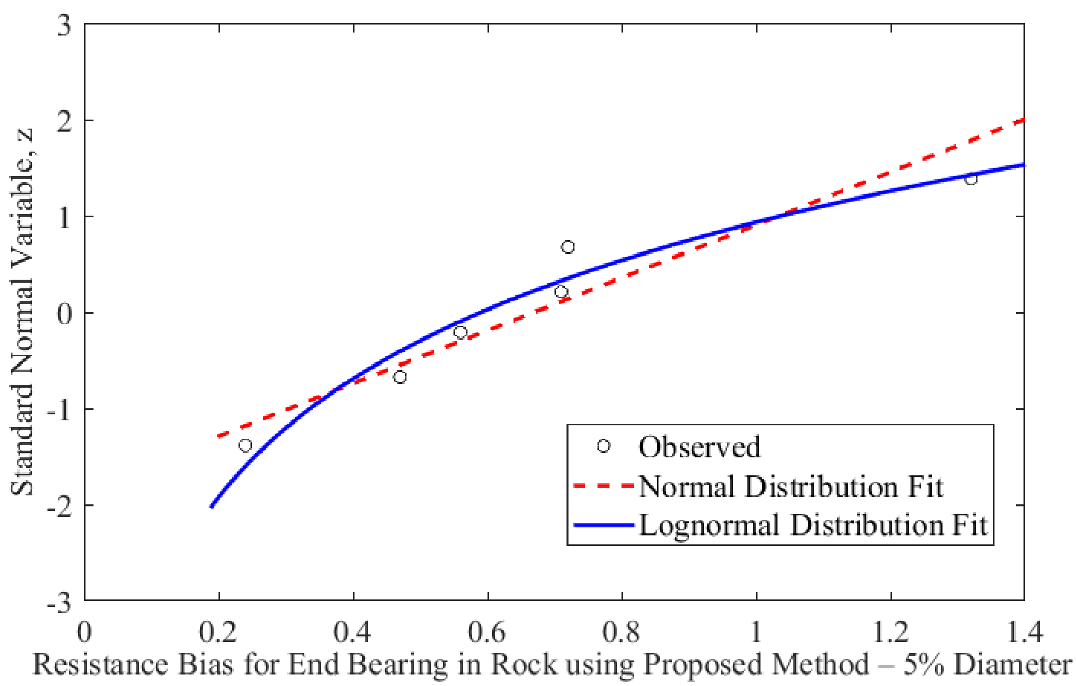

Figure D.52. CDF for end bearing in rock at 5%B using proposed method (2014)

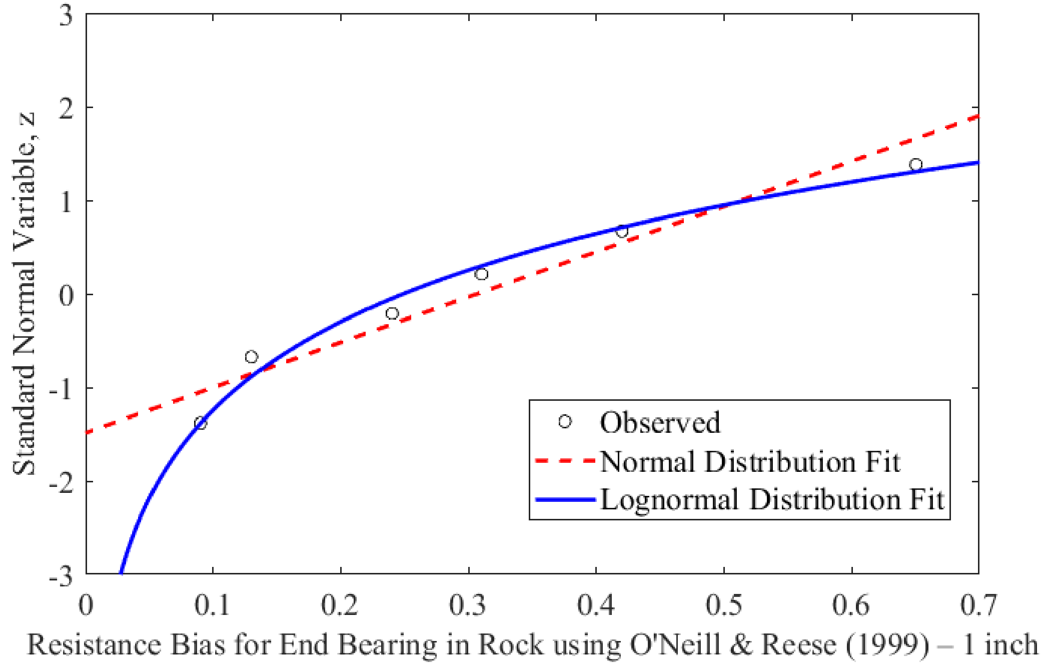

Figure D.53. CDF for end bearing in rock at 1 in. using O'Neill and Reese (1999)

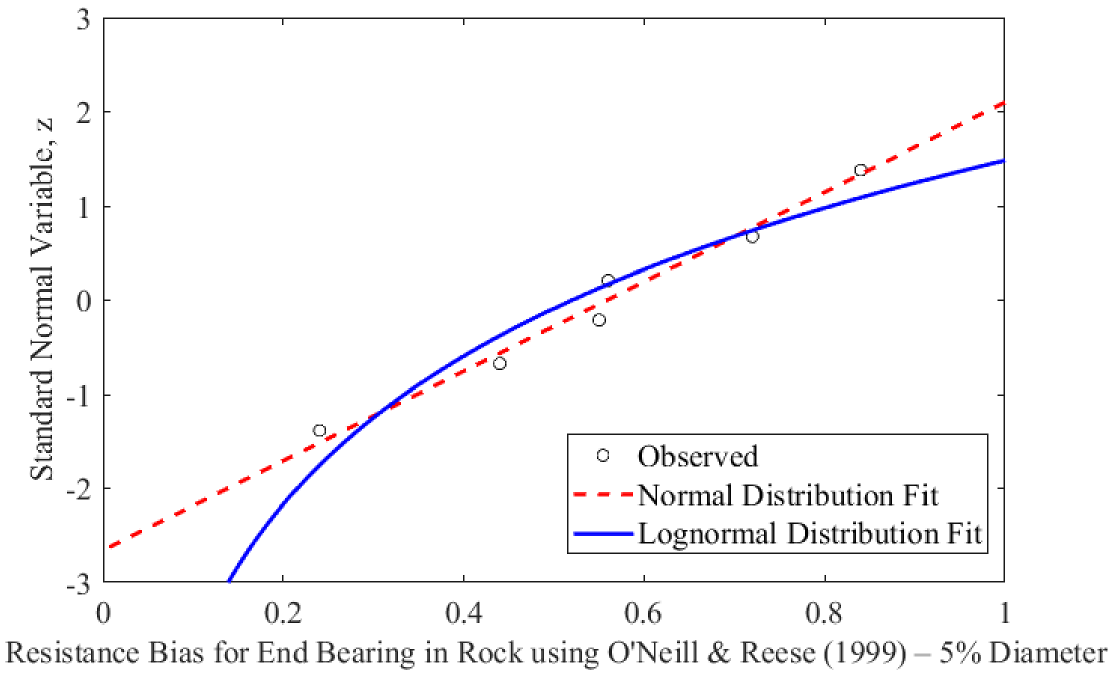

Figure D.54. CDF for end bearing in rock at 5%B using O'Neill and Reese (1999)

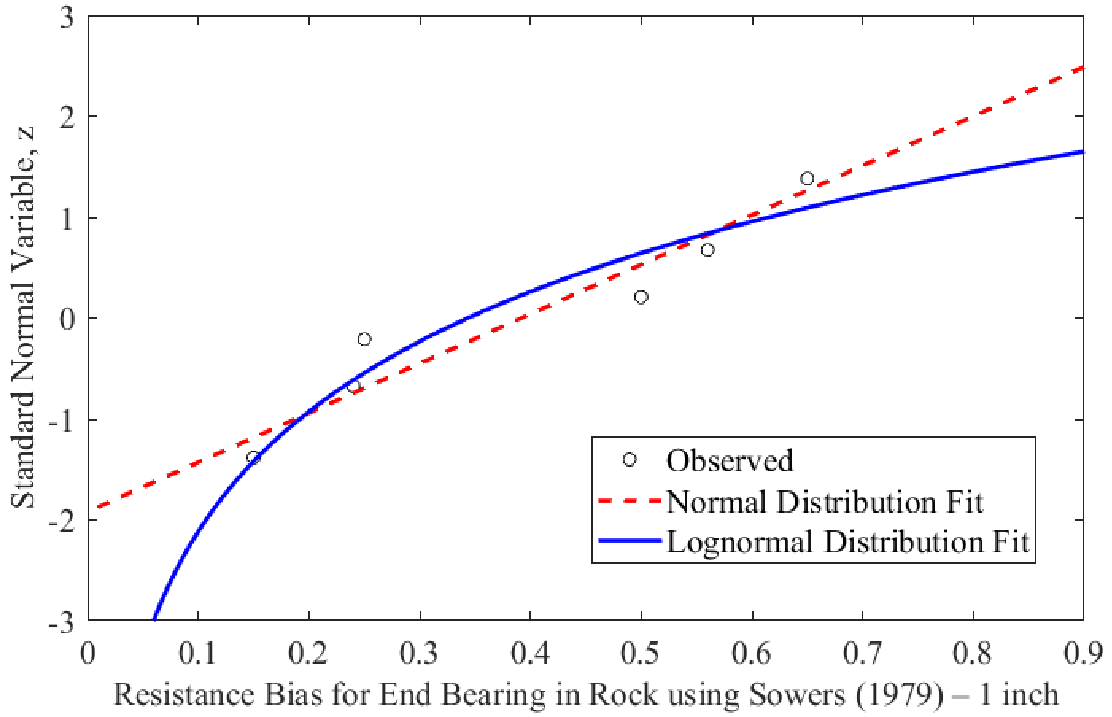

Figure D.55. CDF for end bearing in rock at 1 in. using Sowers (1976)

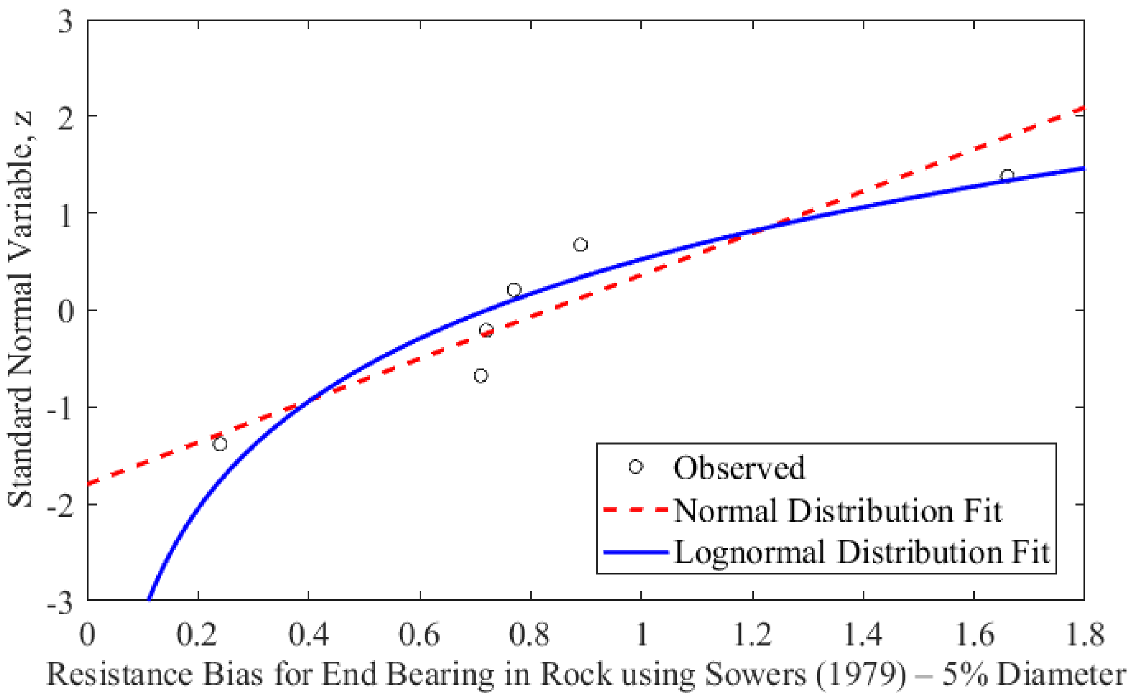

Figure D.56. CDF for end bearing in rock at 5%B using Sowers (1976)

THE INSTITUTE FOR TRANSPORTATION IS THE FOCAL POINT FOR TRANSPORTATION AT IOWA STATE UNIVERSITY.

InTrans centers and programs perform transportation research and provide technology transfer services for government agencies and private companies;

InTrans manages its own education program for transportation students and provides K-12 resources; and

InTrans conducts local, regional, and national transportation services and continuing education programs.

INSTITUTE FOR TRANSPORTATION

IOWA STATE UNIVERSITY

Visit www.InTrans.iastate.edu for color pdfs of this and other research reports.